

NONEQUILIBRIUM FEATURES OF VOLTAGE GATED SODIUM ION CHANNEL

Thesis submitted for the degree of
Doctor of Philosophy (Sc.)

in

Chemistry (Physical)

by

KRISHNENDU PAL

Department of Chemistry
UNIVERSITY OF CALCUTTA

2017

TO MY FAMILY

Acknowledgements

I gladly introduce my thesis as an outcome of the research I have done during my PhD tenure at S.N Bose National Centre for Basic Sciences, Kolkata. Here I take the opportunity to acknowledge all the persons who are directly and indirectly(perhaps more importantly) involved towards the accomplishment of the thesis works.

First of all, I express my sincere gratitude to Prof. Gautam Gangopadhyay for his supervision and the time he invested into my work. He always encouraged me to think and work independently, provided enough space to approach any problem from my viewpoint and gave excellent suggestions and encouragements at times when I was giving up. It's been a wonderful journey with him.

Next I would really like to acknowledge the excellent teachers who inspire me. I am blessed to have teachers like Mr. Brata Samanta(Math), Mr. Bijan Sahu(Math), Prof. Binoy Das(Physics), Prof. Alak Ghosh(Inorganic Chemistry), Prof. Pabitra Chattopadhyay(Analytical Chemistry), Prof. Sanjib Bagchi(Physical Chemistry) and obviously my father(Retd. WBFS), my first brilliant math teacher. Probably this thesis is the direct outcome of the tiniest fraction of the wisdom I could touch from their vast knowledge.

Luckily I have some lovely seniors, friends and juniors who stay very close to my heart. Among the seniors Biswajit Das, Anirban Karmakar, Kinshuk Banerjee and other institutional seniors Arghya-da, Biplob-da, Debmalaya-da, Arindam-da(Ghosh) impressed me with their diverse knowledge and attitude towards life. Friends who I love the most are Anindya, Biswajit, Deep, Anirban, Kaiser, Chandra, Saurjo, Raikishor, Debdas, Meghnath, Buddha, Nirnay, Kartik, Subrata, Abhishek-da. Among juniors I would like to specifically name Snehasish. Also I am thankful to SNB Badminton and Football groups for letting me play two of my favorite sports.

Any word of gratitude feels so inadequate to describe how immensely grateful I am to my family. Needless to say that every success in my life came simply because of the priceless sacrifices my parents made for me. I thank my talented elder sisters for their love, care, concern and affection. I am also blessed with two little nieces, Mistu and Priya and a nephew, Zudo.

Most importantly I would like to thank my girlfriend Miss. Anindita Mukherjee for her unconditional love, everlasting support and encouragement for the last five years. Her never failing faith in me gave me strength and confidence to push my boundaries harder and harder. With out her presence this journey would have been very difficult.

Finally, I thank all the academic and nonacademic stuffs of S. N. Bose National Centre for Basic Sciences, Kolkata for providing me such a global platform with vibrant research atmosphere and beautiful natural scenery which also satisfactorily fed my passion of photography. I am grateful to the Department of Science and Technology, Govt. of India for providing me regular monthly fellowship to carry out my research peacefully.

Krishnendu Pal

Satyendra Nath Bose National Centre for Basic Sciences
Salt Lake, Kolkata, India, July 21, 2017.

ABSTRACT

The research on the voltage-gated sodium ion channel draws immense attention in neuroscience as a target for anesthesia and treatments for genetic diseases in brain, muscle and heart. The sodium ion channel, coupled with the potassium channel initiates the action potential, the most essential requirement for communication between cells. The diverse areas of intense research on sodium ion channel over more than the past six decades include structural, functional and dynamical understanding of channel proteins, inactivation process, inactivation-recovery path of sodium channel, pharmacological channelopathy-toxicology, Markovian modeling of channel kinetics, nonequilibrium response of the channels etc. Sodium channel is mostly investigated experimentally using the patch clamp and voltage clamp techniques where the channel kinetics is studied during the relaxation of channel protein. Here we have investigated the nonequilibrium kinetic and thermodynamic responses of sodium ion channel under stochastic, oscillating and pulsed voltage protocols along with various drug binding situations. The works done in the thesis is briefly given below:

(a) Using oscillating external voltage protocol we have studied the dynamic hysteresis at nonequilibrium steady state and its parametric dependence upon frequency, amplitude, mean voltage of the external voltage protocol. The utilization of energy and associated dissipative work done at nonequilibrium steady state is also investigated.

(b) Comparing closed-state-inactivation and open-state-inactivation path we have explored the energetically optimum processes or the favoring path of inactivation.

(c) We have shown that open state drug blocking is a free energy driven process while closed state blocking is an entropy driven process. Comparing all voltage protocols we have shown that the inactive state blockers are more potent channel blockers than open state blockers.

(d) Considering sodium and potassium channel blockers in single channel model a more realistic picture of drug affected spiking activity of action potential and ionic currents for multiple channels has been studied using Gillespie's exact simulation technique.

(e) Finally we have extended our study from one neuron to two neurons, unidirectionally coupled via electrical synapses. We have shown that the size of patch or channel number fluctuations in individual neurons have very important role in unidirectional synchronization and metabolic energy consumption and these scenario in presence of sodium, potassium drug blockers.

List of Publications

1. **Probing kinetic drug binding mechanism in voltage-gated sodium ion channel: open state versus inactive state blockers,**
K. Pal and G. Gangopadhyay,
Channels, 9, 307 (2015).
2. **Dynamical characterization of inactivation path in voltage-gated Na⁺ ion channel by non-equilibrium response spectroscopy ,**
K. Pal and G. Gangopadhyay,
Channels, 10, 478 (2016).
3. **Nonequilibrium response of a voltage gated sodium ion channel and biophysical characterization of dynamic hysteresis**
K. Pal, B. Das and G. Gangopadhyay,
Journal of Theoretical Biology, 415, 113 (2017).
4. **Role of Patch Size in Synchronization and Metabolic Energy Consumption in Coupled Neurons: Drug Blocking of Sodium and Potassium Channels**
K. Pal and G. Gangopadhyay,
(Submitted)
5. **Study Of The Effect Of Sodium And Potassium Blockers On Action Potential Using Gillespie Simulation Of Modified Hodgkin-Huxley Model**
K. Pal and G. Gangopadhyay,
(Submitted)
6. **Nonequilibrium thermodynamics and a fluctuation theorem for individual reaction steps in a chemical reaction network¹**
Krishnendu Pal, Biswajit Das, Kinshuk Banerjee and Gautam Gangopadhyay,
Journal of Physics: Conference Series, 638, 012002 (2015), STATPHYS-KOLKATA VIII.

¹Not included in the thesis

Contents

1	Introduction	1
1.1	Scope of Thesis	6
1.2	Plan of Thesis	12
2	Topical Review: Background Theory & Literature Survey	20
2.1	Membrane Potential: Neuron	20
2.1.1	Circuit model of the membrane	22
2.1.2	Ion channels	24
2.1.3	Communication between cells: Action potential	25
2.2	Voltage Gated Sodium Ion Channel	29
2.2.1	Structure of the voltage gated sodium channel	30
2.2.2	The dynamical voltage-dependent conformational change	31
2.2.3	Sodium channel family	33
2.3	Inactivation of Sodium Channel	34
2.3.1	Fast inactivation	34
2.3.2	Slow inactivation	35
2.4	Path of Inactivation	35
2.4.1	Inactivation path in sodium channels	35
2.5	Sodium Channelopathy	37
2.5.1	Drug receptor sites of sodium channel	37
2.5.2	Mechanism of drug binding	38
2.5.3	Chemical structures of sodium blockers	39

2.5.4	Sodium channelopathies:	39
2.5.5	Theoretical and computational modeling	41
2.6	Nonequilibrium Response Spectroscopy	42
2.6.1	Nonequilibrium thermodynamics: Entropy balance	42
2.6.2	Adiabatic and nonadiabatic entropy balance	45
2.7	Dynamic Hysteresis	46
2.7.1	Reason of dynamic hysteresis:	47
2.7.2	Memristor	50
2.8	Neuronal Synchronization	51
2.8.1	Chemical synaptic mechanisms of synchronization	52
2.8.2	Gap-junctions and synchronization	52
2.8.3	Synchronizing the Hodgkin-Huxley neurons	53
3	Nonequilibrium Response And Dynamic Hysteresis Of A Voltage Gated Sodium Ion Channel	66
3.1	Introduction	67
3.2	Master Equation and Nonequilibrium Thermodynamic Description	69
3.2.1	Kinetic scheme and master equation description	69
3.2.2	Nonequilibrium thermodynamic features of sodium channel	71
3.3	Voltage Clamp Dynamics	73
3.3.1	Kinetic studies and equilibrium features	73
3.3.2	Steady state solution	75
3.4	Nonequilibrium Response To Oscillating Voltage Protocol	75
3.4.1	Nonequilibrium response dynamics	76
3.4.2	Dynamic hysteresis in sodium channel	76
3.4.3	Ionic current and dissipative work done at nonequilibrium steady state	83
3.5	Approximate Analytical Expressions	87
3.5.1	Low frequency limit	89
3.5.2	High frequency limit	91

3.6	Comparison With Other Models Of Sodium Channel	92
3.7	Conclusion	95
4	Characterization Of Inactivation Path In Voltage-Gated Na⁺ Ion Channel By Non-Equilibrium Response Spectroscopy	102
4.1	Introduction	103
4.2	Dynamical Characterization Of Inactivation	105
4.2.1	Kinetics of CSI and OSI	105
4.2.2	Nonequilibrium thermodynamic characterisation of inactivation path	106
4.3	Constant Voltage Protocol	106
4.3.1	Activation and Inactivation dominated regions	108
4.3.2	Choice of voltage region to study inactivation	108
4.3.3	Waiting Time analysis of inactive states	109
4.3.4	Constant voltage inactivation path	111
4.4	Pulse Train Protocol	111
4.4.1	Kinetics of CSI and OSI in pulse train	113
4.4.2	Non-equilibrium thermodynamics of CSI and OSI in pulse train protocol	115
4.5	Oscillating Voltage Protocol	116
4.5.1	Kinetics of CSI and OSI in oscillating voltage protocol	118
4.5.2	Thermodynamics of CSI and OSI in oscillating voltage protocol	119
4.6	Conclusion	121
5	Investigation Of The Kinetic Drug Binding Mechanism In Voltage-Gated Sodium Ion Channel: Open State Versus Inactive State Blockers	128
5.1	Introduction	129
5.2	Model of Drug Binding	130
5.3	Constant Voltage Clamp Dynamics	132
5.4	Oscillating Voltage Protocol	135
5.5	Pulse Train Protocol	137
5.6	Conclusion	141

6	Effect Of Site Selective Drug Blocking On Single Sodium And Potassium Channel: Gillespie Simulation Algorithm	149
6.1	Introduction	149
6.2	Kinetic Scheme of Markovian Models	151
6.3	Choice of Simulation Technique	154
6.3.1	Gillespie simulation algorithm	155
6.3.2	From microscopic limit to deterministic limit	157
6.4	Effect of Sodium & Potassium Channel Blockers	159
6.4.1	Sodium blocker	159
6.4.2	Potassium blocker	162
6.5	Conclusion	164
7	Effect Of Channel Noise On Synchronization And Metabolic Energy Consumption In Unidirectionally Coupled Two Hodgkin-Huxley Neurons	171
7.1	Introduction	171
7.2	Single Hodgkin-Huxley Neuron: Deterministic Description	174
7.3	Unidirectionally Coupled Two Hodgkin-Huxley Neurons Via Gap Junction: Deterministic Description	177
7.3.1	Kinetic scheme of unidirectionally coupled Neurons	177
7.3.2	Energetic description of the unidirectionally coupled neurons	179
7.4	Effect Of Patch Size In Unidirectionally Coupled Neuron	179
7.4.1	Stochastic generalization of Hodgkin-Huxley model: Langevin description	180
7.4.2	Kinetic picture of synchronization	182
7.4.3	Energetics of the unidirectional synchronization	182
7.4.4	Effect of patch size variation on metabolic energy consumption	183
7.5	Effect Ion Channel Blocking Drugs	186
7.5.1	Sodium channel blockers	187
7.5.2	Potassium channel blockers	188
7.5.3	Total blockers	189
7.6	Conclusion	190

Chapter 1

Chapter 1

Introduction

Voltage-gated ion channels are a particular class of transmembrane protein that form ion selective channels which activates by the change in the electrical potential of the membrane. The subunits of the channel protein are arranged in such a way that a central pore is formed through which ions can travel down their electrochemical gradient. Although the cell membrane is usually impermeable to ions, the conformational change of protein channel leads to the opening and closing of the pore which determines the ion conductivity through the channel pore [1]. In excitable cells namely, neuronal, cardiac and muscle tissues etc, ion channels generate and propagate action potential which is the fundamental requirement of communication through cells. When a stimulus above a particular threshold magnitude arrives, sodium channels burst open and the sodium ions in extracellular space diffuse instantly into the intracellular space and further depolarize the cell membrane and initiates action potential. When the cell is depolarized enough sodium channel inactivates when a part of a channel protein residue gets inside the pore and block ion permeation. After that potassium channel and sodium-potassium pump brings the channel protein back to its resting state by adjusting the resting state ion equilibrium in extracellular and intracellular medium and thereby completes the action potential. Till now sodium, potassium, calcium and chloride ion channels have been found to be responsible mainly for action potential generation.

The research on voltage-gated ion channel is still drawing immense attention in neuroscience over the past six decades. The literature of ion channel research is extremely vast and well grounded by the contribution of eminent biophysicists. Pioneering research performed by Cole, Curtis [2–4], Hodgkin, Huxley [5] and Kratz [6, 7] during the period 1935-1952 is now known as the era of classical biophysics, today which serves as the

foundation of our understanding of how the selective diffusion of ions across the plasma cell membrane results in the generation and propagation of action potential in excitable tissues. Initially debated but later a series of experiments by Hodgkin and Huxley demonstrated that action potentials were an electric signal of ionic origin [5]. Using experiments with the voltage clamp, invented by Cole and Curtis, 1947, Hodgkin and Huxley published five papers [8] in a row at the summer of 1952 describing how ionic currents give rise to the action potential. The final paper of the Hodgkin-Huxley [8] mathematically described the action potential which was a landmark in the history of today's theoretical neuroscience. Their experiments for modeling the action potential using voltage clamp technique has laid the foundation for electrophysiology; for which they shared the Nobel Prize in Physiology or Medicine in 1963. Experiments by Rothenberg, 1950 [9] and Keynes, 1951 [10] demonstrated that propagation of the action potential is associated with an inward flow of sodium ions and the outflow of potassium ions. Experiments done by Hodgkin and Katz [6] demonstrated that the concentration of sodium in the extracellular solution determines the rate of rising and amplitude of the action potential. Later Neher and Sakmann in the late 1970s and early 1980s had advanced this research field by inventing the patch-clamp technique which permits the possibility of measuring ionic current through the individual ion channels [11]. Neher and Sakmann shared the Nobel Prize in Physiology or Medicine in 1991 for this outstanding work. The experimental works by Nossal et al., 1991 [12] and Hille et al., 1992 [1] demonstrated that the individual ion channels are essentially stochastic entities that open and close in a random way. The computational and theoretical works by Skaugen and Walloe, 1979 [13], c1-Strassberg, 1993 [14], DeFelice, 1996 [15], White and co-workers, 1996 [16] produced computer based programming of Markov models to describe the noise properties of clusters of ion channels in a small area of membrane [14,17]. Later Fox et al., 1994 and 1997 [18,19] had given a stochastic description of the kinetics of many ion channels by considering Langevin description. After isolation of individual sodium and potassium ion channels, several workers have studied the single ion channel kinetics experimentally to fit the kinetics to mathematical models. Several Markov models for sodium and potassium channels had been proposed [20–24] then. For example, Zagotta et al [20] had performed an experiment for the selection of the best suited Markov model for the description of potassium ion channel kinetics. The Nobel Prize in Chemistry 2003 was awarded jointly to P. Agre and R. MacKinnon for discoveries concerning channels in cell membranes [25]. MacKinnon and colleagues determined the three-dimensional molecular structure of a potassium channel from an actinobacteria, *Streptomyces lividans*, utilizing X-ray crystallography [26,27]. For modeling sodium channels Horn, 1984 [28], Vandenberg-Bezánilla, 1991 [29], Patlak,

1991 [30], Kuo, 1994 [31], Millonas, 1998 [32], Clancy- Rudy, 2002-2007 [33–35] produced very effective and notable contributions.

Among all types of cation and anion channels, particularly, *Voltage Gated Sodium Ion Channel* is the most studied one which initiates the action potential [1] first hand. Sodium channels are the giant trans-membrane proteins with four interconnected repetitive subunits arranged in such a way that a central pore is formed. That pore can selectively conduct Na^+ ion across the electrochemical gradient from extracellular part to intracellular part. From initiation of action potential by sodium ion selective gates to inactivation of that gate is done by sodium ion channel protein. Sodium ion channel regulates many physiological functions which makes it an optimal drug target for therapeutic action. Particularly, sodium channels are targeted for anesthesia and treatments for genetic diseases in the brain, skeletal muscle, heart and for various other pathologies. These drugs basically block the sodium channels and inhibit generating action potential which leads to the insensitivity of the targeted area. More than fifty-five channelopathies (inherited ion channel diseases that result from genetic defects and disturbance in subunits) have been identified [36, 52]. Some well-known diseases like epilepsy, familial hemiplegic, migraines and familial autism mostly caused by mutations to genes encoding the channel [38]. The worldwide sales of drugs which are mainly ion channel-targeted are estimated to be approximately USD 12 billion [39]. Thus voltage gated sodium ion channel has been a major area of interest in pharmacological, neurological and electrophysiological research. The main theme of research in sodium channel in the context of our proposed thesis can be broadly classified in the following categories: A.) Structural and functional understanding of the sodium channel protein, B.) Inactivation of sodium channel, C.) Activation, inactivation and recovery path of sodium channel, D.) Toxicology and Channelopathy, E.) Markovian modeling for gating kinetics, F.) Nonequilibrium Response of Voltage gated sodium channels. Here we provide a brief survey of literature of the major discoveries in the context of sodium ion channel.

A. Structural and functional understanding of the sodium channel protein:

Beneski and Catterall, 1980 [40] and Hartshorne [41] using photoactive derivative of a scorpion toxin, identified a large molecular weight component which led to the elucidation of the primary structure of sodium channels. This was the major accomplishment to set the groundwork for molecular and mutagenic studies of sodium channels. This study for the first time assigned distinct functional gating roles to regions or residues of channel protein. The recent X-ray crystal structure determination of bacterial sodium channels (Na_vAb , Na_vRh , and Na_vMs from *Arcobacter butzleri*, Alphaproteobacterium

HIMB114, and *Magnetococcus* sp., respectively) has revealed that these channels have different functional states such as closed [42], potentially inactive [43,44], and open [45]. With the help of these studies and combining human sodium channel sequences and bacterial crystallographic data homology models [46] have been build up. Several studies using prokaryotic sodium channels channels have provided insight of the structure and function of bacterial sodium channel channels, translatable to eukaryotic sodium channels [47]. Very recently in 2017 H. Shen et al. [48] has obtained remarkable achievement by determining the crystal structure of eukaryotic sodium channel(Na_vPaS) from American cockroach *Periplaneta americana* which further enhanced our understanding of how eukaryotic sodium channels function at the molecular level.

B. Inactivation of sodium channel: Inactivation is a very important phenomena of sodium channel, it blocks the pore and stops the sodium ions to come inside the cell when the cell is depolarized enough to prevent persistent current and associated troubles such as Long QT-syndrome, hyper excitability, malfunctioning of pacemaker activity etc. The inactivation process of sodium channel has been a very major topic of investigation for sodium channel. Aldrich et al. in 1983 [49] found that voltage-dependent inactivation of Na^+ channels is a consequence of voltage-dependent activation and inactivation is characterized by two distinguishable kinetic components: fast inactivation and a slow inactivation. Stuhmer et al.,1989 [50], Kellenberger et al., 1996 [51], Catterall, 2000 [52] found that hydrophobic triplet (IFMT : Isoleucine, Phenylalanine, Methionine and Threonine) residue works as a latch by blocking the channel pore which plays crucial role for fast inactivation. It holds the fast inactivation gate shut. Contrary to fast inactivation process, Vassilev et al., 1989 [53], Balsler et al., 1996 [54], Vilin et al., 1999 [55] showed that slow inactivation of Na channels is a current-dependent process which resembles C-type inactivation of potassium channels [56,57].

C. Activation, Inactivation and Recovery Path of sodium channel: The protein conformational changes through which sodium channel activates from resting state to ion conducting open state and then inactivates is called open state inactivation path. However, there are ample evidences of another type of inactivation called closed state inactivation where sodium channel could inactivate even without ever being open. In this situation conformational changes of protein is not associated to the pore opening, inactivation occurs from some closed conformation. Inactivation path of sodium ion channel had been a major research interest. Although the original studies by Hodgkin and Huxley, 1952 [8] suggested closed state inactivation(CSI) in sodium channels but first convincing

quantitative evidence for inactivation occurring from pre-open closed states came from investigation done by Bean, 1981 [58] on the Na_v channel in crayfish giant axon by using prepulse protocol. Later Horn et al., 1981 [59], Horn and Vandenberg, 1984 [28], Aldrich and Stevens, 1983 [49], Patlak, 1991 [30], Kuo and Bean, 1994 [31], Armstrong, 2006 [60], Bahring and Covarrubias, 2011 [61] using theoretical, experimental and computation models proved that along with OSI(open state inactivation, after pore opening), CSI(closed state inactivation) is also a prominent inactivation path. Patlak, 1991 [30], Kuo and Bean, 1994 [31] also predicted the recovery from inactivation occurs via CSI path.

D. Toxicology and Channelopathy: The drug binding study of sodium ion channel is probably the most investigated topic of research. Proper functioning of sodium channels regulate most of our physiological processes. A slight malfunctioning in any part of the channel protein, such as improper timing of inactivation etc and other problems occurring due to mutations and inherited disorders can cause chronic ailment, some times proved to be life threatening. The pain killers or the anesthetic drugs basically binds to the ion conducting open state of the channel, thus called open state blockers, block the pore and stops action potential generation process and temporarily desensitize the pain in desired location. Some of these drugs bind to the inactivated conformational state of sodium channels are called inactive state blockers which prevent the sodium channels from reopening to create action potential again. Mutations in sodium channels cause inherited forms of epilepsy. Various sodium channel blockers along with other classes of drugs are used in therapy of epilepsy. Studies with neurotoxins or ion channel blockers like tetrodotoxin (TTX) and saxitoxin (STX) also contributed largely to our today's understanding of the structure and function of sodium channel. Actions of neurotoxins gave us the initial valuable lead in the development of drugs for the diseases in which ion channels are involved. TTX played a great part in the discovery of the voltage gated sodium channel protein [62] and in the determination of the selectivity filter [63] and binding site for pore blockers [64]. Inherited disorders (sodium 'channelopathies') caused due to mutations in genes affects skeletal muscle contraction, cardiac rhythm, or neuronal function. Severity of these diseases range from mild or latent disease to life-threatening or incapacitating conditions. Most sodium channelopathies are dominantly inherited, but some are transmitted by recessive inheritance or appear sporadic. The mechanism of selective blocking of the sodium channel was shown definitively in 1964 by Toshio Narahashi and John W. Moore [65] using the sucrose gap voltage clamp technique. From that first understanding of TTX blocking at 1964, upto the present knowledge of sodium

channel drugs have been a very vast, complicated, rigorous journey which has mostly developed for pharmacological interests [66–71].

E. Markovian modeling of sodium ion channel: From Neher and Sakmann’s landmark work of single-channel study on Nav channels in the late 1970s and 1980, Vandenberg and Horn, 1984 [28] introduced the idea of using statistical methods such as maximum likelihood analysis to rigorously discriminate between different kinetic models by direct fitting single-channel records. Aldrich and Stevens, 1983 [49] and Vandenberg and Horn, 1984 [28] showed that a simple model of Na_v channel gating requires both open- and closed-state inactivation. Later in 1991, Vandenberg and Bezanilla, 1991 [29] provided a nine state model of sodium channel which was until then one of the best model which reproduced the macroscopic currents so efficiently. Today there are so many Markov models available for different types of sodium channels. Such as Clancy-Rudy Model, 1999-2002 [33–35] of cardiac $\text{Na}_v1.5$ channel is a very efficient markov model which fits experimental data with high degree of accuracy and widely being utilized for pharmacological studies.

F. Nonequilibrium Response Spectroscopy: Recently, Millonas et al., 1998 [32] have invented the non-equilibrium response spectroscopy(NRS) to study the ion channels in nonequilibrium situation [72]. Following Millonas et al.’s [32] work Kargol et al., 2002 extended the NRS protocol by using continuously oscillating [73] or fluctuating voltage [74,75] protocol which drives the ion channel far from equilibrium and make it possible to study the ion channel kinetics at the non-equilibrium condition providing various information regarding kinetic and nonequilibrium thermodynamic response properties such as dynamical hysteresis at non-equilibrium steady state(NESS) [76,77]. Pulsed train protocol [78–80] is also a very powerful NRS protocol which is being widely utilized now a days. NRS techniques provide new aspects of ion channel gating kinetics that standard stepped-potential protocols can not provide [75].

1.1 Scope of Thesis

The scope of research in sodium ion channel even just in neuroscience is huge. So here we limit ourself in some specific areas in mainly functional and dynamical aspects of sodium ion channel in isolated patches to whole cell activities. Researches done on sodium channels are mostly experimental in nature which gives an opportunity for theoretical

investigations too. Sodium channel research involves almost all the main stream science fields such as chemistry, physics, neuroscience, electrophysiology, computer science etc. In this thesis we have addressed certain things which were left unexplored previously to our knowledge.

The nonequilibrium dynamical study of sodium channel was almost entirely overlook since the time of Hodgkin and Huxley, until recently Millonas et al. in 1998 introduced Nonequilibrium Response Spectroscopy to study on channels in nonequilibrium environment. The nonequilibrium response properties of sodium channel was not explored earlier. Also the recent development of nonequilibrium thermodynamic quantities like entropy production rates has never been used to study sodium channel earlier. Although dynamic hysteresis arising due to the oscillating voltage has been investigated in mainly Hodgkin-Huxley model, but the explicit sodium channel model in the context of gating has not been used, which gives more realistic results, to study dynamic hysteresis. The nonequilibrium thermodynamics of dynamic hysteresis has not been studied for sodium channel which could provide the energetic information of various gating processes in nonequilibrium situation.

The path of activation, inactivation and recovery have been widely investigated in sodium channel. These studies have been done mostly using constant voltage clamp or patch clamp techniques. But in presence of NRS protocols such as oscillating voltage and pulsed train (these protocols mimic the real system voltage variation in membrane) and in presence of nonequilibrium situation how these paths get modified have never been investigated earlier. Also the entropic cost associated with these paths have never been addressed.

Sodium ion channel research due to its clinical importance is still a very hot topic of research. The complete understanding of the mechanism of blocking by drugs are still not clearly understood. As drug binding kinetics are very much affected by the various types of channel mutations, biological environment and also similar drugs show different binding kinetics in different systems, it was difficult to comprehend drug binding interactions in a general framework. Thus generalization of drug binding kinetics from single channel realization using theoretical approach was required. There are mainly two types of drug binding mechanisms, such as, open state blocker and closed state blocker. Previously these two blocking mechanisms has rarely been inspected separately using mathematical models with proper theoretical background. Also how drug binding kinetics can be estimated through NRS techniques or at nonequilibrium situation has never been investigated in details.

For complete understanding of drug binding mechanism in single sodium channel model one needs to obtain the kinetic and thermodynamic pictures of sodium channel blocking. Thus one can grasp the effect of blockers on sodium channels only but can not give the complete picture of the whole neuron being affected. Thus one needs to see how the drug binding kinetics affect the action potential of a neuron. Along with the sodium channel blockers one can also investigate the potassium blockers to find the complete understanding of the action potential.

As soon as one gets the idea of how the sodium and potassium channel blockers affect the action potential in a single neuron, the most obvious question that arrives in one's mind is how will the drugs affect the slave neuron that is connected to a master neuron: the first step to signal transduction. How the synchronization process gets hampered in presence of drugs has not been investigated earlier. It is also important to study the metabolic energy consumption of sodium and potassium ion channels and how the channel numbers affect the synchronization process.

In the proposed thesis named “**Nonequilibrium Features Of Voltage Gated Sodium Ion Channel**” the research work done by us is summarized as follows:

A. Nonequilibrium response and dynamic hysteresis: We have investigated the dynamic as well as the non-equilibrium thermodynamic response properties of voltage-gated Na-ion channel. Using sinusoidally oscillating external voltage protocol we have both kinetically and energetically shown the non-equilibrium steady state properties of dynamic hysteresis in details. Here we have introduced a method of estimating the work done associated with the dynamic memory due to a cycle of oscillating voltage. We have quantitatively characterized the loop area of ionic current which gives information about the work done to sustain the dynamic memory only for ion conduction, while the loop area of total entropy production rate gives the estimate of work done for overall gating dynamics. We have found that the maximum dynamic memory of Na-channel not only depends on the frequency and amplitude but it also depends sensitively on the mean of the oscillating voltage. We have shown how the system optimize the dynamic memory itself in the biophysical range of field parameters. Our study shows that the relation between the average ionic current with increasing frequency corresponds to the nature of the average dissipative work done at steady state. One of the important understanding of this work is that the utilization of the energy from the external field can not be directly obtained from the measurement of ionic current only but it also requires the study of nonequilibrium thermodynamics.

B. Inactivation path and recovery: Next we have studied the inactivation path of voltage gated sodium channel under various voltage protocols. These voltage protocols actually serve as nonequilibrium response spectroscopic tools to study the ion channel in nonequilibrium environment. In contrast to a lot of effort in finding the crystal structure based molecular mechanism of closed-state(CSI) and open-state inactivation(OSI), our approach is to understand the dynamical characterization of inactivation. The kinetic flux as well as energetic contribution of the closed and open-state inactivation path is compared here for voltage protocols, namely constant, pulsed and oscillating. The nonequilibrium thermodynamic quantities we have used in response to these voltage protocols serve as improved characterization tools for theoretical understanding which not only agrees with the previously known kinetic measurements but also predict the energetically optimum processes to sustain the auto-regulatory mechanism of action potential. We have found that the time dependent voltage pattern governs the population of the conformational states which when couples with characteristic rate parameters, the CSI and OSI selectivity arise dynamically to control the inactivation path. Using constant, pulsed and continuous oscillating voltage protocols we have shown that during depolarization the OSI path is more favoured path of inactivation however, in the hyper-polarised situation the CSI is favoured. It is also shown that the re-factorization of inactivated sodium channel to resting state occurs via CSI path. Here we have shown how the subtle energetic and entropic cost due to the change in the depolarization magnitude determines the optimum path of inactivation.

C. Open state vs. inactive state sodium channel blockers: The kinetics and nonequilibrium thermodynamics of open state and inactive state drug binding mechanisms have been studied here using different voltage protocols in sodium ion channel. We have found that for constant voltage protocol, open state block is more efficient in blocking ionic current than inactive state block. Kinetic effect comes through peak current for mexiletine as an open state blocker and in the tail part for lidocaine as an inactive state blocker. Although the inactivation of sodium channel is a free energy driven process, however, the two different kinds of drug affect the inactivation process in a different way as seen from thermodynamic analysis. In presence of open state drug block, the process initially for a long time remains entropy driven and then becomes free energy driven. However in presence of inactive state blocking, the process remains entirely entropy driven until the equilibrium is attained. For oscillating voltage protocol, the inactive state blocking is more efficient in damping the oscillation of ionic current. From the pulse train analysis it is found that inactive state blocking is less effective in restoring normal repolarisation and blocks peak ionic current. Pulse train protocol also shows that all the inactive states

behave differently as one inactive state responds instantly to the test pulse in an opposite manner from the other two states.

D. Effect of blockers on action potential: Next we switched from single channel study to the whole neuron. We have utilized the site selective drug blocking mechanism of the single sodium and potassium channel to explore the overall action potential. We made a simple but effective modification of the existing Hodgkin-Huxley model by adding drug bound state to study the effect of sodium and potassium blockers on the action potential and ionic currents, using Gillespie's exact Markovian simulation. Our approach provides more realistic picture of drug binding which keeps track each states in real time and enables one to see how gradually the entire population is shifting to the drug bound state. Also we have shown an interesting dependence of sodium and potassium currents on each other in presence of drugs. In presence of sodium blocker the action potential falls off exponentially, but in potassium channel with increasing drug affinity initially a noise induced enhancement of spiking activity of action potential is observed which gradually falls off with increasing drug affinity.

E. Effect of patch size on synchronization between neurons: Finally we have shown the kinetics and energetics of unidirectional synchronization between two coupled neurons. We begin with studying the single neuron kinetics and metabolic energy consumption. Then we have introduced the channel noise or the patch size in the individual neurons of the coupled system. We have found that the size of patch has very important role in unidirectional synchronization and metabolic energy consumption. We have found that there exist three different patch size ranges in which coupled neuron system behaves differently. We have also studied the effect of three types of channel blockers such as sodium, potassium and total blockers and found that they have very interesting and distinct effect on synchronization process and metabolic energy consumption.

Schematic Summary of Thesis

From sodium channel to single neuron and then to two coupled neurons we have covered a broad spectrum of sodium channel research. The entire work in the thesis can be schematically presented as follows.

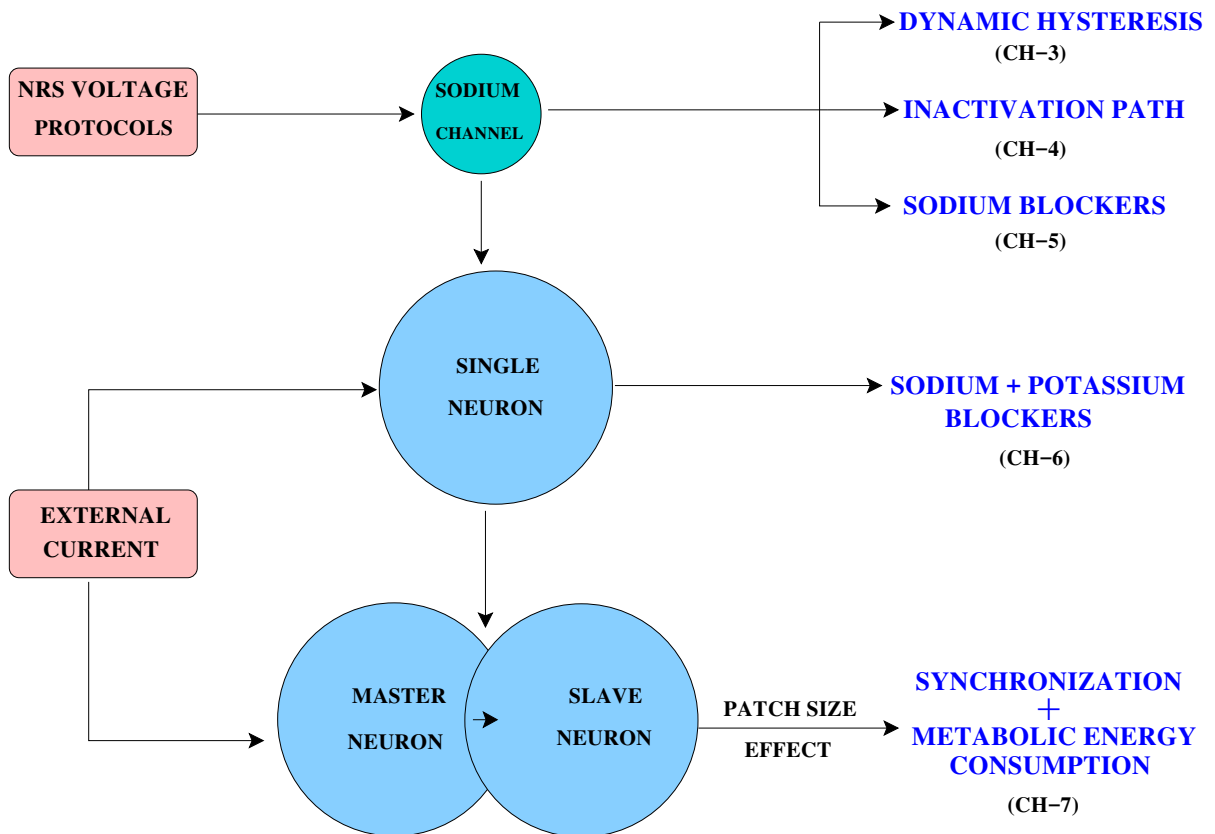


Figure 1.1: Schematic diagram of the thesis works.

1.2 Plan of Thesis

We have presented the contents of the thesis in the following chapters.

1. In **Chapter 2** we have presented the background literature and theory involved.
2. In **Chapter 3**, using oscillating external voltage protocol the nonequilibrium response and dynamical hysteresis of sodium channel and the utilization of energy and associated dissipative work done at nonequilibrium steady state is also investigated.
3. In **Chapter 4**, closed-state-inactivation and open-state-inactivation path is compared using nonequilibrium response spectroscopic tools and the energetically optimum processes or the favoring path of inactivation has been explored here.
4. In **Chapter 5**, the kinetics and time dependent thermodynamic differences of open-state blockers and inactive state blockers have been studied here. Comparing various voltage protocols the more potent blocker is investigated.
5. In **Chapter 6**, considering sodium and potassium channel blockers in single channel model a more realistic picture of drug affected spiking activity of action potential and ionic currents for multiple channels has been studied using Gillespie's exact simulation technique.
6. In **Chapter 7** we have discussed the effect of patch size on the energetics and synchronization between two neurons and how the synchronization process is affected by channel blockers.

Bibliography

- [1] Hille, B., Ionic channels of excitable membranes. 2nd edition, Sinauer Associates, Sunderland, Mass (1992).
- [2] Cole, KS. and Curtis, H.J. Electric Impedance of the Squid Giant Axon during Activity. *J Gen Physiol.*, 22, 649 (1939).
- [3] Cole, KS. Some physical aspects of bioelectric phenomena, *Proc. Natl. Acad. Sci. USA*, 35, 558 (1949).
- [4] Curtis, HJ. and Cole, K.S. Transverse Electric Impedance of the Squid Giant Axon. *J Gen Physiol* 21, 757 (1938).
- [5] Hodgkin AL. Evidence for electrical transmission in nerve Part I. *J Physiol.* 90, 183 (1937);; Hodgkin AL. Evidence for electrical transmission in nerve Part II. *J. Physiol*, 90, 211 (1937);; A. Huxley, From overshoot to voltage clamp, *Trends in Neurosciences*, 25, 553 (2002).
- [6] Hodgkin, AL. and Katz, B. The effect of sodium ions on the electrical activity of giant axon of the squid. *J. Physiol.*, 108, 37 (1949).
- [7] Hodgkin, AL., Huxley, AF. and Katz, B. Measurement of current-voltage relations in the membrane of the giant axon of *Loligo*. *J. Physiol.*, 116, 424 (1952).
- [8] Hodgkin, AL., Huxley, AF. and Katz, B. Measurement of current-voltage relations in the membrane of the giant axon of *Loligo*. *J. Physiol.* 116, 424 (1952);; Hodgkin, AL. and Huxley, AF. The components of membrane conductance in the giant axon of *Loligo*. *J. Physiol.*, 116, 473 (1952);; Hodgkin, AL. and Huxley, AF. Currents carried by sodium and potassium ions through the membrane of the giant axon of *Loligo*. *J. Physiol.*, 116, 449 (1952);; Hodgkin, AL. and Huxley, AF. The dual effect of membrane potential on sodium conductance in the giant axon of *Loligo*. *J.. Physiol.* 116, 497 (1952);; Hodgkin, AL. and Huxley, AF. A quantitative description of membrane current and its application to conduction and excitation in nerve. *J. Physiol.* 117, 500 (1952).
- [9] Rothenberg, MA. Studies on permeability in relation to nerve function, ionic movements across exonal membranes. *Biochim. Biophys. Acta.*, 4, 96 (1950).

-
- [10] Keynes, RD. The ionic movements during nervous activity, *J. Physiol.*, 114, 119 (1951).
- [11] Sakmann, B. and Neher, E. . Patch clamp techniques for studying ionic channels in excitable membranes, *Annual Review of Physiology*, 46: 455 (1984).
- [12] Nossal, R. and Lecar, H. *Molecular and cell Biophysics*, Addison- Wesley, Redwood City, CA (1991).
- [13] Skaugen, E. and L. Walloe, *Physiol. Scand.*, 107, 343 (1979).
- [14] Strassberg, A. and De Felice, LJ. . Limitations of the Hodgkin-Huxley formalism: effects of single channel kinetics on transmembrane voltage dynamics. *Neural Computation*. 5, 843 (1993).
- [15] De Felice, LJ. and Goolsby, WN. Order from randomness: spontaneous firing from stochastic properties of ion channels. In *Fluctuations and Order: The New Synthesis*. M. Millonas, editor. Springer, New York. 331 (1996).
- [16] Chow, CC. and White, JA. Spontaneous action potentials due to channel fluctuations. *Biophys. J.*, 71, 3013 (1996).
- [17] Skaugen, E. Firing behaviour in stochastic nerve membrane models with different pore densities, *Acta. Physiol. Scand.* , 108, 49 (1980).
- [18] Fox, RF. Stochastic versions of the Hodgkin-Huxley equations. *Biophys. J.* , 72, pp. 2069 (1997).
- [19] Fox, RF. and Lu, Y. Emergent collective behavior in large numbers of globally coupled independently stochastic ion channels, *Phys. Rev. E* 49 , 3421 (1994).
- [20] Zagotta, WN., Hoshi, T. and Aldrich, RW., *J. Gen. Physiol.*, 103, 321 (1994).
- [21] Armstrong, CM. Interaction of Tetraethylammonium Ion Derivatives with the Potassium Channels of Giant Axons, *J. Gen. Physiol.*, 58, 413 (1971).
- [22] Armstrong, CM. and Bezanilla, F. Inactivation of the sodium channel. II. Gating current experiments., *J. Gen. Physiol.*, 70, 567 (1977).
- [23] Keener, J. and Sneyd, J., *Mathematical Physiology: I: Cellular Physiology*, Springer, NY, USA (2009).
- [24] Fink M. and Noble D., Markov models for ion channels: versatility versus identifiability and speed, *Phil. Trans. R. Soc. A* , 367, 2161 (2009).
- [25] <https://www.nobelprize.org>.
- [26] MacKinnon, R., Cohen, SL., Kuo, A., Lee, A., Chait, BT. Structural conservation in prokaryotic and eukaryotic potassium channels, *Science*, 280, 106 (1998).
- [27] Doyle, DA., Cabral, J., Pfuetzner, MRA., Kuo, A., Gulbis, JM., Cohen, SL., Chait, BT., MacKinnon, R., *The Structure of the Potassium Channel: Molecular Basis of K⁺ Conduction and Selectivity*, *Science*, 280, 69 (1998).

- [28] Horn, R. and Vandenberg, CA. Statistical properties of single sodium channels, *J. Gen. Physiol.*, 84, 505 (1984).
- [29] Vandenberg, C. A. and Bezanilla, FA sodium channel gating model based on single channel, macroscopic ionic, and gating currents in the squid giant axon, *Biophys. J.*, 60, 1511 (1991).
- [30] Patlak, J. Molecular kinetics of voltage-dependent Na⁺ channels, *Physiol. Rev.*, 71, 1047 (1991).
- [31] Kuo, CC. and Bean, BP. Na⁺ channels must deactivate to recover from inactivation, *Neuron*, 12, 819 (1994).
- [32] Millonas, MM. and Hanck, DA. Nonequilibrium response spectroscopy of voltage-sensitive ion channel gating, *Biophys. J.*, 74, 210 (1998).
- [33] Clancy, CE. and Rudy, Y. Linking a genetic defect to its cellular phenotype in a cardiac arrhythmia, *Nature*, 400, 566 (1999).
- [34] Clancy, CE. and Rudy, Y. Na⁺ channel mutation that causes both Brugada and Long-QT Syndrome phenotypes: A simulation study of mechanism, *Circulation*, 105, 1208 (2002).
- [35] Clancy, CE., Zhu, ZI. and Rudy, Y. Pharmacogenetics and anti-arrhythmic drug therapy: a theoretical investigation, *Am. J. Physiol. Heart. Circ. Physiol.*, 292, H66 (2007).
- [36] Ashcroft, FM. From molecule to malady. *Nature*, 440, 440 (2006).
- [37] Catterall, WA. From ionic currents to molecular mechanisms: the structure and function of voltage-gated sodium channels. *Neuron*, 26, 13 (2000).
- [38] Andavan GSB. and Lemmens-Gruber, R., Voltage-Gated Sodium Channels: Mutations, Channelopathies and Targets, *Current Medicinal Chemistry*, 18, 377 (2011).
- [39] Wickenden, A. , Priest, B. and Erdemli, G., Ion channel drug discovery: challenges and future directions, *Future Med. Chem.*, 4(5), 661 (2012).
- [40] Beneski, DA., and Catterall, WA. Covalent labeling of protein components of the sodium channel with a photoactivable derivative of scorpion toxin. *Proc. Natl. Acad. Sci. USA*. 77:639 (1980).
- [41] Hartshorne, R. P. and Catterall, WA. Purification of the saxitoxin receptor of the sodium channel from rat brain. *Proc. Natl. Acad. Sci. U.S.A.*, 78, 4620 (1981).; Hartshorne, RP., Messner, DJ., Coppersmith, JC. and Catterall, WA. The saxitoxin receptor of the sodium channel from rat brain. Evidence for two nonidentical β subunits. *J. Biol. Chem.* , 257, 13888 (1982).
- [42] Payandeh, J., Scheuer, T., Zheng, N., Catterall, WA. The crystal structure of a voltage-gated sodium channel. *Nature*, 475 (7356), 353 (2011).

- [43] Payandeh, J., Gamal, TM., Scheuer, T., Zheng, N. and Catterall, WA. Crystal structure of a voltage-gated sodium channel in two potentially inactivated states. *Nature* 2012, 486 , 135 (7401).
- [44] Zhang, X., Ren, W., DeCaen, P., Yan, C., Tao, X., Tang, L., Wang, J., Hasegawa, K., Kumasaka, T., He, J., Wang, J., Clapham, DE. and Yan, N. Crystal structure of an orthologue of the NaChBac voltage-gated sodium channel. *Nature* , 486 (7401), 130 (2012).
- [45] McCusker, EC., Bagneris, C., Naylor, CE., Cole, AR., D'Avanzo, N., Nichols, CG., Wallace, BA. Structure of a bacterial voltage-gated sodium channel pore reveals mechanisms of opening and closing. *Nature Commun.*, 3, 1102 (2012).
- [46] Catterall, WA. Structure and function of voltage-gated sodium channels at atomic resolution. *Exp. Physiol.*, 99, 35 (2014).
- [47] Bagneris, C., DeCaen, PG., Naylor, CE., Pryde, DC., Nobeli, I., Clapham, DE., Wallace, BA. Prokaryotic Na^vMs channel as a structural and functional model for eukaryotic sodium channel antagonism. *Proc. Natl. Acad. Sci. U.S.A.*, 111, 8428 (2014); Bagneris, C., DeCaen, PG., Hall, BA., Naylor, C. E., Clapham, DE., Kay, CWM. and Wallace, BA. Role of the C-terminal domain in the structure and function of tetrameric sodium channels. *Nature Commun.*, 4, 3465 (2013).
- [48] Shen, H., Zhou, Q., Pan, X., Li, Z., Wu, J. and Yan, N. Structure of a eukaryotic voltage-gated sodium channel at near atomic resolution, H. Shen et al., *Science* 10.1126/science.aal4326 (2017).
- [49] Aldrich, R.W., Corey, D.P. and Stevens, C. F. A reinterpretation of mammalian sodium channel gating based on single channel recording. *Nature*, 306, 436-441 (1983).
- [50] Stuhmer, W., Conti, F., Suzuki, H., Wang, X., Noda, M., Yahagi, N., Kubo, H. and Numa, S. . Structural parts involved in activation and inactivation of the sodium channel. *Nature*, 339, 597 (1989).
- [51] Kellenberger, S., Scheuer, T. and Catterall, WA. Movement of the Na⁺ channel inactivation gate during inactivation. *J. Biol. Chem.*, 271, 30971 (1996).
- [52] Catterall, WA. From ionic currents to molecular mechanisms: the structure and function of voltage-gated sodium channels. *Neuron*. 26, 13 (2000).
- [53] Vassilev, P., Scheuer, T. and Catterall, WA. Inhibition of inactivation of single sodium channels by a site- directed antibody. *Proc. Natl. Acad. Sci. USA*. 86:8147 (1989).
- [54] Balser, JR., Nuss, HB., Chiamvimonva, N., Perez-Garcia, MT., Marban, E. and Tomaselli, GF. External pore residue mediates slow inactivation in mu 1 rat skeletal muscle sodium channels. *J. Physiol*. 494, 431 (1996).

- [55] Vilin, YY., Makita, N., George, AL. Jr. and Ruben, PC. Structural determinants of slow inactivation in human cardiac and skeletal muscle sodium channels. *Biophys. J.*, 77, 1384 (1999).
- [56] Liu, Y., Jurman, ME. and Yellen, G. Dynamic rearrangement of the outer mouth of a K^+ channel during gating. *Neuron*. 16, 859 (1996).
- [57] Ulbricht, W. Sodium Channel Inactivation: Molecular Determinants and Modulation, *Physiol. Rev.*, 85, 1271 (2005).
- [58] Bean, BP. Sodium channel inactivation in the crayfish giant axon. Must channels open before inactivating? *Biophys. J.* 35, 595 (1981).
- [59] Horn, R., Patlak, J. and Stevens, CF. Sodium channels need not open before they inactivate. *Nature* 291, 426 (1981).
- [60] Armstrong, CM. Na channel inactivation from open and closed states. *Proc. Natl. Acad. Sci. USA*, 103, 17991 (2006).
- [61] Bähring, R. and Covarrubias, M. Mechanisms of closed-state inactivation in voltage-gated ion channels, *J. Physiol.* 589, 461 (2011).
- [62] Agnew, WS., Moore, AC., Levinson, SR. and Raftery, MA. . Identification of a large molecular weight peptide associated with a tetrodotoxin binding protein from the electroplax of *Electrophorus electricus*. *Biochem. Biophys. Res. Commun.* 92, 860 (1980).
- [63] Heinemann, SH., Terlau, H., Stuhmer, W., Imoto, K., and Numa, S.. Calcium channel characteristics conferred on the sodium channel by single mutations. *Nature* 356, 441 (1992).
- [64] Noda, M., Suzuki H., Numa, S. and Stuhmer, W. A single point mutation confers tetrodotoxin and saxitoxin insensitivity on the sodium channel II. *FEBS Lett.* 259, 213 (1989).
- [65] Narahashi, T., Moore J. W. and Scott. W. R. Tetrodotoxin Blockage of Sodium Conductance Increase in Lobster Giant Axons, *The Journal of General Physiology*, 47, 965, (1964).
- [66] Alfred L. and George Jr. Inherited disorders of voltage-gated sodium channels, *J. Clin. Invest.* 115, 1990 (2005).
- [67] Andavan GSB. and Lemmens-Gruber R. Voltage-Gated Sodium Channels: Mutations, Channelopathies and Targets, *Current Medicinal Chemistry*, 18, 377 (2011).
- [68] Catterall, W. A. Sodium Channels, Inherited Epilepsy, and Antiepileptic Drugs, *Annu. Rev. Pharmacol. Toxicol.*, 54,317 (2014).
- [69] Catterall, W. A., Goldin, A. L. and Waxman, S. G. International Union of Pharmacology. XLVII. Nomenclature and Structure-Function Relationships of Voltage-Gated Sodium Channels, *Pharmacol. Rev.* 57, 397 (2005).

- [70] Scholz, A. Mechanisms of (local) anaesthetics on voltage-gated sodium and other ion channels, *British Journal of Anaesthesia*. 89, 52 (2002).
- [71] Ahern, CA., Payandeh, J., Bosmans, F. and Chanda, B. The hitchhiker's guide to the voltage-gated sodium channel galaxy, *J. Gen. Physiol.*, 147, 1 (2015).
- [72] Groot, SRDe. and Mazur, P. *Non-equilibrium Thermodynamics*, North-Holland Publ. Comp., Amsterdam (1951).
- [73] Kargol, A. , Hosein-Sooklal, A. and Constantin, L. and M. Przystalski , Application of oscillating potentials to the Shaker potassium channel., *Gen. Physiol. Biophys.*,23, 53 (2004).
- [74] A. Hosein-Sooklal and A. Kargol , Wavelet Analysis of Nonequilibrium Ionic Currents in Human Heart Sodium Channel (hH1a), *J Membr. Biol.*, **188**, 199 (2002).
- [75] Kargol, A., Smithz, Z. Millonas, MM. Applications of nonequilibrium response spectroscopy to the study of channel gating. Experimental design and optimization, *J. theor. Biol.*, 218, 239 (2002).
- [76] Das, B., Banerjee, K. and Gangopadhyay, G. Entropy hysteresis and nonequilibrium thermodynamic efficiency of ion conduction in a voltage-gated potassium ion channel, *Phys. Rev. E*, 86, 061915 (2012).
- [77] Pal K., Das, B. and Gangopadhyay G., Nonequilibrium response of a voltage gated sodium ion channel and biophysical characterization of dynamic hysteresis, *Journal of Theoretical Biology* , 415, pp. 113 (2017).
- [78] Stramer, CF and Grant, A. O. Phasic ion channel blockade, kinetic model and parameter estimation procedure. *Mol, Pharmacol.*, 28, 348 (2001).
- [79] Vilin, YY., Ruben, PC. Slow inactivation in voltage-gated sodium channels, molecular substrates and contributions to channelopathies. *Cell Biochem Biophys*, 35,171 (2001).
- [80] Pal, K. Gangopadhyay G. Probing kinetic drug binding mechanism in voltage-gated sodium ion channel: open state versus inactive state blockers. *Channels* , 9, 307 (2015).

Chapter 2

Chapter 2

Topical Review: Background Theory & Literature Survey

In this chapter we provide a brief survey of literature and the theoretical backgrounds of the works done in the thesis. We begin from the understanding of the nerve cell and its membrane structure. Then gradually we proceed to discuss how the cells communicate to each other using action potential. Then we go deep into voltage gated sodium channel which is our interest of the thesis. From structural and functional understanding we discuss the process of inactivation and its path, an important property of sodium channel, investigated intensively in past. Then we study the pathological importance of sodium channel. After that we have discussed the recent developments in non-equilibrium thermodynamics and dynamic hysteresis in ion channels. The chapter finally ends with discussing theoretical background of neuronal synchronization.

2.1 Membrane Potential: Neuron

There are many different types of neurons in the mammalian central nervous system. Due to the diverse functions performed by neurons in different parts of nervous system, neurons have wide variety in shape, size, and electrochemical properties. Generally neurons have four functionally important zones: (a) dendritic tree (b) axon hillock, (c) axon (d) synapses. The cell membrane is the most important part of a nerve cell and it's a biological structure that separates the intracellular medium of a cell from the extracellular environment. It controls the movements of substances in and out of cells. Typical cell membrane consists of a protein-lipid-protein bilayer. Proteins orient themselves towards

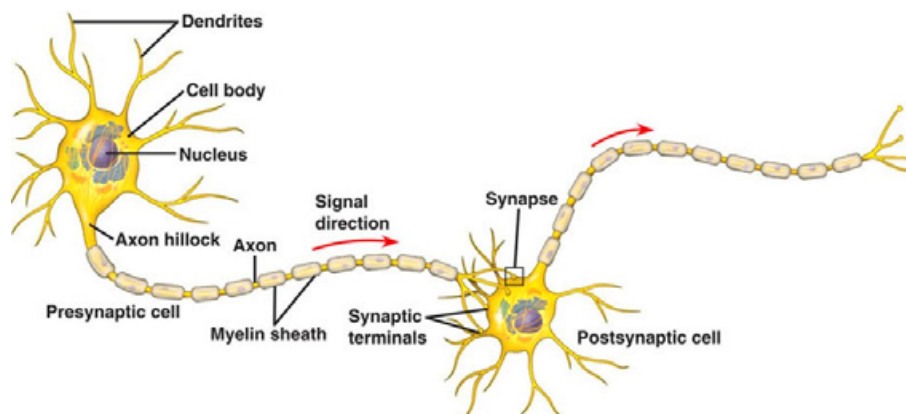


Figure 2.1: Two synaptically connected nerve cell. Source: Reference [1]

the extracellular and intracellular hydrophobic environment whereas the lipids are hydrophobic and they face interior side of the membrane. Proteins help the cell to exchange small polar or charged molecules or ions with the external environment, which otherwise can not cross the membrane because of the interior apolar region. Proteins in the membrane which allow passive diffusion of ions down the concentration gradients are called ion channel proteins and those which actively push ions across the membrane to establish those concentration gradients are called ion transporters or ion pumps. As the ions are present at different concentrations inside and outside the cell, such as $[K^+]_{out} < [K^+]_{in}$ and the opposite is true for Na^+ , Cl^- and Ca^{2+} ions and their movements due to chemical gradients or diffusion and electric field generates a membrane potential. Thus when an electrode is placed inside a cell and a reference electrode is kept in the extracellular fluid, a constant potential difference is observed. This potential difference is negative and of -40 to -80 mV in amplitude. One of the factors that control the excitability of the membrane is its resting potential, which is set by the ion fluxes through the membrane at its resting state. Quantitatively, each type of ions try to drive the membrane potential towards its own equilibrium potential at which the electric force and the chemical-gradient force for the particular ion are balanced such that there is no net flow of the ion (Nernst, 1893). The value of the membrane potential or equilibrium potential (only for one type of ion) at which the net flux of a single ion X is zero is called the reversal potential of ion X (E_X) is given by

$$E_X = \frac{RT}{z_X F} \ln \frac{[X]_{out}}{[X]_{in}}, \quad (2.1)$$

where $R = 8.314472 \text{ J mol}^{-1} \text{ K}^{-1}$ is the universal gas constant, $F = 96485 \text{ C mol}^{-1}$ is the Faraday constant, T is the absolute temperature in K, z_X is the valence of the ion, $[X]_{out}$ and $[X]_{in}$ are the concentrations of the ion X respectively outside and inside the cell in mol m^{-3} . Different types of ions drive the membrane potential towards different voltages.

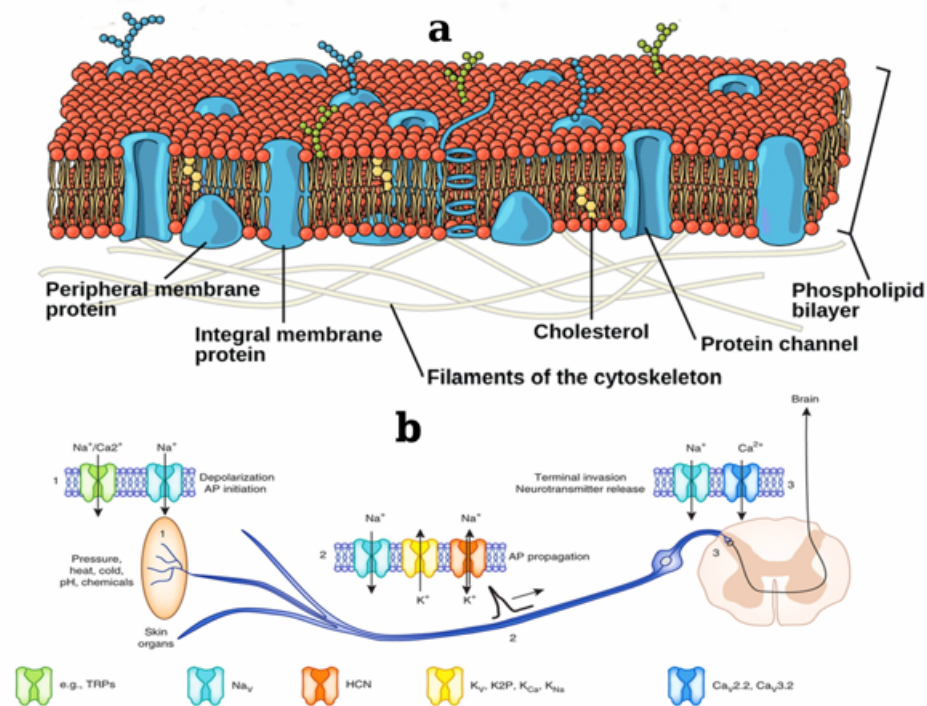


Figure 2.2: In figure (a) a typical membrane of a biological cell is shown. Source: Reference [2], slightly modified. In figure (b) The ion channels across the cell membrane are shown. Source: Reference article of Waxman et al. [3]. The protein channels or the ion channels are shown to have channel or pore which is connected on the both sides of the membrane.

The relative contribution of each ion in setting the membrane potential is weighed by its membrane conductance (in proportion to permeability), as determined by the Goldman-Hodgkin-Katz (GHK) voltage equation. As in neurons, membrane potentials are largely determined by $[Na^+]$, $[K^+]$ and $[Cl^-]$ ions due to their dominant concentrations and permeability through the membrane under physiological conditions. Thus GHK equation is given by

$$E_m = \frac{RT}{F} \ln \frac{P_{Na^+}[Na^+]_{out} + P_{K^+}[K^+]_{out} + P_{Cl^-}[Cl^-]_{in}}{P_{Na^+}[Na^+]_{in} + P_{K^+}[K^+]_{in} + P_{Cl^-}[Cl^-]_{out}} \quad (2.2)$$

where $[ion]_{out}$ and $[ion]_{in}$ are respectively the extracellular and intracellular concentrations of that ion in mol m^{-3} . P_{ion} is the membrane permeability for that ion expressed in ms^{-1} .

2.1.1 Circuit model of the membrane

While the membrane is an insulator, the cytoplasm and extracellular fluids are basically electrolytic solutions and thus they can conduct electricity. Due to the potential differ-

Ion	Internal(mM)	External(mM)	ReversalPot.(mV)
Na^+	49	440	59
K^+	410	22	0
Cl^-	40-100	560	-65
Ca^{2+}	0.0002	10	145

Table 2.1: Intracellular and extracellular concentrations of the ions and their respective reversal potentials for the squid axon.

ence across the membrane there exists unbalanced number of electric charges both inside and outside the cell. As the resting membrane potential is negative and there exist a surplus of negative charges inside the cell and a surplus of positive charges outside, these charges lay on the surface of the membrane. At this situation the phospholipidic bilayer can be represented as a capacitor. As membranes contains ion channels can be passed through charged ions, the electrical representation of the membrane must include resistors connected in parallel with to the capacitor. The conductance of the membrane depends on the number of individual ion channels and their conformational states such as closed, open or inactivated. Figure (2.3) shows the electrical model of the membrane: the three

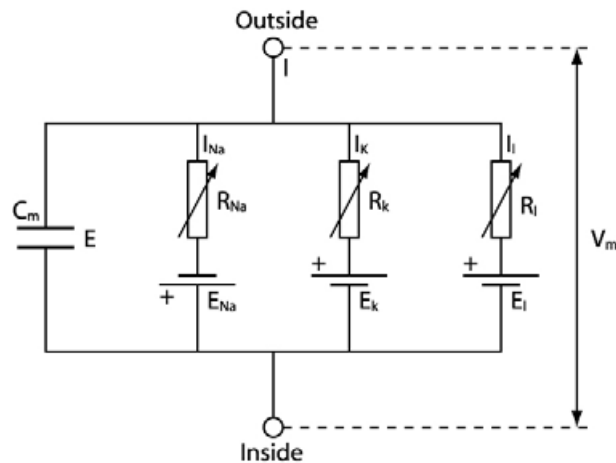


Figure 2.3: Circuit model of membrane.

conductances represent the permeability of the membrane to each particular type of ion, while the three batteries represent the voltage difference driving them, as given by (2.1). This voltage variation of the circuit is described by the first order differential equation

$$C_m \dot{V} = - \sum_{ion} I_{ion}, \quad (2.3)$$

where the individual ionic currents are given by

$$I_{ion} = G_{ion}(V - E_{ion}). \quad (2.4)$$

It is important to note that although the steady-state solution of equation (2.3) gives $I_{ion} = 0$, i.e. the sum of all the ionic currents is zero, but they are not individually (equation 2.4) zero.

2.1.2 Ion channels

Ion channels are integral part of the membrane proteins as shown in figure (2.2) with a aqueous central pore through the cell membrane [4] that allow ions selectively pass the membrane down their electrochemical gradient. These proteins, generally consisting of multiple subunits, together with their special voltage dependent conformation adaptability properties can make the pore closed, so that no ions can pass through or, they can make the pore open to help ions to pass through. Thus there exists mainly two functional conformations, one in which the pore is open (open state) and in the other the pore is closed (closed state). The ion channels have two common major properties: gating and selectivity. Gating is the conformational transition between open and closed state. Depending upon the stimulus dependent pore opening and closing, ion channels can be divided in voltage-gated (responds to the membrane voltage change), ligand-gated (conformation state of the protein changes when it binds to a specific ligand molecule), mechanosensitive (pressure-induced structural changes [5]), pH sensitive (such as KcsA potassium channel [6, 7] ion channels). The selectivity refers to the ability of the channel to recognize a particular ion and let it pass through the pore. Such as a sodium channel is only and only permeable to a sodium ion, not by similar sized potassium or calcium ions. Now it is found that the opening and closing of a voltage gated ion channel is a stochastic process their transition between these two states can be represented as a Markov process as shown in figure (2.4). The α and β in the figure represents the rate

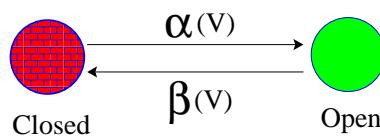


Figure 2.4: Simplest Markov model of ion channels

of voltage dependent transitions between the two states. The continuous macroscopic currents observed in whole-cell patch clamp recordings can be obtained by the ensemble average of a lot of on/off stochastic data of currents of single channels as shown in figure (2.4).

2.1.3 Communication between cells: Action potential

The excitable cells, such as nerve and muscle tissue communicate information to each other in the form of electrical impulse known as an action potential. The generation and propagation of this electrochemical impulse is a highly sophisticated, regulated and controlled process which involves very intelligent machines like ion channels. A slight dysfunction of any of these intricate mechanism can result in life threatening risk. Actually the dysregulation of action potentials are directly linked to variety of pathological conditions such as cardiac arrhythmias, weakness and paralysis of skeletal muscle, extreme pain, and epilepsy. During an action potential, the electrical membrane potential of a

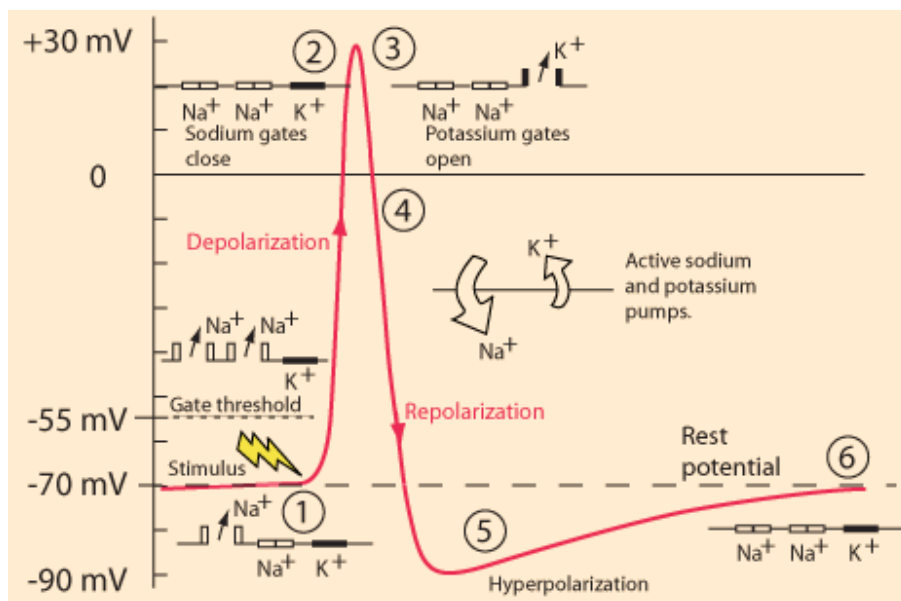


Figure 2.5: Action potential diagram. Source: Reference ([8]).

cell rises and then fall. The processes involved in the generation of action potential is discussed as follows.

(1) When a stimulus is received by dendrites, the Na^+ channels to open. There exist a threshold voltage, i.e -55 mV(generally) bellow which the sodium channels does not respond. But as soon as the stimulus reaches -55 mV all the sodium channels in the vicinity burst open. The action potential is an "All or None" phenomena. Either the depolarization is enough to burst open all the sodium channels or it does not at all.

(2) As the threshold voltage is reached, sodium channels open and more Na^+ ions come inside the cell and further depolarizes the interior part of the cell membrane up to around +30 mV. This process is called depolarization.

(3) As soon as the cell membrane inside the cell rises to +30 mV an important phenomena occurs. The sodium channels automatically inactivates and inhibits further influx of sodium ions inside the cell. At these situation the K^+ channels open and K^+ ions goes out of the cell and slowly repolarize the cell membrane back towards it rest potential.

(5) Actually the repolarization process overshoots the resting membrane potential(-70 mV) and it reaches upto about -90 mV. This process is called hyperpolarization. This hyperpolarization plays very important role for the transmission of information. Hyperpolarization prevents the neuron from receiving another stimulus at this phase by raising the threshold. Hyperpolarization also assures that the signal is proceeding towards one direction.

(6) After hyperpolarization, the Na^+/K^+ pump by throwing 3 Na^+ outside and bringing 2 K^+ ion inside, brings the membrane back to its resting potential at -70 mV. From inactivation to resting state is the re-factorization period or recovery phase of sodium channel. At this time sodium channel gets back to their original state. After that sodium channel is again ready for the next action potential generation. The whole process of action potential takes only a couple of milliseconds to complete.

The electrical signal once initiated by ion channel rapidly propagates along the surface of the cell due to the opening of other ion channels that are sensitive to the voltage change caused by the initial channel opening. Electrical signals travel much faster than chemical signals such as, it can travel the entire length of a human nerve cell as long as one meter of a distance within a few milliseconds.

The Hodgkin-Huxley model

Hodgkin and Huxley [9,10] determined that ionic conductance activate or inactivate according to the membrane voltage They used voltage-clamp technique to record the ionic currents at different voltages and concluded how these ionic currents dynamically gets modulated by voltage. They characterized the kinetics of voltage dependent fast sodium current, I_{Na} and delayed potassium rectifier, I_K , mediated by Na^+ and K^+ , respectively. They proposed a mathematical model that could reproduce the kinetic properties of voltage-dependence as well as could explain the generation of action potentials. The membrane equation for an isopotential compartment is given as,

$$C_m \frac{d}{dt} V(t) = -G_K(t)(V(t) - E_K) - G_{Na}(t)(V(t) - E_{Na}) - G_L(V(t) - E_L) \quad (2.5)$$

where C_m is the membrane capacitance, V is the membrane potential, G_K, G_{Na} and g_L are the membrane conductance for Na^+ , K^+ and leak currents, respectively. E_L, E_{Na} and E_K are their respective reversal potentials, which are given by the Nernst equation. The critical step in the Hodgkin-Huxley model is to calculate the dependence of the conductance $G_K(t)(V)$ and $G_{Na}(t)(V)$ on the membrane potential V . Hodgkin and Huxley proposed that ionic currents originate due to the presence of several independent gating particles which must occupy a specific position in the membrane to allow the Na^+ and K^+ ions to flow. The gating particles bear a net electronic charge such that the membrane potential can switch its position from the inside to the outside or vice-versa. The transition rates α and β between these two states are voltage dependent as shown in figure (2.4). If $x(=m,h,n)$ is defined as the fraction of particles inside the membrane and $(1 - x)$ as the fraction outside the membrane, one obtains the first-order kinetic equation:

$$\dot{x} = \alpha_x(V)(1 - x) - \beta_x(V)x, \quad x = n, m, h. \quad (2.6)$$

They assumed that the particles must occupy inside position to conduct ions and the conductance must be proportional to some function of x , such as,

$$G_K(t) = g_K^{max} n^4 \quad \text{and} \quad G_{Na}(t) = g_{Na}^{max} m^3 h, \quad (2.7)$$

where g_{Na}^{max} and g_K^{max} are the maximal values of the conductances when all gating particles are inside the membrane. \mathbf{m} , \mathbf{h} , \mathbf{n} represents the fraction of those gating particles inside. This equation accurately fit the voltage-clamp data of currents in squid giant axon. They interpreted that to flow through the membrane, Na^+ ions require the assembly of 3 gating particles of type \mathbf{m} and another of type \mathbf{h} , while an assembly of 4 gating particles of type \mathbf{n} is necessary for the flow of K^+ ions. These particles considered to be operating independent of each other, leading to the m^3h and n^4 forms.

Long after Hodgkin and Huxley, it was established that ionic currents are mediated by the opening and closing of individual ion channels. The gating particles were then reinterpreted as gates inside the pore of the channel. The reinterpretation of Hodgkin and Huxley's hypothesis was that the pore of the channel is controlled by four internal gates. These gates operate independently of each other. All the gates must open to conduct ions. Opening of the gates \mathbf{m} and \mathbf{n} in presence of depolarization is called activation. On the other hand, closing of the gate \mathbf{h} is called inactivation. Hodgkin and Huxley (1952) established that three identical activation gates (m^3) and a single inactivation gate (h)

Table 2.2: Parameters of Hodgkin-Huxley equation

C_m	Membrane capacitance	$1 \mu\text{F}/\text{cm}^2$
E_K	K^+ reversal potential	-12.0 mV
ρ_K	K^+ channel density	$18 \text{ channels}/\mu\text{m}^2$
g_K^{max}	Maximal K^+ channel conductance(all K^+ channels are open)	$36.0 \text{ mS}/\text{cm}^2$
γ_K	Single K^+ channel conductance	20 pS
E_{Na}	Na^+ reversal potential	115 mV
ρ_{Na}	Na^+ channel density	$60 \text{ channels}/\mu\text{m}^2$
g_{Na}^{max}	Maximal Na^+ channel conductance(all Na^+ channels are open)	$120.0 \text{ mS}/\text{cm}^2$
γ_{Na}	Single Na^+ channel conductance	20 pS
E_L	Leak reversal potential	10.613 mV
g_L	Leak conductance	$0.3 \text{ mS}/\text{cm}^2$

are necessary to explain the sodium current's characteristics. For potassium current four identical activation gates (n^4) are sufficient.

Thus the Hodgkin-Huxley equation represented together looks as follows,

$$C_m \frac{d}{dt} V(t) = -G_K(t)(V(t) - E_K) - G_{Na}(t)(V(t) - E_{Na}) - G_L(V(t) - E_L)$$

$$\dot{m} = \alpha_m(V)(1 - m) - \beta_m(V)m$$

$$\dot{n} = \alpha_n(V)(1 - n) - \beta_n(V)n$$

$$\dot{h} = \alpha_h(V)(1 - h) - \beta_h(V)h,$$

The rate constants were estimated by fitting empirical functions of voltage to the experimental data (Hodgkin and Huxley, 1952). These functions are as in the original paper as follows:

$$\alpha_m(V) = (0.1(V + 25))(\exp[(V + 25)/10] - 1)^{-1},$$

$$\beta_m(V) = 4 \exp[V/18],$$

$$\alpha_h(V) = 0.07 \exp[-V/20],$$

$$\beta_h(V) = 1 + \exp[(V + 30)/10]^{-1},$$

$$\alpha_n(V) = (0.01(V + 10))(\exp[-(V + 10)/10] - 1)^{-1},$$

$$\beta_n(V) = 0.125 \exp[V/80].$$

For every value of membrane potential V the ionic currents (I_i) sodium and potassium currents can be described by

$$I_{Na} = g_{Na}^{max} m^3 h (V - E_{Na}),$$

$$I_K = g_K^{max} n^4 (V - E_K),$$

and

$$I_L = g_L (V - E_L). \quad (2.8)$$

The total membrane current, $I_M I$ can be written as the summation of capacity current, I_C and ionic current, I_i as

$$I_M I = I_C + I_i, \quad (2.9)$$

where $I_C = C_m dV/dt$.

The propagation of action potential can be described by substituting the value of membrane current for unit length, $I_{MC} = \frac{a}{2r} \frac{\partial^2 V}{\partial x^2}$ in equation (2.9), where a is the radius of the nerve fiber, r is the specific resistance of the axoplasm, x is distance along the fiber and V is the membrane potential. Thus one can write

$$\frac{a}{2r} \frac{\partial^2 V}{\partial x^2} = C_m \frac{dV}{dt} + G_K(t)(V(t) - E_K) + G_{Na}(t)(V(t) - E_{Na}) + G_L(V(t) - E_L). \quad (2.10)$$

The above partial differential equation is not practicable to solve as it stands. During steady propagation, the curve of V against time at any one position is similar in shape to that of V against distance at any one time and it follows that

$$\frac{\partial^2 V}{\partial x^2} = \frac{1}{\theta^2} \frac{\partial^2 V}{\partial t^2},$$

where θ is the velocity of conduction. Therefore, equation (2.10) can be written as

$$\frac{a}{2r\theta^2} \frac{\partial^2 V}{\partial t^2} = C_m \frac{dV}{dt} + G_K(t)(V(t) - E_K) + G_{Na}(t)(V(t) - E_{Na}) + G_L(V(t) - E_L) \quad (2.11)$$

This is an ordinary differential equation and can be solved numerically. This equation describes how the action potential wave propagates with time.

2.2 Voltage Gated Sodium Ion Channel

The knowledge of our understanding of the mechanisms governing the membrane excitability have come a long way since the time of Hodgkin and Huxley. We now know for sure that voltage gated sodium channels by increasing membrane permeability to Na^+ generate the upstroke of action potential. From membrane voltage sensing to pore opening and closing to inactivate sodium channel undergo several conformational changes, or gat-

ing. In the following section we have discussed the background literature on voltage-gated sodium channels which are relevant to this thesis.

2.2.1 Structure of the voltage gated sodium channel

The voltage gated sodium channel protein is composed of 1.) a large alpha subunit (generally around 2000 amino acids long, approx. 260 kDa) [11] and 2.) one or more auxiliary β -subunits of 22-36 kDa [12,13]. Sometimes, the sodium channel associates with other proteins such as calmodulin [14] or annexin II [15].

The α subunit is the principal subunit of the channel complex, responsible for voltage sensing, pore forming, ion selectivity, and ion conduction, inactivation, drug binding. It can function on its own. Although the α subunit is sufficient to produce Na^+ functional properties, but the functions such as channel trafficking, anchoring, localization, and channel conformational change are modulated by the presence of the β -subunits [15,16].

The voltage gated sodium channel being a tetramer is rotationally symmetric. The primary sequence of the alpha subunit folded into four domains (DI-DIV). These domains are similar but non-identical and are arranged in the circumference around the central pore. Large intracellular loops link all the four domains [17]. Each domain contains six transmembrane alpha-helical segments (S1-S6). S1-S4 works as voltage sensing domain and S4 is the voltage sensor. S4 contains several positively charged residues and two hydrophobic residues to sense the voltage change. A narrow ion-selective filter is formed with re-entrant loops between the S5 and S6 helices. The central pore opens when all four voltage sensors activate. The voltage sensing domain and S4-S5 linker pull the S5 and S6 helices outward to open the pore. Neighboring subunits are also forced to move likewise because of tight structural coupling [18,19]. The DIII-DIV linker made of three amino acid residues such as Isoleucine, Phenylalanine, and Methionine are critically important for channel inactivation and are collectively known as inactivation gate or IFM particle. Followed by the channel opening this IFM particle folds into the channel pore and blocks ion conduction from the cytoplasmic side [20]. The β -subunits are cell adhesion molecules which are also viable future therapeutic targets due to their ability to regulate alpha subunits.

For more detailed structure and functional information one can watch the two videos demonstrated by Prof. William Caterrall himself. The links are given in the reference: [22]. The most recent (2017) crystal structure of eukaryotic sodium channel Na_vPaS from

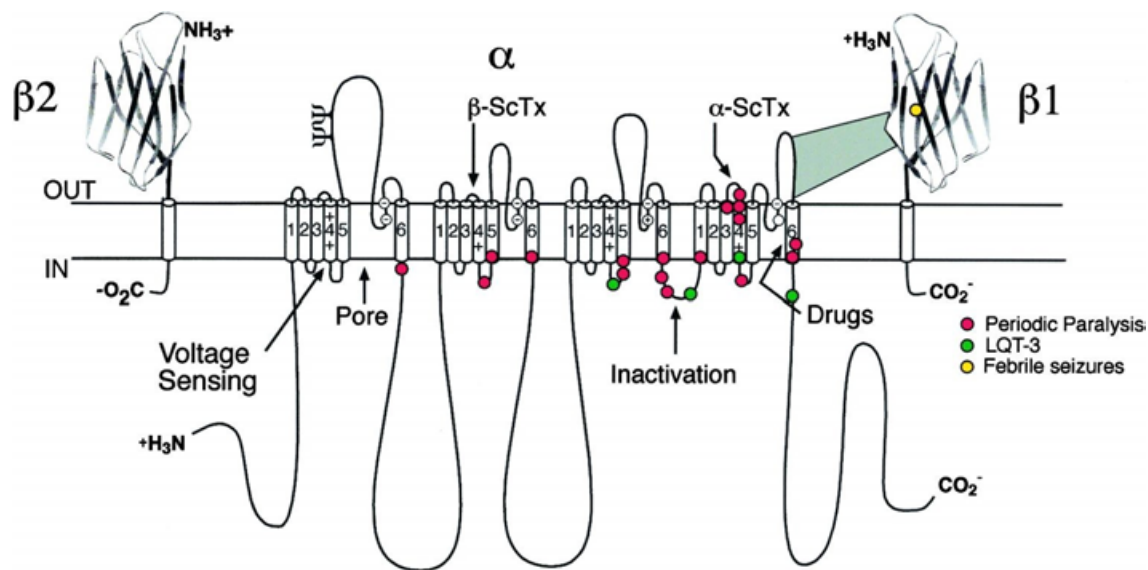


Figure 2.6: Structure of Voltage Gated Sodium Channel. Source: Reference [21]

American cockroach *Periplaneta americana* at a nominal resolution of 3.8 \AA determined using single-particle cryo-EM [28], as shown below.

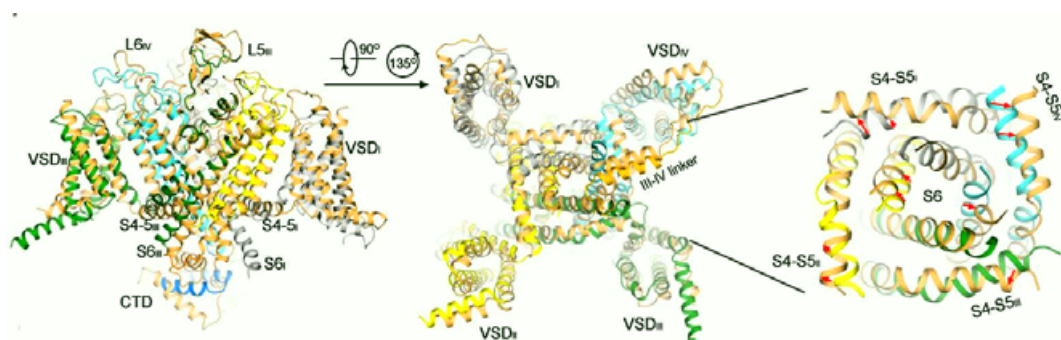


Figure 2.7: The structure of Na_vPaS is shown here. The left one gives the side view of the channel protein, the middle one gives the upper view of the pore and the right one zooms on the pore. The picture is taken from the reference: [28].

2.2.2 The dynamical voltage-dependent conformational change

Sodium influx through the pore is dependent on a series of complex conformational changes in response to altered membrane voltage. In general voltage gated sodium channels exist in one of three state conformations: **closed**(deactivated), **open** (activated), or **inactivated** state. At hyper polarized voltage the channel exists in closed state configuration. In this state no ion permeation across the membrane via voltage gated sodium channel is possible. At cell resting potential i.e, at -70 mV the closed state is the

predominant state. As soon as the membrane voltage is depolarized the transition occurs from from closed state to ion-conducting open configuration in less than a millisecond and allow Na^+ ions to flow into the cell down their electrochemical gradient. Channel activation and opening is voltage dependent processes. Within a few milliseconds of opening, sodium channel goes to a non-conducting or inactivated conformation. The extent of inactivation is apparently voltage-dependent and appears faster at more depolarized potentials. Once inactivated, the channels go to refractory period. At this period sodium channel is unresponsive to further stimulus. Sodium channel does not reactivate until the cell membrane is repolarized to negative resting membrane potential. The time course of recovery from channel inactivation is very important in modulating firing frequency of action potentials in excitable cells.

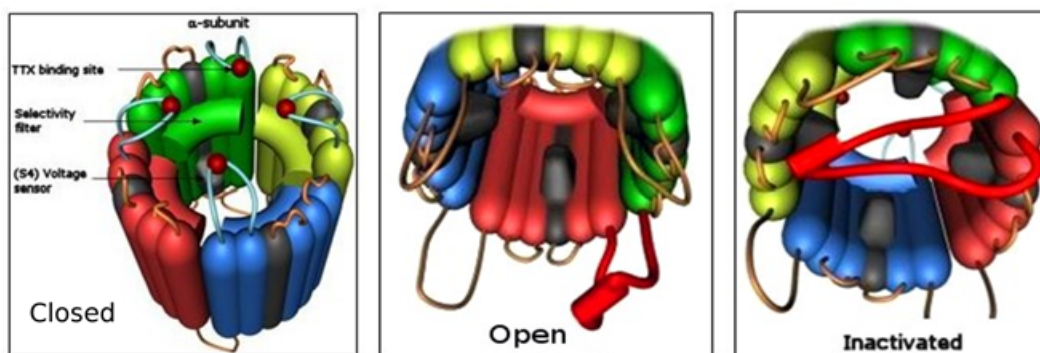


Figure 2.8: Model diagram of closed, open and inactivated state of voltage gated sodium ion channel. Source: Reference [23].

The X-ray crystallographic study of structure elucidation has revealed different functional states such as closed [18], potentially inactive [46,47] and open [26] after determining the bacterial sodium channels and in prokaryotic cells. With the help of these studies and combining human sodium channel sequences and bacterial crystallographic data homology models [58] have been built up.

The simplest possible Markov model [29, 30] for the Na^+ channel with the fewest possible number of states (three) and transitions (four) which is capable of reproducing the essential behaviors is shown in figure (2.9).

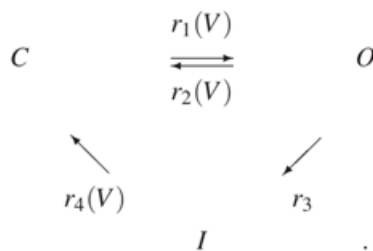


Figure 2.9: Simplest three state model which includes only the main functional states such as Closed(C), Open (O) and Inactivated state(I). In this model inactivation is considered to be voltage independent processes.

2.2.3 Sodium channel family

The standardized nomenclature of sodium channels is currently used from the database maintained by the IUPHAR [11, 31]. The family of sodium channels has nine known members. According to the variety of proteins of these channels are named as $\text{Na}_v1.1$ to $\text{Na}_v1.9$. The gene names are referred to as SCN1A to SCN11A (the SCN6/7A gene is part of the Nax sub-family and has uncertain function). These channels are different not only by their sequence but also they have different kinetics and expression profiles. Some of this data is summarized in Table 2.3, below.

Protein name	Gene	Distribution	TTX sensitivity
$\text{Na}_v1.1$	SCN1A	CNS	TTX-sensitive
$\text{Na}_v1.2$	SCN2A	CNS	TTX-sensitive
$\text{Na}_v1.3$	SCN3A	CNS	TTX-sensitive
$\text{Na}_v1.4$	SCN4A	Skeletal muscle	TTX-sensitive
$\text{Na}_v1.5$	SCN5A	Heart	TTX-resistant
$\text{Na}_v1.6$	SCN8A	CNS	TTX-sensitive
$\text{Na}_v1.7$	SCN9A	PNS	TTX-sensitive
$\text{Na}_v1.8$	SCN10A	PNS	TTX-resistant
$\text{Na}_v1.9$	SCN11A	PNS	TTX-resistant

Table 2.3: Voltage gated sodium channel isoforms can be classified according to their pharmacologic sensitivity to toxin tetrodotoxin (TTX). CNS: Central Nervous System, Peripheral Nervous System.

There are four distinct β -subunits named according to the order of discovery: SCN1B, SCN2B, SCN3B, SCN4B (Table 2.4). $\beta1$ and $\beta3$ interact with the alpha subunit non-covalently, whereas $\beta2$ and $\beta4$ associate with α via disulfide bond [32].

Protein name	Gene link	Assembles with
Na _v β1	SCN1B	Na _v 1.1 to Na _v 1.7
Na _v β2	SCN2AB	Na _v 1.1, Na _v 1.2, Na _v 1.5 to Na _v 1.7
Na _v β3	SCN3B	Na _v 1.1 to Na _v 1.3, Na _v 1.5
Na _v β4	SCN4B	Na _v 1.1, Na _v 1.2, Na _v 1.5

Table 2.4: Voltage gated sodium channel isoforms can be classified according to their pharmacologic sensitivity to toxin tetrodotoxin (TTX). CNS: Central Nervous System, PNS: Peripheral Nervous Syatem.

2.3 Inactivation of Sodium Channel

Inactivation of sodium channel is one of the most crucial step for the normal electrical activity in excitable cells. There are many different types of inactivation, including fast, slow and ultra-slow and each of these can be modulated by cellular factors or accessory subunits [33].

2.3.1 Fast inactivation

Sodium channel opens in response to membrane depolarization and then within 1-2 ms inactivates and restricts further ion flow inside the cell. This fast inactivation process is required to control the excitability in nerve and muscle cells. Site-directed studies showed that the short intracellular loop connecting DIII and DIV of the α subunit is responsible for fast inactivation [34]. This intracellular blocking particle that folds into the channel structure like a hinged lid blocks the pore during inactivation [35]. Cutting this loop by expression of the sodium channel in two pieces greatly slows down the inactivation [36]. The key amino acid sequence required to maintain the closure of inactivation gate [20] is IFM(Isoleucine, Phenylalanine, and Methionine). The peptides containing this inactivation gate sequence can restore fast inactivation to mutant sodium channels [37]. The inactivation gate bends at a key pair of glycine residues and allows it to fold into the intracellular mouth of the pore and then bind within and block sodium conductance as a hinged lid [38,39]. Structural analysis of inactivation gate using NMR showed that it contains a rigid alpha helix preceded by IFM motif and a Threonine residue on their surface [40]. The fast inactivation gate is not present in homotetrameric bacterial sodium channels.

2.3.2 Slow inactivation

The time scale of slow inactivation of sodium channels ranges from 100 ms to 1s. It was also first observed in the squid giant axon [41, 42]. The molecular mechanism of slow inactivation is not well defined as fast inactivation. Many extensive structure-function related studies implicate conformational changes in the selectivity filter [43, 44] and the S6 segment [45] is the key step for slow-inactivation. The wild-type Na_vAb channel shows very prominent use-dependent slow inactivation [18]. An early phase of slow inactivation occurs during test pulses and the composite time constant for this phase of slow inactivation reaches 20 msec at positive membrane potentials. Repetitive depolarizations at slow rates (0.2 Hz or 1 Hz) shows a late phase of slow inactivation that reduces the sodium current to near zero which is very slowly reversible [58]. Wild-type Na_vAb has been found to be crystallized in a conformation which is expected to be of the slow-inactivated state [46]. The selectivity filter, central cavity, and intracellular activation gate have all been modified by an asymmetric pore collapse. During the pore collapsing two of the S6 segments move towards the central axis of the pore and two move away to give a striking dimer-of-dimers arrangement [46, 47]. It is likely that this pore collapse is responsible for the stability of the slow-inactivated state and the long time required for recovery from slow inactivation [58].

2.4 Path of Inactivation

Path of inactivation is an important research in ion channels. Inactivation can occur in two ways. The channel inactivation via pore opening and then inactivation which is called Open State Inactivation, OSI is well know path of inactivation. However, inactivation can occur from pre-open closed states too, without even opening the pore. This is called closed-state inactivation, CSI. In both the cases recovery from inactivation occurs when the membrane potential is returned back to its initial resting potential. Although OSI mechanism is a pretty well understood at biophysical and structural [48, 49] levels, the molecular basis of CSI is not fully understood. The intricate mechanisms involved in CSI requires further investigation.

2.4.1 Inactivation path in sodium channels

Although Hodgkin and Huxley first suggested CSI in Na_v channels but the first convincing quantitative evidence for inactivation occurring from pre-open closed states came

from investigating the sodium channel in crayfish giant axon by Bean, 1981 [50]. In this study the current kinetics in response to a single activating pulse was compared to the inactivation onset kinetics investigated using prepulse protocol. Quantitative inspection of the data showed that the currents took longer time to reach the peak than for prepulse inactivation to develop. From that analysis it was proved that inactivation can occur before the Nav channels open.

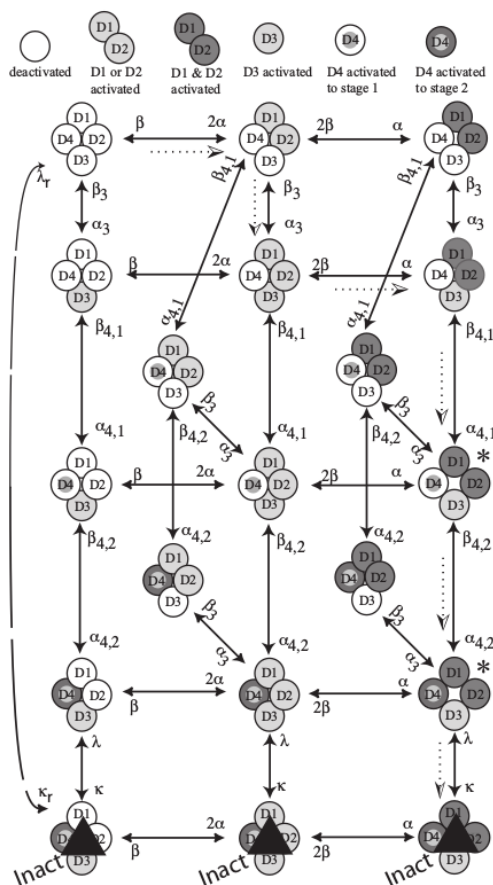


Figure 2.10: State diagram for activation and inactivation. This scheme shows how the domains D1-D4 gradually activates to go to the open state and inactivate states. The dotted lines show the most preferred path of inactivation at 0 mV voltage. The ion conducting states are marked with asterisks. More detailed information is found in reference [57].

By examining the single Nav channel recordings from rat myotubes Horn et al, 1981 [51] found a striking discrepancy between the channel opening probability and inactivation probability clearly which was an indication of CSI. The direct relationship between the inactivation magnitude and the time it takes for the first opening studied in these experiments suggested that inactivation could occur before opening. Further quantitative studies such as maximum likelihood analysis by Horn and Vandenberg, 1984 [52] over

several kinetic schemes confirmed the existence of CSI. After that Aldrich and Stevens, 1983 [54] showed that the open probability is substantially reduced when the activating voltage pulse is provided after a conditioning prepulse that elicits no unitary activity.

Later Kuo and Bean, 1994 [55] demonstrated that channels actually deactivate before they recover from inactivation and the inactivation at hyperpolarized potentials starts with a delay which is nearly electrically silent. These experimental results have qualitatively and quantitatively explained that sodium channel inactivation is a combined process of CSI OSI in Nav channels [50–52, 54–57]. However, some sodium channels undergo more inactivation from the open state and others undergo more inactivation from pre-open closed states. These distinct behaviors are referred to preferential OSI and preferential CSI, respectively [53]. The kinetic scheme provided by Armstrong (2006) for sodium channel inactivation is well accepted model until now. The Armstrong kinetic scheme [57] is shown in figure (2.10).

2.5 Sodium Channelopathy

The physiological importance of the voltage gated sodium channel is association with numerous pathologies which ranges from mild to life-threatening. Drug discovery in this area is difficult. Various neurotoxins that are produced by plants and animals for defence and protection, such as tetrodotoxin, scorpion toxins and batrachotoxin targets Sodium channels. Studies with neurotoxins or ion channel blockers contributed largely to our today's understanding of the structure and function of sodium channel. In this section we briefly discuss the drug receptors of sodium channels, classes of different channelopathies and their treatment strategies and therapies.

2.5.1 Drug receptor sites of sodium channel

Sodium channels are blocked by drugs used clinically as local anesthetics, antiarrhythmics, and antiepileptics [58]. Site-directed mutagenesis studies of sodium channels revealed the receptor site for local anesthetics and related drugs is formed by amino acid residues in the S6 segments in domains I, III, and IV [59–61] as shown in figure (2.11) [62]. These drugs bind to a common receptor site in the pore and impede ion permeation, as seen in figure 2.11(left).

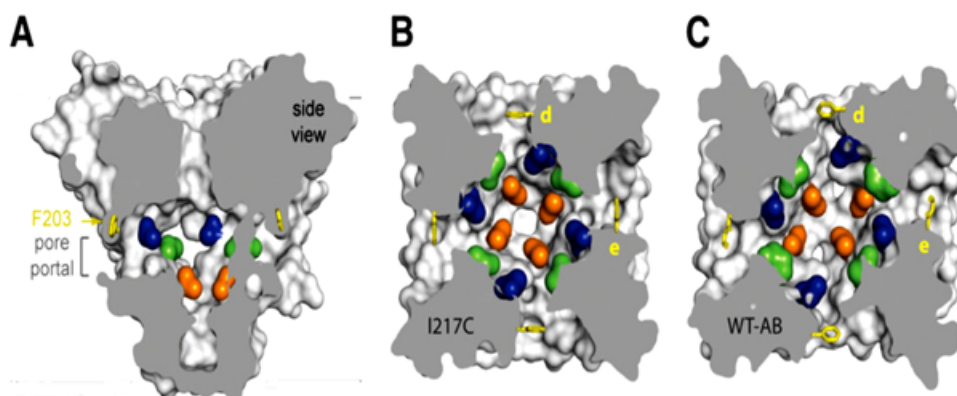


Figure 2.11: Drug-binding sites and fenestrations in NavAb. (A) Side view of the hydrophobic access to central cavity. Phe203 side chains are yellow sticks. Binding sites of Na_vAb residues are: Threonine206 (blue), Methionine209 (green), and Valine213 (orange). (B) Top view sectioned below the selectivity filter colored as in (A). (C) Structure of the drug-binding site in the slow-inactivated state in Na_vAb . Source: Reference [62]

2.5.2 Mechanism of drug binding

Many sodium channel blockers are well studied electrophysiologically. The mechanism of block is rather complex and includes three typical phenomena observed in different experimental protocols. The long-standing explanation for high-affinity LA block is called the *modulated receptor hypothesis* [4] according to which large or *hydrophilic* drugs blockers have different affinities to different functional states of the channel. The affinity to the closed state is the lowest one. The affinity to the open state is bigger, and the inactivated states of the channel have the maximal affinity. Although this general phenomenon of the use dependence significantly vary for different compounds. As also predicted by modulated receptor hypothesis [4], fenestrations lead from the lipid phase of the membrane sideways into the drug receptor site and provides a specific *hydrophobic* access pathway for the binding of small hydrophobic drugs in the resting state of the channel as seen from figure (2.11, left) [18]. Access to the drug binding site in Na_vAb channels is controlled by the side chain of a single amino acid residue, Phe203 (figure 2.11, left) [18]. It control drug access and egress from the local anesthetic receptor site in mammalian cardiac and brain sodium channels. In contrast, phenytoin, carbamazepine, and lamotrigine shows prominent voltage-dependent block due to preferential binding to the inactivated states of sodium channels [63, 64], as shown in figure (2.11, right). Frequency-dependent block allows these agents to selectively prevent sodium channels from initiating rapid action potential firing in nerves that conduct pain signals or from doing so in cardiac myocytes to cause arrhythmias [65].

2.5.3 Chemical structures of sodium blockers

Sodium channel blockers have highly diverse chemical structures. Most LAs are flexible molecules that contain a protonatable amino group at one end, an aromatic moiety at the opposite end, and polar groups in the middle [66]. Classical examples are lidocaine, bupivacaine, and tetracaine. Typical anticonvulsants such as phenytoin, lamotrigine, and carbamazepine (CMZ) are electroneutral molecules. Unlike LAs, they contain nonionizable polar groups at one end of the molecule and an aromatic moiety at the other end [66]. Antidepressants, which block sodium channels, have an ionizable amino group and a polycyclic moiety that contains aromatic and saturated rings. Another group of blockers contains bulky rigid moieties [66]. Examples are cocaine, memantine, and quinidine.

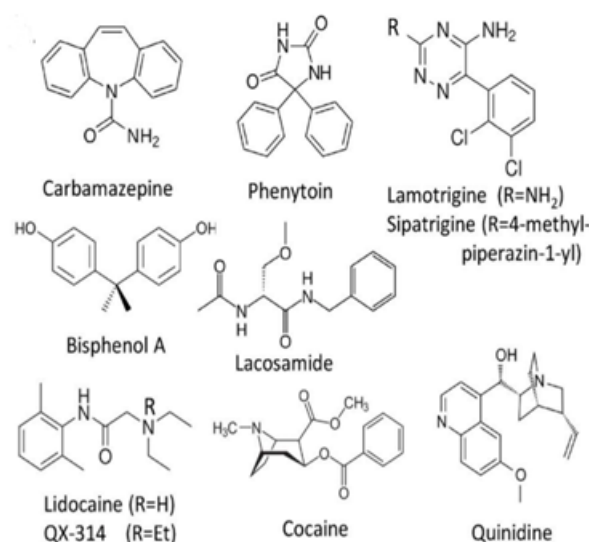


Figure 2.12: Drug-binding sites and fenestrations in NavAb. (A) Side view of the hydrophobic access to central cavity. Phe203 side chains are yellow sticks. Binding sites of Na_vAb residues are : Threonine206 (blue), Methionine209 (green), and Valine213 (orange). (B) Top view sectioned below the selectivity filter colored as in (A). (C) Structure of the drug-binding site in the slow-inactivated state in Na_vAb. Source: Reference [62]

2.5.4 Sodium channelopathies:

The essential nature of Na_v channel is emphasized by the existence of inherited disorders (sodium “channelopathies”) caused by mutations in genes that encode these vital proteins. Nearly 20 disorders affecting skeletal muscle contraction, cardiac rhythm, or neuronal function and ranging in severity from mild or latent disease to life-threatening

or incapacitating conditions have been linked to mutations in human Na_V channel genes. Inherited disorders of Na_V Channel are shown in the following list [67].

Muscle sodium channelopathies (SCN4A)

i) Hyperkalemic periodic paralysis, ii) Paramyotonia congenita, iii) Potassium-aggravated myotonia, iv) Painful congenital myotonia, v) Myasthenic syndrome, vi) Hypokalemic periodic paralysis type 2, vii) Malignant hyperthermia susceptibility.

Although the mechanism of action is poorly understood [68], the carbonic anhydrase inhibitors are found often to be successful for the treatment of periodic paralysis. However certain local anesthetic/antiarrhythmic agents (most common one is Mexiletine) have antimyotonic activity and are often used to treat nondystrophic myotonias [69]. A Flecainide have utility in severe forms of myotonia that are resistant to mexiletine [70]. Long-term treatment of myotonia with these blockers is often limited for side effects.

Cardiac sodium channelopathies (SCN5A)

i) Congenital long QT syndrome (Romano-Ward), ii) Idiopathic ventricular fibrillation (Brugada syndrome), iii) Isolated cardiac conduction system disease, iv) Atrial standstill, v) Congenital sick sinus syndrome, vi) Sudden infant death syndrome, vii) Dilated cardiomyopathy, viii) conduction disorder, ix) arrhythmia.

β -Adrenergic blockers are used for therapy in LQTS although this treatment strategy is less efficacious in the setting of SCN5A mutations [71]. In vitro evidences suggest that mexiletine counteract the aberrant persistent Na^+ current and shorten the QT interval [72] in SCN5A mutation carriers. Flecainide has also been observed to shorten QT intervals in the setting of certain SCN5A mutations [73]. Class III-type antiarrhythmic agents such as quinidine, sotalol etc are beneficial in Brugada syndrome [74].

Neuronal sodium channelopathies

Neuronal channelopathies are divided generally in two classes as follows,

A. Brain sodium channelopathies (SCN1A, SCN2A, SCN1B): i) Severe myoclonic epilepsy of infancy (Dravet Syndrome), ii) Generalized epilepsy with febrile seizures plus (GEFS+), iii) Intractable childhood epilepsy with frequent generalized tonic-clonic seizures, iv) Benign familial neonatal-infantile seizures.

B. Peripheral nerve sodium channelopathies (SCN9A): Familial primary erythralgia.

In principle, the imbalance of excitation and inhibition should be corrected by drug treatment. Unfortunately, treatment with antiepileptic drugs such as phenytoin, carbamazepine, and lamotrigine shows adverse effects on patients with DS [75, 76]. Current best therapy for patients with DS uses combinations of four-drug combination of valproic acid, the benzodiazepine clobazam, topiramate, and stiripentol, which has shown efficacy in the treatment in France and elsewhere in Europe [77] in 2011. Benzodiazepines such as clonazepam and clobazam are broadly effective antiepileptic drugs for GEFS+ epilepsy as well as many other types of epilepsy. Levetiracetam binds to the synaptic vesicle protein SV2 and effectively prevents seizures in GEFS+ and a broad range of epilepsy syndromes [78].

2.5.5 Theoretical and computational modeling

The development of theoretical models of ion channels reflects advancements in our understanding of channel gating. Since most data are collected outside of the physiological cellular environment, the model provides a tool for simulation in physiological conditions that cannot be maintained during experiments. Also using models, we can understand the electrophysiological behavior of the cell in presence of a mutation or drug intervention that alters a single voltage-dependent transition. Thus accurate models for drug testing is important [79].

To date, the majority of models have used Hodgkin-Huxley models although is insufficient to reproduce even basic features of voltage gated channels. Recently Markovian-based models of normal and mutant cardiac Na channels are repeatedly being validated and improved as new experimentally datas are being obtained. The models accurately simulate single channel properties such as latency to first opening, distribution of mean open times, voltage dependence of mean open times, distribution of channel closed times, and gating behavior of single channels. Macroscopic current properties are also accurately reproduced, including current-voltage relations, voltage dependence of activation and availability, and time and voltage dependence of channel recovery from inactivation. These accurate channel models can be used to investigate state-specific binding of drugs to the channels within the complex integrative cell. Clancy-Rudy Model, 1999-2002 [80, 81] of cardiac $\text{Na}_v1.5$ channel is a one notable markov model which fits experimental data with high degree of accuracy and widely being utilized for pharmacological studies now a days.

2.6 Nonequilibrium Response Spectroscopy

Experimentally, the ion channel kinetics is usually studied by the patch clamp technique which is an extension of the voltage clamp technique, used for estimating the multiple ion channel activities. In both cases, a certain voltage pulse is given to ion channel and the ionic current during the relaxation of channel protein to its equilibrium potential [82–84] is measured. Therefore, in this technique the response properties of channel protein is measured during its relaxation from one non-equilibrium state to its equilibrium state. However, in a nerve cell opening and closing of the voltage-gated ion channels occur completely at the non-equilibrium environment [85]. This is due to the fact that for accepting a nerve impulse the equilibrium potential of a nerve cell is changed. For returning back to its equilibrium potential, gradually sodium and potassium channels start opening and as a consequence, action potential propagates along the nerve cell [4]. To understand more about the activity of channel proteins in the non-equilibrium environment recently a new technique, the non-equilibrium response spectroscopy [86,87] is developed. In this technique the response properties of channel protein are measured by applying the continuously oscillating [88] or fluctuating voltage [89]. Continuous supply of energy from the external voltage forces the ion channel to show its response characteristics in the non-equilibrium environment [89]. This sort of nonequilibrium response spectroscopic technique provides new aspects of ion channel gating kinetics that standard stepped-potential protocols can not provide [86]. It is seen that subtle details of the kinetics that are otherwise invisible when conventional stepped pulses are visible if NRS technique is used. As a consequence, the kinetics can be probed in a much more sensitive way by supplementing conventional techniques with measurements of the responses to more complex voltage waveforms.

To study the thermodynamics of the system in nonequilibrium environment we present here some recent literature on the development of the Nonequilibrium Thermodynamics in the next subsection.

2.6.1 Nonequilibrium thermodynamics: Entropy balance

In this thesis we have extensively used nonequilibrium quantities like entropy production rates. Thus we first discuss the entropy balance equation derived previously for a Markovian process [90–95]. Here we consider an open system driven by external agent is in contact with the environment with temperature, T . The total number of states m is finite. Thus the probability to find the system in a state m at time t is denoted by $p_m(t)$

who's evolution with time is described by the master equation as follows:

$$\dot{p}_m(t) = \sum_{m'} W_{m,m'} p_{m'}(t), \quad (2.12)$$

where the transition rate matrix satisfies

$$\sum_m W_{m,m'} = 0. \quad (2.13)$$

Now different mechanisms, ν can cause the transitions between states m . Also, if we suppose these rates to be time dependent via a control variable λ , we have the following situation,

$$W_{m,m'} = W_{m,m'}(\lambda_t) = \sum_{\nu} W_{m,m'}^{\nu}(\lambda_t). \quad (2.14)$$

If the control variable λ_t is time dependent, the system is said to be externally driven. If the rates are “frozen” at a particular values $W_{m,m'}^{\nu}$, we shall get a corresponding unique stationary distribution, p_m^{st} , as the rate matrix is irreducible and the system will always eventually reach that state. It is given by the normalized right eigenvector of zero eigenvalue of the transition matrix,

$$W_{m,m'}(\lambda) p_m^{st}(\lambda) = 0. \quad (2.15)$$

Now the system's Shannon entropy [90, 94, 95] (Boltzmann constant $k_B = 1$) is given by,

$$S(t) = \sum_m p_m(t) \ln p_m(t). \quad (2.16)$$

Using equation (2.12) and (2.13) and omitting (t) from p_m and λ_t from W , we get

$$\begin{aligned} \dot{S} &= - \sum_m \dot{p}_m \ln p_m \\ &= - \sum_{m,m',\nu} W_{m,m'}^{\nu} \ln \frac{p_m}{p_{m'}} \\ &= \frac{1}{2} \sum_{m,m',\nu} [W_{m,m'}^{\nu} p_{m'} - W_{m',m}^{\nu} p_m] \ln \frac{p_{m'}}{p_m} \\ &= \frac{1}{2} \sum_{m,m',\nu} [W_{m,m'}^{\nu} p_{m'} - W_{m',m}^{\nu} p_m] \ln \frac{W_{m',m}^{\nu} p_{m'}}{W_{m,m'}^{\nu} p_m} \\ &\quad + \frac{1}{2} \sum_{m,m',\nu} [W_{m,m'}^{\nu} p_{m'} - W_{m',m}^{\nu} p_m] \ln \frac{W_{m',m}^{\nu}}{W_{m,m'}^{\nu}} \end{aligned} \quad (2.17)$$

Now the term fluxes, $J_{m,m'}^\nu$ and corresponding forces, $X_{m,m'}^\nu$ are defined as,

$$J_{m,m'}^\nu(t) = W_{m,m'}^\nu(\lambda_t)p_{m'}(t) - W_{m',m}^\nu(\lambda_t)p_m(t), \quad (2.18)$$

and

$$X_{m,m'}^\nu(t) = \ln \frac{W_{m',m}^\nu(\lambda_t)p_{m'}(t)}{W_{m,m'}^\nu(\lambda_t)p_m(t)}. \quad (2.19)$$

With this definition the master equation (2.12) can be written as

$$\dot{p}_m(t) = \sum_{m',\nu} J_{m,m'}^\nu(t) = J_{m,m'}(t), \quad (2.20)$$

where we define

$$J_{m,m'}(t) = J_{m,m'}^\nu(t). \quad (2.21)$$

The system's entropy production rate can thus be written as in the familiar form of irreversible thermodynamics [96],

$$\dot{S}(t) = \dot{S}_e(t) + \dot{S}_i(t) \quad (2.22)$$

The quantity $\dot{S}_e(t)$ is called the entropy flow and is expressed as,

$$\begin{aligned} \dot{S}_e(t) &= \frac{1}{2} \sum_{m,m',\nu} J_{m,m'}(t) \ln \frac{W_{m',m}^\nu(\lambda_t)}{W_{m,m'}^\nu(\lambda_t)} \\ &= \sum_{m,m',\nu} W_{m,m'}^\nu(\lambda_t)p_{m'}(t) \ln \frac{W_{m',m}^\nu(\lambda_t)}{W_{m,m'}^\nu(\lambda_t)}, \\ &= - \sum_{m,m',\nu} W_{m,m'}^\nu(\lambda_t)p_{m'}(t) \ln \frac{W_{m,m'}^\nu(\lambda_t)}{W_{m',m}^\nu(\lambda_t)} \end{aligned} \quad (2.23)$$

and the positive quantity $\dot{S}_i(t)$ is called entropy production and it is defined as,

$$\begin{aligned} \dot{S}_i(t) &= \sum_{m,m',\nu} W_{m,m'}^\nu(\lambda_t)p_{m'}(t) \ln \frac{W_{m,m'}^\nu(\lambda_t)p_{m'}(t)}{W_{m',m}^\nu(\lambda_t)p_m(t)} \\ &= \frac{1}{2} \sum_{m,m',\nu} J_{m,m'}^\nu(t)X_{m,m'}^\nu(t) \geq 0 \end{aligned} \quad (2.24)$$

The entropy production, $\dot{S}_i(t)$ is zero only if the detailed balance condition is satisfied, i.e.,

$$W_{m,m'}^\nu(\lambda)p_{m'} = W_{m',m}^\nu(\lambda)p_m \quad (2.25)$$

The above mathematical descriptions can be applied to any system which is described by a master equation. The transitions between states m due to different physical mechanisms(ν) can correspond to exchange of heat with different reservoirs where the transition rates of mechanism ν must obey the local detailed balance condition. It follows that $\dot{S}_i(t)$ is also equal to the total entropy production $\dot{S}_{tot}(t)$ in system plus environment. If the environment remains at equilibrium at all times using detailed balance as in equation (2.25), it will not have its own internal entropy production. The above description in terms of the system alone is not complete, the irreversible processes taking place in the environment also needs to be considered. Thus the entropy flow is equal to the minus of the entropy increase in the reservoir, i.e $\dot{S}_e(t) = -\dot{S}_r(t)$. The microscopic origin of these relations can be found in the reference [97].

2.6.2 Adiabatic and nonadiabatic entropy balance

In equation (2.19) the force X can be split in an adiabatic contribution, A and a nonadiabatic contribution, N such as,

$$X_{m,m'}^\nu(t) = A_{m,m'}^\nu(\lambda_t) + N_{m,m'}(t), \quad (2.26)$$

where

$$A_{m,m'}^\nu(\lambda_t) = \ln \frac{W_{m,m'}^\nu(\lambda_t)p_{m'}^{st}(\lambda_t)}{W_{m',m}^\nu(\lambda_t)p_m^{st}(\lambda_t)} \quad (2.27)$$

and

$$N_{m,m'}(t) = \ln \frac{p_m^{st}(\lambda_t)p_{m'}(t)}{p_{m'}^{st}(\lambda_t)p_m(t)}. \quad (2.28)$$

Thus the total entropy production can be split into an adiabatic and a nonadiabatic contribution as follows,

$$\dot{S}_i(t) \equiv \dot{S}_{tot}(t) = \dot{S}_a(t) + \dot{S}_{na}(t) \quad (2.29)$$

with

$$\dot{S}_a(t) = \frac{1}{2} \sum_{m,m',\nu} J_{m,m'}^\nu(t) A_{m,m'}^\nu(\lambda_t) \geq 0 \quad (2.30)$$

$$= \sum_{m,m',\nu} W_{m,m'}^\nu(\lambda_t)p_{m'}(t) \ln \frac{W_{m,m'}^\nu(\lambda_t)p_{m'}^{st}(\lambda_t)}{W_{m',m}^\nu(\lambda_t)p_m^{st}(\lambda_t)}, \quad (2.31)$$

$$\begin{aligned} \dot{S}_{na}(t) &= \frac{1}{2} \sum_{m,m'} (t) N_{m,m'}(t) \geq 0 \\ &= - \sum_m \dot{p}_m(t) \ln \frac{p_m(t)}{p_m^{st}(\lambda_t)}. \end{aligned} \quad (2.32)$$

There are basically two ways possible by which a system can be brought out of equilibrium: one, by applying steady nonequilibrium constraints (adiabatic contribution) or by driving (nonadiabatic contribution). The term “adiabatic” here does not mean the absence of heat exchange, but it means the instantaneous relaxation to the steady state. Both \dot{S}_a and $\dot{S}_{na}(t)$ are non-negative entropy productions as follows from Jensen’s inequality, $\ln x \geq 1 - x$ for $x > 0$, together with Eqs. (2.13) and (3.15). The non-negativity of these quantities agree with the fact that the trajectory entropies s_a and s_{na} obey detailed fluctuation theorems[33]. The nonadiabatic entropy production is zero in the adiabatic limit $p_m(t) \rightarrow p_m^{st}(\lambda_t)$. The adiabatic entropy production, divided by the temperature of the reservoir is called the house-keeping heat [98, 99].

2.7 Dynamic Hysteresis

Dynamic hysteresis is a phenomenon observed in many physical and chemical systems and had been studied experimentally for more than two decades [100, 101]. Figure (2.13) shows the typical nature of the dynamic hysteresis, (right). This notion often contrasts the common conception of hysteresis. This dynamic hysteresis is different from the general behavior of any protein fixed where response-vs-stimulus relationship is observed as seen from figure (2.13, left). Hysteresis is the signature of memory developed in the system as a result of complex dependence of the system’s response to the external stimulus. Thus it is believed that voltage-gated channels remembers their recent past or they can alter their response(voltage-dependence) to changes occurred in membrane potential. This dynamic voltage dependence in voltage-gated ion channels have strong impact on electrical signaling [102, 103].

One of the earliest examples of hysteresis in channels was reported in 1982 on gating currents in the squid giant axon [104]. The gating currents arise from the movement of intrinsic charges in voltage-gated channel protein [105] which causes conformational changes to occur and therefore various activities of the channel come to play [105, 106]. The relationship between the net mobilized gating charge(Q) and the associated membrane potential(V) for the activation of Na^+ channel in the squid giant axon shifts toward more negative voltages when the membrane is held at 0 mV, instead of -70 mV [104]. This phenomenon indicated that the voltage dependence of channels vary with the type of activity. Similar observations were found with the excitation-contraction coupling in frog skeletal muscles [107]. Studies showed that gating currents from L-type Ca^{2+} [108], voltage gated potassium channels also show hysteretic behavior [109–111]. It was be-

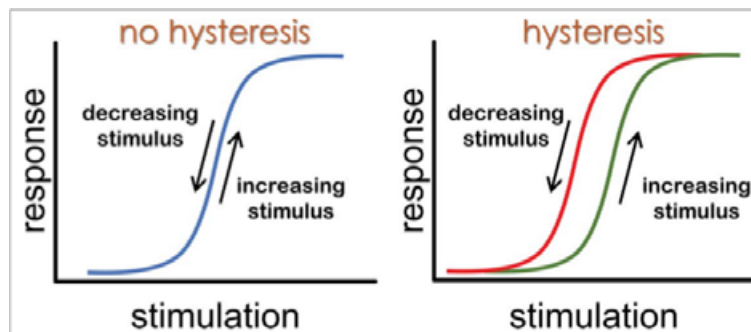


Figure 2.13: Comparison between a non-hysteretic and a hysteretic system. A) The response of a non-hysteretic system is a fixed function of the stimulation. No changes in the responses-stimulus relationship are observed except as the magnitude of a stimulus varies. B) In contrast, the path of activity of hysteretic systems changes as a function of stimulus applied, but also depends on whether the magnitude of the stimulus is decreasing or increasing. Source: Reference [103].

lieved that inactivation processes might have been the reason behind the hysteresis. But the recent studied has refuted such ideas by altering or blocking the inactivation process using pharmacological methods or genetic modulation. Thus inactivation has no significant role in hysteresis [109,111]. The Hyperpolarization-activated cyclic-nucleotide-gated HCN ion channels, also known for the “funny current” [112], essential for the regulation of pacemaking activity in the heart and brain, are recently found to show dynamic hysteresis. Experimental and computer simulation have shown that the stability of electrical rhythmic activity are critically dependent on the hysteretic activity of HCN [113–115]. Recently, the pore-forming protein lysenin has shown hysteresis due to its transport and regulation characteristics similar to ion channels [116–118].

2.7.1 Reason of dynamic hysteresis:

It is observed that when the period of the transmembrane voltage is comparable with the protein relaxation time, the ion current through the channel depends on prehistory and the standard conditions of hysteresis is achieved. A distinctive feature of such channels has high sensitivity of its conformational equilibrium to the transmembrane voltage. As the different conformations of the channel-forming protein has significantly different conductances a strong nonlinearity arises in the channel stationary current-voltage characteristics [4]. Although the equilibration of the channel-forming protein may occur very slowly.

Several theoretical works [119–122] although not many including dynamic hysteresis model has been proposed. Here we briefly discuss the model provided by Pustovoit *et al.* [123]. A membrane containing N channels and each of which can be in one of the two conformational states of differing conductances. The transitions between the two states are Markovian and can be described by the kinetic scheme. The kinetic scheme in 2.14

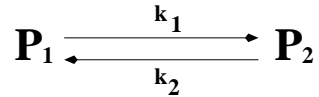


Figure 2.14: **Kinetic Model:** P_1 and P_2 are the probabilities of finding the channel in state 1 and state 2. The transition rates k_1 and k_2 are voltage dependent functions, such as $k_1 = k_1^0 \exp(-\alpha_1 V)$ and $k_2 = k_2^0 \exp(\alpha_2 V)$. k_1^0 and k_2^0 are the rates in the absence of the external voltage and α_i are inversely proportional to the absolute temperature.

was first time was proposed by Mueller and Rudin [124] and demonstrated for individual channels by Ehrenstein *et al.* [125]. The probability P_1 of finding the channel in state 1 at time t can be found by solving the rate equation

$$\begin{aligned} \frac{dP_1(t)}{dt} &= -k_1(t)P_1(t) + k_2(t)[1 - P_1(t)] \\ &= k_2(t) - k(t)P_1(t), \end{aligned} \quad (2.33)$$

where $k(t) = k_1(t) + k_2(t)$. The solution is

$$P_1(t) = P_1(t_0)e^{-\int_{t_0}^t k(t_1)dt_1} + \int_{t_0}^t e^{-\int_{t_1}^t k(t_2)dt_2} k_2(t_1) dt_1. \quad (2.34)$$

The periodic voltage of period T is switched on at $t = 0$. Here $V_T(t)$ is the time-dependent external voltage of the form $V(t) = H(t)V_T(t)$, where $H(t)$ is the Heaviside step function and $V_T(t)$ is a periodic function of t , $V_T(t + T) = V_T(t)$. As $t \rightarrow \infty$, $P_1(t)$ become periodic, $P_1(t + T) = P_1(t)$.

Considering only the probability of finding the channel in state 1 and omitting the subscript in the notation of this probability, i.e. $P_1 \longleftrightarrow P(t)$ and using the solution in (3.29) we can write $P(t)$ for $nT < t < (n + 1)T$, $n = 0, 1, \dots$, denoted by $P(t|n)$ as

$$P(t|n) = P(nT) \exp \left[- \int_{nT}^t k(t_1) dt_1 \right] + \int_{nT}^t k_2(t_2) \exp \left[- \int_{t_2}^t k(t_1) dt_1 \right] dt_2. \quad (2.35)$$

Using Eq. (3.29) one can write a recursion formula connecting the probabilities $P(nT)$ and $P((n + 1)T)$:

$$P((n + 1)T) = \gamma P(nT) + a_0, \quad (2.36)$$

where γ and a_0 are given by

$$\gamma = \exp \left[- \int_0^T k(t) dt \right]$$

and

$$a_0 = \int_0^T k_2(t_2) \exp \left[- \int_{t_2}^T k(t_1) dt_1 \right] dt_2.$$

The recursion formula in Eq. (2.36) helps expressing the $P(nT)$ in terms of $P(0)$ which is the equilibrium probability of finding the channel in state 1 in the absence of external voltage, $P(0) = k_2^0 / (k_1^0 + k_2^0)$. Eventually we obtain

$$P(nT) = \gamma^n \frac{k_2^0}{k_1^0 + k_2^0} + \frac{1 - \gamma^n}{1 - \gamma} a_0 \quad (2.37)$$

Expressions in Eqs. 2.35 and 2.37 give the probability $P(t)$ at any t . As $n \rightarrow \infty$ the probability $P(nT)$ approaches its asymptotic value,

$$\lim_{n \rightarrow \infty} P(nT) = \frac{a_0}{1 - \gamma}. \quad (2.38)$$

Substituting this into Eq. 2.35 we find the asymptotic long-time behavior of the probability $P(t)$, which will be denoted by $P_\infty(t)$,

$$P_\infty(t) = \lim_{n \rightarrow \infty} P(t|n) = \frac{a(t)}{1 - \gamma}, \quad (2.39)$$

where function $a(t)$ is given by

$$a(t) = \int_t^{t+T} k_2(t_2) \exp \left[- \int_{t_2}^{t+T} k(t_1) dt_1 \right] dt_2. \quad (2.40)$$

One can see that $a(0) = a_0$. Function $a(t)$ is periodic, $a(t + T) = a(t)$. As a consequence, $P_\infty(t)$ is also periodic, $P_\infty(t + T) = P_\infty(t)$.

Expressions in Eqs. 2.39 and 2.40 show that $P_\infty(t)$ is prehistory dependent. This dependence disappears in the limiting cases of very slow and very fast variation of the voltage (Fig. 2.15). In these limiting cases $P_\infty(t)$ takes the following form:

$$P_\infty(t) = \frac{k_2(t)}{k(t)} \quad \text{for slow } V(t) \quad (2.41)$$

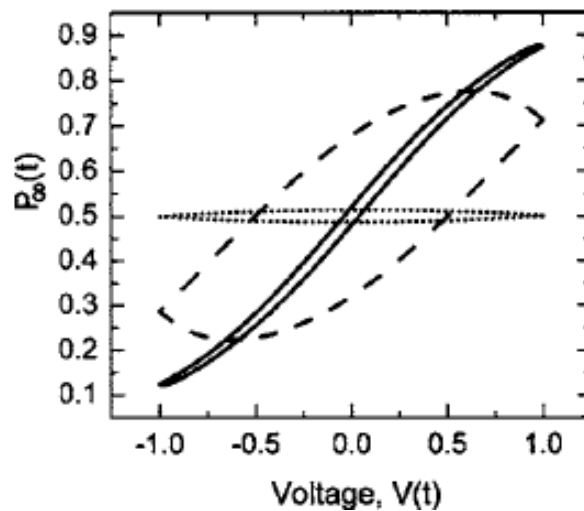


Figure 2.15: Dynamic hysteresis. The loop area vanishes at very low and very high frequency of voltage. In some intermediate frequency the loop has maximum area.

and

$$P_{\infty}(t) = \frac{\langle k_2(t) \rangle}{\langle k(t) \rangle} \quad \text{for fast } V(t) \quad (2.42)$$

where the angular brackets denote averaging over the period of a periodic function $f(t)$. Loop area is an important quantity to measure dynamic hysteresis. It depends on the frequency mean voltage and amplitude of the applied periodic voltage. When the static hysteresis is absent the loop area vanishes in two limiting cases: i) at very slow and ii) at very fast voltage change. When the voltage varies sufficiently slowly, the protein molecule adjusts its conformational distribution to the instantaneous value of the voltage and consequently the ion current being independent of the prehistory does not show hysteresis. Oppositely when the period of the voltage change is much shorter than the characteristic protein relaxation time, the protein molecule cannot follow fast variations of the voltage and sees only its average value. As a consequence, the current through the channel becomes again independent of the prehistory, and the hysteresis loop collapses to a single line. Thus, the loop area first monotonically grows with the frequency of voltage change, reaches a maximum, and then vanishes as the frequency tends to infinity.

2.7.2 Memristor

Dynamic hysteresis is a signature of dynamic memory [126–128] which is also a property of a memristor device originally envisioned in circuit theory [129, 130]. Recent studies show that the sodium and potassium channels behave almost similarly like locally-active memristors. They exhibit all of the fingerprints that a memristor device show such as i)

the characteristic pinched hysteresis in Lissajous figures in the voltage-current plane ii) the vanishing loop areas at very low and very high frequency of the periodic excitation. iii) There exist specific clockwise and anti-clockwise direction of hysteresis curves. However, in ion channels the studies are mainly concentrated on the kinetic properties that too are not performed in biophysical ranges and the energetic aspects were overlooked. A voltage-controlled memristor is defined [128] by,

$$i = G(x_1, x_2, \dots, x_n; v)v$$

$$\frac{dx_k}{dt} = f_k(x_1, x_2, \dots, x_n; v), k = 1, 2, \dots, n, \quad (2.43)$$

where G in the first equation is a piecewise continuous and bounded function of $(x_1, x_2, \dots, x_n; v)$, called the memductance of the memristor. The state variables (x_1, x_2, \dots, x_n) in the second equation depend on the internal state of the memristor and is defined by “n” 1st-order differential equations of states.

A current-control memristor is defined by,

$$v = R(x_1, x_2, \dots, x_n; i)i$$

$$\frac{dx_k}{dt} = f_k(x_1, x_2, \dots, x_n; i), k = 1, 2, \dots, n, \quad (2.44)$$

where R is a piecewise continuous and bounded function of n state variables (x_1, x_2, \dots, x_n) , called the memristance of the memristor.

Just as the Hodgkin-Huxley circuit model has stood the test of time, its constituent potassium ion-channel and sodium ion-channel memristors are destined to be classic examples of locally-active memristors in future textbooks on circuit theory and bi-physics [128].

2.8 Neuronal Synchronization

Neuronal synchronization is described as the correlated appearance of neuronal events occurring at the same time which are associated with various physiological functions. Generally it involves adjustment or phase locking of rhythms between two or more neurons which leads to a stable phase difference of membrane voltage oscillations such as coincidence of action potentials. The existence of synchronization region in brain has been confirmed by Riehle et al. [131] who investigated the rhythm synchronization be-

tween different neurons. Phase synchronization in different regions of brain is associated with complex biological function. Furthermore, the synchronization of gamma wave was observed by Montgomery et al. [132]. Many researchers later investigated the dynamical properties using the well known neuron models [133–135] while some did biological experiments [136, 137]. For example, Gu et al. [136] proposed a new neuron model which can detect complex dynamical behaviors in electrical activities efficiently for larger parameter region. For realistic neuronal systems composed of a large number of neurons with non-identical neurons, it is very important to investigate the collective nature of synchronization in neuronal networks [138, 139]. Due to diversity of realistic systems, phase synchronization [140] between coupled neurons is more acceptable than complete synchronization.

2.8.1 Chemical synaptic mechanisms of synchronization

Synaptic interaction is the most common mechanism of communication between neurons. Neurotransmitter released by presynaptic terminus activate the postsynaptic cell receptor and the generation of inward or outward currents depolarizes or hyperpolarizes the postsynaptic cell [141]. In general both the excitatory and inhibitory synaptic interaction contribute to synchronization of neuronal activity.

2.8.2 Gap-junctions and synchronization

The existence of gap junctions or electrical synapses in the mammalian brain has been known for long times [142]. Electrophysiologists consider gap junctions of great importance by most mammalian. Gap junctions or electrical synapses allow direct flux of ions between connected cells therefore providing a mechanism of communication which is action potential independent [143]. The large internal diameter, approx 1.2 nm, of many gap junction channels allows not only flow of electric current, largely carried by K^+ ions, but also exchange of small metabolites and intracellular signaling molecules. Gap junctions can synchronize electrical activity and may subserve metabolic coupling and chemical communication as well [144]. If few cells are connected through electrical synapses, any change of membrane voltage in one neuron would trigger current flow between coupled neurons leading to corresponding changes of membrane voltage in the latter cells leading to synchronization. In cortical networks, groups of GABA-releasing interneurons [145] and glial cells [146] are interconnected via gap junctions. There is a set of indirect evidences suggesting that electrical coupling may occur between axons of pyramidal neurons [147].

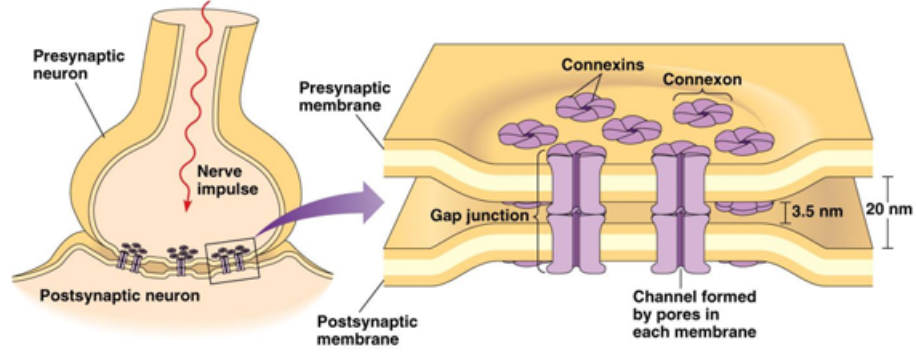


Figure 2.16: Diagram of a typical gap junction. Source: Reference [148] .

2.8.3 Synchronizing the Hodgkin-Huxley neurons

The synchronization between two HH neurons connected via gap junctions is presented as follows. $x_{i,M}$ and $x_{i,S}$ ($i = 1, 2, 3, 4$ and subscripts M, S stand for the master and slave system, respectively) be the four variables V, n, m and h in each system. The master neuron is represented by the following set of equations:

$$\dot{x}_{1,M} = 1/C_{mM}[I_{extM} - g_{K_M}^{max} x_{2,M}^4 (x_{1,M} - E_{K_M}) - g_{Na_M}^{max} x_{3,M}^3 x_{4,M} (x_{1,M} - E_{Na_M}) - g_{l_M} (x_{1,M} - E_{L_M})]$$

$$\dot{x}_{2,M} = \alpha_n(x_{1,M})(1 - x_{2,M}) - \beta_n(x_{1,M})x_{2,M},$$

$$\dot{x}_{3,M} = \alpha_m(x_{1,M})(1 - x_{3,M}) - \beta_m(x_{1,M})x_{3,M},$$

$$\dot{x}_{4,M} = \alpha_h(x_{1,M})(1 - x_{4,M}) - \beta_h(x_{1,M})x_{4,M},$$

and the slave system is proposed to be governed by the equations:

$$\begin{aligned} \dot{x}_{1,S} = 1/C_{mS}[I_{extS} - g_{K_S}^{max} x_{2,S}^4 (x_{1,S} - E_{K_S}) - g_{Na_S}^{max} x_{3,S}^3 x_{4,S} (x_{1,S} - E_{Na_S}) - g_{l_S} (x_{1,S} - E_{L_S}) \\ + C_0(x_{1,M} - x_{1,S}), \end{aligned} \quad (2.45)$$

$$\dot{x}_{2,S} = \alpha_n(x_{1,S})(1 - x_{2,S}) - \beta_n(x_{1,S})x_{2,S},$$

$$\dot{x}_{3,S} = \alpha_m(x_{1,S})(1 - x_{3,S}) - \beta_m(x_{1,S})x_{3,S},$$

$$\dot{x}_{4,S} = \alpha_h(x_{1,S})(1 - x_{4,S}) - \beta_h(x_{1,S})x_{4,S},$$

where the added term $C_0(x_{1,M} - x_{1,S})$ in Eq. (2.45) represents a feedback synchronization force. Normally the parameters such as C_m , $g_{K_M}^{max}$, $g_{Na_M}^{max}$, g_L , E_{Na} , E_K and E_L of the slave

neurons are reduced by very small percentage to keep the two neurons asynchronous, so that they can not “share time solutions”. The term C_0 is interpreted as a synaptic like control current where $C_0 C_{m_M}$ is a constant synaptic conductance.

By solving these coupled differential equations with proper selection of parameters and external current the desynchronized spiking patterns of master and slave system which can be seen to have transition to a regularly synchronized state of the action potentials using control action [149].

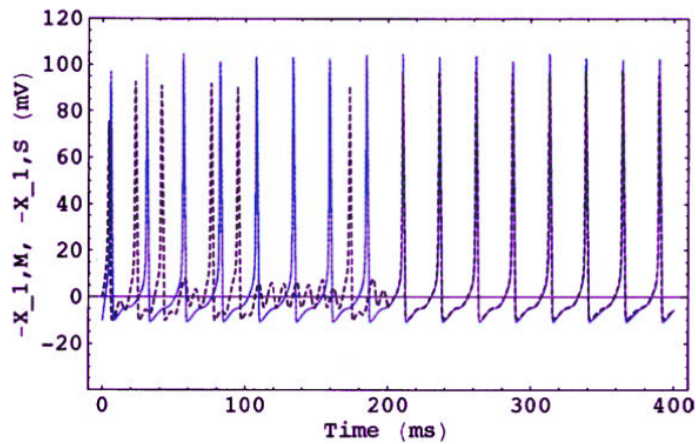


Figure 2.17: Spiking patterns of the master (solid line) and slave (dashed line) systems for the action potentials in desynchronized and synchronized states. The forcing functions amplitude and frequency parameters as specified in the text $I_{ext_M}(t) = 2.58 \sin(0.245t)$; $I_{ext_S} = \sin(0.715t)$. Source: Reference [149].

Bibliography

- [1] www.pmgbiology.files.wordpress.com
- [2] <https://courses.lumenlearning.com/biology1/chapter/the-cell-membrane/>
- [3] Waxman SG and Zamponi GW, Regulating excitability of peripheral afferents, emerging ion channel targets. *Nature Neuroscience*, 17, 15 (2014).
- [4] Hille, B., *Ionic channels of excitable membranes*. 2nd edition, Sinauer Associates, Sunderland, Mass (1992).
- [5] Chang G., Spencer RH., Lee AT., Barclay MT. and Rees DC., Structure of the MscL Homolog from mycobacterium tuberculosis, a gated mechanosensitive ion channel. *Science*, 282, 2220 (1998).
- [6] Schrempf H., Schmidt O., Kummerlen R., Hinnah S., Muller D., Betzler M., Steinkamp T. and Wagner R., A prokariotic potassium ion channel with two predicted transmembrane segments from *Streptomyces lividans*. *Embo J.*, 14, 5170 (1995).
- [7] Cuello L., Romero JG., Cortes DM. and Perozo E., pH-dependent gating in the *Streptomyces lividans* K⁺ channel. *Biochemistry*, 37, 3229 (1998).
- [8] <http://hyperphysics.phy-astr.gsu.edu/hbase/Biology/actpot.html>
- [9] Hodgkin AL. Evidence for electrical transmission in nerve Part I. *J Physiol.*, 90,183 (1937)., Hodgkin AL. Evidence for electrical transmission in nerve Part II. *J. Physiol.*, 90, 211 (1937), A. Huxley, From overshoot to voltage clamp, *Trends in Neurosciences*, 25, 553 (2002).
- [10] Hodgkin, AL., Huxley, AF. and Katz, B. Measurement of current-voltage relations in the membrane of the giant axon of *Loligo*. *J. Physiol.* 116, 424 (1952), Hodgkin, AL. and Huxley, AF. The components of membrane conductance in the giant axon of *Loligo*. *J. Physiol.* 116, 473 (1952), Hodgkin, AL. and Huxley, AF. Currents carried by sodium and potassium ions through the membrane of the giant axon of *Loligo*. *J. Physiol.* 116, 449 (1952), Hodgkin, AL. and Huxley, AF. The dual effect of membrane potential on sodium conductance in the giant axon of *Loligo*. *J. Physiol.* 116, 497 (1952), Hodgkin, AL. and Huxley, AF. A quantitative description of membrane

- current and its application to conduction and excitation in nerve. *J. Physiol.* 117, 500 (1952).
- [11] Catterall, WA., Goldin, AL. and Waxman, SG. International Union of Pharmacology. XLVII. Nomenclature and structure function relationships of voltage-gated sodium channels. *Pharmacol. Rev.*, 57, 397 (2005).
- [12] Messner, DJ. and Catterall, WA. The sodium channel from rat brain. Separation and characterization of subunits. *J. Biol. Chem.*, 260, 10597 (1985).
- [13] Yu, FH., et al. Sodium channel beta4, a new disulfide linked auxiliary subunit with similarity to beta2. *J Neurosci.*, 23, 7577 (2003).
- [14] Herzog, RI., Liu, C., Waxman, SG. and Cummins, TR. Calmodulin binds to the C terminus of sodium channels Nav1.4 and Nav1.6 and differentially modulates their functional properties. *J. Neurosci.*, 23, 8261 (2003).
- [15] Okuse, K., et al. Annexin II light chain regulates sensory neuron specific sodium channel expression. *Nature*, 417, 653 (2002).
- [16] Patino, GA. and Isom, LL. Electrophysiology and beyond, multiple roles of Na⁺ channel beta subunits in development and disease. *Neurosci. Lett.*, 486, 53 (2010).
- [17] , Frank H., and William A. Catterall. Overview of the Voltage Gated Sodium Channel Family. *Genome Biology*, 4, 207 (2003).
- [18] Payandeh, J., Scheuer, T., Zheng, N., Catterall, W. A. The crystal structure of a voltage-gated sodium channel. *Nature*, 475 (7356), 353 (2011).
- [19] Lipkind, GM., and Fozzard, HA. Voltage-gated Na Channel Selectivity, The Role of the Conserved Domain III Lysine Residue. *J Gen Physiol.*,131, 523 (2008).
- [20] West, JW., et al. A cluster of hydrophobic amino acid residues required for fast Na(+) -channel inactivation. *Proc. Natl. Acad. Sci. U.S.A* 89, 10910 (1992).
- [21] Catterall, WA. From Ionic Currents to Molecular Mechanisms, The Structure and Function of Voltage-Gated Sodium Channels, *Neuron*, 26, 13 (2000).
- [22] Part:1) www.youtube.com/watch?v=QnQQkWxAKwI and Part:2) www.youtube.com/watch?v=hfXGsJCOC9A.
- [23] <http://slideplayer.com/slide/5809424/>
- [24] Payandeh, J., Gamal, T. M., Scheuer, T., Zheng, N., Catterall, WA. Crystal structure of a voltage-gated sodium channel in two potentially inactivated states. *Nature*, 486 (7401), 135 (2012).
- [25] Zhang, X., Ren, W., DeCaen, P., Yan, C., Tao, X., Tang, L., Wang, J., Hasegawa, K., Kumasaka, T., He, J., Wang, J., Clapham, DE., Yan, N. Crystal structure of an orthologue of the NaChBac voltage-gated sodium channel. *Nature*, 486 (7401), 130 (2012).

- [26] McCusker, EC., Bagnieris, C., Naylor, CE., Cole, AR., D'Avanzo, N., Nichols, CG., Wallace, BA. Structure of a bacterial voltage-gated sodium channel pore reveals mechanisms of opening and closing. *Nature Commun.*, 3, 1102 (2012).
- [27] Catterall, WA. Structure and function of voltage-gated sodium channels at atomic resolution. *Exp. Physiol.*, 99, 35 (2014).
- [28] Shen, H., et. al. Structure of a eukaryotic voltage-gated sodium channel at near-atomic resolution, H. Shen et al., *Science* 10.1126/science.aal4326 (2017).
- [29] Bush, P. and Sejnowski TJ. Simulations of a reconstructed cerebellar Purkinje cell based on simplified channel kinetics. *Neural Computation*, 3, 321 (1991).
- [30] Destexhe, A., Mainen, ZF. and Sejnowski, TJ. Synthesis of models for excitable membranes, synaptic transmission and neuromodulation using a common kinetic formalism. *J. Computational Neuroscience*, 1, 195 (1994) .
- [31] <http://www.iuphar.org/>
- [32] Isom, LL., et al. Primary structure and functional expression of the beta 1 subunit of the rat brain sodium channel. *Science*, 256 (5058), 839 (1992).
- [33] Goldin, AL. ,Mechanisms of sodium channel inactivation, *Current Opinion in Neurobiology*, 13, 284 (2003).
- [34] Vassilev, PM., Scheuer, T., Catterall, WA. Identification of an intracellular peptide segment involved in sodium channel inactivation. *Science*, 241, 1658 (1988).
- [35] Vassilev, P., Scheuer, T., Catterall, WA. Inhibition of inactivation of single sodium channels by a site directed antibody. *Proc. Natl. Acad. Sci. USA.*, 86, 8147 (1989).
- [36] Stuhmer, W., et al. Structural parts involved in activation and inactivation of the sodium channel. *Nature.*, 339, 597 (1989).
- [37] Eaholtz, G., Scheuer, T., Catterall, WA. Restoration of inactivation and block of open sodium channels by an inactivation gate peptide. *Neuron*, 12, 1041 (1994).
- [38] Kellenberger, S., West, JW., Catterall, WA., Scheuer, T. Molecular analysis of potential hinge residues in the inactivation gate of brain type IIA Na + channels. *J. Gen. Physiol.*, 19,607 (1997).
- [39] S West, JW, Scheuer, T, Catterall, WA. Molecular analysis of the putative inactivation particle in the inactivation gate of brain type IIA Na + channels. *J Gen Physiol.*, 109,589 (1997).
- [40] Rohl, CA., Boeckman, FA., Baker, C., Scheuer, T., Catterall, WA., Klevit RE. Solution structure of the sodium channel inactivation gate. *Biochemistry.*, 38, 855 (1999).
- [41] Adelman, WJ Jr, Palti, Y. The effects of external potassium and long duration voltage conditioning on the amplitude of sodium currents in the giant axon of the squid, *Loligo pealei*. *J. Gen. Physiol.*, 54, 589 (1969).

- [42] Rudy, B. Slow inactivation of the sodium conductance in squid giant axons. Pronase resistance. *J Physiol (Lond.)*, 283,1 (1978).
- [43] Vilin, YY., Fujimoto, E., Ruben, PC. A single residue differentiates between human cardiac and skeletal muscle Na⁺ channel slow inactivation. *Biophys. J.*, 80, 2221 (1999).
- [44] Pavlov, E., et al. The pore, not cytoplasmic domains, underlies inactivation in a prokaryotic sodium channel. *Biophys J.*, 89,232 (2005).
- [45] Zhao, .Y, Yarov -Yarovoy, V., Scheuer, T., Catterall, WA. A gating hinge in Na⁺ channels, a molecular switch for electrical signaling. *Neuron.*, 41, 859 (2004).
- [46] Payandeh, J. et al. Crystal structure of a voltage- gated sodium channel in two potentially inactivated states. *Nature.*, 486, 135 (2012).
- [47] Zhang, X., et al. Crystal structure of an orthologue of the NaChBac voltage-gated sodium channel. *Nature.*, 486, 130 (2012).
- [48] Aldrich, RW. Fifty years of inactivation. *Nature* 411, 643 (2001).
- [49] Kurata, HT. and Fedida, DA. structural interpretation of voltage-gated potassium channel inactivation. *Prog. Biophys. Mol. Biol.* 92, 185 (2006).
- [50] Bean, BP. Sodium channel inactivation in the crayfish giant axon. Must channels open before inactivating? *Biophys. J.* 35, 595 (1981).
- [51] Horn, R., Patlak, J. and Stevens, CF. Sodium channels need not open before they inactivate. *Nature*, 291, 426 (1981).
- [52] Horn, R. and Vandenberg, CA. . Statistical properties of single sodium channels. *J. Gen. Physiol.*, 84, 505 (1984).
- [53] Bahring, R. and Covarrubias, M. Mechanisms of closed-state inactivation in voltage gated ion channels, *J. Physiol.* 589, 461 (2011).
- [54] Aldrich, RW. and Stevens, CF. Inactivation of open and closed sodium channels determined separately. *Cold Spring Harb. Symp. Quant. Biol.*, 48, 147 (1983).
- [55] Kuo, CC. and Bean, BP. Na⁺ channels must deactivate to recover from inactivation. *Neuron* 12, 819 . (1994).
- [56] Patlak, J. Molecular kinetics of voltage-dependent Na⁺ channels. *Physiol. Rev.*, 71, 1047 (1991).
- [57] Armstrong, CM. Na channel inactivation from open and closed states. *Proc. Natl. Acad. Sci. USA* 103, 17991 (2006).
- [58] Catterall, WA. Structure and Function of Voltage-Gated Sodium Channels at Atomic Resolution, *Exp. Physiol.*, 99, 35 (2014).
- [59] Ragsdale, DS., McPhee, JC., Scheuer, T., Catterall, WA. Molecular determinants of state -dependent block of sodium channels by local anesthetics. *Science*, 265, 1724 (1994).

- [60] Wang, GK., Quan, C., Wang, S. A common local anesthetic receptor for benzocaine and etidocaine in voltage-gated mu1 Na⁺ channels. *Pflugers Arch.*, 435, 293 (1998).
- [61] Yarov-Yarovoy, V., Baker, D., Catterall, WA. Voltage sensor conformations in the open and closed states in ROSETTA structural models of K⁺ channels. *Proc. Natl. Acad. Sci. USA*, 103, 7292 (2006).
- [62] Catterall, WA. and Swanson, TM., Structural Basis for Pharmacology of Voltage-Gated Sodium and Calcium Channels, *Mol. Pharmacol.* 88, 141 (2015).
- [63] Catterall, WA. Common modes of drug action on Na⁺ channels, local anesthetics, antiarrhythmics, and anticonvulsants. *Trends Pharmacol. Sci.* 8, 57 (1987).
- [64] Xie, XM., Garthwaite, J. State-dependent inhibition of Na⁺ currents by the neuroprotective agent 619C89 in rat hippocampal neurons and in a mammalian cell line expressing rat brain type IIA Na⁺ channels. *Neuroscience* 73, 951 (1996).
- [65] Hille, B. Local anesthetics, hydrophilic and hydrophobic pathways for the drug-receptor reaction. *J. Gen. Physiol.* 69, 497 (1977).
- [66] Tikhonov, DB. and Zhorov, BS. Mechanism of sodium channel block by local anesthetics, antiarrhythmics, and anticonvulsants, *J Gen Physiol.*, 149, 465 (2017).
- [67] George Jr., AL. Inherited disorders of voltage-gated sodium channels, *J. Clin. Invest.*, 115, 1990 (2005).
- [68] Meola, G. and Sansone, V. Therapy in myotonic disorders and in muscle channelopathies [review]. *Neurol. Sci.* 21, S953 (2000).
- [69] Jackson, CE., Barohn, RJ, and Ptacek, LJ. Paramyotonia congenita, abnormal short exercise test, and improvement after mexiletine therapy. *Muscle Nerve.* 17, 763 (1994).
- [70] Rosenfeld, J., Sloan -Brown, K., and George, AL., Jr. A novel muscle sodium channel mutation causes painful congenital myotonia. *Ann. Neurol.* 42,811 (1997).
- [71] Priori, SG., et al. Association of long QT syndrome loci and cardiac events among patients treated with beta-blockers. *JAMA.* 292, 1341 (2004).
- [72] Wang, DW., Yazawa, K., Makita, N., George, AL., Jr., and Bennett, PB. Pharmacological targeting of long QT mutant sodium channels. *J. Clin. Invest.* 99,1714 (1997).
- [73] Abriel, H., Wehrens, X.H., Benhorin, J., Kerem, B., and Kass, R.S. Molecular pharmacology of the sodium channel mutation D1790G linked to the long -QT syndrome. *Circulation.* 102, 921 (2000).
- [74] Glatzer, KA., et al. Effectiveness of sotalol treatment in symptomatic Brugada syndrome. *Am. J. Cardiol.* 93, 1320 (2004).

- [75] Liao, WP., Shi, YW., Long, YS., Zeng, Y., Li, T., et al. Partial epilepsy with antecedent febrile seizures and seizure aggravation by antiepileptic drugs, associated with loss of function of Na V 1.1. *Epilepsia* 51,1669 (2010).
- [76] Miller, IO., Sotero de Menezes, MA. 2007 (2011). SCN1A-related seizure disorders. In *GeneReviews TM*, ed. RA Pagon, MP Adam, TD Bird, et al. Seattle, Univ. Wash. <http://www.ncbi.nlm.nih.gov/books/NBK1318/>
- [77] Chiron, C. Current therapeutic procedures in Dravet syndrome. *Dev. Med. Child Neurol.* 53, 16 (2011).
- [78] Lynch, BA., Lambeng, N., Nocka, K., Kensel-Hammes, P., Bajjalieh, SM., et al. The synaptic vesicle protein SV2A is the binding site for the antiepileptic drug levetiracetam. *Proc. Natl. Acad. Sci. USA*, 101, 9861 (2004)
- [79] Clancy, CE., Zheng IZ. and Rudy, Y. Pharmacogenetics and anti arrhythmic drug therapy, a theoretical investigation, *Am. J. Physiol. Heart. Circ. Physiol.*, 292, H66 (2007).
- [80] Clancy, CE. and Rudy, Y. Linking a genetic defect to its cellular phenotype in a cardiac arrhythmia, *Nature*, 400, 566, 1999.
- [81] Clancy, CE. and Rudy, Y. Na⁺ channel mutation that causes both Brugada and Long-QT Syndrome phenotypes, A simulation study of mechanism, *Circulation*, 105,1208 (2002).
- [82] Huxley, A. From overshoot to voltage clamp, *Trends in Neurosciences*, 5, 553 (2002).
- [83] Kandel, E., Schwartz, J. and Jessell, T. *Principles of Neural Science*, (4th ed.), McGraw-Hill. 152, New York (2012). bear
- [84] Hamill, OP A., Marty, E. Neher, B. Sakmann and Sigworth, F.J. Improved patch-clamp techniques for high-resolution current recording from cells and cell free membrane patches, *Pflugers Archiv Euro. J. Physiol.*, 391, 85 (1981).
- [85] S. R. De. Groot and P. Mazur, *Non-equilibrium Thermodynamics*, North-Holland Publ. Comp., Amsterdam (1951).
- [86] Kargol, A., Hosein, A-Sooklal, Constantin, L. and Przystalski, M. Application of oscillating potentials to the Shaker potassium channel., *Gen. Physiol. Biophys.*, 3, 53 (2004).
- [87] Millonas, MM. and Hanck, DA. Nonequilibrium response spectroscopy of voltage-sensitive ion channel gating, *Biophys. J.*, 74, 210 (1998).
- [88] Kargol, A., Smithz, B. and Millonas, MM. Applications of nonequilibrium response spectroscopy to the study of channel gating. *Experimental design and optimization*, *J. theor. Biol.*, 18, 239 (2002).
- [89] Hosein-Sooklal, A. and Kargol, A. Wavelet Analysis of Nonequilibrium Ionic Currents in Human Heart Sodium Channel (hH1a), *J Membr. Biol.*, 188, 199 (2002).

- [90] Schnakenberg, J. Network theory of microscopic and macroscopic behavior of master equation systems *Rev. Mod. Phys.* 48, 571 (1976).
- [91] Jiu -Li, L., Van den Broeck, C. and Nicolis, G. Stability criteria and fluctuations around nonequilibrium states, *Z. Phys. B, Condens. Matter* 56, 165 (1984).
- [92] Esposito, M., Harbola, U. and Mukamel, S. Entropy fluctuation theorems in driven open systems, Application to electron counting statistics, *Phys. Rev. E* 76, 031132 (2007).
- [93] Gaspard, P. Time -Reversed Dynamical Entropy and Irreversibility in Markovian Random Prozesse, *J. Stat. Phys.* 117, 599 (2004).
- [94] Ge, H. Extended forms of the second law for general time dependent stochastic processes, *Phys. Rev. E* 80, 021137 (2009).
- [95] Ge, H. and Qian, H. Physical origins of entropy production, free energy dissipation, and their mathematical representations *Phys. Rev. E* 81, 051133 (2010).
- [96] Seifert, U. Entropy Production along a Stochastic Trajectory and an Integral Fluctuation Theorem, *Phys. Rev. Lett.* 95, 040602 (2005).
- [97] Esposito, M. , Lindenberg, K. and Van den Broeck, C. Entropy production as correlation between system and reservoir, *New J. Phys.* 12, 013013 (2010).
- [98] Hatano, T. and Sasa, S. I. Steady-State Thermodynamics of Langevin Systems, *Phys. Rev. Lett.* 86, 3463 (2001).
- [99] Speck, T. and Seifert, U. Integral fluctuation theorem for the housekeeping heat, *J. Phys. A* 38, L581 (2005).
- [100] Zhou, W., Cayabyab, FS., Pennefather, PS., Schlichter, LC. and DeCoursey, TE. HERG-like K⁺ Channels in Microglia, *J. Gen. Physiol.* 111, 781 (1998).
- [101] Mannikko, R., Pandey, S., . Larsson, HP. and Elinder, F. Hysteresis in the voltage dependence of HCN channels, conversion between two modes affects pacemaker properties. *J. Gen. Physiol.* 125, 305 (2005).
- [102] Villalba-Galea CA. New insights in the activity of voltage sensitive phosphatases. *Cell Signal*, 24,1541 (2012) .
- [103] Villalba-Galea, CA. . Hysteresis in voltage-gated channels. *Channels*, 11(2), 140 (2017)
- [104] Bezanilla, F., Taylor, RE., Fernandez, JM. Distribution and kinetics of membrane dielectric polarization. One. Long -term inactivation of gating currents. *J. Gen. Physiol.* , 79, 21 (1982).
- [105] Bezanilla, F. How membrane proteins sense voltage. *Nat. Rev. Mol. Cell. Biol.*, 9, 323 (2008).
- [106] Bezanilla F. Voltage-gated ion channels. *IEEE Trans Nanobioscience*, 4, 34 (2005).

- [107] Brum, G., Rios, E. Intramembrane charge movement in frog skeletal muscle fibres. Properties of charge 2. *J Physiol.*, 387, 489 (1987).
- [108] Shirokov, R., Levis, R., Shirokova, N., Rios, E. Two classes of gating current from L-type Ca channels in guinea pig ventricular myocytes. *J. Gen. Physiol.*, 99,863 (1992).
- [109] Goodchild, SJ., Macdonald, LC., Fedida, D. Sequence of gating charge movement and pore gating in HERG activation and deactivation pathways. *Biophys J.*, 108, 1435 (2015).
- [110] Hull, CM., Sokolov, S., Van Slyke, AC., Claydon, TW. Regional flexibility in the S4-S5 linker regulates Herg channel closed state stabilization. *Pflugers. Arch.*, 466, 1911 (2014).
- [111] Tan, PS., Perry, MD., Ng, CA., Vandenberg, JI., Hill AP., Voltage-sensing domain mode shift is coupled to the activation gate by the N-terminal tail of hERG channels. *J. Gen. Physiol.*, 140, 293 (2012).
- [112] Baruscotti, M., Bottelli, G., Milanesi, R., DiFrancesco, JC., DiFrancesco, D. HCN-related channelopathies. *Pflugers. Arch.*, 460, 405 (2010).
- [113] Elinder, F., Mannikko, R., Pandey, S., Larsson, HP. Mode shifts in the voltage gating of the mouse and human HCN2 and HCN4 channels. *J. Physiol.*, 575, 417 (2006).
- [114] Mannikko, R., Pandey, S., Larsson, HP., Elinder, F. Hysteresis in the voltage dependence of HCN channels, conversion between two modes affects pacemaker properties. *J Gen Physiol.*, 125, 305 (2005).
- [115] Bruening-Wright, A., Larsson, HP. Slow conformational changes of the voltage sensor during the mode shift in hyperpolarization-activated cyclic nucleotide gated channels. *J Neurosci.*, 27,270 (2007).
- [116] Fologea, D., Krueger, E., Lee, R., Naglak, M., Mazur, YI., Henry, R., Salamo, GJ. Controlled gating of lysenin pores, *Biophys. Chem.* 146 25 (2010).
- [117] D. Fologea, E. Krueger, Y.I. Mazur, C. Stith, O. Yui, R. Henry, G.J. Salamo, Bi-stability, hysteresis, and memory of voltage-gated lysenin channels, *Biochim. Biophys. Acta* 1808 (2011) 2933-2939.
- [118] Colibus, L. De., et al. Structures of lysenin reveal a shared evolutionary origin for pore-forming proteins and its mode of sphingomyelin recognition, *Structure*, 20, 1498 (2012).
- [119] Das, B., Banerjee, K. and Gangopadhyay, G. Entropy hysteresis and nonequilibrium thermodynamic efficiency of ion conduction in a voltage-gated potassium ion channel, *Phys. Rev. E*, 86 , 061915 (2012).
- [120] Flyvbjerg, H., et al. Modeling hysteresis observed in the human erythrocyte voltage-dependent cation channel, *Acta Phys. Polon. B* 43 , 2117 (2012).

- [121] Gudowska, E., et al. Hysteresis in channel gating, Unsolved Problems of Noise and Fluctuations, UPoN 2002, Third Annual Conference, American Institute of Physics, 2002.
- [122] Pal, K. and Gangopadhyay, G., Nonequilibrium response of a voltage gated sodium ion channel and biophysical characterization of dynamic hysteresis, *Journal of Theoretical Biology*, 415, pp. 113 (2017).
- [123] Pustovoit, MA., Berezhkovskii, AM., Bezrukov, SM. Analytical theory of hysteresis in ion channels, Two-state model. *The Journal of Chemical Physics* 125, 194907 (2006).
- [124] Mueller, P. and Rudin, DO., *J. Theor. Biol.* 4, 268 (1963).
- [125] Ehrenstein, G., Lecar, H. and Nossal, R. *J. Gen. Physiol.* 55, 119 (1970).
- [126] Chua, LO., Sbitnev, VI . and Kim, H. Hodgkin-Huxley axon is made of memristors, *Int. J. Bifurcation Chaos*, 2, 1230011 (2012).
- [127] Chua, L. Memristor, Hodgkin -Huxley, and edge of chaos, *Nanotechnology*, 4 , 383001 (2013).
- [128] Sah, Mpd., Kim, H. and Chua, LO. Brains Are Made of Memristors, *IEEE circuits and systems magazine*,1531 (2014).
- [129] Chua, LO. Memristor -The missing circuit element *IEEE, Trans Circuit Theory*, 18, 507 (1971).
- [130] Chua, LO. The Fourth Element, *Proc. IEEE*, 100, 1920 (2012).
- [131] Riehle, A., Grun, S., Diesmann, M. Spike synchronization and rate modulation differentially involved in motor cortical function, *Science*, 278, 1950 (1997).
- [132] Montgomery, S.M., Buzsaki, G. Gamma oscillation dynamically couple hippocampal CA3 and CA1 regions during memory task performance, *PNAS*, 104, 14495 (2007) .
- [133] Hindmarsh, JL., Rose, RM. A model of neuronal bursting using three coupled first order differential equations, *Proc. R. Sco. Lond. B* 221 87 (1984) .
- [134] Dhamala, M., Viktor, KJ., Ding, MZ. Transitions to synchrony in coupled bursting neurons, *Phys. Rev. Lett.*, 92, 028101 (2004) .
- [135] Ozer, M., Uzuntarla, M., Perc, M. et al. , Spike latency and jitter of neuronal membrane patches with stochastic Hodgkin-Huxley channels, *J. Theor. Biol.* 261 83 (2009).
- [136] Gu, HG., Pan, BB., Chen, GR., Biological experimental demonstration of bifurcations from bursting to spiking predicted by theoretical models, *Nonlinear Dyn.*, 7 , 391 (2014).
- [137] Gu, HG., Pan, BB. A four dimensional neuronal model to describe the complex non-linear dynamics observed in the firing patterns of a sciatic nerve chronic constriction injury model, *Nonlinear Dyn.*, 81 2107 (2015) .

- [138] Majhi, S., Perc, M., Ghosh, D., Chimera states in uncoupled neurons induced by a multilayer structure, *Sci. Rep.* 6, 39033 (2016).
- [139] Wang, QY., Aleksandra, M., Perc M Taming desynchronized bursting with delays in the Macaque cortical network, *Chinese Phys. B* 20, 040504 (2011) .
- [140] Pikovsky, A., Roseblum, M., Kurths, J. Synchronization, A universal Concept in Nonlinear Sciences, Cambridge University Press, (2001) .
- [141] Singer, W., Gray, CM. Visual feature integration and the temporal correlation hypothesis. *Annu Rev Neurosci.*, 18, 555 (1995).
- [142] Bennett, MVL. Electrical transmission, a functional analysis and comparison with chemical transmission. In *Cellular Biology of Neurons*, vol. I, sec. I, Handbook of Physiology. The Nervous System, E.R. Kandel, ed. (Baltimore, MD, Williams and Wilkins), 357 (1977).
- [143] Perez Velazquez, JL., Carlen, PL. Gap junctions, synchrony and seizures. *Trends Neurosci.*, 23, 68 (2000).
- [144] Bennett, MVL. and Zukin, RS. Electrical Coupling and Neuronal Synchronization in the Mammalian Brain *Neuron*, 41, 495 (2004).
- [145] Gibson, JR., Beierlein, M., Connors, BW. Two networks of electrically coupled inhibitory neurons in neocortex. *Nature*, 402, 75 (1999).
- [146] Mugnaini, EFS., Vernadakis, A., editors. Cell junctions of astrocytes, ependyma, and related cells in the mammalian central nervous system, with emphasis on the hypothesis of a generalized functional syncytium of supporting cells, *Astrocytes*. New York, Academic, New York, 1986. 329 -371.
- [147] Schmitz, D., Schuchmann, S., Fisahn, A., Draguhn, A., Buhl, EH., Petrasch-Parwez, E., Dermietzel, R., Heinemann, U., Traub RD. Axo -axonal coupling a novel mechanism for ultrafast neuronal communication. *Neuron*, 31, 831 (2001).
- [148] www.studyblue.com
- [149] Cornejo-Perez, O. and Femat, R. Unidirectional synchronization of Hodgkin-Huxley neurons, *Chaos, Solitons and Fractals*, 25, 43 (2005).

Chapter 3

Chapter 3

Nonequilibrium Response And Dynamic Hysteresis Of A Voltage Gated Sodium Ion Channel

In this chapter we have studied the dynamic as well as the non-equilibrium thermodynamic response properties of voltage-gated Na-ion channel. Using sinusoidally oscillating external voltage protocol we have both kinetically and energetically studied the non-equilibrium steady state properties of dynamic hysteresis in details. We have introduced a method of estimating the work done associated with the dynamic memory due to a cycle of oscillating voltage. We have quantitatively characterized the loop area of ionic current which gives information about the work done to sustain the dynamic memory only for ion conduction, while the loop area of total entropy production rate gives the estimate of work done for overall gating dynamics. The maximum dynamic memory of Na-channel not only depends on the frequency and amplitude but it also depends sensitively on the mean of the oscillating voltage and here we have shown how the system optimize the dynamic memory itself in the biophysical range of field parameters. The relation between the average ionic current with increasing frequency corresponds to the nature of the average dissipative work done at steady state. It is also important to understand that the utilization of the energy from the external field can not be directly obtained only from the measurement of ionic current but also requires nonequilibrium thermodynamic study.

3.1 Introduction

The study of the voltage-gated sodium ion channel is still gaining intense attention in neuro-physiology as they play an important role in generation and propagation of the action potential [1,2]. A lot of effort [3] has been devoted to understand the individual channel-gating dynamics by fitting the experimentally measured ionic current with that of the theoretical one estimated from the suitable Markov model [4–9]. Experimentally, the ion channel kinetics is usually studied by the patch clamp technique and voltage clamp technique where the ionic currents during the relaxation of channel protein from one non-equilibrium state to its equilibrium state is measured [10–13]. However, in a nerve cell opening and closing of the voltage-gated ion channels occur completely at the non-equilibrium environment [14]. To understand more about the activity of channel proteins [15] in the non-equilibrium environment the non-equilibrium response spectroscopy [16,17] comes handy where energy is continuously supplied to the system from external sources using oscillating [18] or fluctuating voltage [19] protocol which forces the ion channel go far from its equilibrium and allow us to study its response characteristics in the non-equilibrium environment [16].

One of the most interesting non-equilibrium response activity of channel protein is the dynamic hysteresis which is detected by measuring the ionic current at different applied voltages. The special characteristic feature of dynamic hysteresis is that it vanishes at extreme adiabatic (very low frequency) and non-adiabatic (very high frequency) limits [20]. In the voltage-gated ion channel, it is developed when the period of the oscillating external voltage is comparable to the characteristic relaxation time of the conformational transitions between the corresponding Markov states which are responsible for the overall gating-dynamics of the channel protein [21–23]. Several kinetic as well as thermodynamic studies have been carried out by focusing their motivation to find out which external and internal factors controls the stability of the dynamic hysteresis on or how this dynamic memory is related to the biological memristor [24–26] and the corresponding circuit theory based studies of the shape and size [26] of the hysteresis curves. However, in this regard a basic question remains unresolved, namely, the inherent physical meaning of the dynamic hysteresis loop area of the ionic current versus voltage curve. To answer this basic question, several related questions come into the picture which are as follows: (I) The dynamic hysteresis is a signature of the dynamic memory developed in a system. Therefore, by observing the hysteretic nature of ionic current as a function of voltage, we can infer that the dynamic memory developed in an ion channel for ion conduction should be an inherent property of the channel protein. The ionic current is related only with the

open state probability of the channel protein. But the overall gating process of ion channel depends not only on the open state but it also depends on the several physiological states like closed, open and inactivated states [27,28] in Na channel. So a natural question arises whether the kinetically studied ionic current only carries the sufficient information about the memory capacity of channel protein for ion conduction or does it play a fractional role of the overall gating-dynamics? (II) If ionic current just represent partly, then how can we measure dynamic memory developed in the channel protein for the overall gating-process? (III) How this memory depends on the parameters of the external oscillating field *i.e.*, frequency, amplitude and the mean voltage? Is there any optimum amplitude, frequency and mean voltage where the dynamic hysteresis becomes maximum? (IV) What are the thermodynamic signatures of dynamical hysteresis and the physical interpretations of the loop areas? (V) How the ionic current at steady state is related to the dissipative work done in presence of oscillating voltage protocol?

To answer these questions, here we have studied the kinetic as well as the non-equilibrium thermodynamic response properties of a voltage-gated Na-ion channel by considering the sinusoidally oscillating external voltage protocol. A master equation has been constructed on the basis of the familiar nine-state Markov model of Na-ion channel of Vandenberg and Bezanilla [29] which is well established from subsequent other studies [18]. For completeness we have calculated the kinetic and thermodynamic properties of ion channel at constant voltage. For oscillating voltage case, we have thoroughly studied the inherent physical nature of the dynamic hysteresis observed in both kinetic and non-equilibrium thermodynamic response properties of the channel protein. We have also studied the relation between the average ionic current and the dissipative work done at steady state. An approximate analytical solution of the master equation has been provided for oscillating voltage at steady state to estimate the role of the inactivated states.

Layout of this chapter is as follows. In section (2) kinetic scheme of sodium channel master equation and various entropy production rates of nonequilibrium thermodynamics have been discussed. We have described constant voltage clamp technique in section (3). Nonequilibrium response to oscillating voltage protocol is studied in section (4). We have investigated the hysteresis and the dissipative work done at steady state in different subsections. In section (5) we have provided the approximate analytical expressions for qualitative understanding of the numerical results. In section (6) we have given a brief comparison of our results with another popular model of sodium channel. Finally, the chapter is concluded in section (7).

3.2 Master Equation and Nonequilibrium Thermodynamic Description

In this section at first we have described the nine state model of sodium channel and its corresponding master equation and rate parameters. Then the kinetic and nonequilibrium thermodynamic aspect of the channel subjected to constant and time dependent external voltage protocol have been discussed.

3.2.1 Kinetic scheme and master equation description

To describe the kinetics of the Na^+ ion channel, here we have considered the familiar nine state model proposed by Bezanilla and co-workers [29]. In this proposed model we have considered the data of human $\text{Na}_V1.5$ [17] of the sodium channel. Here the ion conducting state or open state is represented by P_5 , whereas the states, P_1 to P_4 are closed states and P_6 to P_8 are the inactivated states. At the resting potential (-70 mV), the most preferred state is P_0 . However, when depolarization occurs after passing through several sequential closed states, the channel goes to the open state and produces the macroscopic ionic current, $I(t)$ by in-fluxing of Na^+ ions into the cell. Then the channel enters into the inactivated states and the inward ionic current is terminated.

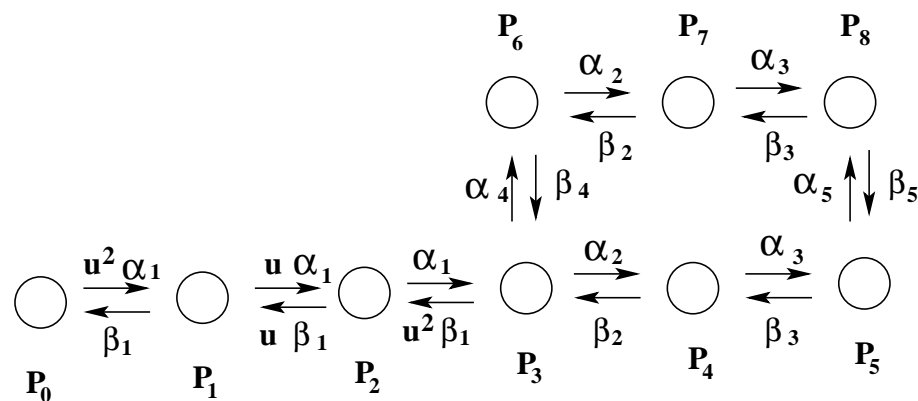


Figure 3.1: The nine state kinetic model [29] of sodium channel is shown here. At resting potential the channel is in P_0 state. During depolarisation, several conformational changes occur in channel protein and it goes from close states P_0 to P_4 , to open state, P_5 and subsequently it enters into the inactive states, P_6 , P_7 and P_8 .

The voltage-dependent forward and backward transition rates, $\alpha_n(V(t))$ and $\beta_n(V(t))$, respectively are given by

$$\alpha_n(V(t)) = \alpha_n(0) \exp \left[\frac{q_n e V(t) \delta_n}{k_B T} \right],$$

and

$$\beta_n(V(t)) = \beta_n(0) \exp \left[\frac{-q_n e V(t) (1 - \delta_n)}{k_B T} \right]. \quad (3.1)$$

Here q_n^\pm (s) are the gating charges involved with each forward and backward transitions, respectively. $\alpha_n(0)$ and $\beta_n(0)$ represents the forward and backward transitions at zero voltage, respectively with $k_B T/e = 24.4$ mV, where e = fundamental electric charge, δ_n is dimensionless fractional electrical distance ($0 < \delta_n < 1$), $u=1.2$, a parameter used in this model [17] and T is the absolute temperature.

The time evolution of the probabilities of the nine states can be written in terms of two general master equations. For convenience we have considered two indices, ‘‘A’’ and ‘‘I’’ which represent the active states (P_0 to P_5) and inactive states (P_6 to P_8), respectively. The master equation corresponding to the active state can be written as:

$$\begin{aligned} \frac{dP_A(i, t)}{dt} = & \omega_{(i-1)}^+(V(t))P_A(i-1, t) + \omega_{(i+1)}^-(V(t))P_A(i+1, t) - \omega_{(i)}^+(V(t))P_A(i, t) - \omega_{(i)}^-(V(t))P_A(i, t) \\ & + \delta_{3,i}[-l_1(V(t))P_A(i, t) + l_{-1}(V(t))P_I(2i, t)] \\ & + \delta_{5,i}[-l_2(V(t))P_A(i, t) + l_{-2}(V(t))P_I(i+3, t)], \end{aligned} \quad (3.2)$$

where $P_A(i, t)$ represents the probability of remaining in the i -th active state at time t . Similar sort of expression holds for inactive state master equation as

$$\begin{aligned} \frac{dP_I(i, t)}{dt} = & \omega_{(i-1)}^+(V(t))P_I(i-1, t) + \omega_{(i+1)}^-(V(t))P_I(i+1, t) - \omega_{(i)}^+(V(t))P_I(i, t) - \omega_{(i)}^-(V(t))P_I(i, t) \\ & + \delta_{6,i}[l_1(V(t))P_A(i/2, t) - l_{-1}(V(t))P_I(i, t)] \\ & + \delta_{8,i}[l_2(V(t))P_A(i-3, t) - l_{-2}(V(t))P_I(i, t)]. \end{aligned} \quad (3.3)$$

For active states with population $P_A(i, t)$, the value of i ranges from 0 to 5, whereas for inactive states, $i = 6, 7$ and 8 . $\omega_i^+(V(t))$ and $\omega_i^-(V(t))$ are designated as the forward and backward transition rates of i -th state. For example, for the state $P_A(3, t)$, the associated rates are $\omega_2^+ = \alpha_1$, $\omega_3^+ = \alpha_2$, $\omega_4^- = \beta_2$ and $\omega_3^- = u^2 \beta_1$ which can be found from the Fig. (3.1). Here $l_1 = \alpha_4$, $l_{-1} = \beta_4$, $l_2 = \alpha_5$ and $l_{-2} = \beta_5$. The parameters associated

with these nine coupled differential equations are given in the following TABLE I. At any instant of time, t the ionic current $I(t)$ is calculated by the following equation,

$$I(t) = g_0 g_V(t)(V(t) - V_r)P_5(t). \quad (3.4)$$

Here g_0 and g_V are experimentally fitted parameters describing the voltage dependence of the sodium ion conductance as described in the caption of the TABLE I.

n	$\alpha_n(0)(s^{-1})$	$\beta_n(0)(s^{-1})$	q_n	δ_n
1	4779	10.3	2.83	0.053
2	5045	12.1	3.16	0.5
3	1684	2360	0.077	0.78
4	19.8	*	*	0.12
5	800	59.8	0.16	0.33

Table 3.1: Model parameters are given here with $\beta_4(V) = \frac{\alpha_4(V)\beta_5(V)}{\alpha_5(V)}$, is a constraint to maintain microscopic reversibility [17]. The total gating charge of the model is 11.8 e. g_V is the instantaneous conductance, fitted by a third order polynomial, expressed as $g_V(t) = g_0 + g_1 V(t) + g_2 (V(t))^2 + g_3 (V(t))^3$, where unit of $g(V)$ is μS and $g_1 = -8.21 \times 10^{-4}$, $g_2 = -4.72 \times 10^{-6}$, $g_3 = 1.49 \times 10^{-8}$. $g_0 = 0.0169$ is the overall scaling factor representing the cell expression rate. These values are obtained from the fit used in the model to account for the instantaneous voltage dependence of the channel conductance [17]. V_r is the reversal potential for the sodium ion channel under study, usually 67.0 mV.

3.2.2 Nonequilibrium thermodynamic features of sodium channel

Here we have provided the nonequilibrium thermodynamic features of the sodium channel in terms of the entropy production rates. Here we have considered that the system remains in contact with the environment with temperature, T . We begin with the definition of system entropy [30] as,

$$S_{sys}(t) = -k_B \sum_{i=0} P_i(t) \ln P_i(t), \quad (3.5)$$

where k_B is the Boltzmann constant. The system entropy production rate (epr) is calculated to obtain the following expression,

$$\dot{S}_{sys}(t) = \frac{k_B}{2} \sum_{i,j} \left[q_{ij}(V(t))P_i(t) - q_{ji}(V(t))P_j(t) \right] \ln \left[\frac{P_i(t)}{P_j(t)} \right]. \quad (3.6)$$

Here, q_{ij} is the transition rate which converts the state from i to j . Similarly reverse transition occurs for q_{ji} . Now the system epr [31, 32] is defined as,

$$\dot{S}_{sys}(t) = \dot{S}_{tot}(t) - \dot{S}_{med}(t), \quad (3.7)$$

where $\dot{S}_{tot}(t)$ is total epr and $\dot{S}_{med}(t)$ is the medium epr, appearing due to entropy flux into the surroundings [33, 34] as follows,

$$\dot{S}_{tot}(t) = \frac{k_B}{2} \sum_{i,j} \left[q_{ij}(V(t))P_i(t) - q_{ji}(V(t))P_j(t) \right] \ln \left[\frac{q_{ij}(V(t))P_i(t)}{q_{ji}(V(t))P_j(t)} \right], \quad (3.8)$$

and,

$$\dot{S}_{med}(t) = \frac{k_B}{2} \sum_{i,j} \left[q_{ij}(V(t))P_i(t) - q_{ji}(V(t))P_j(t) \right] \ln \left[\frac{q_{ij}(V(t))}{q_{ji}(V(t))} \right]. \quad (3.9)$$

Now, for the constant voltage case all the transition rates associated with these eprs are time independent and for oscillating voltage case they are functions of both voltage and time. In addition one should note that when detailed balance holds the total epr vanishes i.e, $\dot{S}_{tot} = 0$ as $q_{ij}(t)P_i(t) = q_{ji}(t)P_j(t)$, which is clearly a case of equilibrium situation where all other eprs are also zero. On the contrary when $\dot{S}_{tot} > 0$, it should go to a nonequilibrium steady state which demands the situation of broken detailed balance, i.e, $q_{ij}(t)P_i(t) \neq q_{ji}(t)P_j(t)$.

There is an another way [35] of expressing total epr as the sum of adiabatic($\dot{S}_a(t)$) and nonadiabatic($\dot{S}_{na}(t)$) contributions which is relevant to our work having time dependent external perturbation that breaks the detailed balance. The expressions are as follows,

$$\dot{S}_a(t) = \frac{k_B}{2} \sum_{i,j} \left[q_{ij}(V(t))P_i(t) - q_{ji}(V(t))P_j(t) \right] \ln \left[\frac{q_{ij}(t)P_i^{st}(V_t)}{q_{ji}(t)P_j^{st}(V_t)} \right], \quad (3.10)$$

and

$$\dot{S}_{na}(t) = \frac{k_B}{2} \sum_{i,j} \left[q_{ij}(V(t))P_i(t) - q_{ji}(V(t))P_j(t) \right] \ln \left[\frac{P_i(t)P_i^{st}(V_t)}{P_j(t)P_j^{st}(V_t)} \right], \quad (3.11)$$

where $P_i^{st}(V_t)$ is the stationary or equilibrium probability the system would have if the driving voltage was frozen at time t at the value, V_t . For very slow driving i.e when the system is in the adiabatic limit the system at all times remains in steady state with $P_i^{ss}(t) \rightarrow P_i^{st}(V_t)$ where $P_i^{ss}(V_t)$ is the steady state probability and consequently the nonadiabatic epr becomes zero. However, for finite rate of driving, the nonadiabatic epr is nonzero. The net flux, $J(t)$ is given by $J(t) = \sum_{i,j} q_{ij}(t)P_i(t) - q_{ji}(t)P_j(t)$.

3.3 Voltage Clamp Dynamics

Generally the voltage clamp technique is used by electro-physiologists to measure the ionic currents through the membrane of excitable cells while holding the membrane voltage at a set level. A series of voltage ramp can be used which allows the membrane voltage to be altered independently of the ionic currents allowing to study the current-voltage relationship of the voltage gated sodium channel (VGSC). In subsection 3.1 we have shown the response of channel in presence of constant voltage in terms of ionic current, probabilities of different states, steady state current and entropy production rates. In subsection 3.2 we have given the steady state expression of the open state probability using detailed balance condition. For the constant voltage case (between two successive applied voltage) the transition rates become time independent as the voltage is kept constant throughout the time course of study.

3.3.1 Kinetic studies and equilibrium features

In this subsection we have studied the constant voltage case using numerical computation using Runge-Kutta algorithm for solving coupled differential equations with $P_0=1$ as initial condition. All the rate constants and the parameters are already given in previous section. Here, we have studied the transient and steady state probabilities, macroscopic current and system, medium and total entropy production rates. From Fig. 3.2(a) it is important to note that with the onset of depolarization, ionic current initially increases with influx of sodium ionic current inside the cell. After passing through a maximum (since $I(t)$ is -ve, as more negative value implies more influx of current into the cell) ionic current decreases and attains a steady value. So the first part of increasing ionic current is called the activation and the decreasing part of ionic current is called inactivation. It is also observed from the graphs of ionic current that with the increasing depolarization, inactivation occurs in a faster rate. Now, from the Fig. 3.2(c) and (d) it is observed that the magnitude of open state probability and the ionic current at steady state is very low indicating that the inactivation has already occurred, as the inactive states, (P_6, P_7, P_8) are much more populated than the open state, P_5 as observed from Fig. 3.2(b), where $V = -30$ mV is taken as an example. Here one should note that the sodium channel works extremely fast as observed from the kinetic picture of the ionic current and probability curves which says it almost immediately activates and then deactivates by completing its task within a few milliseconds which is actually needed for the instantaneous faster generation of action potential.

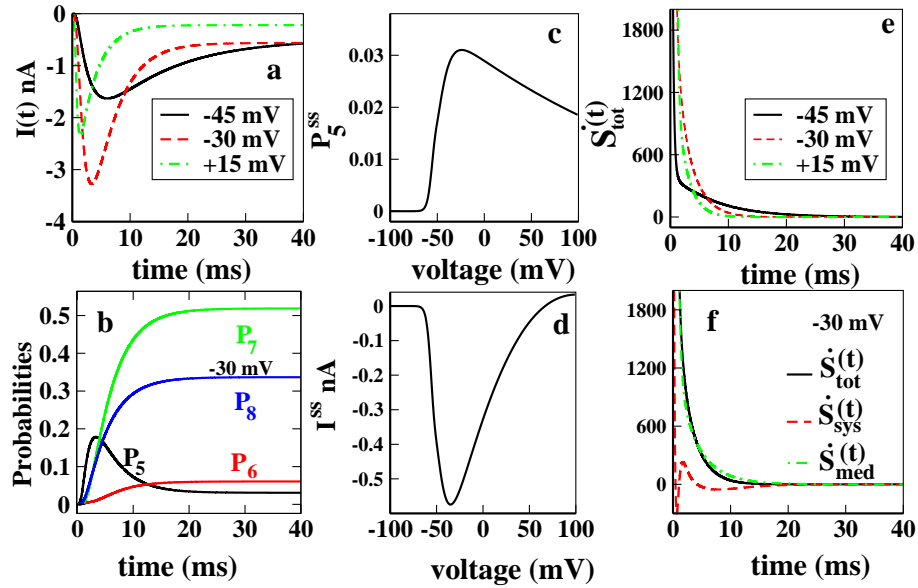


Figure 3.2: Constant voltage case and the equilibrium features are shown in this figure. In Fig. (a) Ionic current at depolarizations $V = -45, -30, +15$ mV at constant is plotted, in Fig. (b) open state probability and three inactive state probabilities are shown in -30 mV. In Fig. (c) steady state probabilities of open state at different voltage has been plotted. In Fig (d) corresponding steady state ionic currents at different voltages are shown. Fig (e) shows that for all depolarisations mentioned in Fig. (a) the total epr ultimately vanishes. In Fig. (f) all three eprs are shown for -30 mV which shows all eprs vanish ultimately. The unit of entropy production rates are $\mathbf{JK}^{-1}\mathbf{S}^{-1}$.

Next we have studied the thermodynamics of the system in terms of three entropy production rates in presence of constant voltage. As seen from the Fig. 3.2(e) that for constant external voltage, (V_t) the system quickly reaches to equilibrium suggested by vanishing $\dot{S}_{tot}(t)$ which also satisfies the detailed balance condition i.e $J^{st} = 0 = q_{ij}(V_t)P_i^{st}(V_t) - q_{ji}(V_t)P_j^{st}(V_t)$. Thus from equation (3.10) and (3.11) we can write,

$$\dot{S}_{tot}^{st} = 0 = \dot{S}_a^{st} = \dot{S}_{na}^{st}. \quad (3.12)$$

Thus if the voltage is fixed at V_t the ion channel ultimately relaxes to equilibrium satisfying $J^{st} = 0$. Thus it is important to note that even when the voltage is time dependent, as $J^{st} = 0$ we shall always have $\dot{S}_a(t) = 0$ for all values of t as seen from equation (3.10) for ion channel. The corresponding \dot{S}_{sys} and \dot{S}_{med} also vanishes independently confirming that the system ultimately equilibrates or adjusts itself with the constant external perturbation as seen from Fig. 3.2(f).

3.3.2 Steady state solution

Here we have estimated the open state probability, P_5^{st} at steady state for constant voltage which indeed allow us to study the steady state current, I^{st} as usually observed in the experiments. At constant voltage case the system reaches at equilibrium. With each different voltage the equilibrium steady state alters and attains new value holding detailed balance. Using the detailed balance and normalizing condition i.e., $\sum_{i=0}^{i=8} P_i^{st} = 1$, we obtain the steady state solution of the probabilities. The expression of the P_5 then becomes,

$$P_5 = \frac{1}{\frac{\beta_2\beta_3}{\alpha_2\alpha_3}(x+y) + \frac{\beta_3}{\alpha_3} + z}, \quad (3.13)$$

where, $x = \frac{u^2\alpha_1\beta_1(\beta_1+\alpha_1)+\beta_1^3}{\alpha_1^3}$, $y = (1 + \gamma_1 + \frac{\gamma_1\alpha_2}{\alpha_3+\beta_2})$, $z = (1 + \gamma_2 + \frac{\gamma_2\beta_3}{\alpha_3+\beta_2})$, $\gamma_1 = \alpha_4/\beta_4$, $\gamma_2 = \alpha_5/\beta_5$. The open state probability of sodium channel does not show powered Boltzmann Distribution [20] but arises in more complex way as shown in Fig. 3.2(c) and the corresponding ionic current is calculated using the expression $I^{st} = g_0g_V(V - V_p)rP_5^{st}$ and the nature of steady state ionic current is shown in Fig. 3.2(d).

3.4 Nonequilibrium Response To Oscillating Voltage Protocol

Motivated by the experimental work of Kargol *et al.* [16], here we have theoretically studied kinetic as well thermodynamic response properties of Na^+ channel by considering the sinusoidal oscillating voltage protocol. This sort of nonequilibrium response spectroscopic technique provides new aspects of ion channel gating kinetics that standard stepped-potential protocols can not provide [19]. Comparing the models of Vandenberg-Bezanilla [29] and Millonas-Hanck [17] for the same system(i.e, human cardiac isoform, hH1a) Kargol [19] showed that both the models fit with the experimental data for the stepped-potential protocols equally well. For custom designed fluctuating voltage pulses that drives the protein molecule far from its equilibrium state, both the models fit the experimental data [19] almost equally well. Therefore we selected this model for studying nonequilibrium response using oscillating voltage protocol.

In this section, at first we have studied the time-dependent variation of the response properties of Na-channel. Then the kinetic and thermodynamic response properties of channel protein have been discussed at steady state. Here we mainly concentrate our discussion to explain the significance of the kinetic and thermodynamic hysteresis loop

areas. Besides in this sub-section we have also discussed about the determination of the optimum frequency, mean voltage as well as the amplitude of the external oscillating voltage where the magnitude of the hysteresis loop area becomes maximum. Finally, with a rigorous thermodynamic analysis we have shown how the ionic current is related to the dissipative work done by the system at steady state as a function of frequency of external protocol with varying amplitudes and mean voltages.

3.4.1 Nonequilibrium response dynamics

Here the sinusoidal external voltage is expressed as $V(t) = V_0 + A \sin(\omega t)$ where $V_0 = -70$ mV is the mean voltage around which it oscillates with amplitude, $A=45$ mV and frequency, ω . Here the transition probabilities evolve dynamically depending on the time dependent voltage, $V(t)$. First we have studied the transient behaviour of the system in Fig. (3.3). In Fig. 3.3(a), (b) and (c) we have plotted $I(t)$, $P_5(t)$ and $\dot{S}_{tot}(t)$ as a function of time for two different frequency values, 50 and 100 Hz of the the oscillating voltage. In Fig. 3.3(d), all the entropy production rates, $\dot{S}_{tot}(t)$, $\dot{S}_m(t)$ and $\dot{S}_{sys}(t)$ are drawn as a function of time for a particular frequency, 100 Hz. Similarly the time variation of $P_6(t)$, $P_7(t)$ and $P_8(t)$ are plotted at frequency, 50 Hz. The common trend in all these figures is that all the kinetic and thermodynamic response properties reach at steady state within a very small time interval and start oscillating around a steady value which is consistent with the experiments done earlier [36]. It is shown that with increasing frequency values, the steady state reaches faster. From Fig. 3.3(c), we observe that the total epr at these two frequencies oscillate around a steady value whose magnitude is always greater than zero indicating the non-equilibrium steady state (NESS) due to non zero flux, $J^{ss}(t) = q_{ij}(V(t))P_i^{ss}(V(t)) - q_{ji}(V(t))P_j^{ss}(V(t)) \neq 0$. Thus at NESS the dissipation function, $\dot{S}_{tot}^{ss}(t) = \dot{S}_{na}^{ss}(t) > 0$ as $\dot{S}_a^{ss}(t) = 0$ for all values of t as stated earlier. The total epr of the channel comes entirely from the non-adiabatic contribution arising due to the external driving. It is also seen from the Fig. (e) that at NESS the inactive states are mainly populated which also oscillate periodically.

3.4.2 Dynamic hysteresis in sodium channel

Dynamic hysteresis is a signature of dynamic memory [24–26] which is also a property of a memristor device originally envisioned in circuit theory [37–40]. The main characterizing feature is the memristor’s electrical resistance which is not constant but depends on the history of current that had previously flowed through the device. There have been lots of

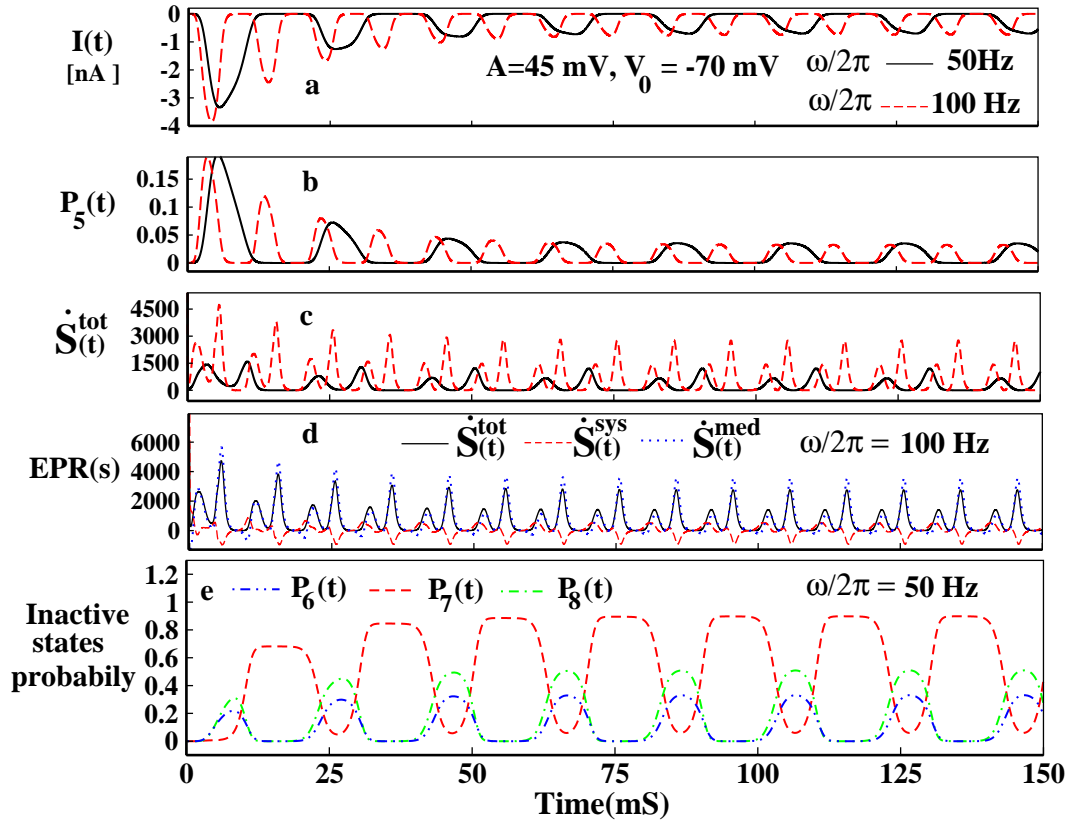


Figure 3.3: Transient kinetic and nonequilibrium thermodynamic behaviors under oscillating voltage protocol is shown here. In Fig. (a) $I(t)$ has been plotted with time for frequencies 50 and 100 Hz at amplitude 45 mV, in (b) Open state probability is plotted for same values with time, in (c) total epr is plotted with time and in (d) all the three entropy production rates are plotted with time at 100 Hz. For all the cases the value of V_0 is kept at -70 mV. The unit of entropy production rates are $\mathbf{JK}^{-1}\mathbf{S}^{-1}$. In Fig. (e) we have plotted the probabilities of the three inactive states at 50 Hz.

studies on memristor mostly from circuit theory perspective and also extended to sodium and potassium ion channels. A memristor shows dynamic hysteresis where loop areas of time variant quantities like ionic current shrinks with increasing frequencies. The hysteresis loops are pinched at single or multiple points with existing specific clockwise and anti-clockwise direction of hysteresis. These newly developed dynamical responses can mimic memristor properties and the learning and memory processes can be directly realized as in circuit theory approaches [26]. However, in ion channels the studies are mainly concentrated on the kinetic properties that too are not performed in biophysical ranges and the energetic aspects are overlooked. Here we have studied the kinetic and nonequilibrium thermodynamic aspects of the memristor properties of the sodium ion channel.

Here we have rigorously investigated the dynamic hysteresis of the channel at NESS under periodic perturbation. We have chosen three different types of frequencies: very low, medium and high frequency. The steady state ionic current, $I^{ss}(t)$ and the open state probability, $P_{open}^{ss}(t)$ are plotted as a function of voltage in Fig. 3.4(a) and (b). From the kinetic experiment we can measure $I^{ss}(t)$ and $P_{open}^{ss}(t)$. To get more biophysical insight we have taken the amplitude of the oscillating voltage, $A = 45$ mV which covers the entire biological range of activation and inactivation depolarisation of sodium channel, i.e. (-115 to -25 mV) and $V_0 = -70$ mV which is the resting potential of the cell. By taking these parameters, we have studied the kinetic response of Na-channel at steady state in one complete cycle of the oscillating voltage. From Fig. (3.4)(a) and (b), we observe that $I^{ss}(t)$ and $P_{open}^{ss}(t)$ shows dynamic hysteresis as a function of voltage which vanishes at very low and high frequencies. At very low and high frequency regime, $I^{ss}(t) - V(t)$ curve has no hysteresis loop indicating that the value of $I^{ss}(t)$ at a particular $V(t)$ will be the same during the voltage variation in the positive direction (-115 mV to -25 mV) as well as in the reverse direction (-25 mV to -115 mV) in an one periodic cycle of the oscillating voltage with $V_0 = -70$ mV and $A = 45$ mV. Now the product of current and voltage, $I(t) \times V(t)$ represents the power or work done per unit time by a system in the unit of JS^{-1} . So at very low and high frequency limits, the magnitude of the area of $I^{ss}(t)-V(t)$ curve created during the voltage variation in the positive direction will be similar but opposite in sign with that of the area of $I^{ss}(t)-V(t)$ curve in the reverse direction as the system returns to the original state in the same path in which it previously travelled in forward direction. Consequently, in an one periodic cycle, the overall power should be zero at these two frequency regime. However, in the medium frequency, the areas of $I^{ss}(t)-V(t)$ curves are originated due to the fact that the response to the voltage variation in the positive direction is not the same with that of the negative direction. As a result, a hysteresis loop area is formed which can be called as a power loop of the ion channel. In the spirit of the studies on estimating the mechanical work and power output of the work loop [41–45] which is used in muscle physiology of skeletal or cardiac muscle contractions via in vitro muscle testing of whole muscles or single muscle fibers, here we have calculated the work done per cycle associated with the dynamic hysteresis. Actually the area of the power loop signifies the amount of work done associated the dynamic memory over a periodic cycle of the oscillating voltage at steady state.

As the hysteresis is a signature of the memory [24–26, 46–48], so we can say that the loop area of $I^{ss}(t)-V(t)$ curve carries the information about the memory of the channel protein. Alternatively, in the energetic term, we can say that the loop area indicates the

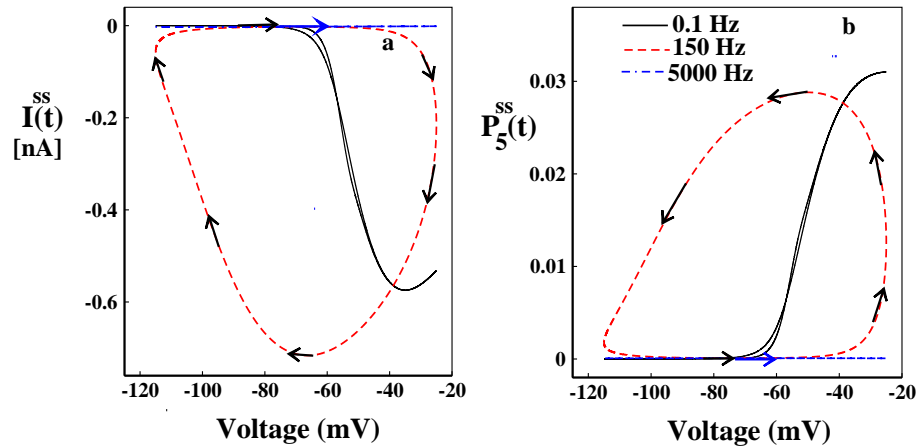


Figure 3.4: **Kinetics of hysteresis at $V_0 = -70$ mV, $A = 45$ mV is shown here.** In Fig. (a) $I(t)$ is plotted in one complete oscillation of voltage at 0.1 Hz, 150 Hz and 5000 Hz. (b) Open state probability is plotted for similar frequencies. The blue arrow indicates the starting point of loop.

amount of work done by the channel protein per unit time maintained by the dynamic memory [26] of the Na-channel. This dynamic memory is mainly generated due to the ion conduction of the channel protein in presence of periodic voltage variation. To investigate the work done by the channel protein or the power loop, we have calculated the area of the loop by using the formula

$$A_h^{cur} = \oint Q(V(t))dV, \quad (3.14)$$

where, $Q = I^{ss}(t)$ and A_h^{cur} is the magnitude of the hysteresis loop area of $I^{ss}(t)-V(t)$ curve. Here in Fig. (3.5)(a), (b) and (c), we have plotted the normalized loop area as a function of frequency, mean voltage and amplitude, respectively. From Fig. 3.5(a) it is seen that the hysteresis loop area of ionic current or the work done by the ion-channel gradually increases with frequency of external voltage and after passing through a maximum around 150 Hz with a magnitude of approximately 47.0 JS^{-1} , it again decreases down. This curve indicates that at a particular amplitude and mean voltage, the ion channel works at its maximum for an optimum frequency. This maximum work is done by the ion channel corresponds to the maximum dynamic memory developed in the Na-channel due to non-linear response of the channel protein against an oscillating voltage. This optimum frequency depends on the mean voltage as well as the amplitude of the oscillating voltage.

For more detailed study, we kept the amplitude and frequency fixed at 45 mV and 150 Hz, respectively and varied the mean voltage which is shown in Fig. (3.5)(b). We have found that around $V_0 = -55$ mV, the channel works at its maximum with a magnitude

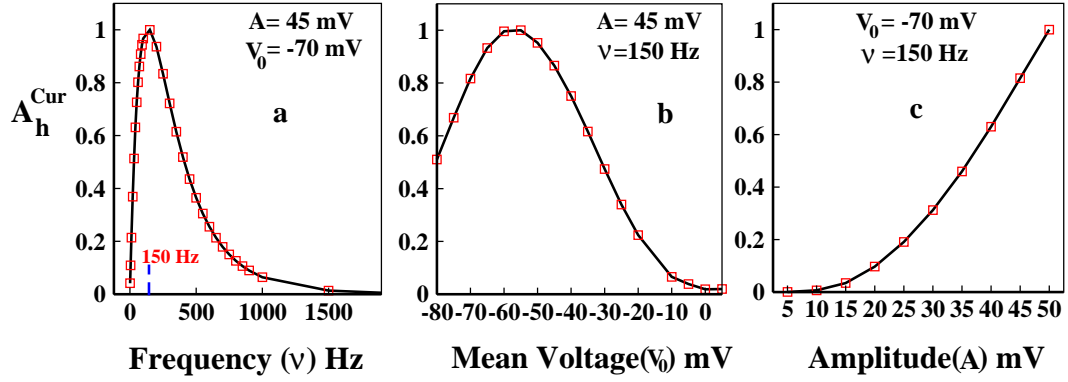


Figure 3.5: Normalised loop area of ionic current for different parameters are plotted here. In Fig. (a) hysteresis loop area of ionic current at amplitude 45 mV and $V_0 = -70$ mV is plotted. The hysteresis loop area of ionic current at amplitude 45 mV and frequency 150 Hz has been plotted as a function of mean voltage V_0 in Fig. (b). In Fig. (c) the area of current is plotted as a function of amplitude keeping mean voltage fixed at -70 mV and frequency at 150 Hz.

of approximately 57.0 JS^{-1} . It indicates that the capacity of the ionic conduction of Na-channel becomes optimum at a certain mean voltage where the loop area of open state probability at steady state should be maximum as the ionic current is directly related with the open state probability. With increasing mean voltage, the vanishing ionic conduction indicates the decrement of the value of the open state probability at steady state. From numerical study we observe that with increase in the mean voltage, the probability of the inactive states increases and simultaneously the closed and open state probabilities decrease. Therefore, from this curve we can say that the maximum dynamic hysteresis of Na-channel not only depends on the frequency but it also depends on the mean of the external oscillating voltage. To investigate how the loop area varies with amplitude, here we have plotted the normalized loop area of $I^{ss}(t)-V(t)$ curve as a function of amplitude which is shown in Fig. (3.5)(c). We observe that with increasing the amplitude the the loop area also increases and the maximum area shown here is approximately 58.0 JS^{-1} . The nature of the curve is pretty predictable in terms of the energetics. The energy accepted by the channel from the oscillating voltage is proportional to the square of the amplitude of the oscillating voltage. So at a particular frequency and mean voltage, if the amplitude of the oscillating voltage is increased, the ion channel absorbs more energy for its activation. Thus the ion conducting capacity of the ion-channel increases and as a result the dynamic memory also increases. But giving excess energy to ion channel may damage the channel protein and so determining the maximum amplitude needs a proper experimental verification. However, here we choose the amplitude 45 mV so that

the voltage variation should remain almost in the range of the action potential where the Na-channel works in the living nerve cell [15].

To investigate more on the dynamic memory from current-voltage curve a natural question arises whether the dynamic memory depends only on the open state probability, P_5 due to the overall gating dynamics of the Na-channel or it only provides the information about the dynamic memory of the channel protein generated due to conduction of ions. To clarify this, we have plotted the thermodynamic quantities per unit voltage variation at steady state like the system entropy production rate as $T\dot{S}_{sys}^{ss}(t)/V(t)$, the medium entropy production rate as $T\dot{S}_{med}^{ss}(t)/V(t)$ and the total entropy production rate as $T\dot{S}_{tot}^{ss}(t)/V(t)$ as a function of voltage in steady state which are depicted in Fig. (3.6) (a),(b) and (c), respectively. The dimension of all of these thermodynamic loop areas are of power in JS^{-1} . From the previous discussion we have observed that the dimension of the loop area of $I^{ss}(t)-V(t)$ curve is also power. So what are the differences these kinetic and thermodynamic loop areas implying? Actually, the thermodynamic quantities, namely epr are calculated by considering the net flux-force formulation between the Markov states in Na-channel scheme. Therefore, the loop area of $T\dot{S}_{tot}^{ss}(t)/V(t)$ vs. $V(t)$ is the total power or work done by the ion channel per unit time associated the dynamic memory developed for all over gating dynamics, including the dynamic memory for the ion conduction. From Fig. (3.6)(d) the normalized loop area shows how the work done is carried out with increasing frequencies by the ion channel for maintaining the dynamic memory for overall gating dynamics. With increasing frequency the magnitude of the loop areas of $T\dot{S}_{tot}^{ss}(t)/V(t)$ vs. $V(t)$ increases upto shown frequency range 5000 Hz. It should decrease down at a very high frequency which we have verified from the numerical study. However, to remain in a biophysical range and to tally with the loop area curve of $I^{ss}(t)-V(t)$, we have drawn the figure for the highest frequency of 5000 Hz. From this study one can be sure that the meaning of the kinetic and thermodynamic loop areas are different and they carry different physical features. The kinetic loop area gives partial information such as the idea of work done associated with the memory for ion conduction process which may not represent the overall gating dynamics in presence of periodic external drive. Thus thermodynamic study is essential for understanding the dynamic memory developed for overall gating dynamics.

It is also interesting to point out that for ionic current at low frequency (ν) region the loop area increases linearly with frequency and in the high frequency region it shows the $\frac{1}{\nu}$ dependency for periodic perturbation [23]. But for sodium channel within the biologically favourable kinetic range the total epr with growing hysteresis loop area depends on frequency as $(1 - e^{-\frac{\nu}{\nu_0}})$, where ν_0 is the approximate rate of increment of area or the

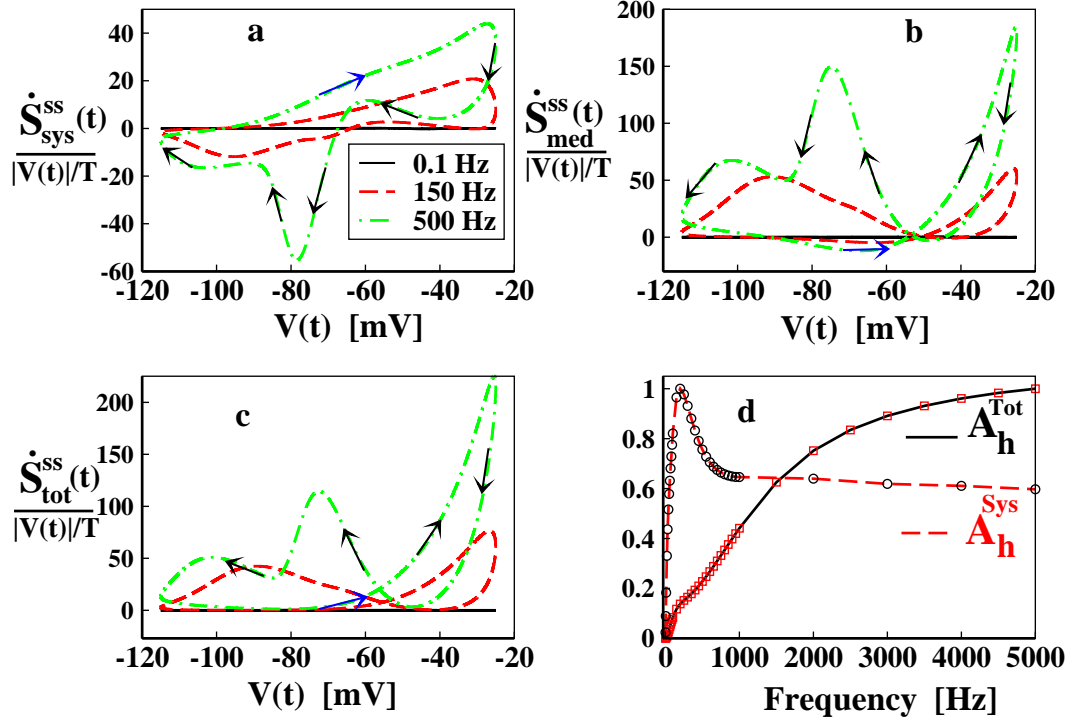


Figure 3.6: Thermodynamic quantities showing dynamic hysteresis is plotted here at $V_0 = -70$ mV and $A = 45$ mV. In Fig. (a) system epr, in Fig. (b) medium epr and in Fig. (c) total epr has been plotted for 0.1 Hz, 150 Hz and 500 Hz scaled by $\frac{|V(t)|}{T}$ to keep the loop areas in the unit of power. In every case the blue arrow is the starting point of clockwise direction. In all the cases the value of V_0 is kept at -70 mV and amplitude is kept at 45 mV. The unit of total entropy production rates are $\text{JK}^{-1}\text{S}^{-1}$. In Fig. (d) the black solid line is the normalised loop area of scaled total epr and the red dashed line is the normalised loop area of the system entropy (see equation 3.5), both plotted as a function of frequency.

slope of the curve. Here the normalised area of the system entropy, A_h^{Sys} in a complete cycle has been plotted using equation (3.5) in figure 3.6(d). It shows similar trends in very low frequency as loop area of ionic current showing a maximum at 200 Hz having a magnitude approximately 61.0 unit and then gradually decreases down very slowly with increasing frequency. The area of system entropy shows the amount of information stored in the system dynamically. Thus at an amplitude 45 and mean voltage -70 mV the system stores maximum information corresponding to the dynamic memory at around 200 Hz.

3.4.3 Ionic current and dissipative work done at nonequilibrium steady state

Next we have made a closer inspection of the time dependent energetics at NESS. To do that we have plotted the average dissipative work, W_d^{ss} over a complete cycle of oscillation at NESS with increasing frequencies ranging from very low to very high region. Here we consider cycle average of total epr at NESS as $\langle \dot{S}_{tot}^{ss}(t) \rangle = 1/\tau \int_0^\tau \dot{S}_{tot}^{ss}(t) dt$, where τ is the time period of oscillation. One should note that $\dot{S}_{sys}^{ss}(t)$ being a state function, $\langle \dot{S}_{sys}^{ss}(t) \rangle = 0$, as well as $\langle \dot{S}_{ad}(t) \rangle = 0$ for all t as discussed earlier. The state function, internal energy energy, $U(t)$ at time t is defined as $U(t) = -k_B T \sum_i P_i(t) \ln P_i^{st}(V_t)$. Now at NESS over a complete cycle the change in internal energy is also zero, i.e, $1/\tau \int_0^\tau \dot{U}(t) dt = 0$. Thus we have the following situation at NESS as,

$$\langle \dot{S}_{sys}^{ss}(t) \rangle = \langle \dot{S}_a^{ss} \rangle = \langle \dot{U}^{ss}(t) \rangle = 0. \quad (3.15)$$

Using the definition of total epr and equation (3.15) we can write

$$\langle \dot{S}_{tot}^{ss}(t) \rangle = \langle \dot{S}_{med}^{ss}(t) \rangle = \langle \dot{S}_{na}^{ss}(t) \rangle. \quad (3.16)$$

We know the dissipative work, $W_d(t)$ is related to total heat dissipation, (h_d) by the following equation [34]

$$\dot{U}(t) + h_d(t) = W_d(t) + T\dot{S}_a(t), \quad (3.17)$$

where $h_d(t) = T\dot{S}_{med}^{ss}(t)$. Now taking average on both sides of the equation (3.17) and using equation (3.15) we can write $T \langle \dot{S}_{med}^{ss}(t) \rangle = \langle W_d^{ss}(t) \rangle$. Again using equation (3.16) we get the following expression for the average dissipative work

$$\langle W_d^{ss}(t) \rangle = T \langle \dot{S}_{tot}^{ss}(t) \rangle. \quad (3.18)$$

So in case of a strictly periodic external driving the cycle-averaged dissipative work done and dissipative heat are synonymous which is also a measure of medium entropy production rate. Thus at periodically driven NESS the average total entropy production rate multiplied by temperature is the measure of dissipative work done by the system.

In Fig. 3.7(a) and (b), we have shown the average ionic current, $\langle I^{ss}(t) \rangle$ and the average dissipative work done scaled with temperature, $\langle W_d^{ss}(t) \rangle / T$ at NESS as a function of frequency for several amplitudes of the oscillating voltage by keeping $V_0 = -70$ mV. From Fig. 3.7(a) it is observed that at very low frequency limit, $\langle I^{ss}(t) \rangle$

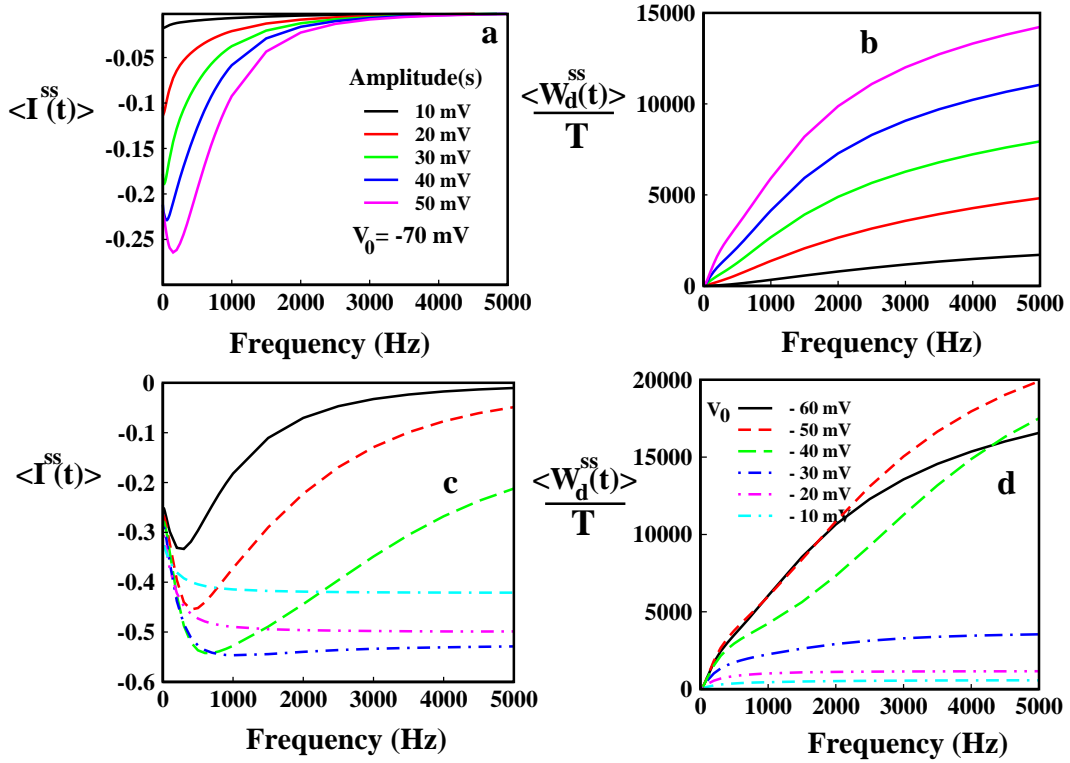


Figure 3.7: In Fig. (a) $\langle I^{ss}(t) \rangle$ has been plotted with frequencies for amplitudes 10, 20, 30, 40, 50 mV and in (b) similar graph for $\langle W_d^{ss}(t) \rangle$ at NESS at amplitude 45 mV and mean voltage -70 mV. In Fig. (c) and (d) the average ionic current and average total epr has been plotted with the frequencies for mean value of external field at -60, -50, -40, -30, -20 and -10 mV respectively at amplitude of 45 mV. The unit of $W_d^{ss}(t)$ is JS^{-1} and $\langle I^{ss}(t) \rangle$ is nA .

gradually increases with increasing the frequency values. However, after passing through a maximum it decreases down with increasing the frequencies. At extreme high frequency, $\langle I^{ss}(t) \rangle$ becomes independent of the amplitude of the oscillating voltage, whereas the magnitudes of $\langle W_d^{ss}(t) \rangle / T$ increases with increasing the amplitude values with a constant rate. This is due to the fact that at extreme high frequency, say above the frequency 4,000 Hz, the ion channel totally fails to respond according to the fast time varying voltage. But it responds according to the average value of the oscillating voltage *i.e.*, the mean voltage, $V_0 = -70$ mV. In this scenario, the population of the closed states become maximum, whereas, the population of other states such as P_3 to P_8 become zero which is confirmed from our numerical study and from the approximate analytical understanding of high frequency region, discussed in the next section. Therefore, in this condition as the open state probability becomes zero for any amplitude of the oscillating voltage, the ionic current which strictly depends on P_5 , becomes independent of the amplitude. However, $\langle W_d^{ss}(t) \rangle / T$ depends on all the fluxes and forces associated with

the channel. So with increasing amplitude $\langle W_d^{ss}(t) \rangle / T$ or the average dissipative work done also increases. From Fig. 3.7(b), we also observe that at very low frequency, the values of $\langle W_d^{ss}(t) \rangle / T$ are very close to zero indicating that the system remains very close to equilibrium. However, at high frequency, it has a finite value which indicates that system remains at NESS. Therefore, although the extreme low and high frequency regimes are associated with vanishing hysteresis but they are definitely thermodynamically distinguishable.

For more clarity, we have plotted $\langle I^{ss}(t) \rangle$ and $\langle W_d^{ss}(t) \rangle / T$ as a function of frequency for several mean voltage, V_0 keeping the amplitude, $A = 45$ mV as constant. The curves are drawn in Fig. 3.7(c) and (d), respectively. In Fig. 3.7(c), we observe that for $V_0 = -60$ mV to -40 mV, $\langle I^{ss}(t) \rangle$ first increases with frequency and after passing through a maximum it again decreases down. In these mean voltage, the maxima are shifted towards high frequencies with increasing the values of V_0 . However, from $V_0 = -30$ mV to -10 mV, $\langle I^{ss}(t) \rangle$ gradually increases with increasing frequencies but it finally achieves a steady value which is quite independent of frequency. In these mean voltage, the magnitude of $\langle I^{ss}(t) \rangle$ decreases with increasing the values of V_0 giving a clear trend at high frequency. That means with increasing V_0 , $\langle I^{ss}(t) \rangle$ first increases but after a certain mean voltage it decreases down. That trend is quite similar to the curve of the normalized loop-area of ionic current as a function of mean voltage which is already shown in Fig. 3.4(b). Furthermore, from this observation we can say that at high frequency regime, $\langle P_5^{ss}(t) \rangle$ also follows the same trend as ionic current. This is due to the fact that with increasing mean voltage, the inactivated states become more populated and the open state probability becomes very small. It is also confirmed from our numerical analysis. In the moderate frequency regime $\langle I^{ss}(t) \rangle$ as well as the $\langle P_5^{ss}(t) \rangle$ depends on the frequency values and the variation of $\langle I^{ss}(t) \rangle$ and $\langle P_5^{ss}(t) \rangle$ with V_0 also follows the similar trends as that of the high frequency regime. However, in the extreme low frequency the trend is not followed by $\langle I^{ss}(t) \rangle$. In Fig. 3.7(d), we have also plotted $\langle W_d^{ss}(t) \rangle / T$ as a function of frequency for similar mean voltage with keeping amplitude, $A = 45$ mV as constant. From Fig. 3.7(d), we have observed that at very low frequency the value of $\langle W_d^{ss}(t) \rangle / T$ remains quite close to zero. However, with increasing frequency $\langle W_d^{ss}(t) \rangle / T$ increases and it finally reaches to a steady value. In this case we observe that variation of $\langle W_d^{ss}(t) \rangle / T$ with V_0 at high as well as moderate frequency does not follow the similar trend with that of the variation of $\langle I^{ss}(t) \rangle$ with V_0 . Here we see that at moderate frequency regime with increasing V_0 , the values of $\langle W_d^{ss}(t) \rangle / T$ decreases gradually. At this regime, for $V_0 = -60$ and -50 mV, the values of $\langle W_d^{ss}(t) \rangle / T$ is quite same. However, in the other V_0 values $\langle W_d^{ss}(t) \rangle / T$ decreases with increasing V_0 . In the high frequency regime, the trend remain same for

$V_0 = -30, -20$ and -10 mV. But for $V_0 = -60, -50$ and -40 mV it becomes totally different.

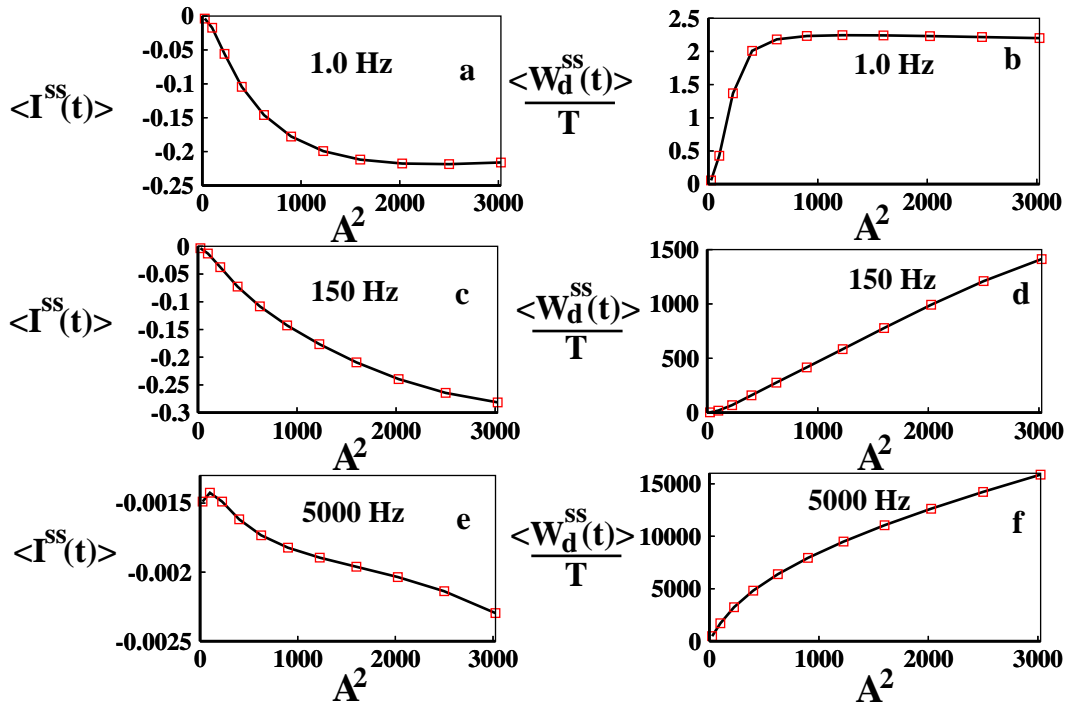


Figure 3.8: In Fig. (a) and (b) $\langle I^{ss}(t) \rangle$ and $\langle W_d^{ss}(t) \rangle$ has been plotted with the power of external field at frequency 1.0 Hz. In Fig. (c) and (d) same have been plotted for 150 Hz and in (e) and (f) for frequency 5000 Hz. For all the cases $V_0 = -70$ mV. The unit of A^2 is $(\text{mV})^2$.

Now for finding out how $\langle I^{ss}(t) \rangle$ and $\langle W_d^{ss}(t) \rangle / T$ depends on the input energy accepted by the channel protein from the oscillating voltage, here we have plotted them as a function of the amplitude square of the external voltage, A^2 at three different frequencies: low, 1.0 Hz; medium, 150 Hz and extreme high, 5000 Hz. We have chosen the parameter A^2 as it is directly proportional to the energy received by the system from one cycle of the oscillating voltage at steady state. In Fig. 3.8 (a), (c) and (e), $\langle I^{ss}(t) \rangle$ versus A^2 has been plotted for low, medium and high frequencies, respectively, whereas, $\langle W_d^{ss}(t) \rangle / T$ for these three different frequencies have been depicted in Fig. 3.8 (b), (d) and (f), respectively. From Fig. 3.8(a) and (b) we observe that $\langle I^{ss}(t) \rangle$ as well as $\langle W_d^{ss}(t) \rangle / T$ at NESS initially increase with increasing A^2 and then get saturated. It indicates that the capacity of channel protein to consume energy reaches a steady value for producing the ionic current as well as for driving the overall gating-process over a periodic cycle. The magnitude of $\langle W_d^{ss}(t) \rangle / T$ shows that system is very close to equilibrium. However, this capacity increases with increasing the frequency values which we can predict by observing the variation of $\langle I^{ss}(t) \rangle$ and $\langle W_d^{ss}(t) \rangle / T$ in Fig.

3.8 (c) and (d). In these two figures we see that at frequency 150 Hz, $\langle I^{ss}(t) \rangle$ and $\langle W_d^{ss}(t) \rangle / T$ gradually increase with increasing values of A^2 almost linearly. This behaviour can be explained clearly in terms of the consumption of energy by the channel protein associated with the dynamic memory developed inside it due to ion-conduction as well as for the overall-gating dynamics. At this frequency, ion channel shows a significant dynamic memory for ion conduction. From the previous discussion we have observed that the dynamic memory capacity increases with increasing the amplitude of the oscillating voltage which can be verified from Fig. 3.5(c). So for this reason, here $\langle I^{ss}(t) \rangle$ and $\langle W_d^{ss}(t) \rangle / T$ increases with increasing A^2 or the energy supply. However, in Fig.3.8(e) and (f), we observe a different trend in the variation at very high frequency, 5000 Hz. In this region, the magnitude of $\langle I^{ss}(t) \rangle$ becomes very very small, almost zero, whereas $\langle W_d^{ss}(t) \rangle / T$ increases almost linearly with A^2 . This is due to the reason that at high frequency with mean voltage of -70 mV, the population of open state probability and related ionic current vanishes, but the population of P_0 to P_2 gradually increases. As the involvement of all other states, such as P_3 to P_8 reduces in overall gating process, thus with more supply of energy system will dissipate more, which is reflected in Fig. 3.8(f).

3.5 Approximate Analytical Expressions

Here we want to develop some qualitative ideas of the system dynamics under oscillating voltage through some approximate analytical expressions. It is observed from Fig. (3.3)(d) of numerical section that asymptotically inactive states get much more populated than the actives states at steady states. Thus we want to solve the time dependent solution of P_6, P_7, P_8 using oscillating voltage protocol at limiting conditions, from low to moderately high frequency region. Thus writing the probability equations of inactive states and using the normalizing conditions $\sum_{i=0}^8 P(i, t) = 1$ and after rearrangement we get following three equations,

$$\begin{aligned} \frac{dP_6}{dt} &= -x_1P_6 - x_2P_7 - x_3P_8 + y_1 \\ \frac{dP_7}{dt} &= -x_4P_6 - x_5P_7 - x_6P_8 + y_2 \\ \frac{dP_8}{dt} &= -x_7P_6 - x_8P_7 - x_9P_8 + y_3 \end{aligned} \quad (3.19)$$

where, $x_1 = (\alpha_4 + \alpha_2 + \beta_4)$, $x_2 = (\alpha_4 - \beta_2)$, $x_3 = \alpha_4$, $x_4 = -\alpha_2$, $x_5 = (\beta_2 + \alpha_3)$, $x_6 = -\beta_3$, $x_7 = \alpha_5$, $x_8 = (\alpha_5 - \alpha_3)$, $x_9 = (\alpha_5 + \beta_5 + \beta_3)$, $y_1 = (1 - P_0 - P_1 - P_2 - P_4 - P_5)$, $y_2 = 0$, $y_3 = (1 - P_0 - P_1 - P_2 - P_3 - P_4)$. Thus the equations can be written in matrix notation

as follows,

$$\frac{d}{dt}\bar{\mathbf{P}}(t) = -\mathbf{A}(t)\bar{\mathbf{P}}(t) + \bar{\mathbf{Y}}(t) \quad (3.20)$$

where, $\mathbf{A}(t)$ is a (3×3) matrix with transition probabilities and $\bar{\mathbf{P}}(t)$ and $\bar{\mathbf{Y}}(t)$ are the (3×1) column matrices. $\mathbf{A}(t) = \begin{pmatrix} x_1 & x_2 & x_3 \\ x_4 & x_5 & x_6 \\ x_7 & x_8 & x_9 \end{pmatrix}$, $\bar{\mathbf{P}}(t) = \begin{pmatrix} P_6 \\ P_7 \\ P_8 \end{pmatrix}$, and $\bar{\mathbf{Y}}(t) = \begin{pmatrix} y_1 \\ 0 \\ y_3 \end{pmatrix}$.

Now the solution of the above time dependent equation (3.20) with suitable limit ($t_0 < t' < t$) gives us the following expression,

$$\bar{\mathbf{P}}(t) = \exp \left[- \int_{t_0}^t \mathbf{A}(t') dt' \right] \bar{\mathbf{P}}(t_0) + \int_{t_0}^t \exp \left[- \int_{t'}^t \mathbf{A}(t'') dt'' \right] \bar{\mathbf{Y}}(t') dt'. \quad (3.21)$$

Using the above expression we can write $\bar{\mathbf{P}}(t)$ for $mT < t < (mT + t)$ as,

$$\bar{\mathbf{P}}(mT + t) = \exp \left[- \int_{mT}^{mT+t} \mathbf{A}(t') dt' \right] \bar{\mathbf{P}}(mT) + \int_{mT}^{mT+t} \exp \left[- \int_{t'}^{mT+t} \mathbf{A}(t'') dt'' \right] \bar{\mathbf{Y}}(t') dt', \quad (3.22)$$

where T is the time period of the oscillating voltage and $m(=0,1,2,3..etc)$ is the index of the oscillating period. When $t=T$, it becomes

$$\bar{\mathbf{P}}[(m+1)T] = \exp \left[- \int_{mT}^{[(m+1)T]} \mathbf{A}(t') dt' \right] \bar{\mathbf{P}}(mT) + \int_{mT}^{[(m+1)T]} \exp \left[- \int_{t'}^{[(m+1)T]} \mathbf{A}(t'') dt'' \right] \bar{\mathbf{Y}}(t') dt'. \quad (3.23)$$

and for $m=0$,

$$\bar{\mathbf{P}}[(m+1)T] = \exp \left[- \int_0^T \mathbf{A}(t') dt' \right] \bar{\mathbf{P}}(mT) + \int_0^T \exp \left[- \int_{t'}^T \mathbf{A}(t'') dt'' \right] \bar{\mathbf{Y}}(t') dt'. \quad (3.24)$$

Defining

$$\Phi = \exp \left[- \int_0^T \mathbf{A}(t') dt' \right],$$

and

$$\Delta_0 = \int_0^T \exp \left[- \int_{t'}^T \mathbf{A}(t'') dt'' \right] \bar{\mathbf{Y}}(t') dt', \quad (3.25)$$

equation (3.24) can be rewritten as,

$$\bar{\mathbf{P}}[(m+1)T] = \Phi \bar{\mathbf{P}}(mT) + \Delta_0, \quad (3.26)$$

where Φ is a (3×3) matrix, and Δ_0 is a (3×1) column matrix. Now, putting $m=0,1,2,3..etc$, and using the recursion relation using $\bar{\mathbf{P}}(mT)$ and $\bar{\mathbf{P}}[(m+1)T]$ and using

the sum rule of geometric progression we can write,

$$\bar{\mathbf{P}}(mT) = \Phi^m \bar{\mathbf{P}}(0) + \left[\mathbf{I} - \Phi^m \right] \left[\mathbf{I} - \Phi \right]^{-1} \Delta_0, \quad (3.27)$$

where $\bar{\mathbf{P}}(0)$ is the matrix having the initial probabilities of P_6, P_7, P_8 , i.e., $\bar{\mathbf{P}}(0) = \begin{pmatrix} P_6 \\ P_7 \\ P_8 \end{pmatrix} = \begin{pmatrix} 0 \\ 0 \\ 0 \end{pmatrix}$. Now, when $m \rightarrow \infty$, $\Phi^m \rightarrow 0$ and $\bar{\mathbf{P}}(mT)$ reaches its asymptotic value,

$$\lim_{m \rightarrow \infty} \bar{\mathbf{P}}(mT) = \left[\mathbf{I} - \Phi \right]^{-1} \Delta_0. \quad (3.28)$$

By substituting the above expression into equation (3.22) and taking the asymptotic long time limit of the probability, $\bar{\mathbf{P}}(mT + t)$, which is denoted by $\bar{\mathbf{P}}^{ss}(t)$, we get,

$$\bar{\mathbf{P}}^{ss}(t) = \lim_{m \rightarrow \infty} \bar{\mathbf{P}}(mT + t) = \left[\mathbf{I} - \Phi \right]^{-1} \Delta(t), \quad (3.29)$$

where the expression of $\Delta(t)$ is defined as,

$$\Delta(t) = \int_t^{(t+T)} \exp \left[- \int_t^{(t+T)} \mathbf{A}(t'') dt'' \right] \bar{\mathbf{Y}}(t') dt'. \quad (3.30)$$

At this stage we separately show the expression of $\bar{\mathbf{P}}^{ss}(t)$ for low and high frequency limits.

3.5.1 Low frequency limit

At a very low frequency, as $T \rightarrow \infty$, $\Phi \rightarrow 0$, equation (3.29) becomes,

$$\bar{\mathbf{P}}^{ss}(t) = \int_0^T \exp \left[- \int_0^t \mathbf{A}(t - t'') dt'' \right] \bar{\mathbf{Y}}(t - t') dt'. \quad (3.31)$$

As $\mathbf{A}(t')$ and $\bar{\mathbf{Y}}(t')$ are slow varying functions in low frequency limit, so we can expand them using Taylor expansion around t as, $\mathbf{A}(t - t'') \simeq \mathbf{A}(t) - t'' \dot{\mathbf{A}}(t)$, $\bar{\mathbf{Y}}(t - t') \simeq \bar{\mathbf{Y}}(t) - t' \dot{\bar{\mathbf{Y}}}(t)$. Now, putting the above expansion we get,

$$\exp \left[- \int_0^t \mathbf{A}(t - t'') dt'' \right] = \left(\mathbf{I} + \frac{1}{2} \dot{\mathbf{A}}(t) t'^2 \right) \exp[-\mathbf{A}(t) t']. \quad (3.32)$$

Thus we have to evaluate the following integration,

$$\bar{\mathbf{P}}^{ss}(t) = \int_0^T \left[(\mathbf{I} + \frac{1}{2} \dot{\mathbf{A}}(t)t'^2) \exp[-\mathbf{A}(t)t'] \left[\bar{\mathbf{Y}}(t') - t' \dot{\bar{\mathbf{Y}}}(t') \right] dt' \right]. \quad (3.33)$$

To find the integration, we have neglected the orders higher than 2 of t' and we obtain an expression as,

$$\bar{\mathbf{P}}^{ss}(t) = \mathbf{Q}(t) - [\mathbf{A}(t)]^{-1} \dot{\mathbf{Q}}(t), \quad (3.34)$$

where, $\mathbf{Q}(t) = [\mathbf{A}(t)]^{-1} \bar{\mathbf{Y}}(t)$. Now, for slowly varying voltage the 2nd term is neglected to obtain the final expression as,

$$\bar{\mathbf{P}}^{ss}(t) = \mathbf{Q}(t) = [\mathbf{A}(t)]^{-1} \bar{\mathbf{Y}}(t). \quad (3.35)$$

Thus we finally obtain the expressions of P_6, P_7, P_8 at low frequency as follows,

$$\begin{aligned} P_6^{ss}(t) &= (1/D) \left[a_{11}y_1 + a_{13}y_3 \right] \\ P_7^{ss}(t) &= (1/D) \left[a_{21}y_1 + a_{23}y_3 \right] \\ P_8^{ss}(t) &= (1/D) \left[a_{31}y_1 + a_{33}y_3 \right], \end{aligned} \quad (3.36)$$

where D is the determinant of the matrix \mathbf{A} and the value of the $a_{ij}(s)$ are given in the table below.

$a_{11} =$	$(x_5x_9 - x_6x_8)$	$b_{11} =$	$(\langle x_5 \rangle \langle x_9 \rangle - \langle x_6 \rangle \langle x_8 \rangle)$
$a_{13} =$	$(x_2x_6 - x_3x_5)$	$b_{13} =$	$(\langle x_2 \rangle \langle x_6 \rangle - \langle x_3 \rangle \langle x_5 \rangle)$
$a_{21} =$	$(x_6x_7 - x_4x_9)$	$b_{21} =$	$(\langle x_6 \rangle \langle x_7 \rangle - \langle x_4 \rangle \langle x_9 \rangle)$
$a_{23} =$	$(x_3x_4 - x_1x_6)$	$b_{23} =$	$(\langle x_3 \rangle \langle x_4 \rangle - \langle x_1 \rangle \langle x_6 \rangle)$
$a_{31} =$	$(x_4x_8 - x_5x_7)$	$b_{31} =$	$(\langle x_4 \rangle \langle x_8 \rangle - \langle x_5 \rangle \langle x_7 \rangle)$
$a_{33} =$	$(x_1x_5 - x_2x_4)$	$b_{33} =$	$(\langle x_1 \rangle \langle x_5 \rangle - \langle x_2 \rangle \langle x_4 \rangle)$

Table 3.2: In this table the expressions of a_{ij} for low frequency and b_{ij} for high frequency are given.

Constant Voltage Steady State Limit

From equation (3.21) for constant voltage we can write

$$\bar{\mathbf{P}}(t) = (\mathbf{A})^{-1} \left[\mathbf{I} - e^{(-\mathbf{A}t)} \right] \bar{\mathbf{Y}}. \quad (3.37)$$

where \mathbf{A} and $\bar{\mathbf{Y}}$ are constant in time and $\bar{\mathbf{P}}(t_0) = \begin{pmatrix} P_6 \\ P_7 \\ P_8 \end{pmatrix} = \begin{pmatrix} 0 \\ 0 \\ 0 \end{pmatrix}$.

Now at steady state i.e, at $t \rightarrow \infty$ the equation (3.37) gets reduced to,

$$\bar{\mathbf{P}}_{eq} = (\mathbf{A})^{-1}\bar{\mathbf{Y}}. \quad (3.38)$$

The difference between equations (3.35) and (3.38) is that the former is time dependent and the later is constant in time. The nature of the equation at very low frequency and constant voltage case are almost similar except the oscillating case has slow time dependence.

3.5.2 High frequency limit

For the high frequency region, $T \rightarrow 0$, then Φ can be written as follows,

$$\Phi = \mathbf{I} - \int_0^T \mathbf{A}(t') dt'$$

or

$$\Phi = \mathbf{I} - T \langle \mathbf{A} \rangle. \quad (3.39)$$

Thus, $\bar{\mathbf{P}}^{ss}(t)$ becomes,

$$\bar{\mathbf{P}}^{ss}(t) = (\mathbf{I} - \Phi)^{-1} \Delta(t) = (1/T) \langle \mathbf{A} \rangle^{-1} \Delta(t) = (1/T) \langle \mathbf{A} \rangle^{-1} \left[\int_t^{t+T} \exp\left[-\int_{t'}^{t+T} \mathbf{A}(t'') dt''\right] \bar{\mathbf{Y}}(t') dt' \right]. \quad (3.40)$$

Now rearranging the above expression in the high frequency limit as,

$$\bar{\mathbf{P}}^{ss}(t) = (1/T) \langle \mathbf{A} \rangle^{-1} \left[\int_t^{t+T} \bar{\mathbf{Y}}(t') dt' - \int_{t'}^{t+T} \mathbf{A}(t'') dt'' \int_t^{t+T} \bar{\mathbf{Y}}(t') dt' \right],$$

or,

$$\bar{\mathbf{P}}^{ss}(t) = (1/T) \langle \mathbf{A} \rangle^{-1} \left[\int_t^{t+T} \bar{\mathbf{Y}}(t') dt' - \delta(t) \right]. \quad (3.41)$$

As $\delta(t) \rightarrow 0$, we get

$$\bar{\mathbf{P}}^{ss}(t) = \langle \mathbf{A}(t) \rangle^{-1} \langle \bar{\mathbf{Y}}(t) \rangle, \quad (3.42)$$

$$\text{where, } \langle \mathbf{A}(t) \rangle^{-1} = \begin{pmatrix} \langle x_1 \rangle & \langle x_2 \rangle & \langle x_3 \rangle \\ \langle x_4 \rangle & \langle x_5 \rangle & \langle x_6 \rangle \\ \langle x_7 \rangle & \langle x_8 \rangle & \langle x_9 \rangle \end{pmatrix}^{-1} \quad \text{and } \langle \bar{\mathbf{Y}}(t) \rangle = \begin{pmatrix} \langle y_1 \rangle \\ 0 \\ \langle y_3 \rangle \end{pmatrix}$$

Thus we finally obtain the expressions of P_6, P_7, P_8 at high frequency as follows,

$$\begin{aligned} P_6^{ss}(t) &= (1/E) \left[b_{11} \langle y_1 \rangle + b_{13} \langle y_3 \rangle \right] \\ P_7^{ss}(t) &= (1/E) \left[b_{21} \langle y_1 \rangle + b_{23} \langle y_3 \rangle \right] \\ P_8^{ss}(t) &= (1/E) \left[b_{31} \langle y_1 \rangle + b_{33} \langle y_3 \rangle \right], \end{aligned} \quad (3.43)$$

where, E is the determinant of the matrix $\langle \mathbf{A} \rangle$, and the value of the $b_{ij}(s)$ are given in TABLE II, the low frequency and high frequency expressions of the probabilities have been checked directly with the numerical results, and have been found to match almost entirely. Now the time dependent part, $\delta(t) \rightarrow 0$ has a significant physical meaning. In the high frequency limit system fails to understand the tremendously fast variation of external perturbation, and sees an average value. Thus the time dependent part vanishes and the probabilities can be defined with the average values of system parameters. The explicit time dependent expressions of these three inactive states are not easy to calculate as they are coupled with other resting and active states. In very high frequency range, i.e, above 5000 Hz, the system hardly responds to the external perturbation as if it fails to sense the extremely fast voltage variation and sees the average value which is -70 mV. At this potential system remains in resting state. We have found that the probability of P_0 becomes ≈ 1.0 . In such a condition the elements y_1 and y_3 in $\bar{\mathbf{Y}}(t)$ of equation(3.20) also vanish giving $P_6^{ss}(t) = P_7^{ss}(t) = P_8^{ss}(t) = 0$.

3.6 Comparison With Other Models Of Sodium Channel

Here we have given a brief comparison of our results with another popular model of sodium channel. Although there exists many models of sodium channel [5, 17, 49–53] the main problem in comparing with the model associated study using oscillating voltage protocol is that it requires the voltage dependent expression of rate constants and instantaneous conductance which is normally not available always. Most of the studies have considered specific rates fitted for specific voltages. Also with time the model of sodium channel has

improved a lot. Here we have taken the wild type (WT) sodium channel model of Clancy and Rudy [54] for comparison.

This model satisfies almost all the experimental features as far as the current knowledge of sodium channel are concerned. For example, a fast inactivation state (IF) and two intermediate inactivation states (IM₁ and IM₂) are there to reproduce the complex fast and slow recovery features of inactivation. Representation of the closed-state inactivation is included by two closed-inactivation states (IC₂ and IC₃). This allows for channel inactivation from any of the closed available states, providing accurate representation of channel availability throughout the physiological voltage range. This wild-type (WT) Na model was developed on the basis of a wide range of data presented in the experimental literature and also the model parameters were fitted over the wide physiological range (-140 to +70 mV). Microscopic reversibility is ensured by fixing the products of the forward and reverse transition rates of closed loops in the model. This model has also been tested for drug binding kinetics [55] lately and found to be working satisfactorily. The model is shown in Fig. (3.9). The functional form of voltage dependency of rate constants here are very different from the rates in the Vandenberg-Bezanilla, 1991b model. The connectivity of states along with the coupling rate constants are also very different in above two models.

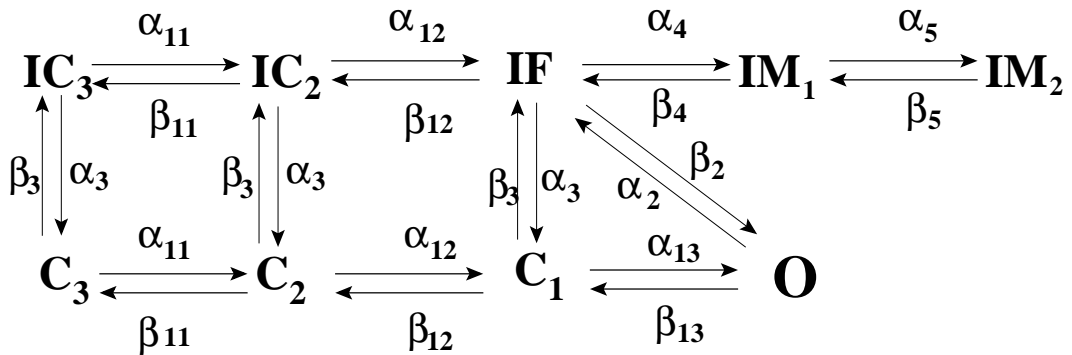


Figure 3.9: Wild-type (WT) sodium channel model of Clancy & Rudy, 2002 [54]: C_3, C_2, C_1 are closed states, O is the conducting state or open state. IC_2 and IC_3 are closed-inactivation states. IF is the fast inactivation state and two intermediate inactivation states, IM_1 and IM_2 are there to reproduce the complex fast and slow recovery features of inactivation. Here $\alpha_{11} = 3.802 / (0.1027 \exp(-V/17.0) + 0.20 \exp(-V/150))$, $\beta_{11} = 0.1917 \exp(-V/20.3)$, $\alpha_{12} = 3.802 / (0.1027 \exp(-V/15.0) + 0.23 \exp(-V/150))$, $\beta_{12} = 0.20 \exp(-(V-5)/20.3)$, $\alpha_{13} = 3.802 / (0.1027 \exp(-V/12.0) + 0.25 \exp(-V/150))$, $\beta_{13} = 0.22 \exp(-(V-10)/20.3)$, $\alpha_2 = (9.178 \exp(V/29.68))$, $\beta_2 = (\alpha_{13} \alpha_2 \alpha_3) / (\beta_{13} \beta_3)$, $\alpha_3 = 3.7933 \times 10^{-7} \exp(-V/7.7)$, $\beta_3 = (0.0084 + 0.00002 \times V)$, $\alpha_4 = \alpha_2 / 100$, $\beta_4 = \alpha_3$, $\alpha_5 = \alpha_2 / (9.5 \times 10^4)$ and $\beta_5 = \alpha_3 / 50$. The $I(t)$ is calculated as $I(t) = G_{Na} P(O)(V - E_{Na})$ where $G_{Na} = 23.5 \text{ mS}/\mu\text{F}$ and the numerical value of E_{Na} is taken as 67.0 mV.

The important results of the model of Clancy and Rudy are shown in Fig. (3.10) where we have compared the nature of time and voltage dependence of current and total epr for the constant and oscillating voltage protocol with our previous results. In Fig. (3.10) (a) we have plotted the $I(t)$ for voltages -40, -30 and -20 mV, respectively. The corresponding vanishing $\dot{S}_{tot}(t)$, in Fig. (3.10)(b) indicates the relaxation to equilibrium. In Fig.(3.10) (c) the NESS ionic current is plotted for frequencies 0.1 to 100 Hz. It also shows the dynamic hysteresis with the similar trend of vanishing loop areas at very low and high frequencies. Similar trend of dynamic hysteresis is seen from the total epr curves too as seen from Fig. (3.10) (d). It is also seen that with increasing frequency the magnitude of the total epr gradually increases which eventually shows similar trend as obtained from Fig. (3.7) (b). It also leads to similar trend of power dependence as seen from Fig. (3.8) (b),(d) and (f). From this comparison we can conclude that depending upon the state connectivity and rate constants, the time and voltage dependence of the kinetic and thermodynamic quantities may differ in shape and magnitude from model to model. However, the qualitative nature of frequency, mean voltage and amplitude dependence of the hysteresis and average dynamical response properties are very generic in nature.

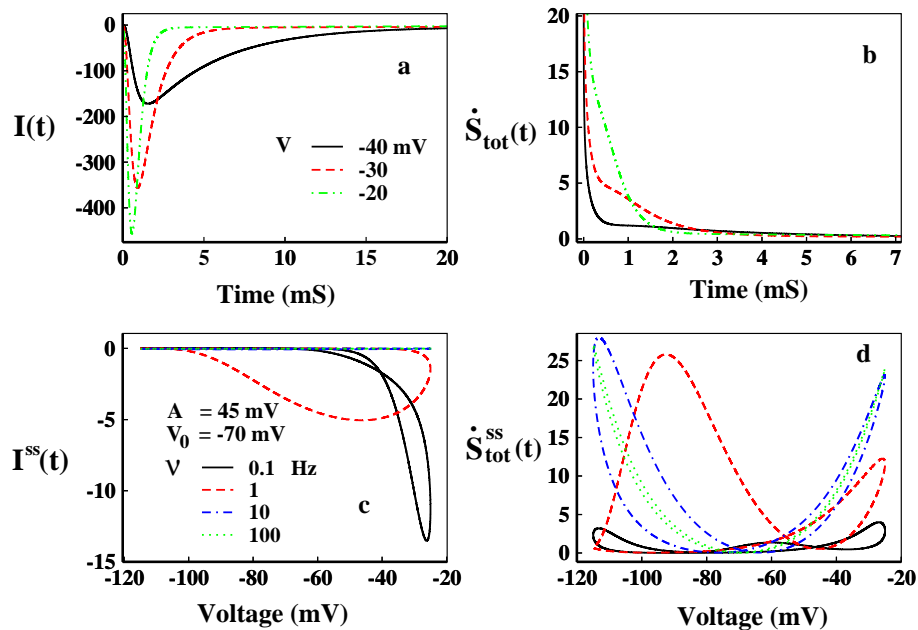


Figure 3.10: For constant voltage protocol, in Fig. (a) $I(t)$ and in (b) $\dot{S}_{tot}(t)$ have been plotted with time for voltages, -40, -30, -20 mV. For oscillating voltage protocol, in Fig. (c) $I^{ss}(t)$ and in (d) $\dot{S}_{tot}^{ss}(t)$ have been plotted for $\nu = 0.1, 1, 10$ and 100 Hz with $V_0 = -70$ mV and $A = 45$ mV. For oscillating voltage case, ionic current, $I^{ss}(t)$ is plotted here in the scale of $G_{Na}(V(t))$, as the voltage dependence of the instantaneous conductance is not available here. The unit of ionic current is $\mu\text{A } \mu\text{F}^{-1}$ and $\dot{S}_{tot}(t)$ is $\text{JK}^{-1}\text{S}^{-1}$.

3.7 Conclusion

We have provided a biophysical characterization of sodium ion channel through nonequilibrium response spectroscopy in presence of oscillating voltage protocol. In addition to the kinetic description, using the theory of nonequilibrium thermodynamics developed recently in the last decade we have shown some important features which have not been reported earlier.

(1) From thermodynamic analysis it is found that for constant voltage the system goes to equilibrium, indicated by the vanishing total entropy production rate. This means that system always adjusts itself with the existing constant perturbation. For oscillating voltage system goes to a nonequilibrium time periodic steady state, indicated by the non-zero total entropy production rate.

(2) Using nonequilibrium response approach, we have found that the ionic current shows vanishing dynamic hysteresis at low and high frequency of external voltage but these two domains are thermodynamically distinguishable.

(3) Although the various Markov models have been theoretically investigated for sodium channel involving the studies of dynamic hysteresis through ionic current only, they lack the precise understanding by more physically relevant quantities like work done associated with dynamic memory loops. Performing an analysis of the hysteresis loop areas similar to the concept of the work loop used in muscle physiology to evaluate the mechanical work and power output, we have quantitatively characterised that loop area of ionic current gives us information about the work done by the channel protein sustaining the dynamic memory for ion conduction, while the thermodynamic loop areas gives the information of work done sustaining memory for overall gating dynamics. Thus making thermodynamic characterization essential for studying the role of dynamic hysteresis of ion channel in addition to the traditional studies of ionic current.

(4) The maximum dynamic memory of Na-channel not only depends on the frequency and amplitude but it also depends on the mean of the external oscillating voltage. Fixing any of the two parameters one can obtain optimum value for other parameter where the work done for the dynamic memory is maximum. The choice of mean voltage is very subtle for sodium channel with sensitive dependence on frequency in the intermediate range. At extremely high frequency system responds according to the mean voltage applied.

(5) The relation between the average ionic current and average dissipative work done or energy loss to the surrounding with increasing frequency is of corresponding nature at

the biophysical range. It is important to understand from this study that the utilization of the energy from the external field can not be directly obtained from the measurement of ionic current only.

(6) Here we have given a brief comparison of our results with another popular model of sodium channel by Clancy and Rudy. It is shown that depending upon the state connectivity and rate constants, the time and voltage dependence of the kinetic and thermodynamic quantities may differ in shape and magnitude from model to model, however, the general trend of the frequency, mean voltage and amplitude response of the hysteresis and average other dynamical properties are model independent.

Bibliography

- [1] A. L. Hodgkin and A. F. Huxley, A quantitative description of membrane current and its application to conduction and excitation in nerve, *J. Physiol.* (1952) **117**,500 (1952).
- [2] B. Sakmann and E. Neher, *Single-Channel Recording*, 2nd ed. (Plenum Press, New York, 1995).
- [3] H. Lodish, A. Berk and SL. Zipursky, *et al*, *Molecular Cell Biology*. 4th edition, W. H. Freeman, New York (2000).
- [4] C. M. Armstrong, Interaction of Tetraethylammonium Ion Derivatives with the Potassium Channels of Giant Axons, *J. Gen. Physiol.*, **58**, 413 (1971).
- [5] C. M. Armstrong and F. Bezanilla, Inactivation of the sodium channel. II. Gating current experiments., *J. Gen. Physiol.*, **70**, 567 (1977).
- [6] J. Keener and J. Sneyd , *Mathematical Physiology: I: Cellular Physiology*, Springer, NY, USA (2009).
- [7] M. Fink and D. Noble, Markov models for ion channels: versatility versus identifiability and speed, *Phil. Trans. R. Soc. A* , **367**, 2161 (2009).
- [8] W. J. Bruno, J. Yang and J. E. Pearson, Using independent open-to-closed transitions to simplify aggregated Markov models of ion channel gating kinetics, *Proc. Natl. Acad. Sci. USA*, **102**, 6326 (2005).
- [9] M. Gurkiewicz and A. Korngreen, A Numerical Approach to Ion Channel Modelling Using Whole-Cell Voltage-Clamp Recordings and a Genetic Algorithm, *PLoS Computational Biology*, **3**, 1633 (2007).
- [10] A. Huxley, From overshoot to voltage clamp, *Trends in Neurosciences*, **25**, 553 (2002).
- [11] E. Kandel, J. Schwartz and T. Jessell, "Principles of Neural Science" (4th ed.), McGraw-Hill. pp. 152-3, New York (2012).
- [12] M. F. Bear, B. W. Connors, and A. Michael, eds. (2006) [1996]. *Neuroscience: Exploring the Brain* (3rd ed.). Philadelphia, Baltimore: Lippincott Williams and Wilkins. p. 84. ISBN 978-0-7817-6003-4.

- [13] O.P. Hamill, A. Marty, E. Neher, B. Sakmann and F.J. Sigworth, Improved patch-clamp techniques for high-resolution current recording from cells and cell-free membrane patches, *Pflugers Archiv Euro. J. Physiol.*, **391**, 85 (1981).
- [14] S.R.De. Groot and P. Mazur, *Non-equilibrium Thermodynamics*, North-Holland Publ. Comp., Amsterdam (1951).
- [15] B.Hille, *Ionic channels of excitable membranes*. 2nd edition, Sinauer Associates, Sunderland, Mass. (1992).
- [16] A. Kargol, A. Hosein-Sooklal, L. Constantin, and M. Przystalski , Application of oscillating potentials to the Shaker potassium channel., *Gen. Physiol. Biophys.*, **23**, 53 (2004).
- [17] M. M. Millonas and D. A. Hanck, Nonequilibrium response spectroscopy of voltage-sensitive ion channel gating, *Biophys. J.*, **74**, 210 (1998).
- [18] A. Kargol, B. Smithz and M. M. Millonasz, Applications of nonequilibrium response spectroscopy to the study of channel gating. Experimental design and optimization, *J. theor. Biol.*, **218**, 239 (2002).
- [19] A. Hosein-Sooklal and A. Kargol , Wavelet Analysis of Nonequilibrium Ionic Currents in Human Heart Sodium Channel (hH1a), *J Membr. Biol.*, **188**, 199 (2002).
- [20] B. Das, K. Banerjee and G. Gangopadhyay, Entropy hysteresis and nonequilibrium thermodynamic efficiency of ion conduction in a voltage-gated potassium ion channel, *Phys. Rev. E*, **86**, 061915 (2012).
- [21] W. Zhou, F. S. Cayabyab, P. S. Pennefather, L. C. Schlichter and T. E. DeCoursey, HERG-like K⁺ channels in microglia, *J. Gen. Physiol.*, **111**, 781 (1998).
- [22] R. Mannikko, S. Pandey, H. P. Larsson and F. Elinder, Hysteresis in the voltage dependence of HCN channels: conversion between two modes affects pacemaker properties, *J. Gen. Physiol.*, **125**, 305 (2005).
- [23] M. A. Pustovoit, A. M. Berezhkovskii and S. M. Bezrukov, Analytical theory of hysteresis in ion channels: two-state model, *J. Chem. Phys.*, **125**, 194907 (2006).
- [24] L. O. Chua, V. I. Sbitnev and H. Kim , Hodgkin-huxley axon is made of memristors, *Int. J. Bifurcation Chaos*, **22**, 1230011(1) (2012).
- [25] L. Chua, Memristor, Hodgkin-Huxley, and edge of chaos, *Nanotechnology*, **24**, 383001 (2013).
- [26] M. Pd. Sah , H. Kim, and L.O. Chua, "Brains Are Made of Memristors " *IEEE circuits and systems magazine*, 1531-636X (2014).
- [27] W. A. Catterall, Structure and Function of Voltage-Gated Ion Channels, *Annu. Rev. Biochem.*, **64**, 493 (1995).
- [28] Marban E, Yamagishi T and Tomaselli GF, Structure and function of voltage-gated sodium channels, *J. Physiol.*, **508**, 647 (1998).

- [29] C. A. Vandenberg, F. Bezanilla, A sodium channel gating model based on single channel, macroscopic ionic, and gating currents in the squid giant axon, *Biophys. J.*, **60**, 1511 (1991).
- [30] J. Schnakenberg, Network theory of microscopic and macroscopic behavior of master equation systems, *Rev. Mod. Phys.*, **48**, 571 (1976)
- [31] L. Jiu-li, C. Van den Broeck and G. Nicolis, Stability criteria and fluctuations around nonequilibrium states, *Z. Phys. B*, **56**, 165 (1984).
- [32] G. Nicolis, Fluctuations around nonequilibrium states in open nonlinear systems, *J. Stat. Phys.*, **6**, 195 (1972).
- [33] U. Seifert, Entropy Production along a Stochastic Trajectory and an Integral Fluctuation Theorem, *Phys. Rev. Lett.*, **95**, 040602 (2005).
- [34] H. Ge and H. Qian, Physical origins of entropy production, free energy dissipation, and their mathematical representations, *Phys. Rev. E*, **81**, 051133 (2010).
- [35] M. Esposito and C. Van den Broeck, Three Detailed Fluctuation Theorems, *Phys. Rev. Lett.*, **104**, 090601 (2010).
- [36] J. F. Fohlmeister and W. J. Adelman Jr., Gating current harmonics. I. Sodium channel activation gating in dynamic steady states, *Biophysical Journal*, **48**, 375 (1985).
- [37] L. O. Chua, Memristor-The missing circuit element *IEEE, Trans Circuit Theory*, **18**, 507 (1971).
- [38] L. O. Chua and S. M. Kang, Memristive devices and systems, *Proc. IEEE*, **64**, 209 (1976).
- [39] L. O. Chua, Device modeling via nonlinear circuit elements, *IEEE Trans. Circuits Syst.*, **27**, 1014 (1980).
- [40] L. O. Chua, The Fourth Element, *Proc. IEEE*, **100**, 1920 (2012).
- [41] R. K. Josephson, Mechanical power output from striated muscle during cyclic contraction, *J. exp. Biol.*, **114**, 493 (1985).
- [42] R. L. Marsh, How muscles deal with real-world loads: the influence of length trajectory on muscle performance, *J. Exp. Biol.*, **202**, 3377 (1999).
- [43] G. N. Askew and R. L. Marsh, The mechanical power output of the pectoralis muscle of blue-breasted quail (*Coturnix chinensis*): the in vivo length cycle and its implications for muscle performance, *J. Exp. Biol.*, **204**, 3587 (2001).
- [44] A. A. Biewener, K. P. Dial and G. E. Goslow, Pectoralis muscle force and power output during flight in the starling, *J. Exp. Biol.*, **164**, 1 (1992).
- [45] A. N. Ahn, R. J. Monti and A. A. Biewener, In vivo and in vitro heterogeneity of segment length changes in the semimembranosus muscle of the toad, *J. Physiol.*, **549.3**, 877 (2003).

-
- [46] S. M. Rappaport, O. Tejjido, D. P. Hoogerheide, T. K. Rostovtseva, A. M. Berezhkovskii and S. M. Bezrukov, Conductance hysteresis in the voltage-dependent anion channel, *Eur. Biophys. J.*, **44**, 465 (2015).
- [47] Y. V. Pershin and M. D. Ventra, Experimental demonstration of associative memory with memristive neural networks *Neural Networks*, Elsevier, **23**, 881 (2010).
- [48] S. H. Jo, T. Chang, I. Ebong, B. B. Bhadviya, P. Mazumder, and W. Lu, Nanoscale Memristor Device as Synapse in Neuromorphic Systems, *Nano Lett.*, **10**, 1297 (2010).
- [49] W. Ulbricht, Sodium Channel Inactivation: Molecular Determinants and Modulation, *Physiol. Rev.*, **85**, 1271 (2005).
- [50] J. Patlak, Molecular kinetics of voltage-dependent Na⁺ channels, *Physiol. Rev.*, **71**, 1047 (1991).
- [51] R. Horn and C. A. Vandenberg, Statistical properties of single sodium channels, *J. Gen. Physiol.*, **84**, 505 (1984).
- [52] C. C. Kuo and B. P. Bean, Na⁺ channels must deactivate to recover from inactivation, *Neuron*, **12**, 819 (1994).
- [53] L. A. Irvine, M. S. Jafri, and R. L. Winslow, Cardiac sodium channel markov model with temperature dependence and recovery from inactivation, *Biophysical Journal*, **76**, 1868 (1999).
- [54] C. E. Clancy and Y. Rudy, Na⁺ channel mutation that causes both Brugada and Long-QT Syndrome phenotypes: A simulation study of mechanism, *Circulation*, **105**, 1208 (2002).
- [55] C. E. Clancy, Z. I. Zhu and Y. Rudy, Pharmacogenetics and anti-arrhythmic drug therapy: a theoretical investigation, *Am. J. Physiol. Heart. Circ. Physiol.*, **292**, H66 (2007).

Chapter 4

Chapter 4

Characterization Of Inactivation Path In Voltage-Gated Na⁺ Ion Channel By Non-Equilibrium Response Spectroscopy

Inactivation path of voltage gated sodium channel has been studied in this chapter under various voltage protocols as it is the main governing factor for the periodic occurrence and shape of the action potential. These voltage protocols actually serve as nonequilibrium response spectroscopic tools to study the ion channel in non-equilibrium environment. In contrast to a lot of effort in finding the crystal structure based molecular mechanism of closed-state(CSI) and open-state inactivation(OSI); here our approach is to understand the dynamical characterization of inactivation. The kinetic flux as well as energetic contribution of the closed and open- state inactivation path is compared here for voltage protocols, namely constant, pulsed and oscillating. The non-equilibrium thermodynamic quantities used in response to these voltage protocols serve as improved characterization tools for theoretical understanding which not only agrees with the previously known kinetic measurements but also predict the energetically optimum processes to sustain the auto-regulatory mechanism of action potential and the consequent inactivation steps needed. The time dependent voltage pattern governs the population of the conformational states which when couple with characteristic rate parameters, the CSI and OSI selectivity arise dynamically to control the inactivation path. Using constant, pulsed and continuous oscillating voltage protocols we have shown that during depolarization the OSI path is more favoured path of inactivation however, in the hyper-polarised situation the

CSI is favoured. It is also shown that the re-factorisation of inactivated sodium channel to resting state occurs via CSI path. Here we have shown how the subtle energetic and entropic cost due to the change in the depolarization magnitude determines the optimum path of inactivation.

4.1 Introduction

Introduction Inactivation of sodium ion channel [1,2] is a self-controlled process necessary to sustain the firing pattern of axon potential in excitable tissues [3,4,6,14]. In excitable cells like neurons, muscles, cardiac and endocrine cells, the action potential is initiated when a stimulus causes the membrane potential to reach a threshold which subsequently results in depolarization. After the membrane potential reaches a threshold, voltage gated sodium channels open, allowing an influx of positively charged sodium ions into the cell and further depolarize it [7]. When the cell is depolarised enough the inactivation of sodium channel occurs which inhibits the cell from further excitation [3]. Inactivated state of sodium channel temporarily prevents the channel from reopening until the cell is brought back to the resting potential by potassium channel by out-fluxing the K^+ ions from the cell. If this inactivation process is hampered, various physiological problems appear, like cardiac arrest, hyper excitability, hysteria, epilepsy etc [8–10]. The persistent current has special functions associated with this inactivation process, such as integration of synaptic potentials and acceleration of firing rates etc [11–13]. Various mutations and hereditary diseases also affect the proper inactivation process which makes the sodium channel an optimal drug target [14].

Inactivation of the Na^+ conductance in a squid giant axon was first characterized by Hodgkin and Huxley [15]. Since then a lot of investigation on inactivation of sodium ion channel at the functional and structural levels [4,16–20] had been performed. These studies showed that the inactivation process involves mainly two distinct and complex molecular mechanisms. The well-known first type of the inactivation is the mechanism that occurs from the open-state, so called open-state inactivation (OSI), at strongly depolarized membrane potentials. The other type of inactivation occurs from pre-open closed states, the closed-state inactivation (CSI), at hyper-polarized and modestly depolarized membrane potentials. Thus voltage-gated Na^+ channel utilizes both OSI and CSI [16,17,21,22] paths. Although detailed mechanistic description of OSI is there [23], much less is known about the CSI in this regard [24–26].

For the previous few decades the majority of the studies of inactivation had been performed by electrophysiologists using usual voltage clamp and patch clamp techniques. But recently developed non-equilibrium response spectroscopic technique [27, 28] has become popular method to study the ion channels in non-equilibrium environment [29], using continuously oscillating voltage protocol [30] or fluctuating voltage [31] or pulse train voltage protocol. This sort of non-equilibrium response spectroscopic technique provides new aspects of ion channel gating kinetics which standard stepped-potential protocols cannot provide [30]. Beside all these although a great deal of effort has been exercised to kinetically understand the molecular mechanism of inactivation, the nonequilibrium thermodynamics in the problems of inactivation has never been applied. The study of nonequilibrium parameters like total entropy production rates can be used to confirm the kinetic results [32]. For oscillating voltage protocol, with its biophysically chosen amplitude, frequency and mean voltage, the system replicates the neuronal oscillation which arises due to oscillatory nature of the membrane depolarization. Also the pulse train protocol is applied here which activates and then deactivates the channel providing a scope to study the path of activation and then the recovery path from inactivation to resting state during refractory period. Using these voltage protocols and nonequilibrium response properties we have characterised the inactivation path both kinetically and thermodynamically which has not been studied earlier. In this respect we are mainly interested here to understand the dynamical mechanism of inactivation in contrast to the molecular mechanism which are traditionally searched for. More specifically using the model of Vandenberg and Bezanilla [33] for various protocols here we have explored the following queries regarding sodium ion channel inactivation:

1. How the channel does react to the constant voltage protocol and what is the favoured path of inactivation in terms of CSI and OSI?
2. What is the preferred path of inactivation during test pulse and base pulses of pulse train protocol and continuously oscillating voltage protocol?
3. How does the non-equilibrium thermodynamic quantities like total entropy production rate contribute to the kinetic understanding?
4. How do these different voltage protocols collectively contribute towards our general understanding of inactivation path or how the different response natures towards different protocols enlighten the mechanism of channels inactivation path?

4.2 Dynamical Characterization Of Inactivation

For the past few decades characterisation of inactivation has been an important topic of research. Various models and theories [14, 16, 17] regarding fast, slow and ultra-slow inactivation [3] have come up. Even though the crystal structure of sodium channel in potentially two inactive states [34, 35] are found, still the path of inactivation happens to be a matter of debate. Almost all recent studies involve molecular structure related information which are very hard to speculate from theoretical perspective. Besides proper non-equilibrium energetics of inactivation path has never been considered. Also how does the different voltage protocols used in the experiments for characterizing the sodium channel inactivation collectively contribute towards our basic understanding of inactivation path is still not addressed in a general framework. Thus studying the simple kinetic flux analysis and thermodynamic contribution of total entropy production rates associated with these inactivation paths we have characterized the dynamical profiles of CSI and OSI in this chapter. Before going to the different voltage protocols used, here we have briefly discussed the kinetics and thermodynamics of inactivation path in the following subsections.

4.2.1 Kinetics of CSI and OSI

There are two possible ways of inactivation as seen from the model (3.1). One is from pre-open closed state, i.e. from P_3 to P_6 (CSI, closed state inactivation) and another is from open-state, i.e. from P_5 to P_8 (OSI, open-state inactivation) [21, 26]. Both of the paths are responsible for inactivation but depending on the kinetic rate parameters and voltage protocols applied we can qualitatively understand here which one is the most favourable path for inactivation, simply by calculating the net flux direction and magnitude. Here we designate the CSI and OSI as follows,

$$CSI(t) = [\alpha_4 P_3(t) - \beta_4 P_6(t)] \quad \text{and} \quad OSI(t) = [\alpha_5 P_5(t) - \beta_5 P_8(t)] \quad (4.1)$$

We have studied the total amount of flux associated with the closed-state inactivation and open-state inactivation. Thus we have calculated the following quantities, which provide the net amount of CSI and OSI occurred in a certain voltage up to the respective steady-state.

$$A_{CSI} = \int_0^{t_s} CSI(t) dt \quad \text{and} \quad A_{OSI} = \int_0^{t_s} OSI(t) dt \quad (4.2)$$

4.2.2 Nonequilibrium thermodynamic characterisation of inactivation path

We concentrate on the total entropy production rates associated with the CSI and OSI path. Thus the total entropy production rate of the CSI path is written as,

$$\dot{S}_{tot}^{CSI}(t) = \left[\alpha_4(V(t))P_3(t) - \beta_4(V(t))P_6(t) \right] \ln \left[\frac{\alpha_4(V(t))P_3(t)}{\beta_4(V(t))P_6(t)} \right]. \quad (4.3)$$

Similarly for open state inactivation path the total entropy production rates associated can be written as,

$$\dot{S}_{tot}^{OSI}(t) = \left[\alpha_5(V(t))P_5(t) - \beta_5(V(t))P_8(t) \right] \ln \left[\frac{\alpha_5(V(t))P_5(t)}{\beta_5(V(t))P_8(t)} \right]. \quad (4.4)$$

Next we have defined here quantities such as F-CSI and F-OSI which are the percentages of the total epr associated with the close state inactivation path and open state inactivation paths, respectively. These quantities are given as follows.

$$F - CSI(\%) = \left[\frac{\dot{S}_{tot}^{CSI}(t)}{\dot{S}_{tot}(t)} \right] \times 100,$$

and

$$F - OSI(\%) = \left[\frac{\dot{S}_{tot}^{OSI}(t)}{\dot{S}_{tot}(t)} \right] \times 100. \quad (4.5)$$

These nonequilibrium thermodynamic quantities like total entropy production rates provide the information about the entropic cost associated with these two paths. The CSI-epr and OSI-epr actually shows the dissipation of energy via these two paths. A path which is more dissipative is more favoured by the system. The CSI-epr and OSI-epr actually shows which path is more favourable during various depolarizations.

4.3 Constant Voltage Protocol

Generally the constant voltage clamp technique is used by electrophysiologists to measure the ionic current through the membrane of excitable cells, while holding the membrane voltage at a set level. The voltage clamp allows the membrane voltage to be manipulated independently of the ionic current, allowing it to study the current-voltage relationship of the voltage gated sodium channel. For the constant voltage case the transition rates

become time independent as the voltage is kept constant throughout the time course of the study. Before we start characterising the inactivation we have studied the ionic currents, probabilities at different voltages numerically. We have used Runge-Kutta algorithm for solving nine coupled differential equations here. All the rate constants and the parameters are already given in the section of kinetic scheme.

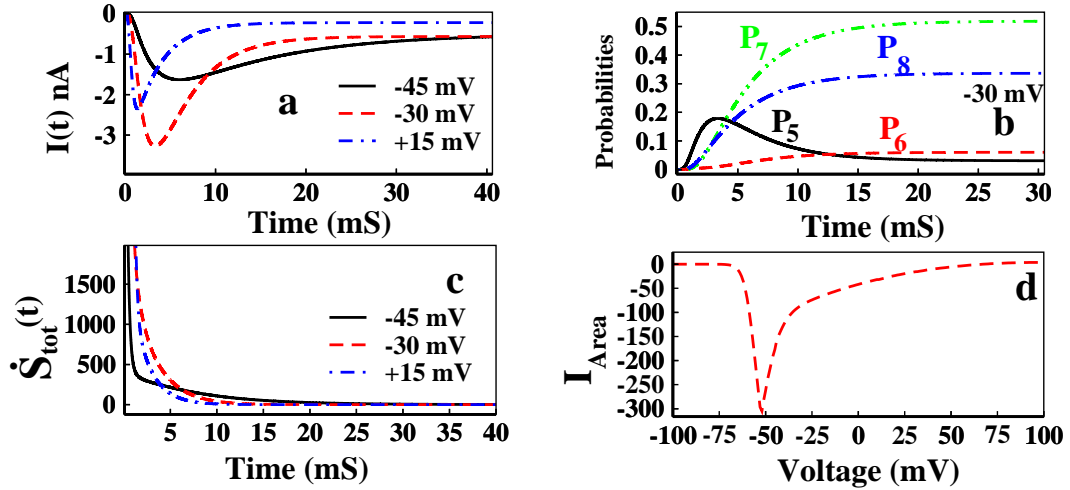


Figure 4.1: Characterization of inactivation at constant voltage. In (a) ionic current at constant values of depolarization such as -45, -30, +15 mV are shown. In (b) open-state, P_5 and inactive states, P_6 , P_7 , P_8 probabilities with time at a depolarization of -30 mV is shown and in (c) total epr, $\dot{S}_{tot}(t)$ vs. time has been plotted for -45, -30 and +15 mV, respectively. In (d) the integrated ionic current vs. various depolarization up to their steady state points, t_s have been shown

From the figure 4.1(a) it is seen that with the onset of depolarization ionic current initially increases, allowing influx of sodium ion current inside the cell membrane, and after passing through a maxima (maxima, because, $I(t) = -ve$, the more negative, the more influx of current into the cell) ionic current decreases. Generally the first part of increasing ionic current is called the activation and the decreasing part of ionic current is called inactivation. From figure 4.1(b) it is observed that open-state probability P_5 gradually decreases and the inactive states start rapidly and takes higher values than P_0 to P_5 states, inferring that the system ultimately goes to inactivated state.

In figure 4.1(c) we have plotted the total epr with time for -45, -30 and +15 mV. For all the voltages it is seen that the system quickly attains the equilibrium as seen from vanishing total epr [41]. For the constant depolarization system always adjust itself with it and equilibrate finally. With the increase in depolarization, system goes to equilibrium in a faster rate. Now as details balance holds in equilibrium with all opposite fluxes are balanced by each other, thereby CSI and OSI also vanish. For this reason if we want to study the paths of inactivation in terms of CSI and OSI, we have to keep the system

driven or out of equilibrium by applying some external time dependent voltage protocol, as discussed in the next two sections.

4.3.1 Activation and Inactivation dominated regions

It is also observed from 4.1(a) that with the increasing depolarization inactivation occurs in a faster rate. As the activation and inactivation process occurs simultaneously it is hard to differentiate this to process as they are mutually coupled to each other. We can at least find the region of voltages where the activation process predominates and vice versa. So, if we calculate the net amount of ionic current in-fluxed into the cell by calculating the area under the curve of ionic currents in various depolarizations, up to their respective steady states, we must observe a region of voltage in which the channel will allow more and more current with more depolarizations. After a certain value of depolarization the channel will close with much faster rate, inhibiting ion influx. The integrated ionic current stated above is calculated as

$$I_{Area} = \int_0^{t_s} I(t) dt, \quad (4.6)$$

where t_s is the time to achieve the steady state for a certain voltage. t_s changes as voltage changes. As the voltage increases from -ve region to +ve region the t_s decreases. In 4.1(d), I Area is plotted against various depolarizations. From this figure it is observed that up to ≈ -70 mV there was no current influx as -70 mV is the resting potential of the cell. Above ≈ -70 mV, the integrated ionic current, I Area increases and that is why it is called as the activation dominated region(-70 to -50 mV). After that the integrated ionic current decreases and so the rest of the part is inactivation dominated region. Given the rate constants the ranges of these domains vary in different sodium channels.

4.3.2 Choice of voltage region to study inactivation

Choice of voltage region to study inactivation is one of the important task we have to do in constant voltage protocol. To extract information about inactivation it is instructive to study the system in a voltage region where inactivation predominates, especially for the model oriented studies, where activation phenomena can affect the inactivation less. Beside the kinetic model and rate parameters also determine the region where one should study the model for inactivation. In our model we have found that for constant voltage case, it is worth studying inactivation above -55 mV. In the figure (4.2) we have plotted the sum of the probabilities of all three inactive states, ($P_6 + P_7 + P_8$) along with the

three resting states, $(P_0 + P_1 + P_2)$. From the curves we can see that the channel actually gains probability of attaining inactivated state above -55 mV, below which the probability of remaining in the resting states is very high or the system hardly activates. Thus for constant voltage protocol it is worth studying the system above -55 mV where the channel has maximum probability of attaining inactivation. Once again we want to mention that this voltage region varies from model to model and with associated rate parameters. Thus for the next analysis regarding the inactivation, we have applied the voltage starting from -55 mV to above.

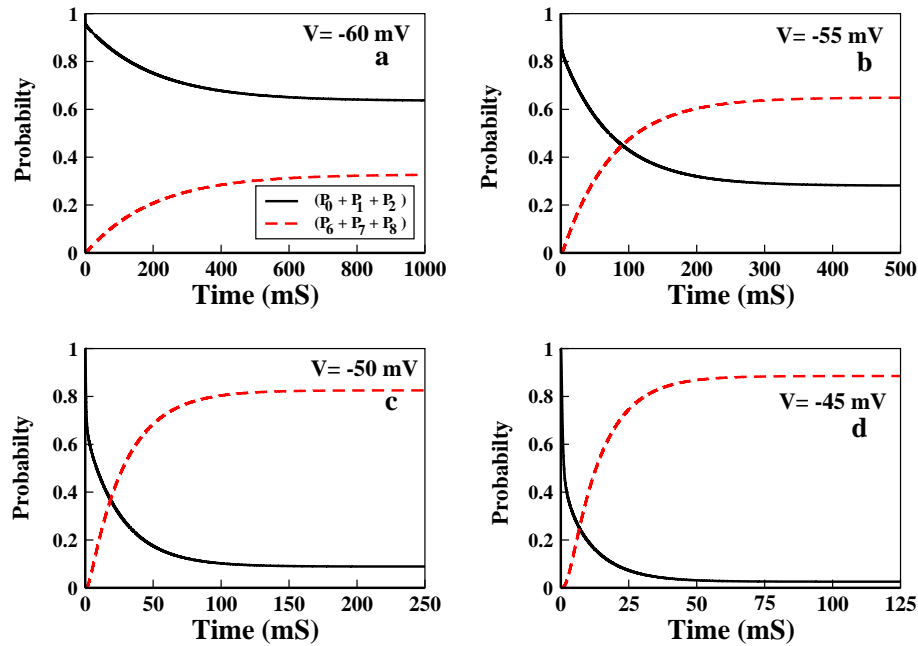


Figure 4.2: Choice of voltage range. In (a to d) The collective probability of the resting states(see text) and the inactive states have been plotted for voltage -60 , -55 , -50 and -45 mV, respectively.

4.3.3 Waiting Time analysis of inactive states

To characterize the inactivation process we want to study the mean waiting time for inactivation in different voltages. The inverse of this quantity shows an approximate rate of inactivation. Now we calculate the mean waiting time as follows,

$$\langle t_{wt}^{in} \rangle = \int_0^{t_s} \frac{d(P_6 + P_7 + P_8)}{dt} dt, \quad (4.7)$$

where we calculate the mean waiting time of overall inactivation including all the inactive states such as P_6 , P_7 and P_8 . Then we plot the mean waiting time as a function of voltage.

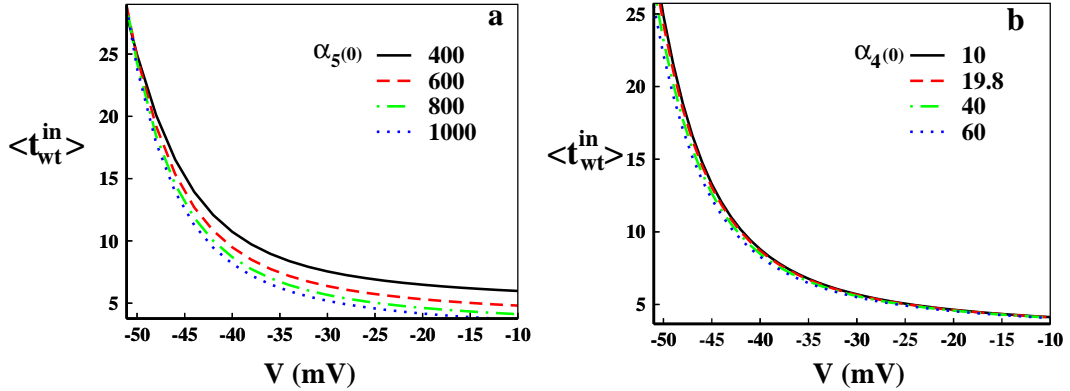


Figure 4.3: Waiting time analysis. In (a) waiting time analysis at different voltages with $\alpha_5(0) = 1000, 800(\text{original}), 600$ and 400 s^{-1} have been plotted up to their steady-states. In (b) similar waiting time analysis is done for $\alpha_4(0) = 60, 40, 19.8(\text{original})$ and 10 s^{-1} .

In figure 4.3(a) and (b), the mean waiting time has been plotted for various depolarizations. It is seen that from -50 mV the mean waiting time gradually decreases with increasing depolarization. As with increasing depolarization inactivation occurs with faster rate the mean waiting time decreases. This result is also consistent with the result of figure 4.1(c).

As we are interested in the inactivation path, next we have shown the effect of change in the rate constants associated with the CSI and OSI paths. The change of rate constants can be physically attributed to the mutation originated disorders. Various mutations and hereditary diseases can change the rates of the path of inactivation. Here we have changed the rate constants a 5 and a 4 to observe the effect in mean waiting time associated with OSI and CSI, respectively. In figure 4.3(a) we have varied the $\alpha_5(0)$ from 400 to 1000 s^{-1} , where green dot-dashed line with 800 s^{-1} is the original rate constant as mentioned in Table 1. Similar plots have been done for figure 4.3(b) for $\alpha_4(0)$ from 10 to 60 s^{-1} . It is quite expected that with increasing rate constants, the mean waiting time should decrease as the rate of inactivation increases. This is also evident from figure 4.3(a) and (b). It is worth mentioning that the change in the rate constants of CSI path do not affect the mean waiting time or rate to a considerable amount. But the change in the rate constant of OSI path affects the overall rate of inactivation considerably which intern also concludes that the OSI path of inactivation occurs in a much greater extent than CSI in this voltage region.

4.3.4 Constant voltage inactivation path

Now we have come to our desired goal of characterization of the inactivation path in constant voltage protocol. Here we have observed the total amount of flux associated with the closed-state inactivation and open-state inactivation. Thus we have calculated the following quantities, which provide the net amount of CSI and OSI occurred in a certain voltage up to the respective steady-state.

$$A_{CSI} = \int_0^{t_s} CSI(t)dt \quad \text{and} \quad A_{OSI} = \int_0^{t_s} OSI(t)dt. \quad (4.8)$$

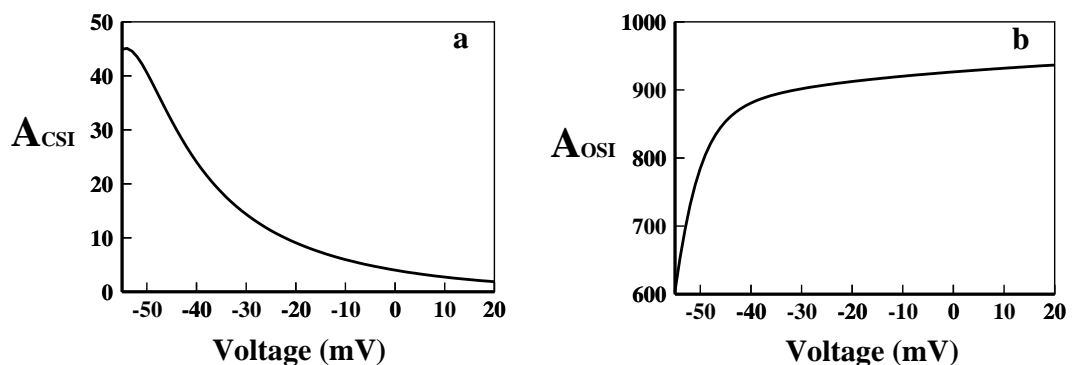


Figure 4.4: Path of inactivation in constant voltage protocol. In (a) the A_{CSI} (see text) and in (b) the A_{OSI} (see text) are plotted for various voltages, respectively.

The definitions of CSI and OSI have been taken from equation (4.1). In figure 4.4(a) and (b) A_{CSI} and A_{OSI} are plotted. It is seen that the net amount of CSI is lesser than the OSI for all voltages. Also it is seen that with increasing depolarization the amount of CSI decreases but OSI increases. Thus it is observed that in this region of depolarization OSI is the most preferred path of inactivation. In general most of the sodium channels use both CSI and OSI. However some channels undergo more inactivation from the open-state and others undergo more inactivation from CSI. These distinct behaviors can be classified as preferential OSI and preferential CSI [21]. The results show that our system is a preferential OSI system.

4.4 Pulse Train Protocol

The pulse train protocol is a popular and a very powerful nonequilibrium spectroscopic tool to study the channel gating process, inactivation procedure and recovery from inactivation [42–45]. Here we want to investigate the path of inactivation in presence of

consecutive test pulses and base pulses. The pulse train is applied in the following manner. First, a base pulse of -80 mV is provided to the system for few milliseconds and then test pulse train of -45 mV is initiated. Each test pulse in the pulse train is brought back to -80mV base voltage and then again fired to test voltage. The applied pulse train is shown in figure 4.5(a). This important nonequilibrium spectroscopic tool replicates the real biological situation where sodium channel responds to a repetitive stimulus. Here the -45mV test pulse activates the system and the base pulse causes necessary refractory changes to the system to prepare it ready for the next incoming pulse. An interesting advantage of using pulse train protocol is that we can actually control the population of various states as desired. As for example the test pulse of -45mV will populate the open-state and inactive states while the base pulse will again depopulate them and will populate the resting state. While populating the resting states, it will provide us a scope to identify the path of re-factorization to the resting state, which has been a major part of investigation [25]. In figure 4.5(b) the corresponding ionic current is shown. It is seen that after the first pulse the peak of the ionic current is gradually reduced as seen in the experiments done earlier [44]. For our purpose of characterization of the inactivation path

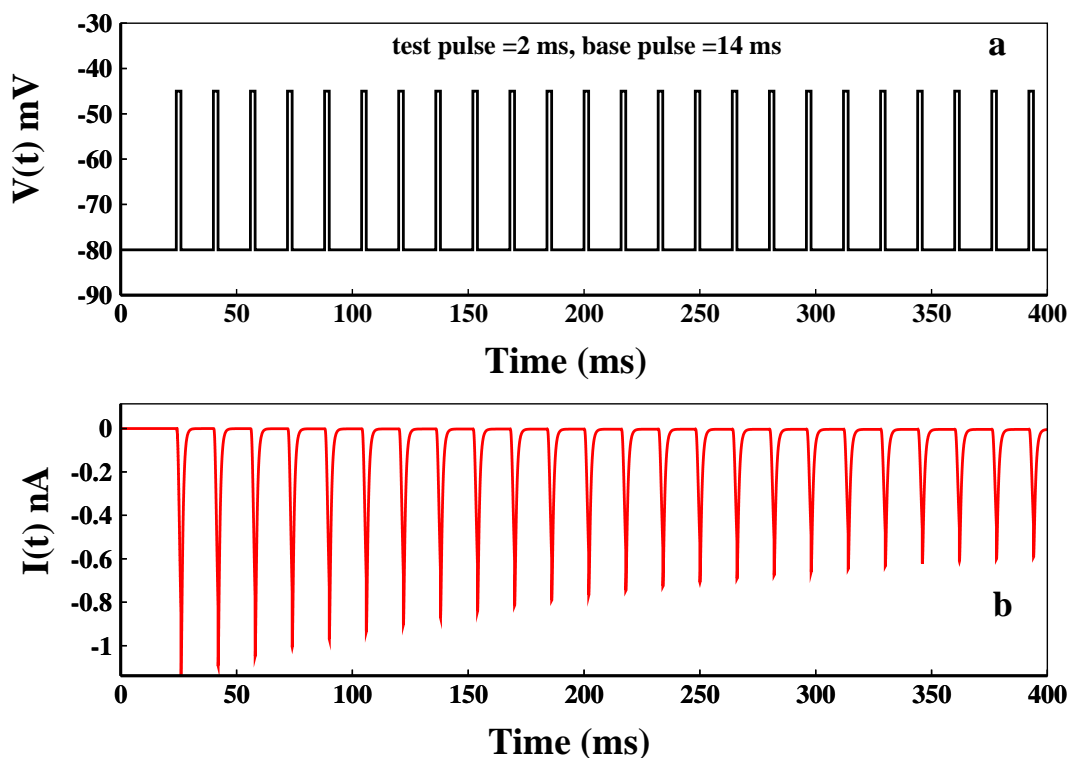


Figure 4.5: Pulse train protocol. In (a) at first the voltage is kept at -45 mV and after few milliseconds it is brought back to base -80 mV after that the pulse train begins. Here the base pulse duration is 14 ms and test pulse duration is 2 ms. In (b) the corresponding ionic current is plotted.

we concentrate on the first 200 ms of the pulse train and for studying the kinetic and the thermodynamic contribution of the closed- state and open-state inactivation. It enables us to understand which path is more favored during test pulse and during refactoring base pulse.

4.4.1 Kinetics of CSI and OSI in pulse train

Here we designate the forward flux of CSI path as CsF and the backward flux as CsB. They are expressed as $CsF = \alpha_4 P_3$ and $CsB = \beta_4 P_6$. Similarly for OSI path, $OsF = \alpha_5 P_5$ and $OsB = \beta_5 P_8$. Now comparing the figures 4.6(b) and (f) it is clearly seen that during the test pulses the net OSI is almost 10 times of the magnitude of the net CSI and also the magnitude of the OSI is +ve, indicating that during the test pulse the open-state inactivation path is preferred. The magnitude of CSI is 10 times lesser than OSI indicating very small probability of occurring inactivation through CSI path. Also it is seen that the magnitude of the CSI and OSI during the test pulses is gradually decreasing. Thus with time both types of inactivation gradually decreases down. One thing we have noticed that the CSI during base pulses gradually becomes more negative after each pulses as seen from the inset of igure 4.6(b) but the OSI remains almost zero during base pulses for all the time. Now to understand the increasing negative magnitude of CSI and the nature of OSI which is almost zero all the time during base pulses, we need to look at the forward and backward fluxes associated with these paths.

Now as we defined $CSI = (CsF - CsB)$ and $OSI = (OsF - OsB)$, if CSI is +ve then the path P_3 to P_6 is followed. Again if CSI is -ve, then the path P_6 to P_3 is followed and similarly for OSI path. Now comparing the figure 4.6(c) and (g) it is seen that during the test pulse CsF is almost 10 times lesser than OsF. Thus closed state inactivation during test pulse also occurs along with open-state inactivation but with negligibly less amount. During the test pulse the OsF is the most favored path. It is worth mentioning that in figure 4.6(h) the OsB flux is seen to be gradually increasing. It is just a mathematical interpretation of the fact that the inactive states are gradually populating or the channel's inactivation via open-state is gradually decreasing. It does not mean that the system reverts back from inactive state to open-state, which is not true in real situation. To hold the microscopic reversibility each Markov model has forward and backward rates. It is thus always instructive to study the net flux which is OSI/CSI instead of giving much of emphasis on individual fluxes, especially for the model oriented kinetic study. Studying individual fluxes are necessary for detailed theoretical understanding of the dynamics of the system but sometimes in reality they are more or less irreversible.

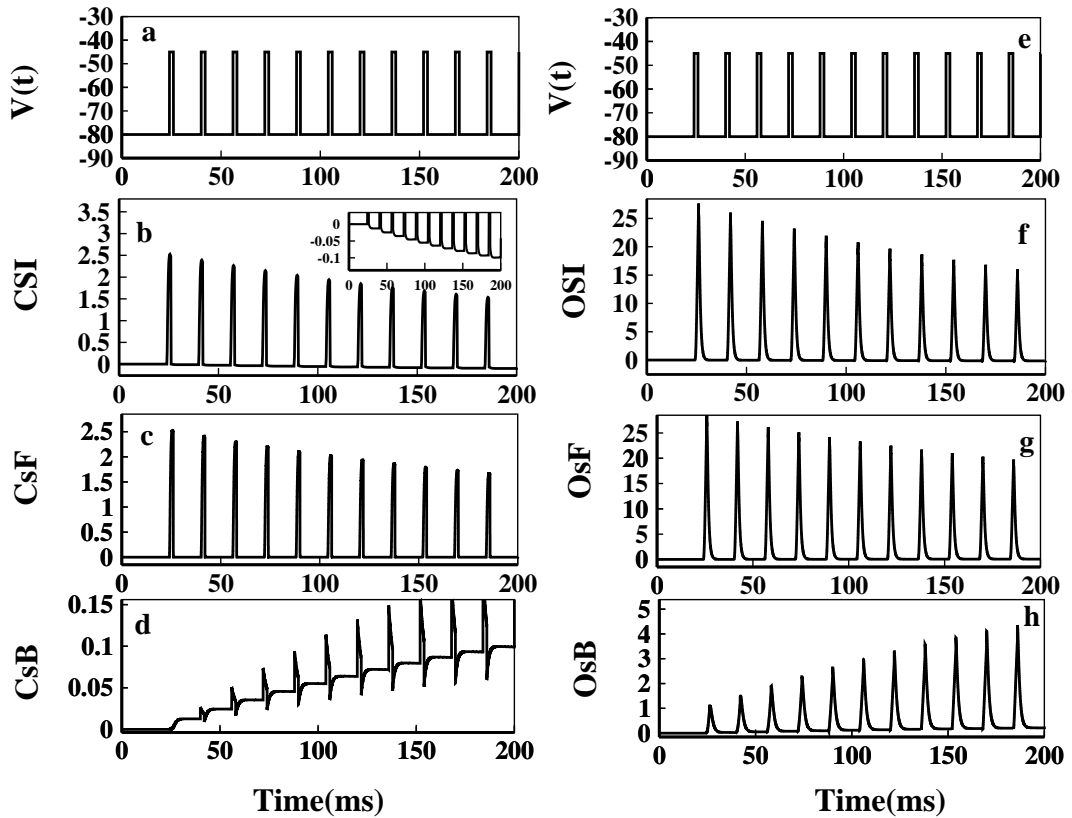


Figure 4.6: Pulse train fluxes. The left panel(a-d) corresponds to the fluxes of closed-state inactivation(CSI) and the right panel(e-h) corresponds to the open-state inactivation(OSI) path. In (a) and (e) the selected first 200ms pulses of figure 4.5(a) has been plotted. In (b) and (f) net CSI and net OSI has been plotted respectively. In (c) and (g) forward flux(CsF) of CSI path and forward flux(OsF) of OSI path are plotted respectively. In (d) and (h) backward flux(CsB) of CSI path and backward flux(OsB) of OSI path are plotted, respectively. The inset figure of (b) shows the gradual increase of negativity of CSI during base pulses.

Now an interesting feature is seen in the base pulses. During the base pulses CsF is close to zero but the CsB is -ve and the negativity gradually increases with time with each base pulse as seen from figure 4.6(d) making the CSI more and more -ve during base pulses as seen in figure 4.6(b)(inset). Here OsF and OsB are approximately zero, indicating that during repolarisation the OSI fluxes has almost no contribution to the system dynamics. This clearly says that during the base pulses the system reverts back to resting state via closed state via CsF path. Shab K+ [46] channels and most of the sodium channels bypasses the open-state during recovery from inactivation [47]. Our analysis certainly agrees with that. Also the rate of recovery from inactivation increases after each pulse with increase in the inactive states population [44]. Thus we have the following situation during the test pulse and base pulse as seen in figure 4.7.

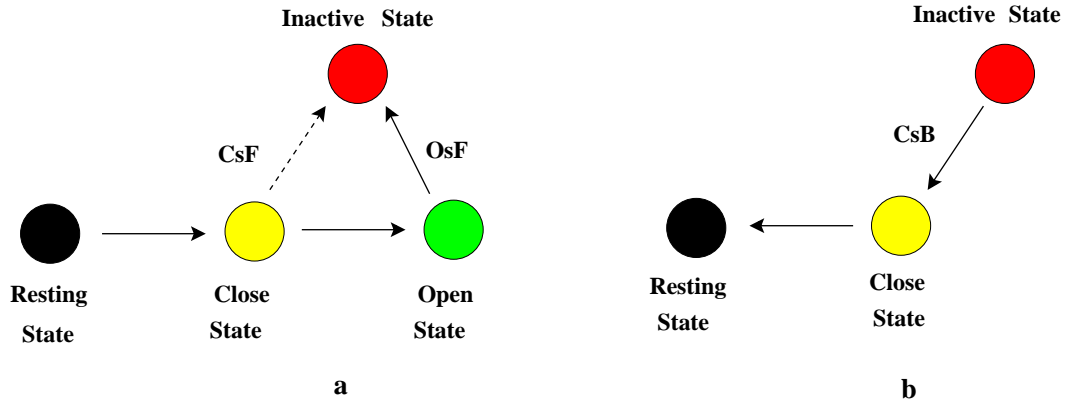


Figure 4.7: Path during activation and recovery from inactivation. In (a) the test pulse path of inactivation has been shown. During the test pulse the system from resting state P_0 goes to closed-state P_3 to P_5 and then via OsF path goes to inactivation. There is a small probability of occurring inactivation via CsF path. The bold solid arrow line indicates the most preferred path of inactivation, OsF. In (b) the recovery from inactivation or refractory path during base pulse is shown. During the base pulse the system from inactivated state goes to resting state via CsB path.

4.4.2 Non-equilibrium thermodynamics of CSI and OSI in pulse train protocol

In figure 4.8 we have plotted the time dependent entropy production rates for pulses starting from 0 ms to 300 ms. From Figure 9B it is seen that the total entropy production rates shows sharp peaks instantly after onset of both test pulses and base pulses. But the peak height gradually decreases down. With the onset of test or base pulses system goes far from the equilibrium as seen by the non-zero values of the dissipation function or the total epr at the peaks. Any change in the depolarization instantly changes the state of the system. Here we want to mention that within this 2 ms test pulse duration the system cannot reach the equilibrium and also during the 14 ms base pulse duration system does not achieve the equilibrium but remains very close to it. These durations are purposefully set so small so that we can study the relaxation or the response dynamics in nonequilibrium environment.

In this situation, we have seen the entropic contributions arising due to closed-state inactivation and open-state inactivation. From the figure 4.8(c) we can see that the entropic contribution of CSI path during the test pulses gradually decreases down. Also during the test pulse $\dot{S}_{tot}^{OSI}(t)$ has significantly higher magnitude than the $\dot{S}_{tot}^{CSI}(t)$ as seen from figure 4.8(d). Oppositely during the base pulse the CSI contribution gradually increases as seen from the inset of figure 4.8(c) but $\dot{S}_{tot}^{OSI}(t)$ remains zero all the time during base pulses. As the population of inactive states increase with each test pulse, re-factorization

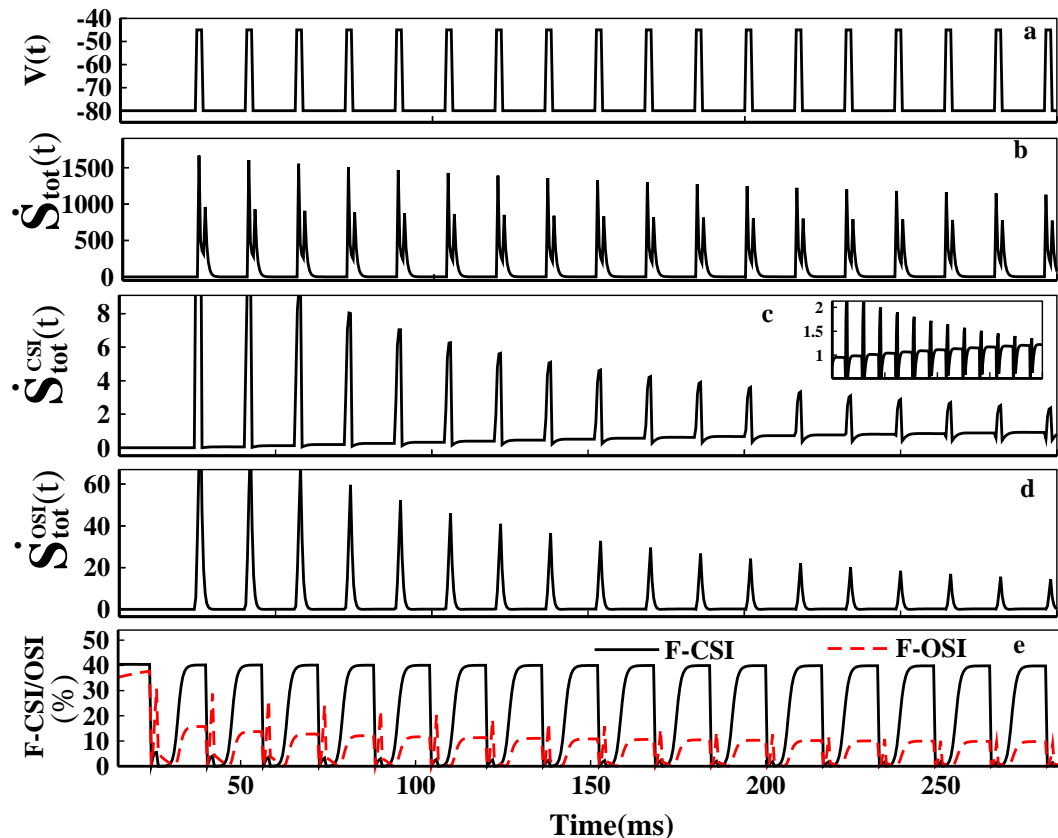


Figure 4.8: Non-equilibrium dissipation. In (a) the pulse train is shown for the first 300 ms. In (b) $\dot{S}_{tot}(t)$ is plotted. In (c) $\dot{S}_{tot}^{CSI}(t)$ and in (d) $\dot{S}_{tot}^{OSI}(t)$ has been plotted. The F-CSI (%) and F-OSI (%) is plotted in (e).

entropy production rate increases with each base pulses. From this thermodynamic analysis we can conclude in correspondence with the kinetic analysis done earlier that during the test pulse OSI path is favored and during base pulse CSI path is favored. The figure 4.8(e) shows the percentage of CSI and OSI contributions of total entropy production rate, respectively. Here in both the graphs the responses are slightly left sifted due to the complex natures of the F-CSI and F-CSI functions. But the general trend is similar to the kinetic trend with more clarity now i.e., during the depolarization OSI fraction of the total epr is greater than CSI. But during the repolarization the CSI fraction is greater than OSI. With each test pulse the OSI fraction gradually decreases down.

4.5 Oscillating Voltage Protocol

Oscillating voltage protocol is an emerging technique to study the ion channels in non-equilibrium environment [27, 29]. In individual neuron the oscillation may appear due to

the oscillating nature of action potential and membrane depolarization. Here we have theoretically studied the kinetic as well the thermodynamic response properties of Na⁺ channel by considering the sinusoidal oscillating voltage protocol. Here the sinusoidal external voltage that we apply is expressed as, $V(t) = V_0 + A \sin(\omega t)$, where $V_0 = -70$ mV is the mean voltage around which it oscillates as well as is the resting potential of the neuron, A is the amplitude of the oscillation and ω is the frequency as shown in figure 4.9(a). To get more biophysical insight we have taken the amplitude of the oscillating voltage, $A = 45$ mV which covers the entire biological range of activation and inactivation depolarization of sodium channel, i.e. (-115 to -25 mV). By taking these parameters, we have studied the kinetic and thermodynamic response at steady state in one complete cycle of the oscillating voltage. Here the transition rates are time as well as voltage dependent. The idea is to study the inactivation paths and their thermodynamic contributions to the total epr.

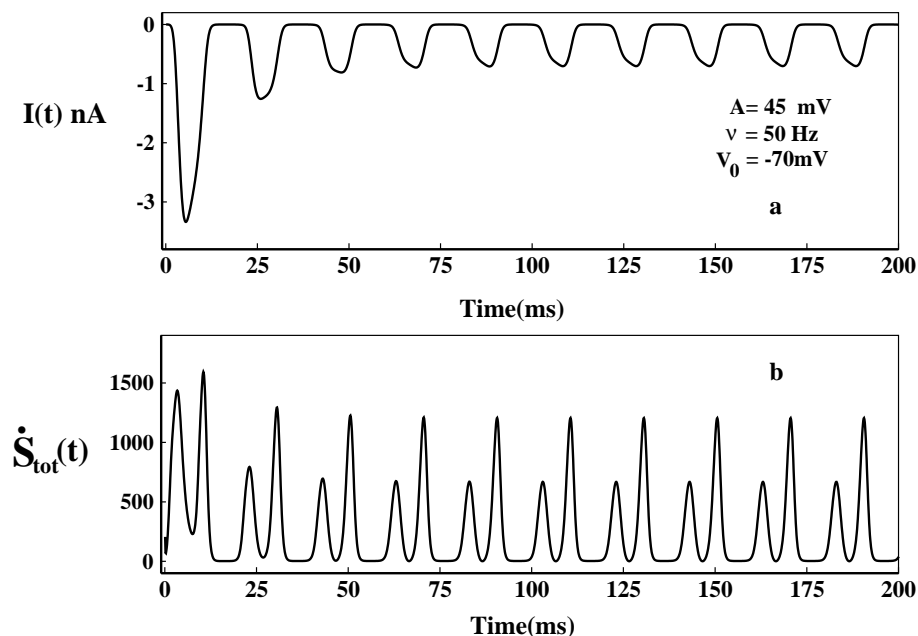


Figure 4.9: Ionic current and total epr in oscillating voltage protocol. In (A) the ionic current and in (B) the corresponding total epr has been plotted.

In figure 4.9(a) the ionic current is plotted at frequency 50 Hz. The ionic current initially oscillates with larger amplitude and then gradually amplitude decreases and it attains a time periodic steady value. Similarly the total epr finally attains a time periodic steady value. As the total epr is always greater than zero, the system is always out of equilibrium and the steady-state is a nonequilibrium steady state (NESS) or dynamic steady-state [48]. At NESS we have studied the directions of the fluxes to understand the OSI and CSI and their contribution to total epr.

4.5.1 Kinetics of CSI and OSI in oscillating voltage protocol

In the figures 4.10(a) and (b) the voltage of the last oscillation or the NESS voltage variation are shown with time. In figures 4.10(c) and (d) the CSI and the OSI has been plotted, respectively. It is seen that in the first half of the cycle where the voltage is more depolarizing, i.e., (-70 to -25) mV, the magnitude of the OSI is much larger than the CSI path. But in the 2nd half when the voltage is in the hyper-polarizing region, i.e. (-70 to -115) mV, the CSI is -ve and OSI is zero almost. This is pretty consistent with the constant and pulse train protocol. It means during the depolarization OSI is more favored than CSI. But during hyperpolarization CSI is favored than OSI.

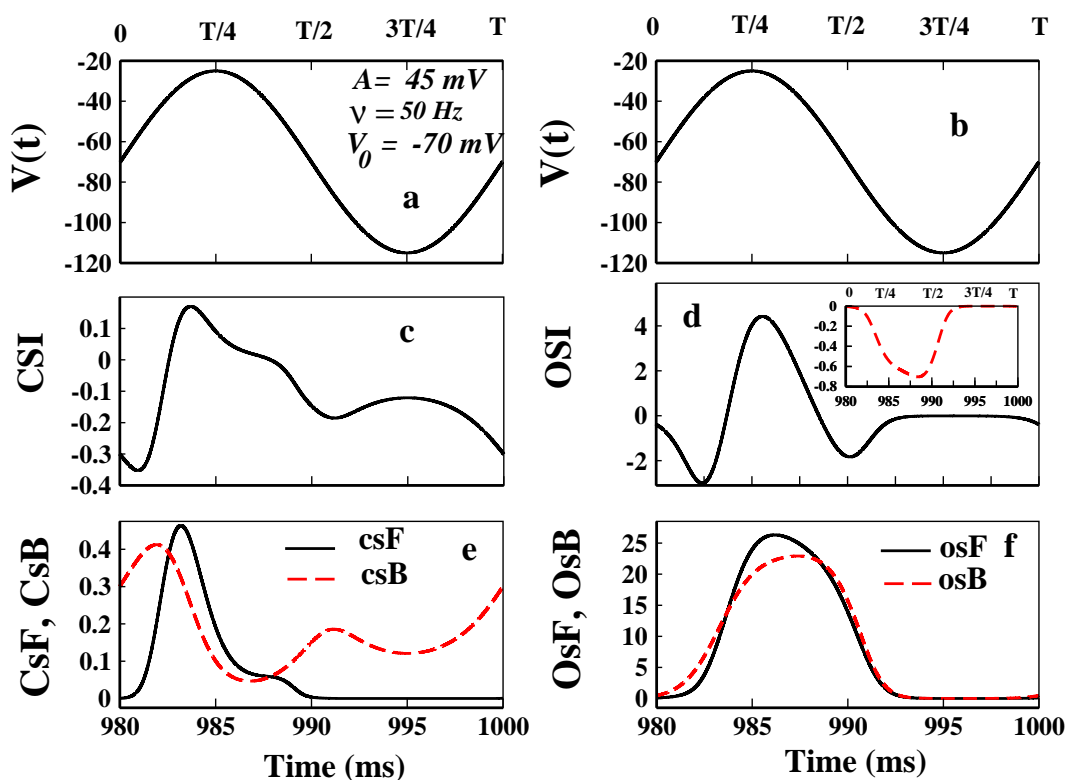


Figure 4.10: Flux analysis at NESS in oscillating voltage protocol. In (a) and (b) the NESS voltage variation for a cycle has been plotted. In (c) and (d) CSI and OSI have been plotted. The inset shows the ionic current at NESS. It shows that the first $T/8$ time is electrically silent. In (e) CsF and CsB and in (f) OsF and OsB have been shown.

It is worth mentioning that the negative magnitude at the very beginning of the OSI arising from the kinetic analysis of such kind may infer some phenomenon which does not happen in reality. The negativity of OSI denotes that system from inactive state goes to open-state again. If so then it could not be an electrically silent process [25] then. From the inset of figure 4.10(e), we can see that the first $T/8$ ms where OSI is negative is actually electrically silent as it is silent during hyper-polarized region. The negativity of

OSI comes from the mathematical construction of the model to maintain the microscopic reversibility which indeed does not show up in the ionic current. This happens because the population of P_8 gradually increases with time. Initially the OsF remains greater than OsB . As the time passes the population of inactive states increases such that at NESS $P_8 \gg P_5$, but the forward and backward fluxes becomes comparable. The case of oscillating voltage is somewhat different from the pulsed train. As it is a continuous voltage change, so the system shows somewhat continuity in responses at the beginning or in the end of the each oscillating pulse. It does not change suddenly. However, recovery from inactivation on sodium channel using oscillating voltage protocol still can be a subject of experimental verification as recovery process is a highly voltage dependent [47]. Now from figures 4.10(e) and (f) it is clear that in the first half of the oscillation OSI is favored than CSI and in the second half CsB is the path during re-polarization, as also seen in pulsed train protocol.

4.5.2 Thermodynamics of CSI and OSI in oscillating voltage protocol

Next we have seen the thermodynamic contribution of CSI and OSI path. In the left panel of figure (4.11) the eprs are plotted with time and in the right panel the eprs are plotted with voltage. The total epr of the system at NESS is plotted in figure 4.11(b) which shows asymmetric response in the 2 halves of the oscillation. It shows the response is more evident on the left side of the oscillation, i.e., between 0 to $T/2$. After the $T/2$ the total epr contribution is negligible, which is correct as in the hyper-polarized region only the CsB path contributes, not all states contributes to the total epr. The total epr is plotted with voltage in figure 4.11(g) which also shows hysteresis property. The kinetic [49] and thermodynamic analysis [41] of dynamic hysteresis of ion channel proves that the ion channel behaves like a memristor device [50]. In figure 4.11(c) the $\dot{S}_{tot}^{CSI}(t)$ is plotted which shows the contribution mainly arises in the second half of the oscillation that is between $T/2$ to T . In this hyper polarized voltage range (-70 to -115 mV) CSI path shows more contribution than the OSI path as seen after comparing OSI the figure 4.11(d) where the $\dot{S}_{tot}^{OSI}(t)$ mainly contributes to the total epr in the first half of the cycle with more depolarised(-70 to -25mV) voltage case. The F-CSI (%) and F-OSI(%) in figures 4.11(e) and (f) shows it clearly that the CSI contribution arises in the hyper polarized region while OSI contribution arises in more depolarised region. This behavior is consistent with the pulse train analysis where we have seen that OSI contribution comes in test

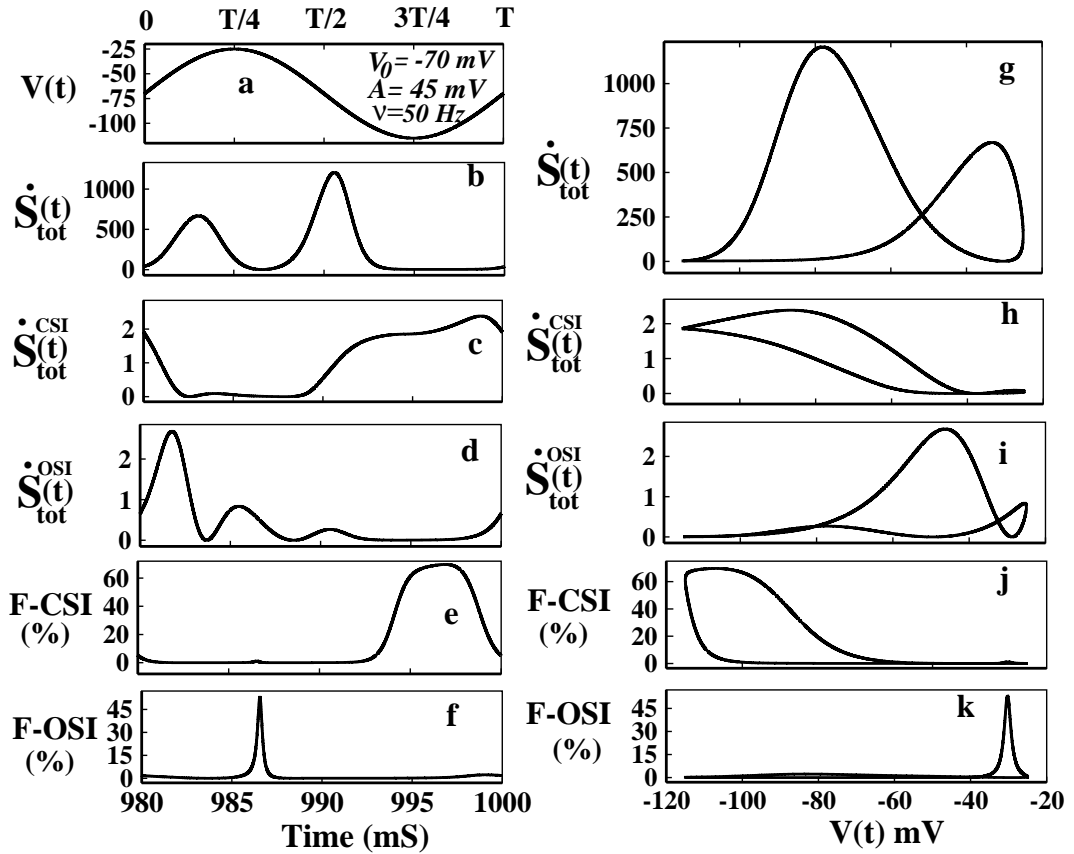


Figure 4.11: Entropy production rate contributions at NESS in oscillating voltage protocol. In (a) the applied voltage at NESS is shown. In (b) and (g) the total epr with time and voltage has been plotted respectively. In (c) and (h) $\dot{S}_{tot}^{CSI}(t)$ has been plotted with time and voltage respectively and in (d) and (i) $\dot{S}_{tot}^{OSI}(t)$ has been plotted with time and voltage respectively. In (e) and (j) F-CSI (%) has been plotted with time and voltage respectively and in (f) and (k) F-OSI (%) has been plotted with time and voltage, respectively.

pulses (depolarizing voltage) and CSI contribution comes in base pulses (hyper-polarizing voltage).

The aforesaid fact is also evident from the right panel figures where the similar quantities have been plotted with voltages. From the figure 4.11(h) it is seen that the loop area of $\dot{S}_{tot}^{CSI}(t)$ is more on the hyperpolarizing voltage region and the loop area of $\dot{S}_{tot}^{OSI}(t)$ is more on the depolarised voltage region as seen from figure 4.11(i). Besides the shape of the hysteresis loop areas of CSI and OSI are clearly distinct to each other. So these two paths are also thermodynamically distinguishable or they have distinct thermodynamic signatures. Also we found that the dynamic memory of these two paths depends heavily on the frequency and mean voltage, which are not reported here. The fact that OSI occurs in depolarised voltage and refractory changes occur via CSI during hyperpolariza-

tion is vivid from the graphs of F-CSI (%) and F-OSI (%) versus voltage in figures 4.11(j) and (k), respectively. Thus the thermodynamic analysis very clearly and more efficiently depicts the pathway of activation and re-factorization than kinetic analysis.

4.6 Conclusion

Inactivation dynamics of sodium channel has been studied here under non-equilibrium environment. By changing the voltage protocols from constant through pulsed to continuously oscillating voltage, we have studied the kinetic flux as well as energetic contributions of the closed and open-state inactivation path. The recently developed non-equilibrium thermodynamic properties used here serves as an improved tool for theoretical understanding of the energetically optimum processes to sustain the auto-regulatory mechanism of inactivation which has not been done earlier. Our approach of non-equilibrium dynamical characterization of inactivation path can invite new avenues in experimental and theoretical research of inactivation, especially for drug blocking and dynamic hysteresis. The conclusions drawn here are mainly as follows.

1. We have characterized the activation and inactivation dominated region of ionic current as a function of voltage.
2. In presence of the constant voltage the path of inactivation is characterized. In a preferential OSI system the OSI path is more favored than CSI for inactivation in moderate to high depolarization. The CSI gradually decrease with increasing depolarizations while OSI increases.
3. From the pulse train analysis it is seen that system follows OSI path to respond to test pulses and comes back to resting states or recovery from inactivation occurs via CSI path during base pulse or refractory period. Recovery from inactivation is relatively a slower process than inactivation and it gradually increases after each pulses with increasing population of inactive states.
4. From the oscillating voltage it is seen that during the hyperpolarised voltage, the system follows CSI path and for depolarized voltage system prefers OSI path.
5. From constant to continuously oscillating voltage protocol, the general conclusion is that during depolarised voltage OSI is most favored path and during hyperpolarised voltage CSI is favored.

6. The results of pulse train and oscillating voltage protocols are both kinetically and thermodynamically established. The calculation of fraction of total epr serves as a supporting tool for theoretical understanding of kinetic results. The thermodynamic results also confirm that these paths show characteristic dynamical hysteretic nature. The study of path of inactivation or the validity of the model gets a strong thermodynamic backup which has not been shown earlier. It is also established that only the kinetic study is not sufficient, the thermodynamic study of inactivation is equally important.

7. For all the voltage protocols, the effect of open-state blocker, Mexilitine shows a characteristic decrease in the relative magnitude of the OSI and CSI path. But the CSI path is least affected by the open-state drug blocking in constant voltage protocol. The dynamical profile of inactivation of the channel can in principle be utilized to estimate the presence of drug and vice versa.

Bibliography

- [1] Yu FH, Catterall WA. Overview of the voltage-gated sodium channel family. *Genome Biology* 2003; 4:207.
- [2] Marban E, Yamagishi T, Tomaselli GF, Structure and function of voltage-gated sodium channels, *J.Physiol.* 1998; 508:647.
- [3] Goldin AL, Mechanisms of sodium channel inactivation, *Current Opinion in Neurobiology* 2003;13:284-290.
- [4] Aldrich RW. Fifty years of inactivation. *Nature* 2001; 411: 643-644.
- [5] Catterall WA. From ionic currents to molecular mechanisms: the structure and function of voltagegated sodium channels. *Neuron* 2000; 26:13-25.
- [6] Ulbricht W. Sodium Channel Inactivation: Molecular Determinants and Modulation. *Physiol. Rev.* 2005; 85:1271-1301.
- [7] B. Hille, *Ionic channels of excitable membranes*. 2nd edition, Sinauer Associates, Sunderland, Mass. 1992.
- [8] Featherstone DE, Fujimoto E, Ruben PC, A defect in skeletal muscle sodium channel deactivation exacerbates hyperexcitability in human paramyotonia congenita, *Journal of Physiology* 1998; 506.3:627-638.
- [9] Devor M. Sodium Channels and Mechanisms of Neuropathic Pain. *The Journal of Pain* 2006; 7:S3-S12.
- [10] Noebels JL. How a Sodium Channel Mutation Causes Epilepsy. *Epilepsy Currents* 2003; 3:70-71.
- [11] Kiss T. Persistent Na-channels: origin and function. A review. *Acta Biologica Hungarica* 2008; 59 (Suppl.):1-12.
- [12] Stafstrom CE. Persistent Sodium Current and Its Role in Epilepsy. *Epilepsy Curr.* 2007 Jan; 7(1):15-22.
- [13] Aman TK, Grieco-Calub TM, Chen C, Rusconi R, Slat EM, Isom LL, Raman IM. Regulation of Persistent Na Current by Interactions between Subunits of Voltage-Gated Na Channels. *J.Neurosci.* 2009; 29(7):2027-2042.

- [14] Catterall WA, Goldin AL, Waxman SG. International Union of Pharmacology. XLVII. Nomenclature and Structure-Function Relationships of Voltage-Gated Sodium Channels. *Pharmacol. Rev.* 2005; 57:397-409.
- [15] Hodgkin AL, Huxley AF. The dual effect of membrane potential on sodium conductance in the giant axon of *Loligo*. *J. Physiol.* 1952; 116:497-506.
- [16] Aldrich RW, Stevens CF. Inactivation of open and closed sodium channels determined separately. *Cold Spring Harbor Symposia on Quantitative Biology* 1983; XLVIII:147-153.
- [17] Goldman L. Sodium channel inactivation from closed states: evidence for an intrinsic voltage dependency. *Biophys. J.* 1995; 69:2369-2377.
- [18] Horn R, Vandenberg CA. Statistical properties of single sodium channels. *J Gen Physiol.* 1984; 84:505- 534.
- [19] Groome JR, Lehmann-Horn F, Holzherr BD, Open and closed-state fast inactivation in sodium channels: Differential effects of a site-3 anemone toxin. *Channels* 2011; 5(1):65-78.
- [20] Armstrong CM, Bezanilla F. Inactivation of the sodium channel. II. Gating experiments. *J.Gen. Physiol.* 1977; 70:567-590.
- [21] Bähring R, Covarrubias M. Mechanisms of closed-state inactivation in voltage-gated ion channels. *J. Physiol.* 2011; 589.3:461-479.
- [22] Bean BP. Sodium channel inactivation in the crayfish giant axon. Must channels open before inactivating? *Biophys.J.* 1981; 35:595-614.
- [23] Yellen G. The moving parts of voltage-gated ion channels. *Q. Rev. Biophys.* 1998; 31:239-295.
- [24] Patlak J. Molecular kinetics of voltage-dependent Na⁺ channels. *Physiol. Rev.* 1991; 71:1047-1080.
- [25] Kuo CC, Bean BP. Na⁺ channels must deactivate to recover from inactivation. *Neuron* 1994; 12:819- 829.
- [26] Armstrong CM. Na channel inactivation from open and closed states. *Proc. Nat. Aca. Sci.* 2006; 103:17991-17996.
- [27] Millonas MM, Hanck DA. Nonequilibrium response spectroscopy of voltage-sensitive ion channel gating. *Biophys J* 1998; 74:210-29.
- [28] Kargol A, Smithz B, Millonas MM, Applications of Nonequilibrium Response Spectroscopy to the Study of Channel Gating. *Experimental Design and Optimization. J. theor. Biol.* 2002; 218:239.
- [29] Groot SRD, Mazur P. *Non-equilibrium Thermodynamics*, North Holland Publ. Comp., Amsterdam 1951.

- [30] Kargol A, Hosein-Sooklal A, Constantin L, Przewalski M. Application of oscillating potentials to Shaker potassium channel. *Gen Physiol Biophys* 2004; 23:53-75.
- [31] Hosein-Sooklal A, Kargol A. Wavelet analysis of non-equilibrium ionic currents in human heart sodium channel (hH1a). *J Membr Biol* 2002; 188:199-212.
- [32] Pal K, Gangopadhyay G, Probing kinetic drug binding mechanism in voltage-gated sodium ion channel: open state versus inactive state blockers. *Channels* 2015; 9:5, 307-316.
- [33] Vandenberg, CA, Bezanilla F. A sodium channel gating model based on single channel, macroscopic ionic, and gating currents in the squid giant axon. *Biophysics. Journal* 1991; 60:1511.
- [34] Payandeh J, Gamal El-Din TM, Scheuer T, Zheng N, Catterall WA. Crystal structure of a voltage-gated sodium channel in two potentially inactivated states. *Nature Letter* 2012; 136, vol 486.
- [35] Zhang X, Ren W. , DeCaen P, Yan C, Tao X, Tang L, Wang J, Hasegawa K, Kumasaka T, He J, Wang J, Clapham DE, Yan N. Crystal structure of an orthologue of the NaChBac voltage-gated sodium channel. *Nature* 2012; 130, vol 486.
- [36] Schnakenberg J. Network theory of microscopic and macroscopic behavior of master equation systems. *Rev. Mod. Phys.* 1976; 48:571.
- [37] Jiu-li L., Van den Broeck C, Nicolis G. Stability criteria and fluctuations around nonequilibrium states. *Z. Phys. B* 1984; 56:165.
- [38] Nicolis G. Fluctuations around nonequilibrium states in open nonlinear systems. *J. Stat. Phys.* 1972; 6:195.
- [39] Seifert U. Entropy Production along a Stochastic Trajectory and an Integral Fluctuation Theorem. *Phys. Rev. Lett* 2005; 95:040602.
- [40] Ge H, Qian H. Physical origins of entropy production, free energy dissipation, and their mathematical representations. *Phys. Rev. E* 2010; 81: 051133.
- [41] Das B, Banerjee K, Gangopadhyay G, Entropy hysteresis and nonequilibrium thermodynamic efficiency of ion conduction in a voltage-gated potassium ion channel, *Phys. Rev. E*, 86, 061915 (2012).
- [42] Majumdar, S., Foster G. and Sikdar, S. K. Induction of pseudo-periodic oscillation in voltage gated sodium channel properties is dependent on the duration of the prolonged depolarization. *Euro. J. Neurosci.* 2004; 20:127-143.
- [43] Raman IM, Bean BP. Inactivation and Recovery of Sodium Currents in Cerebellar Purkinje Neurons: Evidence for Two Mechanisms. *Biophysical Journal* 2001; 80:729-737.
- [44] Colbert CM, Magee JC, Hoffman DA, Johnston D. Slow recovery from inactivation of Na⁺ channels underlies the activity dependent attenuation of dendritic action

- potentials in Hippocampal CA1 pyramidal neurons. *The Journal of Neuroscience*. 1997; 17:6512-6521.
- [45] Chanda B, Blunck R, Faria LC, Schweizer, Mody, Bezanilla F. A hybrid approach to measuring electrical activity in genetically specified neurons. *Nature Neuroscience* 2005; 8:1619-1626.
- [46] Olguin IIA, Carrillo E, Islas LD, Lagunas FG. Recovery from slow inactivation of Shab K⁺ channels. *Channels* 2013; 7:225-228.
- [47] Kuo CC, Yang S. Recovery from inactivation of T-type Ca²⁺ channels in rat thalamic neurons. *The journal of Neuroscience* 2001; 21:1884-1892.
- [48] Fohlmeister JF, Adelman WJ Jr. Gating current harmonics. I. Sodium channel activation gating in Dynamic Steady states. *Biophysci. J.* 1985; 48:375-390.
- [49] Pustovoit MA, Berezhkovskii AM, Bezrukov SM, Analytical theory of hysteresis in ion channels: two-state model, *J. Chem. Phys.*, 125,194907 (2006).
- [50] M. Pd. Sah , H. Kim, and L.O. Chua, "Brains Are Made of Memristors " *IEEE circuits and systems magazine*,1531-636X (2014).
- [51] Scholz A. Mechanisms of (local) anaesthetics on volt- age-gated sodium and other ion channels. *Br J Anaesth* 2002; 89:52-61.
- [52] Fozzard HA, Lipkind GM. The tetrodotoxin binding site is within the outer vestibule of the sodium channel. *Marine Drugs* 2010; 8:219-34.
- [53] Starmer CF, Lastra AA, Nesterenko VV, Grant AO. Proarrhythmic response to sodium channel blockade. Theoretical model and numerical experiments. *Circulation* 1991; 84:1364-77.
- [54] Stramer CF. How antiarrhythmic drugs increase the rate of sudden cardiac death. *Int J Bifurcation Chaos* 2002; 12:1953.
- [55] Clancy CE, Zhu ZI, Rudy Y. Pharmacogenetics and anti arrhythmic drug therapy: a theoretical investigation. *Am. J. Physiol. Heart Circ. Physiol.* 2007; 292:H66-75.
- [56] Fozzard H.A, Lipkind G. M. The Tetrodotoxin Binding Site Is within the Outer Vestibule of the Sodium Channel. *Marine Drugs* 2010; 8:219.
- [57] Nygren A, Fiset C, Firek L, Clark JW, Lindblad DS, Clark RB, Giles WR. Mathematical mode of an adult human atrial cell: The role of K⁺ currents in repolarization. *Cir. Res.* 1998; 82: 63-81.
- [58] MacCannell KA, Bazzazi H, Chilton L, Shibukawa Y, Clark, Giles WR. A mathematical model of electronic interactions between ventricular myocytes and fibroblasts. *Biophys. J.* 2007; 92:4121- 4132.
- [59] Clancy CE, Tateyama M, Liu H, Wehrens XHT, Kass RS. Nonequilibrium gating in cardiac Na⁺ channels: an original mechanism of arrhythmia. *Circulation.* 2003; 107:2233-2237.
- [60] Clancy CE, Kass RS. Theoretical investigation of the neuronal Na⁺ channel SCN1A: Abnormal gating and epilepsy. *Biophys. J.* 2004; 86: 2606-2614.

Chapter 5

Chapter 5

Investigation Of The Kinetic Drug Binding Mechanism In Voltage-Gated Sodium Ion Channel: Open State Versus Inactive State Blockers

The kinetics and nonequilibrium thermodynamics of open state and inactive state drug binding mechanisms have been studied in this chapter using different voltage protocols in sodium ion channel. We have found that for constant voltage protocol, open state block is more efficient in blocking ionic current than inactive state block. Kinetic effect comes through peak current for mexiletine as an open state blocker and in the tail part for lidocaine as an inactive state blocker. Although the inactivation of sodium channel is a free energy driven process, however, the two different kinds of drug affect the inactivation process in a different way as seen from thermodynamic analysis. In presence of open state drug block, the process initially for a long time remains entropy driven and then becomes free energy driven. However in presence of inactive state block, the process remains entirely entropy driven until the equilibrium is attained. For oscillating voltage protocol, the inactive state blocking is more efficient in damping the oscillation of ionic current. From the pulse train analysis it is found that inactive state blocking is less effective in restoring normal repolarisation and blocks peak ionic current. Pulse train protocol also shows that all the inactive states behave differently as one inactive state responds instantly to the test pulse in an opposite manner from the other two states.

5.1 Introduction

The sodium ion channel [1–4] is an optimal drug target for therapeutic action as inactivation plays an important role by temporarily preventing the channel from reopening even though the cell is still depolarized. If the inactivation process is hampered, various physiological problems appear, like cardiac arrest, hyper excitability, hysteria etc, due to the persistent current [5–8]. In particular, sodium channels are targeted for anesthesia and treatments for genetic diseases in the brain, skeletal muscles, and heart [9]. The physiological importance of the voltage gated sodium channel is associated with numerous pathologies namely cardiovascular, neuronal, neuromuscular, musculoskeletal, metabolic, and respiratory systems [10, 11] due to the inherited ion channel diseases due to mutations [12, 13]. Discovery of drug to cure these diseases are difficult owing to the fact that thorough molecular approaches are ineffective and most ion channel drugs are discovered using lab cultured tissues and animal based pharmacological methods [14–16] which cannot be tested on human beforehand. The complete understanding of the mechanism of blocking of drugs and how the intrinsic properties of channel gating affect drug access, binding affinity and unblocking are still not clearly understood. Many existing drugs thus failed to reduce mortality [17, 18] due to incomplete knowledge of drug binding mechanism in ion channels and little knowledge of the molecular and physiochemical basis of drug receptor interaction. Thus the understanding of the drug binding kinetics and its energetics in presence of various membrane depolarisations is one of our goals in this chapter.

For the previous few decades the study of inactivation had been a major investigation for many electrophysiologists studying the cell under voltage clamp and patch clamp techniques. Many drugs or blocks like TTX [19], conotoxins [20], pronase [21], mexiletine [22], lidocaine [22] have been evolved which specifically target binding with the open state or the inactive states of the sodium channel, leading to ceased sodium current influx. Most of the studies involve the discovery of various blockers, their region of binding to the channel protein and the structural change of the channel protein caused in presence of drugs. As drug binding kinetics are very much affected by the various types of channel mutations, biological environment and also similar drugs show different binding kinetics [23, 24] in different systems, it is difficult to comprehend drug binding interactions in a general framework. To generalize drug binding kinetics from single channel realization, we present here simple probabilistic approach using the state model of Bezanilla [25] for cardiac sodium channel. In spite of a great deal of effort to understand the drug binding kinetics the nonequilibrium thermodynamic characterization of binding have been still overlooked. Thus in our study we investigate the following questions: (1) What are the

basic kinetic difference between a drug blocking open state and a drug accessing directly the inactive state of the channel with the variation of drug concentration and voltage? (2) For constant depolarisation which type of drug binding is more effective in blocking the ionic current? (3) What is the thermodynamic difference between a normal inactivation process and a drug induced inactivation? (4) Are these drugs binding processes entropy driven or free energy driven? (5) How these 2 types of drug binding kinetics differ from constant voltage case in presence of oscillating voltage protocol, emerging as nonequilibrium response spectroscopic technique [26–28] which also mimic the neuronal oscillations [29, 30] in membrane potential? (6) How the channel and its drug binding mechanism responds to the pulse train voltage protocol and its varying pulse width.

In this context we have taken a standard single sodium ion channel model which we have extended with drug bound states corresponding to the open state and inactive state blocking, considering local anesthetics such as mexiletine and lidocaine as open state and the inactive state blockers, respectively.

5.2 Model of Drug Binding

The study of local anesthetics (LA) and their binding kinetics to the binding site of sodium ion channel has been important since past few decades [31–33]. Hille [34] in his modulated receptor hypothesis explains the shift of inactivation in presence of use-dependent block of sodium currents during repetitive pulses [35–37]. The hypothesis predicted that the open and inactivated states of voltage gated Na channels have higher affinities toward LA drugs than that of the resting state. The guarded-receptor model emphasizes the dependence of hydrophilic or hydrophobic path of the drug in binding and unbinding kinetics [38]. There have been a lot of drugs [39, 40] invented which binds with sodium channel, can be broadly divided into 2 classes [41, 42], as open state blocker and inactive state stabilizing blocker. From clinical stand point, drugs that have strong open channel blocking potency are called class 1a antiarrhythmics, such as quinidine, mexilitine and disopyramide whereas class 1b antiarrhythmics like lidocaine preferentially block peak over late current [43]. Unlike most positively charged local anesthetics the neutral tricyclic anticonvulsant drugs, namely phenytoin, carbamazepine, and lamotrigine etc have similar blocking affinities for both open or inactivated-state [44]. Till now the clear distinction between activities of open state blocker and inactive state blocker is yet not clear and well established. Various experimental protocols such as constant voltage clamp, oscillating voltage as nonequilibrium response spectroscopic technique and pulse train protocol have

been used enormously but how these protocols affect the drug binding is not yet clear. We consider the drug binding model based on the single sodium ion channel model presented by Vandenberg and Bezanilla [25].

We take the example of an open state drug blocker as mexiletine and inactive state blocker as lidocaine [22]. Thus here we add an extra drug bound state P_5^M with P_5 for the study of mexiletine drug binding kinetics and we add three drug bound states such as P_6^L , P_7^L and P_8^L with P_6 , P_7 and P_8 , respectively to study the kinetics in presence of lidocaine. The models are given in figure (5.1). For simplicity we consider a drug binds to an open state and inactive state with similar binding affinity. We have taken the forward rate constant for binding $k_{on} = [D] \times 10^5 s^{-1}$, where $[D]$ is the molar drug concentration $[M]$ and $k_{off} = 10^{-2} s^{-1}$ [31]. For simplicity we keep the rate constants same for mexiletine and lidocaine. For system under constant, oscillating and pulse train voltage protocols we use these drug binding rates which are not voltage dependent in any case.

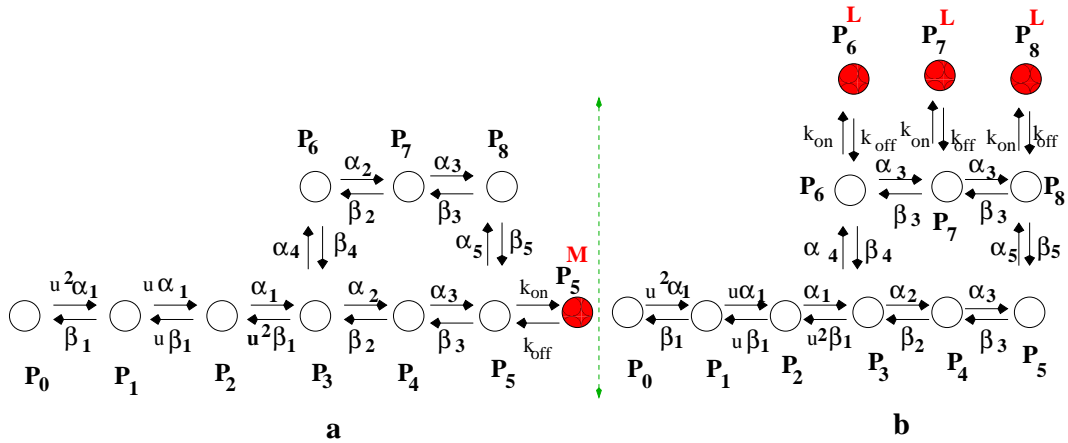


Figure 5.1: Kinetic model of drug binding is shown in this figure. Figure (a) model of open state drug blocker is a ten state model and (b) model for inactive state drug blocker is a twelve state model. We add an extra drug bound state P_5^M with P_5 for the study of open state blockers(eg. Mexilitine) binding kinetics and we add three states such as P_6^L , P_7^L , P_8^L with P_6 , P_7 and P_8 , for inactive state blockers(eg. Lidocaine). We have taken the forward rate constant for binding $k_{on} = [D] \times 10^5 s^{-1}$, where $[D]$ is the molar drug concentration $[M]$ and $k_{off} = 10^{-2} s^{-1}$ [31].

Next we study the effect of three types of voltage protocols for these drug blockers. First we have kept the voltage constant as used in constant voltage clamp dynamics. Secondly we use oscillating voltage protocol, a protocol which helps us to study the system in nonequilibrium environment. Next we have studied the system under pulse train protocol. Here we vary the pulse durations of the base pulse and test pulse and their effect is studied in presence of open state blocker and inactive state blocker with

various concentrations. How the alteration of pulse duration affects or facilitates the drug binding is one of the goals of this part. In each protocol we are comparing whether inactive state blockers or the open state blockers are more effective in blocking the ionic current.

5.3 Constant Voltage Clamp Dynamics

Constant voltage clamp dynamics has been widely used protocol to study ion channels since the work of Hodgkin-Huxley [1, 2]. The voltage clamp technique is used by electrophysiologists to measure the ionic current through the membrane of excitable cells while holding the membrane voltage at a set level. A series of voltage ramp can be used which allows the membrane voltage to be altered independently of the ionic currents allowing to study the current-voltage relationships of the voltage gated sodium channel. Here we have plotted the ionic current at different concentrations of mexiletine and lidocaine keeping the voltage constant i.e, -20 mV. From figure 5.2(a) it is seen that the ionic current is suppressed with the increase in the drug concentration. It is also observed that the peak of the ionic current is also decreased but from the figure 5.2(b) it is seen that lidocaine block has no effect on the peak current which affects the current after the peak is reached that is at tail part only. The effect of the mexiletine is clearly visible for a wide range of drug concentration but the effective range of visible change for lidocaine is very small, i.e., in the very low concentration range, 0.005-0.01 M, after that or the concentration greater than that does not change the kinetics appreciably and the graphs overlap, as for example $[D]=10$ M, overlaps on $[D]=0.1$ M.

Next we have investigated the relation between peak-current and various constant depolarising voltages for different drug concentrations. Here we first put the system in -70 mV depolarisation (a resting potential for the cell), and send it to a steady state until all the parameters become time independent. Then we switch on the drug block sites along with the depolarising voltage and let the system settle down to steady state and then estimate the peak current. From figure 5.2(c) it is seen that for a particular mexiletine concentration the peak of ionic current gradually increases with depolarisation and then after passing through a maximum it decreases again. With increase in mexiletine concentration there is a relative reduction of peak current clearly visible. But in the case of lidocaine a different nature is observed. For a particular lidocaine concentration the peak current shows similar nature as mexiletine but for increasing lidocaine concentration there is no effect on peak current as seen from figure 5.2(d). It is worth mentioning that

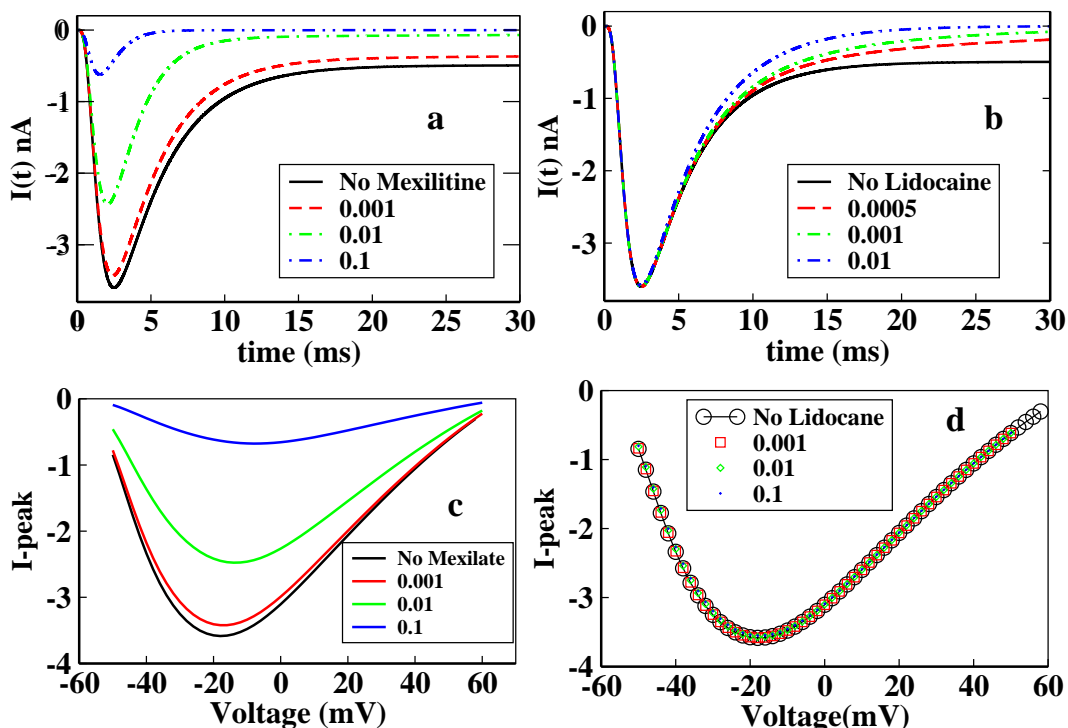


Figure 5.2: Effect of open state and inactive state blocker on ionic current and its peak in presence of constant voltage protocol. Figure (a) Effect of open state blocker for concentrations 0.001 M, 0.01 M, 0.1 M. and (b) inactive state blocker for concentrations 0.0005 M, 0.001 M, 0.01 M. on ionic current are shown here. In (c) with increasing open state blocker concentration relative reduction of peak current clearly visible, which is absent in inactive state blocker in (d).

although there is no effect on peak current due to increasing concentration of lidocaine but there is a clear change in the peak over late current. The late current sharply decreases with the increase in the lidocaine concentration as seen from figure 5.2(b). This behaviour of lidocaine is also consistent with the experiments done earlier as was previously reported that lidocaine was more effective in late component of Na^+ current than peak current in ΔKPQ channels expressed in mammalian cells [45–49]. Lidocaine preferentially blocked late over peak current and the blockade was equally effective in all three channels having mutations N1325S, R1644H and ΔKPQ expressed in *Xenopus oocytes* [50]. Lidocaine inhibits dispersed reopening in single channels without affecting mean open times. Clinical studies showed that the late current is more sensitive than peak current to block by class Ib [4] antiarrhythmic drugs like lidocaine [45, 47, 52].

Next we have studied the nonequilibrium thermodynamics of the system in presence of drug. For that reason we assume that the system is in contact with an isothermal bath at temperature T . The total internal energy $U(t)$, the free energy, $F(t)$ and the system

entropy, $S(t)$ is given as follows [53],

$$U(t) = -T \sum_i P_i(t) \ln P_i^e, \quad (5.1)$$

$$S(t) = - \sum_i P_i(t) \ln P_i(t), \quad (5.2)$$

$$F(t) = U(t) - TS(t) = T \sum_i P_i(t) \ln \left(\frac{P_i(t)}{P_i^e} \right). \quad (5.3)$$

Now we have calculated $\Delta U(t)/T$, $\Delta F(t)/T$ and $\Delta S(t)/T$ which gives us the information about how far the system is from the equilibrium in terms of these thermodynamic parameters namely,

$$\Delta U/T = U^e/T - U(t)/T, \quad (5.4)$$

where $U^e = -T \sum_i P_i^e \ln P_i^e$ is the internal energy of the system at equilibrium and P_i^e is the probability of the i_{th} state at equilibrium. Similarly we can write

$$\Delta F/T = F^e/T - F(t)/T, \quad (5.5)$$

and

$$\Delta S = \Delta U/T - \Delta F/T. \quad (5.6)$$

From the figure 5.3(a) it is seen that without the presence of drug the process is initially entropy driven and soon after the inactivation process starts it becomes free energy driven as seen from the figure 5.3(a). It remains free energy driven upto the equilibrium until all of the three quantities become zero at equilibrium. It may be concluded that the normal inactivation process in sodium channel is free energy driven without the presence of any drug. From figure 5.3(b) it is seen that in presence of 0.001 M mexilitine the process is also initially entropy driven and then after a long time it becomes free energy driven. In figure 5.3(c) it is seen that in presence of lidocaine the process entirely remains entropy driven till the equilibrium reaches. The ionic current graphs are plotted below for each case which shows the similar time scales for reaching the equilibrium. It is observed here from both the graphs of ionic current and thermodynamic potentials that lidocaine blocks faster than that of mexilitine [54, 55].

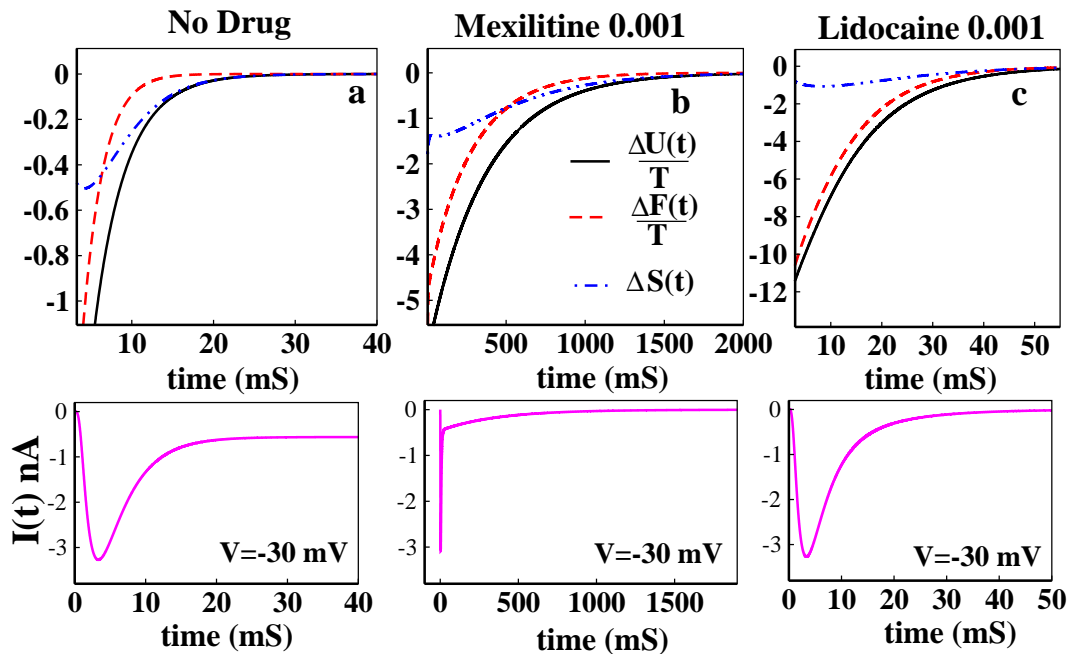


Figure 5.3: Thermodynamic properties of drug binding is shown here. The figure (a) $\Delta U/T$, $\Delta F/T$ and ΔS have been shown without the presence of drug. In (b) the same thermodynamic parameters have been studied in presence of 0.001 M mexilitine and in (c) 0.001 M lidocaine. The black solid curve stands for the $\Delta U/T$, the red dashed curve stands for $\Delta F/T$ and the blue dot-dashed curve stands for ΔS . For all the cases voltage has been kept fixed to -30 mV. The ionic current graphs are plotted below for each case which show the similar time scale for reaching equilibrium.

5.4 Oscillating Voltage Protocol

Oscillating voltage protocol is an emerging technique [27, 28] to study the ion channels in nonequilibrium environment. In individual neurons the oscillations may appear due to oscillating nature of action potential and membrane depolarisation [29, 30].

To realize the effect of drug in ionic current in presence of inherent gating kinetics of channel the oscillating voltage protocol may give the nearly similar cell situation in terms of neuronal oscillation. The functional form of the voltage, $V(t)$ that we have used is $V(t) = V_0 + A \sin(\omega t)$, where V_0 is the mean voltage taken as zero and $\omega = 2\pi\nu$ with amplitude, $A=30$ mV and frequency, $\nu = 30$ Hz consistent with biological range. We have studied the total dissipation function or the total entropy production rate (epr) with time in presence of drug.

Left panel of figure (5.4) is the ionic current and in the right panel the corresponding total epr are shown. From figure 5.4(a) it is seen that without the presence of drug the ionic current oscillates and ultimately attains a time periodic steady value. From

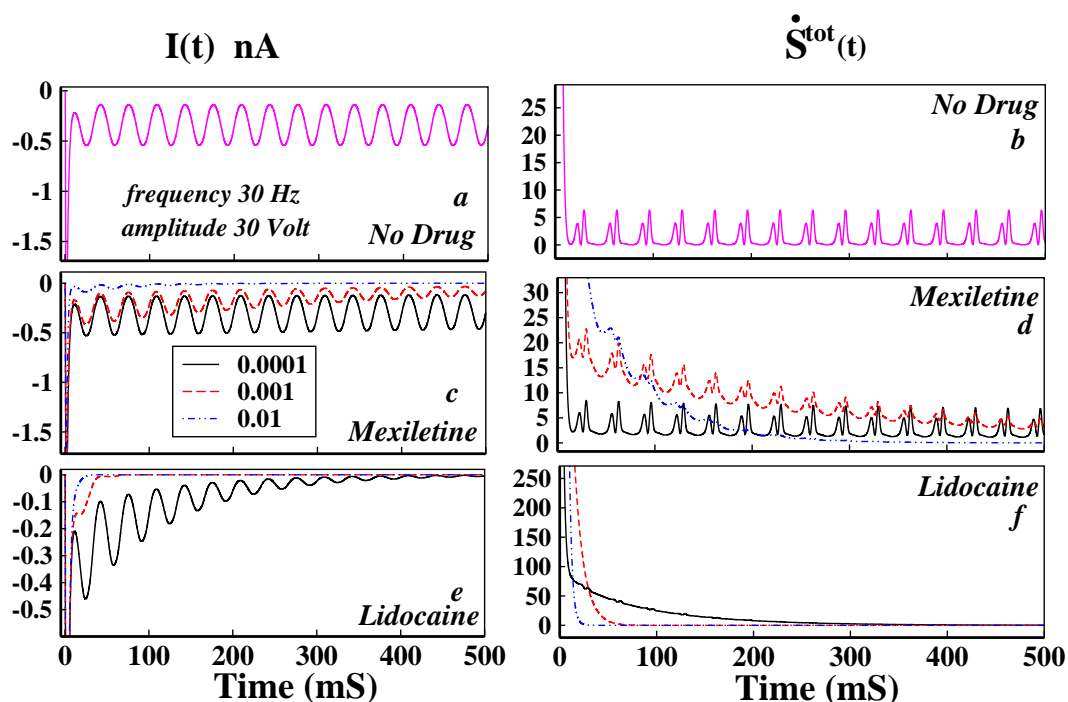


Figure 5.4: Effect of oscillating voltage protocol in ionic current and total entropy production rate leading to damping is plotted here. In the left panel the ionic current and in right panel the total epr has been plotted. In (a) ionic current without the presence of any drug has been plotted and in (b) the corresponding total epr has been plotted. In (c) the ionic current in presence of mexiletine, in (d) the corresponding total epr has been shown. In figure (e) and (f) ionic current and total epr in presence of lidocaine has been plotted, respectively. In figure (c), (d), (e) and (f) the black solid line indicates drug concentration of 0.0001 M, the red dashed line indicates drug concentration of 0.001 M and the blue dot-dashed line indicates 0.01 M drug concentration.

the figure 5.4(b) it is seen that the total entropy production rate is always positive and the system shows a time periodic steady nature of dissipation. Thus it goes to a driven nonequilibrium steady state in presence of oscillating voltage. But in presence of drugs of both kinds the system ultimately relaxes to equilibrium as seen from the figure 5.4(d) and (f). Thus the thermodynamics of the system entirely changes in presence of drug for oscillating external perturbation. In presence of drug the external oscillation cannot hold the system to nonequilibrium steady state any more but relaxes to the equilibrium due to the fact that these drugs have very very high binding affinities to the channel sites. The rate of relaxing to equilibrium in presence of lidocaine is much faster than the mexiletine for a particular drug concentration.

However, one important observation is that the ionic current in presence of drug gradually damps down as seen from figure 5.4(c) and (e). The total epr also gradually damps down to equilibrium. Damping of these kinetic and thermodynamic quantities

in presence of drug is directly related to the fact that the action potential also damps down [4]. It is seen that even with a minute concentration, lidocaine damps down both the ionic current and total epr in a much faster rate to equilibrium than mexilitine which is evident from the comparative study of the graphs in presence of drug.

5.5 Pulse Train Protocol

The pulse train protocol is also being widely used to understand the channel gating and inactivation procedure [56, 57]. These studies mainly involve characterisation of time course for inactivation or more precisely the time course of recovery from inactivation [58–60]. Here we want to investigate how the inactivation of sodium channel plays a role in ionic current when subjected to various depolarising pulse train separated by recovery intervals. First we keep the voltage at -20 mV for few seconds and then bring back the system to base voltage which is -80 mV and then after few milliseconds we start the test pulse train of -20 mV. Each pulse in the pulse train is brought back to base voltage for few milliseconds and then again fired to test voltage again. Here we are changing the base pulse and test pulse duration and studying how the system reacts to it. This study is important as it replicates the biological situation where a pulse comes and sodium channel responds to it and within few milliseconds system goes to inactivation followed by termination of ionic current influx until the potassium channel brings the system back to the resting potential which is more or less -80 mV. Thus here the test pulse (-20 mV) perturbs the system and the base pulse causes refractory changes to get the system ready for the next incoming pulse. Another interesting fact of using such protocol is that one can actually control the population of a state as desired. For example the test pulse will populate the open state and inactive states while the base pulse will again depopulate them. Here we have studied the system with and without presence of open state binding drug, mexiletine and inactive state binding drug, lidocaine with changing duration of the test pulse and base pulse.

First of all we would like to see how the system reacts to pulse train in presence of two kinds of drug already mentioned in different concentrations. We have considered the drug concentrations 0.01 , 0.001 , 0.0005 and 0.0001 M for both the two types of drugs. We kept the test pulse duration at 0.03 seconds and the base pulse duration at 0.01 seconds. The figure 5.5(a) shows how the pulse train is applied. In figure 5.5(b) we have plotted the ionic current in presence of mexiletine drug. It shows that with gradual increase in the drug concentration the peak of the ionic current gradually decreases down. With

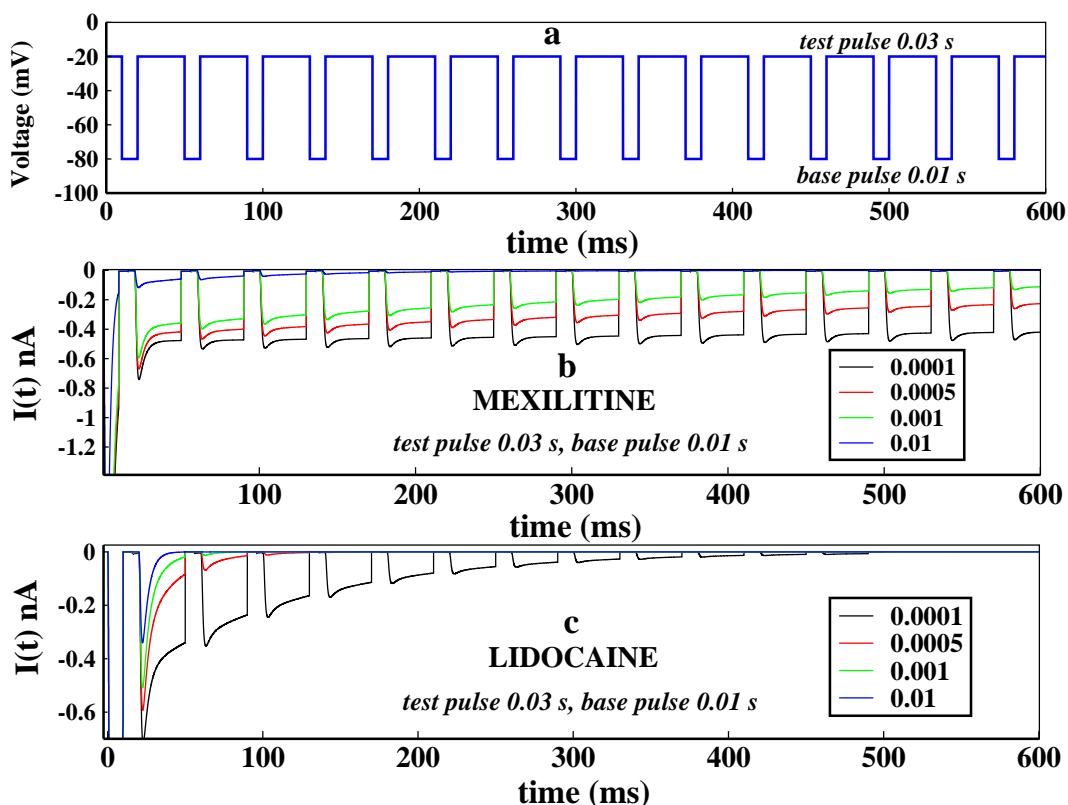


Figure 5.5: Effect of concentration of drugs in ionic current, in presence of pulse train protocol is shown here. In figure (a) first voltage is kept at -20 mV and after few milliseconds it is brought back to base -80 mV after that the pulse train begins. Here the base pulse duration is 0.01s and test pulse duration is 0.03 s. In figure (b) The effect of Mexilitine in ionic current is shown for increasing concentrations such as 0.0001, 0.0005, 0.001 and 0.01 M respectively. In figure (c) similar plot is shown for lidocaine. For both the cases the test pulse is kept for 0.03 s and the base pulse is kept for 0.01 s.

increasing drug concentration the open state blocking occurs with faster rate leading to a gradual decrease in ionic current. In figure 5.5(b) the effect of lidocaine is shown. Lidocaine being an inactive state stabilizing drug stabilizes the inactive states at much faster rate and almost have no impact on refractory period or base pulse in it, leading to the faster termination of ionic current. With a concentration more than 0.01 M, lidocaine permanently prohibits the channel from reopening [22]. Comparing the above two pictures of drug binding it is seen that lidocaine is more effective and faster ionic current blocker than mexiletine, as also observed from oscillating and constant voltage protocol in previous subsections.

Next we focused on the effects of change of base and test pulse durations in ionic currents keeping the drug concentrations same at 0.001 M. For that purpose we have chosen 2 pulse regions. We start with the very short pulse regions where we keep the test

pulse at 0.0008 seconds and base pulse at 0.0002 seconds and also see the effect just altering the pulse durations of each other. In figure 5.6(a) we have plotted the ionic currents at a test pulse duration of 0.0008 seconds and in figure 5.5(b) the test pulse durations are kept at 0.0002 seconds. Comparing the two figures it is seen that the system actually responds to the larger test pulse than the smaller one. As the test pulses are very short in figure 5.6(b), system fails to understand the fast depolarisation and the channel almost remains closed all the time. The inset graphs of figure 5.6(a) and (b) are the asymptotic values of ionic currents in presence of drugs.

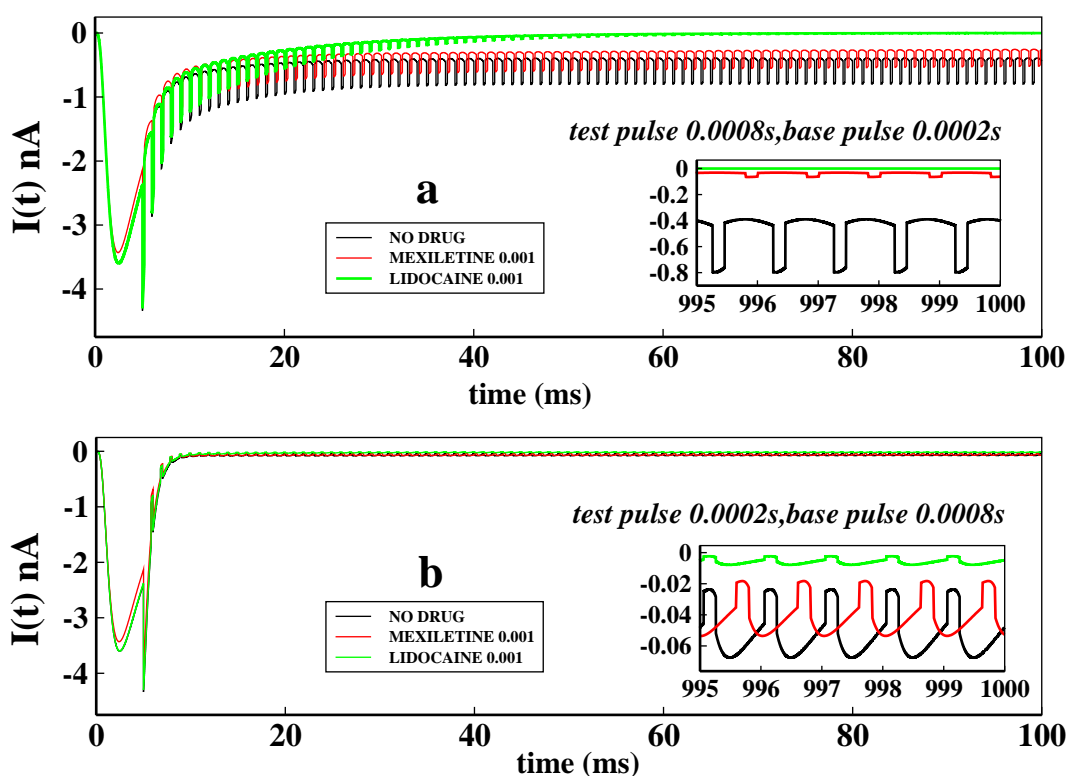


Figure 5.6: Effect of very short test pulse and base pulse durations on ionic current is shown here. In figure (a) the ionic current is plotted with time for no drug, in presence of mexilitine and in presence of lidocaine. The test pulses are kept for 0.0008s and the base pulse is kept for 0.0002 s. In figure (b) similar plot is done but with test pulses duration of 0.0002s and the base pulse duration of 0.0002s. All the drug concentrations are kept at 0.001 M.

In 5.7(a) we have plotted similar curves as in figure 5.7, but with pulse durations of larger time scales, such as test pulses of 0.03 s and base pulse durations of 0.01 seconds. In figure 5.7(b) the alternate duration of pulses are plotted. Comparing the figures 5.7(a) and b) it is important to note that the lidocaine almost immediately blocks the ionic current after the first two or three pulses in larger time scales, than in very short pulses. This is because due to the longer exposure to the depolarisation the lidocaine stabilises

the inactive states more effectively. The plot for shorter test pulse of 0.01 seconds have been shown in figure 5.7(b), which shows that system partially responds to the voltage change and the peak currents are higher than in figure 5.6(b). In addition one can observe from the asymptotic values of ionic current that mexilitine more effectively blocks the ionic current in presence of longer test pulses. For both the cases lidocaine shows less sensitivity toward pulse durations as it almost immediately inhibits the ionic current.

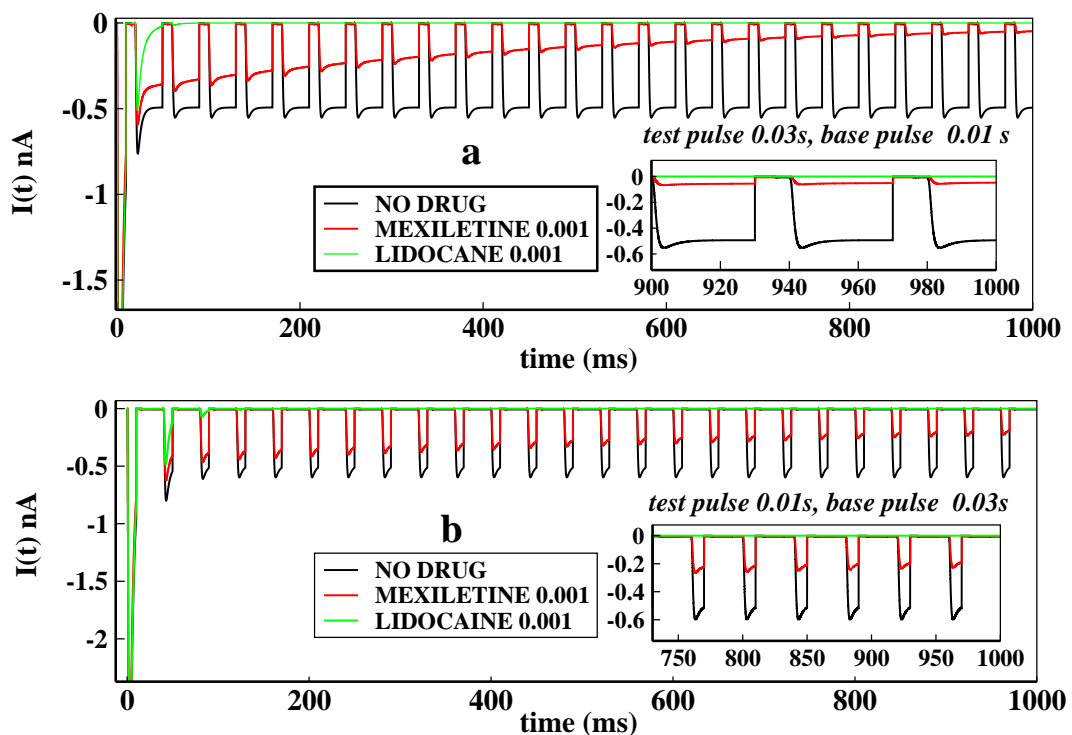


Figure 5.7: Effect of longer test pulse and base pulse durations on ionic current is shown here. In figure (a) the ionic current is plotted with time for no drug, in presence of mexilitine and in presence of lidocain. The test pulses are kept for 0.03 s and the base pulse is kept for 0.01 s. In figure (b) similar plot is shown but with test pulses duration of 0.01s and the base pulse duration of 0.03s. All the drug concentrations are kept at 0.001 M.

Next we have focused on the probabilities of the states which actually have the detailed information of the system responding to the pulse train protocol in presence of the drug. Thus we have studied the probabilities in presence of mexilitine and lidocaine with pulse durations as mentioned in figure (5.8). Here we have particularly seen the system dynamics for consecutive 4 pulses. The probabilities of the original 9 states of the system responds almost similarly but with different magnitudes in presence of mexilitine and lidocaine but their time dependences are almost the same. For convenience we have plotted only the mexilitine in presence of 0.001 M concentration.

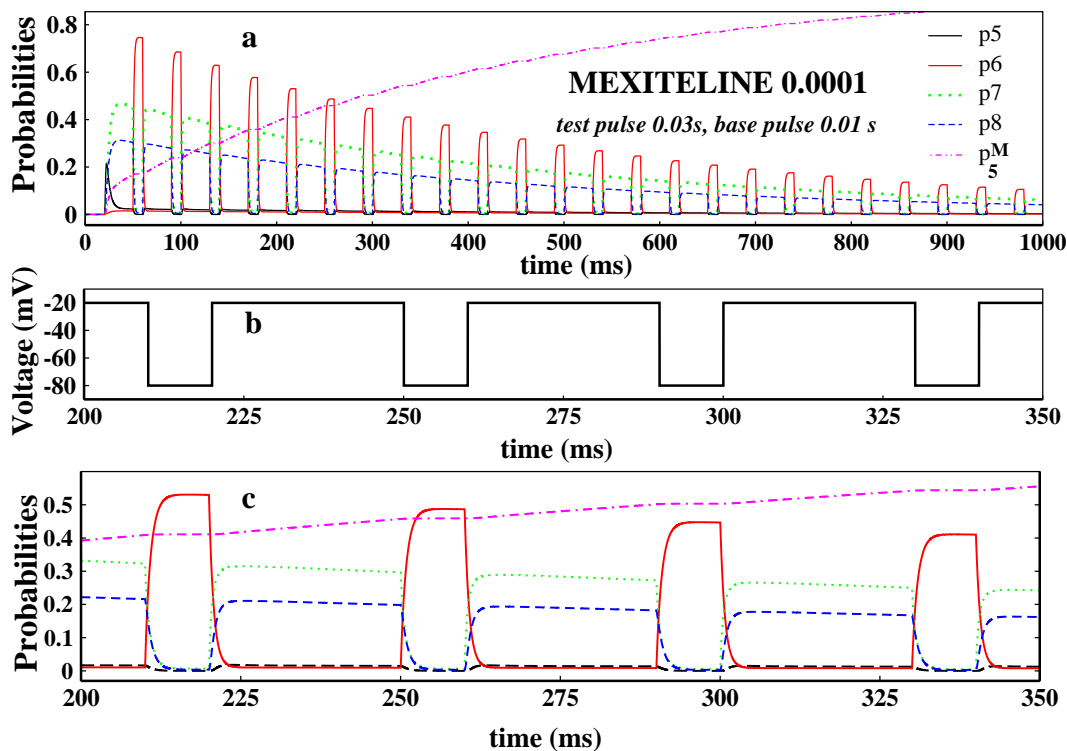


Figure 5.8: The probabilities of important states are shown here. In figure (a) The open state probability and the three inactive state probabilities and the drug binding state probabilities have been plotted in presence of 0.0001 M mexilitine concentration and in presence of pulses mentioned. In (b) the four test pulses of figure (a) which have been studied is shown here. In (c) the aforesaid probabilities are plotted for the above four pulses.

In figure 5.8(a) we have plotted the probabilities of open state, P_5 and the inactive states, P_6 , P_7 and P_8 and the drug binding state, P_5^M for mexilitine. Figure 5.8(b) shows the four pulses of which probabilities have been studied in figure 5.8(c). From the Figure 5.8(c) it is seen that P_6 increases at the test pulse peaks, whereas the P_7 and P_8 increases in the base pulses and vice versa. There is a clear phase lag in the activities of P_6 , P_7 and P_8 . P_7 and P_8 responds almost similarly but with a slight difference in amplitudes. P_6 responds instantly at the test pulse, whereas the other two states are responding in a opposite manner and the magnitudes of the P_7 and P_8 depend on the details of the inactivation path [61] and rate constants

5.6 Conclusion

In general we have studied the drug binding kinetics of voltage gated sodium ion channel in presence of two types of drug binding mechanisms, one which binds to the open state

of the channel such as mexilitine and other binding to the inactive states of the channel such as lidocaine. We have studied kinetics in presence of voltage protocols using constant, oscillating and pulse train where the first one is used by the electrophysiologist in voltage clamp and patch clamp techniques while the oscillating voltage basically mimics the neuronal oscillation which can be caused by the periodic change of membrane voltage. The pulse train protocol is useful which gives the sodium channel a refractory period in which the channel reactivates from the inactivation. Here we have shown the interesting dependence of drug binding mechanism on voltage variation which helps us to understand the toxic activity of drugs in living biological cell.

In constant voltage case the open state blocker acts more slowly than the inactive state blocker in blocking the ionic current. Open state blocker has drastic effect on peak ionic current in presence of constant voltage case but inactive state blocker does not show any observable effect on peak ionic current and only affects the tail part of it. The system in absence of any drug relaxes to equilibrium initially driven by entropy and then driven by free energy. The inactivation of sodium ion channel may be inferred as a free energy driven process. In presence of open state drug blocker the process initially for a long time remains entropy driven and then becomes free energy driven. But in presence of inactive state blocker the process entirely remains entropy driven till the equilibrium reaches. Thus these two types of drug binding are thermodynamically distinguishable which can be compared through calorimetric measurement.

For oscillating voltage protocol, inactive state blocker blocks the current in a faster rate than the open state blocker and also more sensitive to change in concentration than that of the constant voltage case. For equal concentrations inactive state blocker damps the ionic current and the total epr with higher extent than the open state blocker. From the pulse train analysis it is again established that inactive state blocker is a better ionic current blocker than open state blocker thereby inactive state blocking is less effective in restoring normal repolarisation and blocks the peak current. The longer test pulse is actually sensed by the system for both small and large time scales but it is not effectively sensed by the system when it is subjected to shorter test pulse. Open state blocker shows considerable blocking ability towards longer test pulse duration than shorter test pulse duration. From pulse train protocol it is revealed that not all inactive states respond to the external voltage in a similar manner. The one which is directly attached to closed states responds instantly at the test pulse, whereas the other two inactive states are responding in a delayed manner depending on the inactivation paths and rate constants.

Bibliography

- [1] A. L. Hodgkin, Evidence for electrical transmission in nerve Part I , J. Physiol., 90, 183 (1937).
- [2] A. L. Hodgkin, Evidence for electrical transmission in nerve Part II , J. Physiol., 90,211 (1937).
- [3] W. A. Catterall, Sodium Channels, Inherited Epilepsy, and Antiepileptic Drugs, Annu. Rev. Pharmacol. Toxicol., 54, 317 (2014).
- [4] A. Scholz, Mechanisms of (local) anaesthetics on voltage-gated sodium and other ion channels British Journal of Anaesthesia, 89, 52 (2002).
- [5] T. Kiss Persistent Na-channels: origin and function. A review. Acta Biologica Hungarica, 59, 1 (2008).
- [6] Mustafa B.A. Djamgoz and Rustem Onkal, Persistent Current Blockers of Voltage-Gated Sodium Channels: A Clinical Opportunity for Controlling Metastatic Disease, Recent Patents on Anti Cancer Drug Discovery, 8, 66 (2013).
- [7] Lin WH, Wright DE, Muraro NI and Baines RA, Alternative splicing in the voltage-gated sodiumchannel DmNav regulates activation, inactivation, and persistent current, Journal of Neurophysiology, 102, 1994 (2009).
- [8] Wayne E. Crill ,Persistent sodium current in mammalian central neurons , Annu. Rev. Physiol., 58, 34 (1996).
- [9] Catterall, William A., Alan L. Goldin, and Steven G. Waxman, International Union of Pharmacology. XLVII. Nomenclature and Structure-Function Relationships of Voltage-Gated Sodium Channels., Pharmacol Rev., 57, 397 (2005).
- [10] Catterall WA. From ionic currents to molecular mechanisms: the structure and function of voltage-gated sodium channels. Neuron, 26, 13 (2000).
- [11] Ashcroft FM., From molecule to malady , Nature, 440, 440 (2006).
- [12] Dichgans M., et.al, Mutation in the neuronal voltage-gated sodium channel SCN1A in familial hemiplegic migraine , Lancet, 366, 371 (2005).
- [13] George AL Jr., Inherited disorders of voltage-gated sodium channels , J. Clin. Invest., 115, 1990 (2005).

- [14] Wickenden A1, Priest B and Erdemli G., Ion channel drug discovery: challenges and future directions, *Future Med. Chem.*, 4, 661 (2012;).
- [15] Jeffrey J Clare, Targeting Ion Channels for Drug Discovery , *Discov. Med.*, 9, 253 (2010).
- [16] Trevor Perrior, Overcoming Bottlenecks in drug discovery , *Drug Discovery World*, 31, Fall 2010.
- [17] Echt DS, Liebson PR, Mitchell LB, Peters RW, Obias-Manno D, Barker A H, Arensberg D, Baker A, Friedman L, Greene HL. Mortality and morbidity in patients receiving encainide, flecainide, or placebo. The Cardiac Arrhythmia Suppression Trial. *N. Engl. J. Med.* 324, 781 (1991).
- [18] Task Force of the Working Group on Arrhythmias of the European Society of Cardiology, The Sicilian gambit. A new approach to the classification of antiarrhythmic drugs based on their actions on arrhythmogenic mechanisms . *Circulation*, 84, 1831 (1991).
- [19] E Carmeliet, Voltage-dependent block by tetrodotoxin of the sodium channel in rabbit cardiac Purkinje fibers , *Biophys J.*, 51, 109 (1987).
- [20] Siddhartha P. Sarma, et al., Solution Structure of δ -Am2766: A Highly Hydrophobic delta-Conotoxin from *Conus amadis* That Inhibits Inactivation of Neuronal Voltage-Gated Sodium Channels *Chemistry and Biodiversity*, 2, 535 (2005).
- [21] C.M. Armstrong, F Bezanilla, E.Rojas, Destruction of Sodium Conductance Inactivation in Squid Axons Perfused with Pronase . *The Journal of General Physiology*, 62, 375 (1973).
- [22] Colleen E. Clancy, Zheng I. Zhu, and Yoram Rudy, Pharmacogenetics and anti arrhythmic drug therapy: a theoretical investigation , *Am. J. Physiol. Heart. Circ. Physiol.*, 292, H66 (2007).
- [23] Zamponi W. Gerald, Doyle D. Donald and French J. Robert, State-dependent Block Underlies the Tissue Specificity of Lidocaine Action on Batrachotoxin-activated Cardiac Sodium Channels, *Biophysical J.*, 65, 91 (1993).
- [24] Zamponi W. Gerald and French J. Robert, Dissecting lidocaine action: die Diethylamide and Phenol Mimic Separate Modes of Lidocaine Block of Sodium Channels from Heart and Skeletal Muscle , *Biophysical J.*, 65, 2335 (1993).
- [25] Vandenberg, C.A., Bezanilla, F., A sodium channel gating model based on single channel, macroscopic ionic, and gating currents in the squid giant axon. *Biophysics. Journal.*, 60, 1511 (1991).
- [26] M. M. Millonas and D. A. Hanck, Nonequilibrium Response Spectroscopy of Voltage-Sensitive Ion Channel Gating, *Biophys. J.*, 74, 210 (1998).

- [27] A. Hosein-Sooklal and A. Kargol, Wavelet analysis of nonequilibrium ionic currents in human heart sodium channel (hH1a) . *J. Membr. Biol.*, 188, 199 (2002).
- [28] A. Kargol, A. Hosein-Sooklal, L. Constantin and M. Przystalski, Application of oscillating potentials to Shaker potassium channel , *Gen. Physiol. Biophys.*, 23, 53 (2004).
- [29] R. Llinas and Y. Yarom, Oscillatory properties of guinea-pig inferior olivary Neurons and their pharmacological modulation: An in vitro study , *J. Physiol.*, 376, 163 (1986).
- [30] R. R. Llinas, Anthony A. Graces and Y Yarom, In vitro neurons in mammalian cortical layer 4 exhibit intrinsic oscillatory activity in the 10- to 50-Hz frequency range , *Proc. Natl. Acad. Sci. USA*, 88, 897 (1991).
- [31] H.A. Fozzard and G. M. Lipkind, The Tetrodotoxin Binding Site Is within the Outer Vestibule of the Sodium Channel , *Marine Drugs*, 8, 219 (2010).
- [32] C. F. Starmer, A. A. Lastra, V. V. Nesterenko and A O Grant., Proarrhythmic response to sodium channel blockade. Theoretical model and numerical experiments, *Circulation*, 84, 1364 (1991).
- [33] C. F. Stramer, How antiarrhythmic drugs increase the rate of sudden cardiac death , *International Journal of Bifurcation and Chaos*, 12, 1953 (2002).
- [34] Hille B., Local anesthetics: Hydrophilic and hydrophobic pathways for the drug receptor reaction, *J.Gen. Physiol.*, 69, 497 (1977).
- [35] G.K. Wang and G. R. Strichartz, State-Dependent Inhibition of Sodium Channels by Local Anesthetics: A 40-Year Evolution , *Biochem. (Mosc) Suppl. Ser. A Membr Cell Biol.*, 6, 120 (2012).
- [36] Khodorov BI, Shishkova L, Peganov E, Revenko S., Inhibition of sodium currents in frog Ranvier node treated with local anesthetics. Role of slow sodium inactivation , *Biochim Biophys Acta.*, 433, 409 (1976).
- [37] Courtney KR, Mechanism of frequency-dependent inhibition of sodium currents in frog myelinated nerve by the lidocaine derivative GEA , *J. Pharm. Exp. Therop.*, 195, 225 (1975).
- [38] Peter J. Lee, Akihiko Sunami and Harry A. Fozzard, Cardiac specific external paths for lidocaine, defined by isoform-specific residues, accelerate recovery from use-dependent block , *Circ Res.*, 89, 1014 (2001).
- [39] W. J. Crumb, Jr. and C. W. Clarkson, Characterization of cocaine induced block of cardiac sodium channels , *Biophys. J.*, 57, 589 (1990).
- [40] C. H. Lee and P. C. Ruben, Interaction between voltage-gated sodium channels and the neurotoxin, tetrodotoxin , *Channels*, 2, 407 (2008).

- [41] Gregory M. Lipkind and Harry A. Fozzard, Molecular Modeling of Local Anesthetic Drug Binding by Voltage-Gated Sodium Channels ,*Molecular Pharmacology* , 68, 1611 (2005).
- [42] F. Roosevelt Gilliam III, C. Frank Starmer, and Augustus O. Grant, Blockade of Rabbit Atrial Sodium Channels by Lidocaine Characterization of Continuous and Frequency-Dependent Blocking , *Circulation Research*, 65, 723 (1989).
- [43] T. J. Campbell, K. R. Wyse and R. Pallandi. Differential effects on action potential of class IA, B and C antiarrhythmic drugs: modulation by stimulation rate and extracellular K⁺ concentration. *Clin. Exp. Pharmacol. Physiol.* 18, 533 (1991).
- [44] Gregory M. Lipkind and Harry A. Fozzard, Molecular Model of Anticonvulsant Drug Binding to the Voltage-Gated Sodium Channel Inner Pore , *Mol Pharmacol*, 78, 631 (2010).
- [45] An R. H., R. Bangalore, S. Z. Rosero and R. S. Kass, Lidocaine block of LQT-3 mutant human Na channels . *Circ. Res*, 79, 103 (1996).
- [46] P. B. Bennett, K. Yazawa, N. Makita, and George A. L. Jr, Molecular mechanism of an inherited cardiac arrhythmia , *Nature*, 376, 683 (1995).
- [47] R. Dumaine, Q. Wang, M. T. Keating, H. A. Hartmann, P. J. Schwartz, A. M. Brown, and G. E. Kirsch, Multiple mechanisms of Na⁺ channel linked long-QT syndrome, *Circ. Res.*, 78, 916 (1996).
- [48] B. P. Bean, C. J. Cohen, and R. W. Tsien, Lidocaine block of cardiac sodium channels . *J. Gen. Physiol.*, 81, 613 (1983).
- [49] P. B. Bennett, C. Valenzuela, L. Q. Chen, and R. G. Kallen. On the molecular nature of the lidocaine receptor of cardiac Na⁺ channels. *Circ. Res.*, 77, 584 (1995).
- [50] R. Dumaine and G. E. Kirsch, Mechanism of lidocaine block of late current in long Q-T mutant Na⁺ channels , *American Physiological Society*, 274, H477 (1998).
- [51] L. M. Hondeghem, Interaction of class I drugs with the cardiac sodium channel. In: *Antiarrhythmic Drugs* , edited by E. M. Vaughan Williams. Berlin: Springer-Verlag, 1989, p. 157174.
- [52] D. W. Wang, K. Yazawa, N. Makita, George A. L. Jr. and P. B. Bennett, Pharmacological targeting of long QT mutant sodium channels, *J. Clin. Invest.*, 99, 1714 (1997).
- [53] Hao Ge and Hong Qian, Physical origins of entropy production, free energy dissipation, and their mathematical representations , *Phys. Rev. E* 81, 051133 (2010).
- [54] M. Ono, A. Sunami, T. Sawanobori and M. Hiraoka. External pH modifies sodium channel block by mexiletine in guinea pig ventricular myocytes , *Cardiovasc. Res.*, 28, 973 (1994).

- [55] M. Ono, A. Sunami and M. Hiraoka. Interaction between external Na⁺ channel in guinea-pig ventricular Myocytes , *Pugers Arch.*, 431, 101 (1995).
- [56] C. F. Stramer and Augustus O. Grant, Phasic ion channel blockade, kinetic model and parameter estimation procedure , *Molecular Pharmacology*, 28, 348 (1985).
- [57] Y. Y. Vilin and P. C. Ruben, Slow Inactivation in Voltage-Gated Sodium Channels, *Molecular Substrates and Contributions to Channelopathies* , *Cell Biochemistry and Biophysics*, 35, 171 (2001).
- [58] C H Luo and Y Rudy, A dynamic model of the cardiac ventricular action potential. I. Simulations of ionic currents and concentration changes , *Circulation Research* 74, 1071 (1994).
- [59] C. E. Clancy and Y. Rudy, Na(+) Channel Mutation That Causes Both Brugada and Long-QT Syndrome Phenotypes A Simulation Study of Mechanism , *Circulation*, 105, 1208 (2002).
- [60] J. R. Groome, F. Lehmann-Horn and B. D. Holzherr, Open- and closed-state fast inactivation in sodium channels Differential effects of a site-3 anemone toxin , *Channels*, 5, 65 (2011).
- [61] C. M. Armstrong, Na channel inactivation from open and closed states, *Proc. Nat. Acad. Sci.*, 103, 17991 (2006).

Chapter 6

Chapter 6

Effect Of Site Selective Drug Blocking On Single Sodium And Potassium Channel: Gillespie Simulation Algorithm

Here we have done a simple but effective modification of the existing Hodgkin-Huxley model by adding drug bound state to study the effect of sodium and potassium blockers on the action potential and ionic currents using Gillespie's exact Markov model simulation. Our approach provides more realistic picture of drug binding which can keep track each states in real time and we can see how gradually the entire population is shifting to the drug bound state. Also our result shows interesting dependence of sodium and potassium currents on each other in presence of drugs. In presence of sodium blocker the action potential falls of exponentially, but in potassium channel with increasing drug affinity initially a noise induced enhanced spiking activity of action potential is seen which gradually falls off with increasing drug affinity.

6.1 Introduction

Ion channels comprising around 1.5% of the human genome are typically very complex, multimeric, transmembrane proteins [1] which exhibits a high degree of both structural and functional diversity [2]. They have very distinct electrical potential dependent “gating” mechanisms where the protein structures can adopt several conformational states

such as closed, open and inactive states in which states they can either transport ions across the membrane creating pores or restrict the ion permeability when required [3]. The physiological importance of the voltage gated ion channels are associated with numerous pathologies namely cardiovascular, neuronal, neuromuscular, musculoskeletal, metabolic, and respiratory systems [1, 4] due to the inherited or non-inherited ion channel diseases including epilepsy, diabetes, cancer, hypertension, and even chronic pain due to mutations [5–8]. Ion channels are thus optimal targets of many therapeutic actions. Although drugs which targets ion channels were developed without detailed knowledge of the molecular interactions between each other [7]. Many existing ion channel blocking drugs thus failed to be effective in managing diseases or to reduce mortality [9, 10]. These poor outcomes exist in part because the majority of drugs were developed when little was known about their interaction with ion channels [11].

Markov modeling and computation simulation have been proved to be a promising methodologies to reveal fundamental biological principles and mechanisms about how these drugs affect the normal biological process and provides knowledge about the interactions between the drugs and ion channels. For better understanding new computational methods are being developed with the help high-performance computing technologies and strong interdisciplinary connection [12, 13]. Incorporating properties of single ion channel into models of their electrophysiological function requires a Markovian formulation which is represented as discrete kinetic states [14]. Single channel Markov models can simulate state specific channel properties and their alterations by mutations, disease or drug binding. As Markov models can be developed both at the level of single channel activity and at the macroscopic state, they provide an implicit relationship between the single channel records and the macroscopic current [15–19]. Markov models of ion channels have been used to study the ion channel functioning during action potentials [14, 20, 21]. The consequence of mutations [21, 22] and action of therapeutic drugs [23] are also studied with the help of Markov model simulation [24]

The famous model of Hodgkin and Huxley [25] is based on an assumption that the ion permeation processes can be approximated as both continuous and deterministic [25]. However, the permeation processes existing within active membrane are known to be neither continuous nor deterministic. Active membrane is studded with discrete ion channels undergoing random fluctuations between open and closed stable states [26]. There have been few studies of the relationship between these two levels of description, the discrete stochastic behavior of the microscopic ion channels versus the continuous deterministic behavior of their macroscopic membrane currents [27]. Recent works also reveals that fluctuations in the states of these devices may be physiologically important in small neu-

ronal structures like nodes of Ranvier [28–30]. It is well known that the Hodgkin-Huxley model simulated with discrete Markovian ion kinetics instead of the usual continuous rate equations leads to spontaneous generation of action potentials [28, 30–34]. At low patch size or low membrane area or when less number of ion channels are considered the spontaneous firing can occur even without the presence of injected external current. The firing arises due to the stochastic fluctuations of the ion channels. These spontaneous firings decreases with the increase in the size of the membrane patch. There exist critical channel number where the spontaneous action potentials cease to exist. A highly accurate theoretical model using a detailed stochastic analysis of the Hodgkin-Huxley system with random Markovian ion kinetics is given by Fox and Lu (1994) [35, 36] solving Langevin equation.

Although similar Markov models have been extensively used to reproduce the action potentials, the studies of Local Anesthetics such as sodium channel blockers(e.g.Saxitoxin, TTX, Mexilitine, Lidocain etc) and potassium channel blockers(e.g. Tetraethylammonium (TEA), Amiodarone etc) [8] are lacking. Thus here we have studied the effect of drugs on action potential using Gillespie’s simulation algorithm [37, 38]. We have separately studied the effect of both the sodium and potassium blockers on the action potential and ionic conduction, spiking activity etc to find out the effect of both the blockers.

Layout of the chapter is as follows. In section 2. we have given the kinetic scheme for drug binding . Then in section 3 we have discussed how the Gillespie simulation technique is incorporated and its advantages over different other simulation technique. In section 4, we have studied the effect of drugs and under different subsections we have studied the effect of sodium and potassium blockers in action potential and ionic conductance. Finally in section 5, we conclude the chapter.

6.2 Kinetic Scheme of Markovian Models

Stochastic behavior of ion channels can be modeled well [19, 39, 40] as continuous-time discrete-state Markovian jumping processe [42–45]. The Hodgkin and Huxley(1952) [25] gating mechanism consists of four activating n gates for potassium channel and the Markov models consider 5 states, such as, n_0 (when all four gates are closed), n_1 (only one gate is open), n_2 , n_3 and n_4 (Open state or Ion conducting state, when all four gates are open). Potassium channel thus have 8 transition rates between these 5 states. The sodium channel have three activating m gates with four distinct states and one inactivating h gate with two distinct states according to the Hodgkin-Huxley model, the kinetic scheme

based on Markov process theory has eight states, $m_0h_1, m_1h_1, m_2h_1, m_3h_1$ (open state or ion conducting state), m_0h_0, m_1h_0, m_2h_0 , and m_3h_0 with 20 transition rates designated by $\alpha'_{h,m}$ s and $\beta'_{h,m}$ s. Thus a whole there are 28 transitions and 13 states to be considered for simulating action potential while the contributions of other channels are ignored [46]. Each channel randomly fluctuates between a finite number of discrete states. Markov assumptions such as transition rates are dependent on the present stable state only and the present membrane voltage and are independent of the duration for which this present stable state has been occupied are used to interpret the data from patch-clamp experiments on single ion channels [26, 27, 47–49]

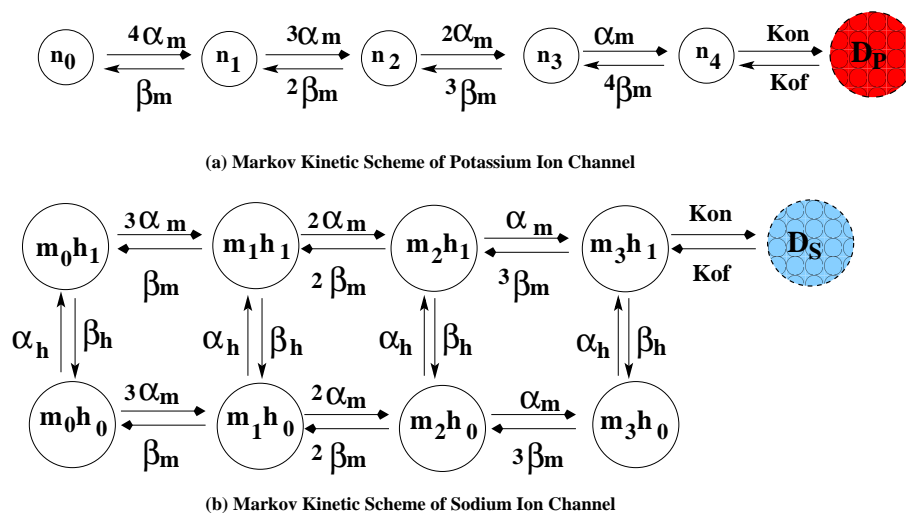


Figure 6.1: Markov model of Potassium and Sodium ion channel. The potassium channel in figure (a) is a 5 state model where we added an extra Drug bound state, D_P . Similarly in figure (b) sodium channel is a 8 state model where we added an sodium blocker state, D_S

Now to study the effect of open state sodium and potassium blockers we have added an extra states in both the channels. For potassium channel it is designated as D_P and for sodium channel it is D_S . The transition rates are given as ‘ k_{on} ’ and ‘ k_{off} ’. Now it is known that these rates are usually expressed as $k_{on} = k_b * [D]$, where k_b is the binding constant of the drug and $[D]$ is the concentration of the drug and k_{off} is independent of the drug concentration. As we do not know what are the values of k_{on} and k_{off} which will fit properly with this model we use trial and error method and change the values of k_{on} keeping k_{off} constant always. Here we have gradually increased the k_{on} from 0.0001 to 1.0 or more keeping $k_{off} = 0.0001$ constant. Increasing k_{on} means increasing drug concentration. Now when we have studied the effect of sodium blockers we do not consider the state D_P and vice versa. Thus our proposed drug binding model now have 14 states and 30 transition rates.

The expressions of the voltage dependent rates [50–52] are given as follows

$$\alpha_m(V) = (0.1(V + 40))(1 - \exp[-(V + 40)/10])^{-1}$$

$$\beta_m(V) = 4 \exp[-(V + 65)/18]$$

$$\alpha_h(V) = 0.07 \exp[-V + 65)/20]$$

$$\beta_h(V) = 1 + \exp[-(V - 35)/10]^{-1}$$

$$\alpha_n(V) = (0.01(V + 55))(1 - \exp[-(V + 55)/10])^{-1}$$

$$\beta_n(V) = 0.125 \exp[-(V + 65)/80]$$

. The V is in mV unit and the rates are in ms^{-1} . The Hodgkin-Huxley [25] transmembrane voltage, V is given by the equation,

The well known Hodgkin-Huxley equation [25] for the squid giant axon without action potential propagation is given as

$$C_m \frac{d}{dt} V(t) + G_K(t)(V(t) - E_K) + G_{Na}(t)(V(t) - E_{Na}) + G_L(V(t) - E_L) = I_{ext}(t). \quad (6.1)$$

Parameters are taken from the references of Gerhard Schmid, Igor Goychuk and Peter Hanggi [50–52] and their descriptions are given Table 6.1.

Table 6.1: Parameters of Hodgkin-Huxley equation

C_m	Membrane capacitance	$1 \mu\text{F}/\text{cm}^2$
E_K	K^+ reversal potential	-77.0 mV
ρ_K	K^+ channel density	$18 \text{ channels}/\mu\text{m}^2$
g_K^{max}	Maximal K^+ channel conductance(all K^+ channels are open)	$36.0 \text{ mS}/\text{cm}^2$
γ_K	Single K^+ channel conductance	20 pS
E_{Na}	Na^+ reversal potential	50.0 mV
ρ_{Na}	Na^+ channel density	$60 \text{ channels}/\mu\text{m}^2$
g_{Na}^{max}	Maximal Na^+ channel conductance(all Na^+ channels are open)	$120.0 \text{ mS}/\text{cm}^2$
γ_{Na}	Single Na^+ channel conductance	20 pS
E_L	Leak reversal potential	-54.4 mV
g_L	Leak conductance	$0.3 \text{ mS}/\text{cm}^2$

The potassium and sodium membrane conductances for a discrete stochastic channel populations are expressed as by the following equation,

$$G_K(V, t) = [g_K^{max}/N_K] N_{n_4} \quad \text{and} \quad G_{Na}(V, t) = [g_{Na}^{max}/N_{Na}] N_{m_3 h_1}, \quad (6.2)$$

where N_{n_4} and N_{Na} are the number of open potassium and sodium channels, respectively and N_K and N_{Na} are the total number of potassium and sodium channels, respectively.

6.3 Choice of Simulation Technique

Computer simulation algorithms can be categorized into two groups:

1. Approximation algorithm: Langevin's equation provided by Fox and Lu [35, 36] where the gating variables m , h and n are considered to be induced by independent Gaussian white noise, $\eta_x(t)$ such as,

$$\dot{x} = \alpha_x(V)(1 - x) - \beta_x(V)x + \eta_x(t), \quad x = n, m, h.$$

The Gaussian white noise with zero mean takes into account the fluctuations of the number of open gates. The noise strengths depend on the membrane voltage. The noise correlations have the following form for an excitable membrane patch with N_{Na} number of sodium and N_K number of potassium ion channels [35, 36], respectively,

$$\langle \eta_x(t)\eta_x(t') \rangle = \frac{2}{N_i} \frac{\alpha_x \beta_x}{\alpha_x + \beta_x} \delta(t - t') \quad i = Na, K, \quad (6.3)$$

where $N_{Na} = \rho_{Na}A$ and $N_K = \rho_K A$ are the numbers of sodium and potassium ion channels in a particular patch size of area A .

2. Exact algorithm: Conductance arises due to Markov jumping process between states. The exact simulation thus possible by solving Markov models using stochastic algorithms. The exact algorithms again can be classified into two algorithms, such as, i) Channel-State-Tracking(CST) algorithms and ii) Channel-Number-Tracking(CNT) algorithms. The CST algorithm tracks the *states of each channel* and superimposes individual channel currents corresponding to the states. This algorithm is although simple but it is computationally very intensive. It has been utilized by Clay and DeFelice [27] in 1983, Strassberg and DeFelice [33] in 1993, and Rubinstein [30] in 1995. However an easy alternative algorithm is Gillespie algorithm [37] in 1977 used by Skaugen and Walloe [32] and Chow and White [38] in 1996 tracks the *number of channels in each state* with the assumption that multi channel systems are independent and memoryless. This Channel Number Tracking(CNT) algorithm provides much greater efficiency in cases where many channels are simulated as the algorithm calculates an effective transition rate associated

the multi-channel system allows only one transition among all states in a random time interval.

6.3.1 Gillespie simulation algorithm

We have done the simulation using the following steps.

1. Initially we have fixed the number of Sodium and Potassium channels to be simulated. $N_{Na} = \rho_{Na}A$ and $N_K = \rho_KA$ are the numbers of sodium and potassium ion channels in a particular patch of area $A \mu m^2$.

2. Then at a resting membrane potential, i.e. at -70 mV the steady state values of the gating variables n, m and h are solved using the following steady state equations,

$$n = \frac{\alpha_n}{\alpha_n + \beta_n}, m = \frac{\alpha_m}{\alpha_m + \beta_m} \text{ and } h = \frac{\alpha_h}{\alpha_h + \beta_h}. \quad (6.4)$$

3. Next at $t=0$ we have assigned the population of the drug bound state, $D_{Na/K} = 0$ for respective sodium and potassium blocker simulations. All the other 13 states are binomially distributed as given by Skaugen and Walloe, 1979 [32],

$$N_{Na}^{kj} = {}^3 C_j h^k (1-h)^{(1-k)} m^j (1-m)^{(3-j)} N_{Na},$$

$$N_K^j = {}^4 C_j n^j (1-n)^{(4-j)} N_K, \quad (6.5)$$

where N_{Na}^{kj} and N_K^j denotes the population of the states where k number of h gates, m number of m gates and j number of n gates are open. Here N_{Na}^{kj} and N_K^j are integers which fluctuate around their expected values.

4. Then we put a initial voltage of -60 mV and start the simulation. First we calculate the individual propensities (a_{ij} for sodium ion channel and (a_k) for potassium channels of all the 30 reactions (including the drug bound state). The propensities a_{ij} or a_k are expressed as the sum of the rates leaving the states multiplied by the population of that state, ($m_i h_j$), e.g. the propensity of the reactions from the state ($m_2 h_0$) is given by $a_{20} = (\alpha_m + 2\beta_m + \alpha_h) N_{m_2 h_0}$. Similarly a_3 for the state n_3 is given as, $a_3 = (\alpha_n + 3\beta_n) N_3$. This way we calculate 30 propensities corresponding to 30 reactions.

5. Next we calculate the total propensity, a_{tot} by summing all the propensities as calculated in the previous step. The sum can be expressed simply for sodium channel

blockers as,

$$a_T = \left[\sum_0^{22} a_{ij} \right] + \left[\sum_0^8 a_k \right].$$

and for potassium channel blockers,

$$a_T = \left[\sum_0^{20} a_{ij} \right] + \left[\sum_0^{10} a_k \right].$$

6. Next we calculate the time required to take the next reaction to occur by calculating τ , which is given as

$$\tau = \frac{1}{a_T} \ln(1/r_1),$$

where r_1 is a pseudo-random number called from a uniform distribution $[0,1]$. As soon as the τ is achieved, the time is incremented as $t = t + \tau$.

7. In the next step we calculate which one of the 30 reactions has taken place in that τ time. A random integer μ is assigned which designate the reaction number. So μ varies from 1 to 30 in our case including the drug bound state. Then an another random number r_2 from an uniform distribution of unit interval is called. Then we calculate the quantity, $(r_2 \times a_T)$. Then the reaction number μ is calculated using the following relation

$$\sum_{\nu=1}^{\mu-1} a_{\nu} < (r_2 \times a_T) \leq \sum_{\nu=1}^{\mu} a_{\nu}$$

. This is actually adding the successive propensities, such as $a_{00} + a_{01} + a_{10} + a_{11} + \dots + a_{30} + a_{31} + a_0 + a_1 + \dots + a_4$ under the μ do-loop ($1 \geq \mu \leq 30$) until their sum is equal or just exceed $(r_2 \times a_T)$, and the μ is then set equal to the index of the last a_{ν} , term added, i.e. the loop index or reaction number index μ . This is how the reaction taken place is identified.

8. As soon as the reaction number index, μ is identified, the population of the states associated with that reaction is updated by ± 1 . The population of the state from which the transition occurred is updated with -1 and the population of the state where to the transition has occurred is updated with +1.

9. Then the sodium and potassium conductances are calculated using equation 7.2 and the corresponding sodium, I_{Na} and potassium ionic, I_K currents are given by the equation

$$I_K = G_K(V, t)(V - E_K) \quad \text{and} \quad I_{Na} = G_{Na}(t)(V - E_{Na}). \quad (6.6)$$

For the first step the $V = -60$ mV here, as mentioned in step 4.

10. Then membrane potential is simply integrated with a time step τ as follows,

$$V_i = V_{i-1} + \frac{1}{C_m} [(I_{ext} - I_{int})\tau],$$

where $I_{int} = I_K + I_{Na} + I_L$. We have taken here the $I_{ext} = 6.9$.

11. Then again the process is repeated from step 4, with the new value of membrane potential and updated rates and propensities in that V.

12. To calculate the spike frequency of action potential we run the program for a very long time and then count the spike number in 10000 ms to calculate the frequency in Hz unit. The program is written in Fortran 90.

6.3.2 From microscopic limit to deterministic limit

In this section we shall study the action potentials and conductances of sodium and potassium channels under no external current, $I_{ext} = 0.0 \mu A/cm^2$ starting from very low patch size $A = 0.5 \mu m^2$ to deterministic limit such as $A = 200 \mu m^2$. Here the presence of drug is not considered. Thus here we used the Gillespie's simulation considering 13 states and 28 reactions. In figure (6.2) we have shown how the action potentials vary

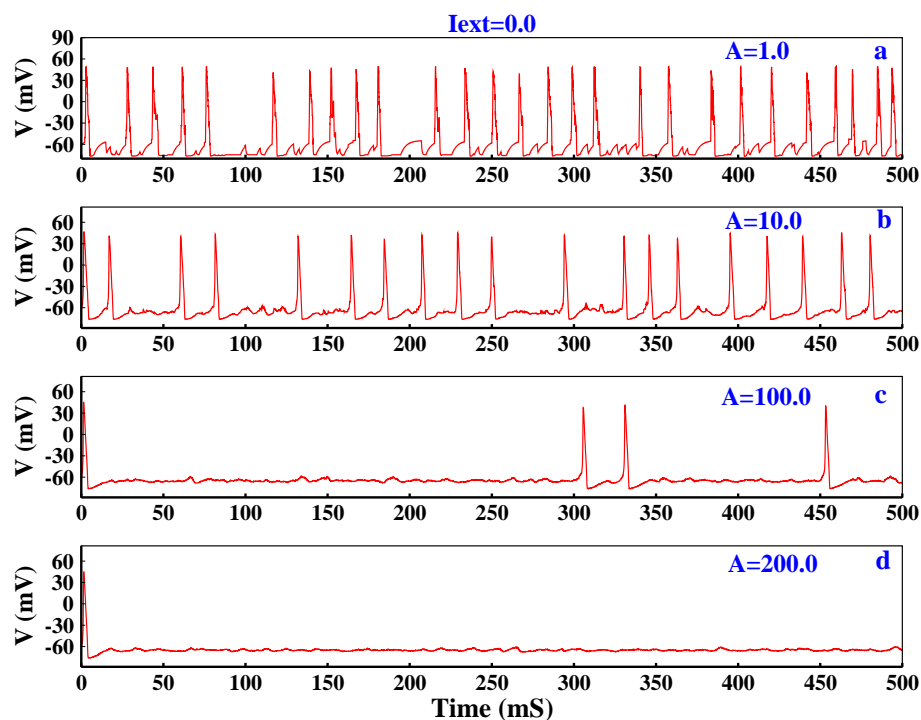


Figure 6.2: Action potentials at various patch sizes is plotted here. From (a) to (d) the action potentials are shown for $A = 1.0, 10.0, 100.0, 200.0 \mu A/cm^2$. $I_{ext} = 0.0 \mu A/cm^2$.

from patch size, $A=1.0$ to $200 \mu\text{m}^2$. In figure 6.2(a) the action potential for $A = 1.0 \mu\text{m}^2$ is plotted where approximately 60 sodium channels and 18 potassium channels take part in action potential generation. At very low patch size channel noise play very important role. At low patch size these number fluctuations or channel noise can alone generate spiking activities as already known to literature [50–52]. As soon as the patch size is increased the rate of spontaneous generation of spikes decreases. As we can see at very high patch size, for example $A = 200 \mu\text{m}^2$, the spiking phenomenon vanishes away and system behaves similarly as it does in deterministic limit at $I_{ext} = 0.0 \mu\text{A}/\text{cm}^2$.

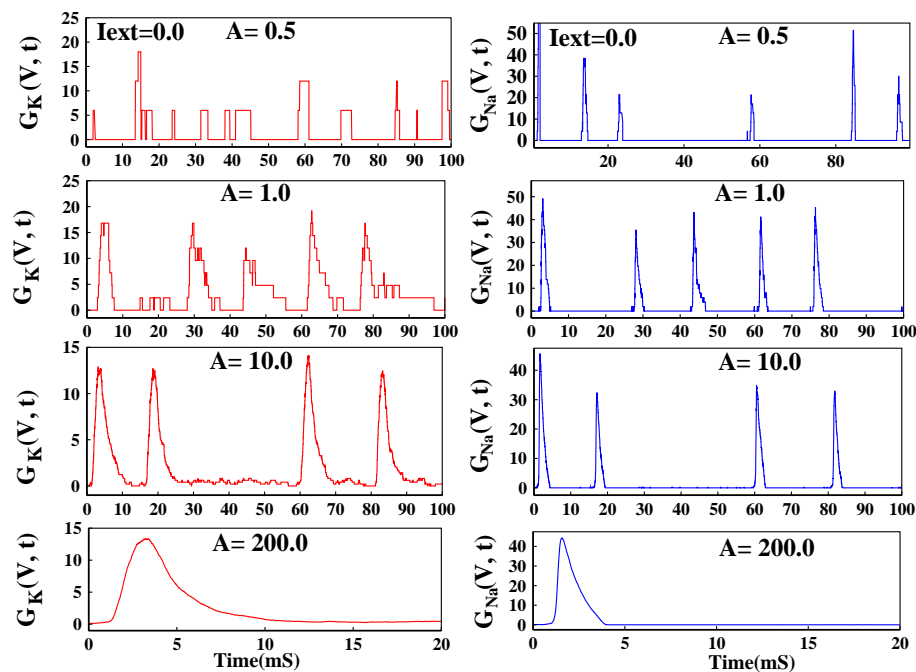


Figure 6.3: Conductance curves for sodium and potassium channels from microscopic system to deterministic limit. In the left panel potassium and in the right panel the sodium channel conductances are plotted for $A = 0.5, 1.0, 10.0, 200 \mu\text{A}/\text{cm}^2$ at $I_{ext} = 0.0 \mu\text{A}/\text{cm}^2$ for first few mS.

The stochastic nature of conductance for both sodium and potassium channels are well observed from the figure (6.3). At high patch size the conductance curves behave similar to the response in deterministic limit.

6.4 Effect of Sodium & Potassium Channel Blockers

In this section we shall study the effect of sodium and potassium blockers separately using Gillespie's simulation for the model shown in figure (6.1) for $I_{ext} = 6.9 \mu A/cm^2$.

6.4.1 Sodium blocker

Here we have considered only open state sodium channel blockers to study the effect of blockers on action potential and ionic currents. Thus only D_S state is present not D_P . From figure (6.4) it is seen that with increasing drug concentration the number of action

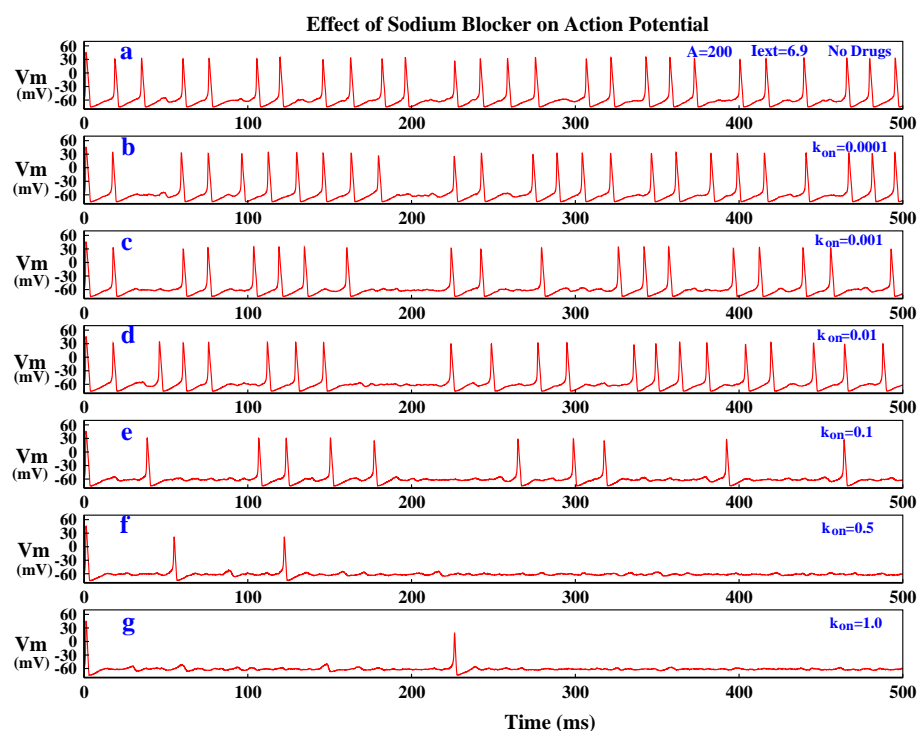


Figure 6.4: Action potentials in presence of various sodium blocking affinities is plotted here. In figure (a) the action potentials are plotted without the presence of any drug. From figure (b) to (g) the action potentials are plotted for $k_{on}=0.0001, 0.001, 0.01, 0.1, 0.5$ and 1.0 . for $A= 200 \mu A/cm^2$ and $I_{ext} = 6.9 \mu A/cm^2$

potential gradually decreases and at very high value of $k_{on}=1.0$ the system totally fails to regenerate action potentials. As the rate of drug binding increases more and more channels go to the state and get trapped. Thus the available open sodium channels gradually decrease and thus that patch fails to generate action potentials. As the action potentials on that patch are not generating, the patch fails to send signals to the nervous

system and the nervous system with out getting any response from that patch can not feel its existence. This is the intricate mechanism of local anesthesia.

Next we have seen how the sodium and potassium ionic currents get modified with increasing drug binding rates. From figure (6.5) we can see that with increasing drug

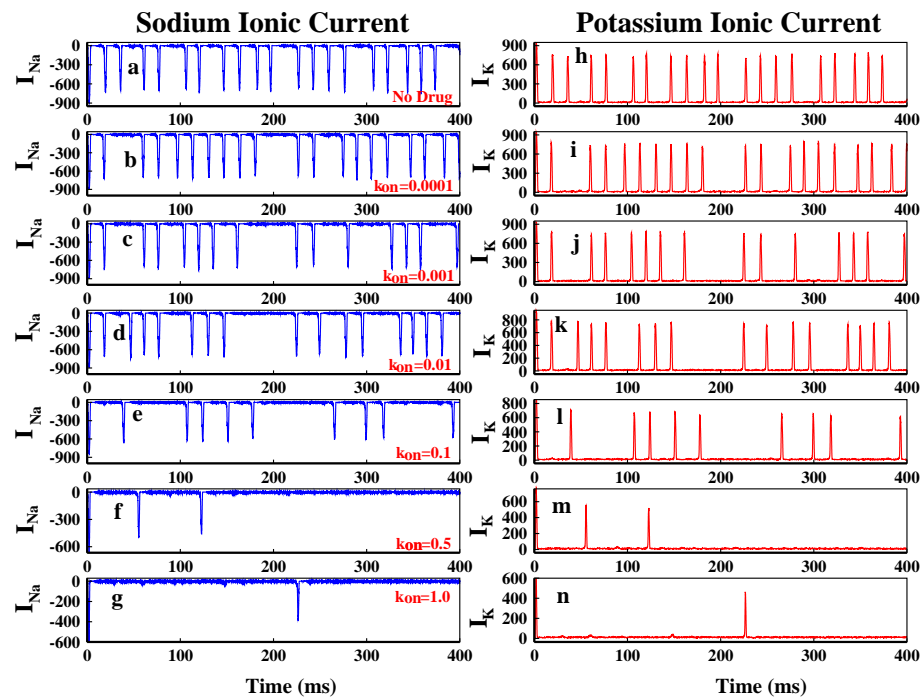


Figure 6.5: In the left panel from figure (a) to (g) the sodium ionic current and in the right panel from figure (h) to (n) potassium ionic current is plotted for $A = 200 \mu A/cm^2$ and $I_{ext} = 6.9 \mu A/cm^2$.

concentration as the available open state of sodium channels decreases rapidly, the sodium ionic current also decreases. At very high concentration such as $k_{on}=1.0$ the sodium ionic current almost vanishes. Interestingly the effect of drug is not only evident on sodium ion current, it directly affect the potassium currents too. This happens because sodium and potassium channels together works for action potentials. The number of spike of sodium ionic current is equal to the number of spike for potassium ionic current.

Next we have shown the population of the drug bound state with increasing k_{on} . It is seen that with increasing k_{on} rate the population of the drug binding state increases rapidly. Next we have shown the spiking frequency of the action potentials with increasing k_{on} in figure (6.7). It is seen that the spiking rate almost falls off exponentially from high concentration to low concentration.

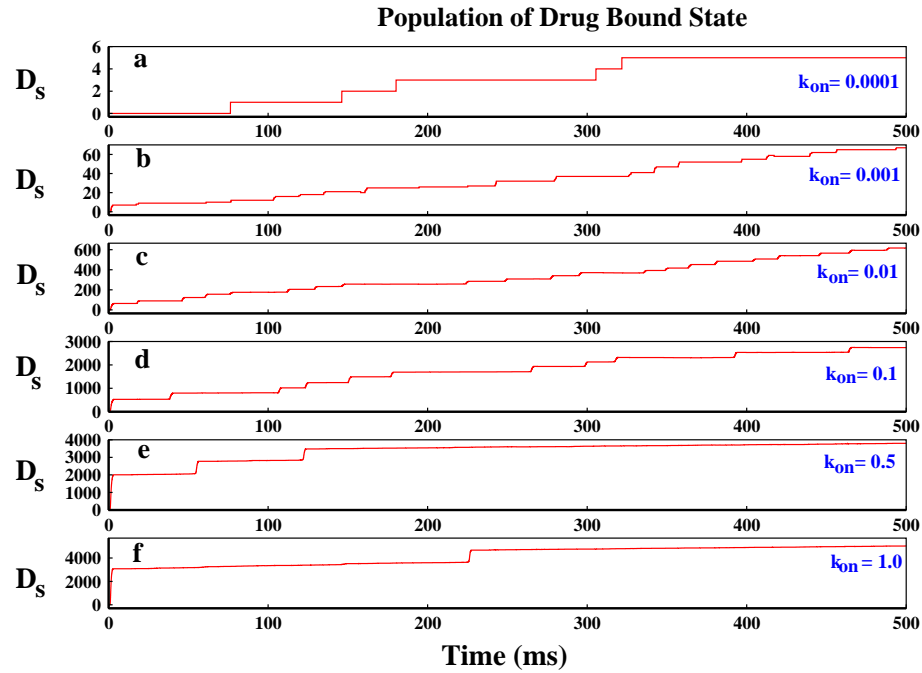


Figure 6.6: Population of D_s or sodium drug bound state is plotted for $k_{on} = 0.0001$ to 1.0 from figure (a) to (f) for $A = 200 \mu A/cm^2$ and $I_{ext} = 6.9 \mu A/cm^2$.

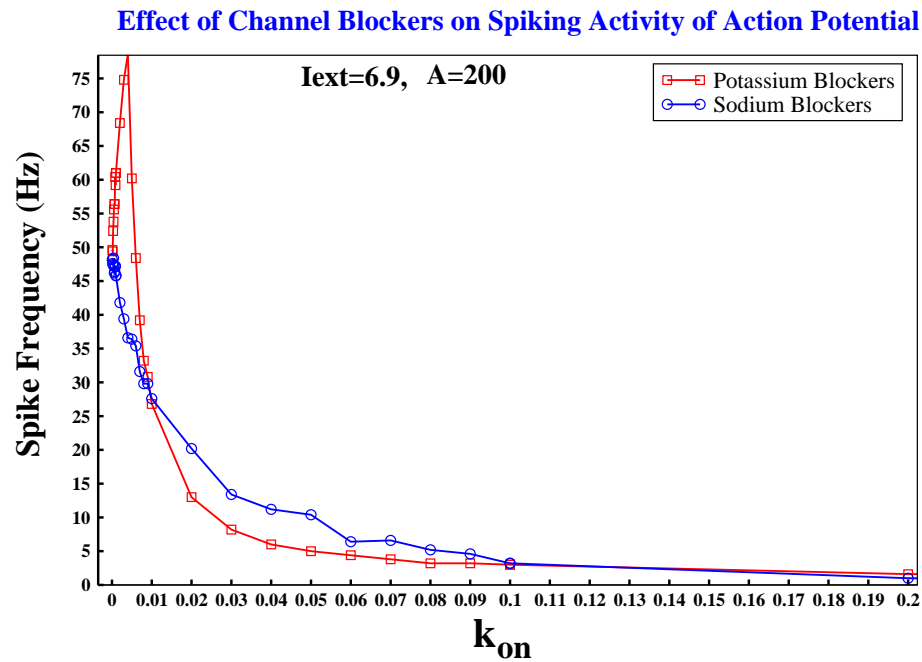


Figure 6.7: Spiking frequency(Hz) of the action potentials in presence of increasing channel blockers, k_{on} ranging from 0.0001 to 1.0 is plotted for $A = 200 \mu A/cm^2$ and $I_{ext} = 6.9 \mu A/cm^2$. The spiking frequency is calculated over a long simulation run upto 10s. The circled-blue-solid line and the squared-red-solid line shows the frequency of spiking of action potentials in presence of sodium and potassium channel blockers, respectively.

6.4.2 Potassium blocker

Here we have studied the effect of Potassium blockers on action potential, ionic currents and spiking activity. Here the D_P state is only considered, not D_S state. In figure (6.8) the

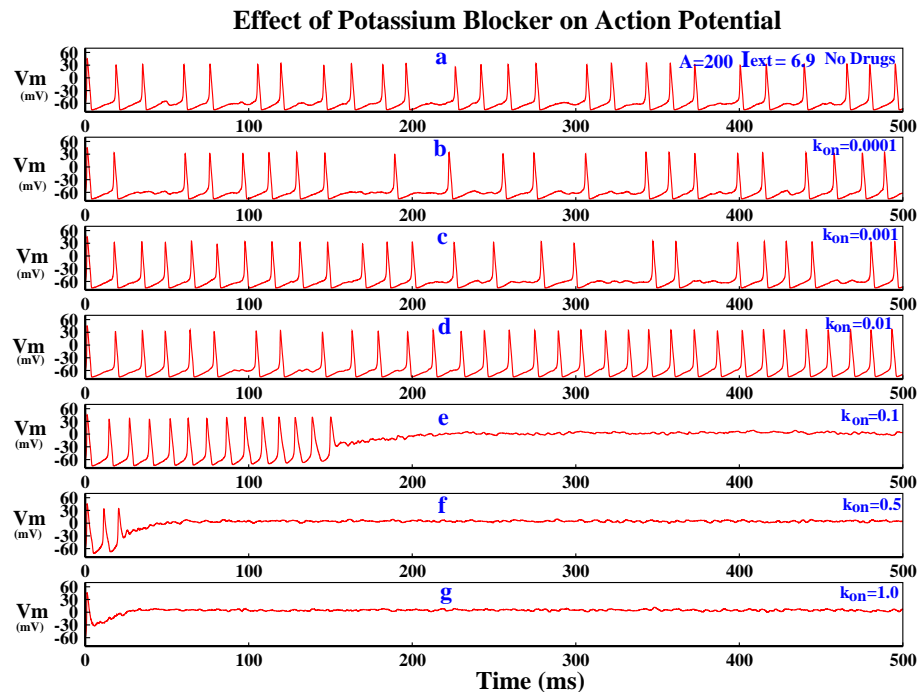


Figure 6.8: Action potentials in various blocking affinities are plotted here. In figure (a) the action potentials are plotted with out the presence of any drug. From figure (b) to (g) the action potentials are plotted for $k_{on}=0.0001, 0.001, 0.01, 0.1, 0.5$ and 1.0 . for $A=200 \mu A/cm^2$ and $I_{ext} = 6.9 \mu A/cm^2$

action potentials for various k_{on} is plotted here. We have found an interesting dependence of k_{on} here. Initially with increasing k_{on} the spiking activity increases unlike sodium channel and then decreases. This initial increase is consistent with the literature [52]. With increasing drug concentration number of potassium channel decreases and that causes and increase in the internal channel noise. As we have already seen from the figure (6.2) that channel noise can play important role and can spontaneously generate spiking activities. There exists a competition between the overall conduction of the potassium current and the channel noise. Initially the influence o the channel noise dominates and thus the spiking activity increases. After a certain k_{on} value the spiking activity decreases. In this case the influence of overall potassium conductance dominates. The potassium conductances falls of drastically due to lack of available open potassium channels. Thus it is seen that due to the lack of available potassium channels the depolarization process gets hampered and the action potential generation does not complete. As is it is not

complete further re-factorization of membrane depolarization is not possible and thus no action potential generation is possible as seen from figure 6.8(e-f).

Next we have plotted the potassium and sodium ionic currents in the figure (6.9). For all the k_{on} values both the sodium and potassium currents have 1:1 correspondence

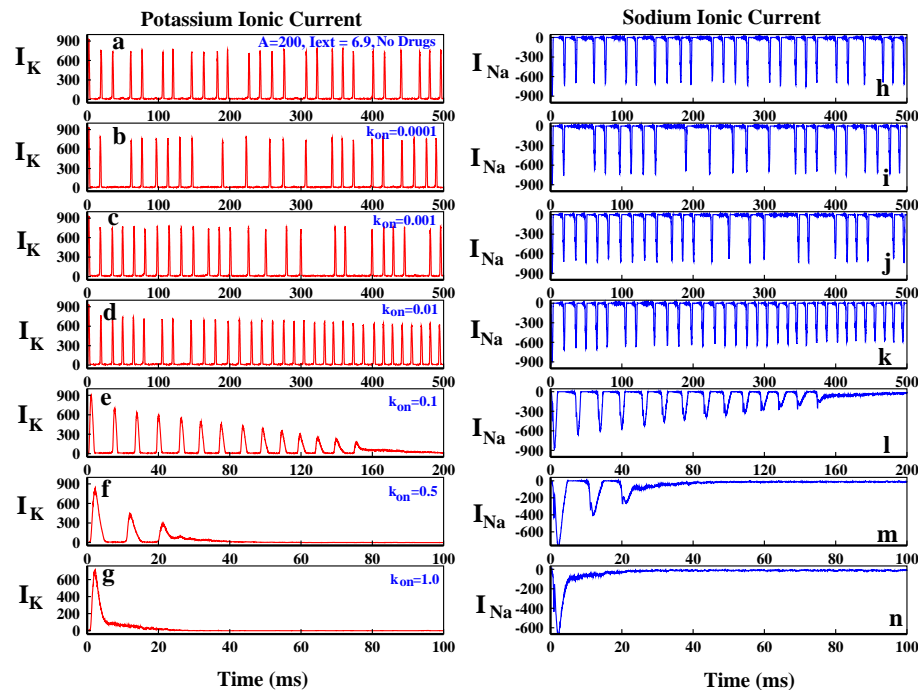


Figure 6.9: In the left panel from figure (a) to (g) the potassium ionic current and in the right panel from figure (h) to (n) sodium ionic current is plotted for $A = 200 \mu A/cm^2$ and $I_{ext} = 6.9 \mu A/cm^2$.

regarding the spike numbers. With increasing k_{on} initially the spikes of both ionic increases and then decreases as seen from the action potentials. Also the ionic currents for higher k_{on} falls off and never re-initiates. In figure (6.10) we have plotted the population of the potassium blockers.

Next we have plotted the spike frequency of the action potentials with increasing k_{on} . As mentioned earlier initially with increasing drug concentration the spiking activity increases, we see that the spiking frequency initially increases as channel noise increases and then it decreases as the overall potassium conduction decreases as seen from figure (6.7).

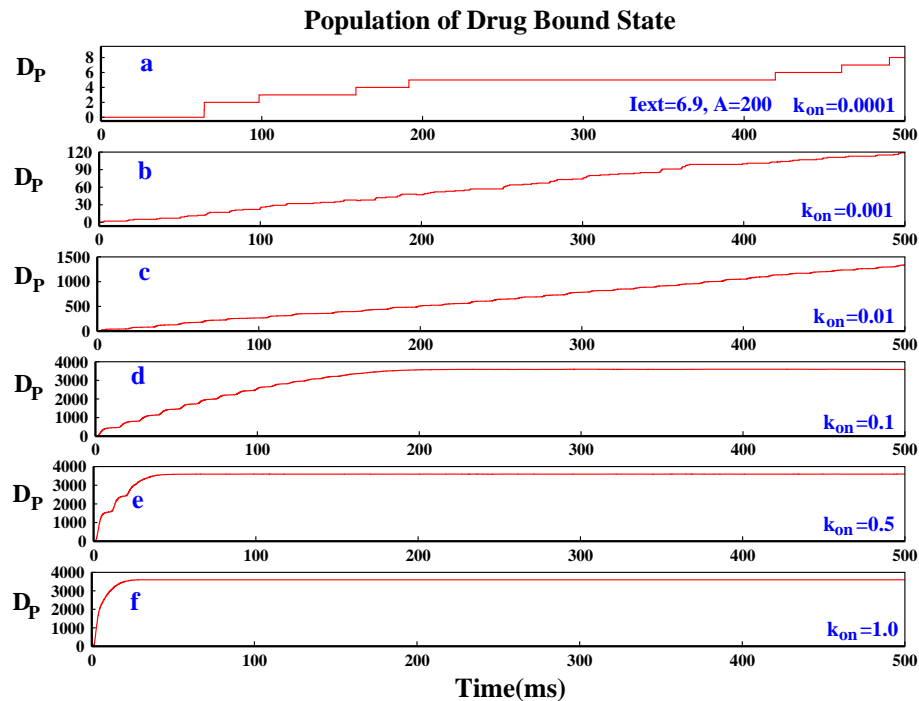


Figure 6.10: Population of D_P or potassium drug bound state is plotted for $k_{on} = 0.0001$ to 1.0 from figure (a) to (f) for $A = 200 \mu A/cm^2$ and $I_{ext} = 6.9 \mu A/cm^2$.

6.5 Conclusion

In this chapter we have introduced a simple but realistic approach to understand the effect of sodium and potassium blockers all the way from microscopic level to deterministic level. We have utilized the site selective drug blocking mechanism of the single sodium and potassium channel to explore the overall action potential. The existing literature of drug blockers using Langevin description [52] discards the drug blocked channels before hand and calculate the action potential using the available channels which are not blocked yet.

But in our approach we can track each states in real time and we can see how gradually the entire population is shifting to the drug bound state. The conductance or population of open states is real time updated with population changes. Thus this approach provides more realistic picture of drug binding.

We have understood that the number of sodium current spike will always be equal to the potassium spikes. In case of sodium channels blockers although the spiking activity decreases, the action potentials generated are of complete shape because of available potassium channels but in case of potassium blockers at higher values of k_{on} due to the lack of potassium channels the shape of action potential can not complete and as the

re-factorization process gets hampered, the action potential can not regenerate or the spiking activity is completely destroyed.

We have also seen that in case of sodium blockers the increase in drug binding affinity directly leads to decrease in number of action potential generation whereas for potassium channel with increasing drug binding affinity initially the channel noise come into play which enhances spiking frequency and then it gradually behaves similarly like sodium blockers.

Bibliography

- [1] Ashcroft, FM. From molecule to malady. *Nature* 440, 440 (2006).
- [2] Venter, JC et al. The sequence of the human genome. *Science* 291, 1304-51, (2001).
- [3] Clare, JJ. Functional expression of ion channels in mammalian systems. In Clare, J.J. and Trezise D.T. (Eds.) *Expression and Analysis of Recombinant Ion Channels*. Wiley-VCH, Weinheim, Germany,79-109, (2006).
- [4] Catterall, WA. From ionic currents to molecular mechanisms, the structure and function of voltage-gated sodium channels. *Neuron*, 26, 13 (2000).
- [5] Dichgans, M., et.al, Mutation in the neuronal voltage-gated sodium channel SCN1A in familial hemiplegic migraine, *Lancet*, 366, 371 (2005).
- [6] George, AL Jr., Inherited disorders of voltage-gated sodium channels, *J. Clin. Invest.*, 115, 1990 (2005).
- [7] Ballester, G F., Carvajal, A F., Gonzalez-Ros J M. , Montiel, A F. Ionic Channels as Targets for Drug Design, A Review on Computational Methods, *Pharmaceutics*, 3, 932-953 (2011).
- [8] Pal, K., Gangopadhyay, G., Probing kinetic drug binding mechanism in voltage-gated sodium ion channel, open state versus inactive state blockers. *Channels* , 9(5), 307-16 (2015).
- [9] Echt, DS., Liebson, PR., Mitchell, LB., Peters, RW, Obias, Manno D., Barker, A. H., Arensberg, D., Baker, A., Friedman, L., Greene, HL. Mortality and morbidity in patients receiving encainide, flecainide, or placebo. The Cardiac Arrhythmia Suppression Trial. *N. Engl. J. Med.* 324, 781 (1991).
- [10] Task Force of the Working Group on Arrhythmias of the European Society of Cardiology, The Sicilian gambit. A new approach to the classification of antiarrhythmic drugs based on their actions on arrhythmogenic mechanisms. *Circulation*, 84, 1831 (1991).
- [11] Clancy CE., Zhu Z.I., Rudy Y., Pharmacogenetics and anti arrhythmic drug therapy, a theoretical investigation, *Am. J. Physiol. Heart. Circ. Physiol.*, 292, H66 (2007).

- [12] Zemzemi N., Bernabeu MO., Saiz J., Cooper J., Pathmanathan P., Mirams GR., et al. Computational assessment of drug-induced effects on the electrocardiogram, from ion channel to body surface potentials. *Br J Pharmacol.*, 168, 718-33 (2013).
- [13] Vladimir YY., Allen TW. , Clancy CE., Computational models for predictive cardiac ion channel pharmacology, *Drug Discovery Today, Disease Models*, 14, 3-10 (2014).
- [14] Rudy Y., Silva JR. Computational biology in the study of cardiac ion channels and cell electrophysiology. *Q. Rev. Biophys.* 39, 57-116 (2006).
- [15] Nekouzadeh A., and Rudy Y., Statistical properties of ion channel records. Part II. Estimation from the macroscopic current. *Math. Biosci.* 210, 315-334 (2007).
- [16] Nekouzadeh A., and Rudy Y., Statistical properties of ion channel records. Part I. Relationship to the macroscopic current. *Math. Biosci.* 210, 291-314 (2007).
- [17] Aldrich RW., Corey DP., Stevens CF. A reinterpretation of mammalian sodium channel gating based on single channel recording. *Nature.* 306, 436-441 (1983).
- [18] Anderson CR., Stevens CF. Voltage-clamp analysis of acetylcholine produced end-plate current fluctuations at frog neuromuscular junction. *J. Physiol.* 235, 655-691 (1973).
- [19] Neher E., Steinbach JH. Local anesthetics transiently block currents through single acetylcholine-receptor channels. *J. Physiol.* 277, 153-176 (1978).
- [20] Silva J., Rudy Y. Subunit interaction determines IKs participation in cardiac repolarization and repolarization reserve. *Circulation.* 112, 1384-1391 (2005).
- [21] Faber, GM., Silva J., Livshitz L., Rudy Y. Kinetic properties of the cardiac L-type Ca²⁺ channel and its role in myocyte electrophysiology, a theoretical investigation. *Biophys. J.* 92, 1522-1543 (2007).
- [22] Clancy, C. E., and Y. Rudy. Linking a genetic defect to its cellular phenotype in a cardiac arrhythmia. *Nature.* 400, 566-569 (1999).
- [23] Clancy, C.E., Z. I. Zhu, and Y. Rudy. Pharmacogenetics and anti-arrhythmic drug therapy, a theoretical investigation. *Am. J. Physiol. Heart Circ. Physiol.* 292, H66-H75 (2007).
- [24] Nekouzadeh A., Silva J.R., Rudy Y., Modeling Subunit Cooperativity in Opening of Tetrameric Ion Channels, *Biophysical Journal.* 95(7), 3510-3520 (2008).
- [25] Hodgkin, AL. Evidence for electrical transmission in nerve Part I. *J Physiol* ; 90, 183 (1937).
- Hodgkin, AL. Evidence for electrical transmission in nerve Part II. *J. Physiol* ; 90, 211 (1937).
- Hodgkin, A.L., Huxley, A.F., A quantitative description of membrane current and its application to conduction and excitation in nerve, *J. Physiol.* ; 117, 500 (1952).

- Huxley, A. , From overshoot to voltage clamp, *Trends in Neurosciences*, 25, 553 (2002).
- [26] Hille, B., *Ionic channels of excitable membranes*. 2nd edition, Sinauer Associates, Sunderland, Mass (1992).
- [27] Clay, J., and DeFelice, L. Relationship between membrane excitability and single channel open-close kinetics. *Biophys. J.* 42, 151-157 (1983).
- [28] Lecar, H., and R. Nossal. Theory of threshold fluctuations in nerves. *Biophys. J.* 11, 1048 -1067, (1971).
- [29] Sigworth, F. J. The variance of sodium current fluctuations at the node of ranvier. *J. Physiol. (London)* 307, 97-129 (1980).
- [30] Rubinstein, J. T. Threshold fluctuations in an N sodium channel model of the node of Ranvier. *Biophys. J.* 68, 779-785 (1995).
- [31] Lecar, H., Nossal, R. Theory of threshold fluctuations in nerves. I. Analysis of various sources of membrane noise. *Biophys. J.* 11, 1068-1084 (1971b).
- [32] Skaugen, E., and L. Wall0e. Firing behaviour in a stochastic nerve membrane model based upon the Hodgkin-Huxley equations. *L. Acta Physiol. Scand.* 107, 343-363 (1979).
- [33] Strassberg, A., and L. J. De Felice. 1993. Limitations of the Hodgkin-Huxley formalism, effects of single channel kinetics on transmembrane voltage dynamics. *Neural Computation.* 5, 843-855.
- [34] De Felice, L. J., and W. N. Goolsby. 1996. Order from randomness, spontaneous firing from stochastic properties of ion channels. In *Fluctuations and Order, The New Synthesis*. M. Millonas, editor. Springer, New York. 331-342.
- [35] Fox, R. F. Stochastic versions of the Hodgkin-Huxley equations. *Biophys. J.* , 72, 2069-2074 (1997).
- [36] R.F. Fox, Y. Lu, Emergent collective behavior in large numbers of globally coupled independently stochastic ion channels *Phys. Rev. E* 49 , 3421 (1994).
- [37] Gillespie, D. T. Exact stochastic simulation of coupled chemical reactions. *J. Phys. Chem.* 81, 2340-2361 (1977).
- [38] Chow, C. C., and J. A. White. Spontaneous action potentials due to channel fluctuations. *Biophys. J.* , 71,.3013-3021 (1996).
- [39] Colquhoun, D., and A. G. Hawkes. Relaxation and fluctuations of membrane currents that flow through drug-operated channels. *Proc. R. Soc. London, Ser. B* 199, 231-262 (1977).
- [40] Colquhoun, D., and A. G. Hawkes. On the stochastic properties of single ion channels. *Proc. R. Soc. London, Ser. B* 211, 205-235 (1981).

-
- [41] Neher, E., and C. F. Stevens. Conductance fluctuations and ionic pores in membranes. *Annu. Rev. Biophys. Bioeng.* 6, 249-273 (1977).
- [42] Papoulis, A. *Probability, Random Variables, and Stochastic Processes*, 2nd ed. Singapore, McGraw-Hill (1985).
- [43] Armstrong, C. M., and F. Bezanilla.. Inactivation of the sodium channel. II. Gating current experiments. *J. Gen. Physiol.* 70, 567-590 (1977).
- [44] Armstrong, C. M., and W. F. Gilly.. Fast and slow steps in the activation of sodium channels. *J. Gen. Physiol.* 74, 691-711 (1979).
- [45] Gilly, W. F., and C. M. Armstrong. Divalent cations and the activation kinetics of potassium channels in squid giant axons. *J. Gen. Physiol.* 79, 965-996 (1982).
- [46] H Iroyuki Mino , Jay T. Rubinstein , and John A. White, Comparison of Algorithms for the Simulation of Action Potentials with Stochastic Sodium Channels, *Annals of Biomedical Engineering*, Vol. 30, 578-587, (2002)
- [47] Strassberg, A. F., and DeFelice, L. J. Limitations of the Hodgkin-Huxley formalism. *Computation and Neural Systems Program-Memo 24*, California Institute of Technology (1992).
- [48] Kienker, P.. Equivalence of aggregated Markov models of ion-channel gating. *Proc. R. SOC. London B* 236,269-309 (1989).
- [49] Conti, F., DeFelice, L. J., and Wanke, E. Potassium and sodium ion current noise in the membrane of the squid giant axon. *J. Physiol. (London)* 248,45- 82. (1975).
- [50] Schmid, G., Goychuk, I., Hanggi, P. Channel noise and synchronization in excitable membranes, *Physica A* , 325, 165 -175 (2003).
- [51] Hanggi, P., Schmid, G., Goychuk, I., Excitable membranes: Channel Noise, Synchronization, and Stochastic Resonance. *Advances in Solid State Physics* , 42, 359-370 (2002).
- [52] Schmid, G., Goychuk, I., Hanggi, P. Stochastic resonance as a collective property of ion channel assemblies. *Europhys. Lett.*, 56 (1), 22-28 (2001).

Chapter 7

Chapter 7

Effect Of Channel Noise On Synchronization And Metabolic Energy Consumption In Unidirectionally Coupled Two Hodgkin-Huxley Neurons

In this chapter the stochastic generalization of single Hodgkin-Huxley neuron is further extended to unidirectionally coupled neurons. Our main focus is to elucidate the kinetics and energetics of unidirectional synchronization between two coupled neurons as a function of patch size. We have found that the size of the patch is playing the pivotal role in unidirectional synchronization and metabolic energy consumption. For example, there exist three different patch size ranges in which coupled neuron system behaves differently from noise enhanced phase to dead range before reaching the deterministic limit. We have also found that the sodium and potassium channel blockers have distinct kinetic and energetic effects on synchronization process and metabolic energy consumption rate.

7.1 Introduction

The action potential is the basic unit of signaling used by nerve and muscle tissue for cellular communication. Generation of action potential to maintain neural activity requires high metabolic energy [1–4]. In humans, the brain has only 2% of the body mass but

it consumes 20% of the human metabolic energy [1] which is a large fraction. The generation of the firing sequences of action potentials to transmit information [2] consumes a large fraction of brain's total metabolic energy consumption. The action potential involves influx of Na^+ ions and efflux of K^+ ions through voltage-gated ion channels, which charge the membrane capacitance to the peak of the action potential and then discharge it back to resting potential. This whole process consumes huge energy. Ion pumps extrude ions through the cell membrane against their concentration gradient consuming ATP molecules. There are three basic reasons why action potential demand huge energy. Firstly, making a robust signal requires the membrane capacitance to be charged by more than 50 mV to the peak of the action potential. Secondly, the total area of the membrane covered by action potential during its propagation through axons, collaterals and dendrites is very large and so the capacitance must be charged to the peak voltage. Thirdly, the flux of Na^+ and K^+ ions exceeds the minimum required to charge the membrane to peak potential because the Na^+ and K^+ currents overlap [5, 6]. Energy consumed by a neuron during an action potential is estimated by recording some action potentials and then computing theoretically the number of sodium ions required to enter into the cell to produce the same membrane depolarization [5–11]. The Hodgkin-Huxley [12] circuit model is the most frequently used model in the study of actual neurons [13–16]. The average metabolic energy consumption can be estimated by calculating the total derivative of the electrochemical energy in the circuit [17, 18].

Speaking of coupled neuron system obviously brings the topic of synchronization. Although the synchronization process in physical and biological system is a well known [19–23] but the neuronal synchronization process is one of the most important biological phenomena. Neural activities like selective attention [24–26], cognition [27], memory, learning [28, 29] and some diseases relate to the synchronization process [30–33]. Controlled synchronization of coupled neuron systems have been widely investigated [34, 35] like many studies to understand the biological information transfer process in neural networks. Experimentally [36, 37] it is seen that in large ensembles of neurons the synchronization plays significant role in information processing. Experimentally it is also seen that two coupled living neurons can be synchronized by depolarizing external DC current [38]. Theoretically various modern control methods [39–41], like feedback control, back stepping design, and nonlinear control were successfully applied to neuronal synchronization. Signals are transferred from one neuron to another through synaptic junctions which are mainly of two types, such as chemical or electrical. Electrical synapses or gap junctions are efficient and robust to transmit signal from one neuron to another [42]. Although energetics and synchronization process of unidirectionally coupled neurons is well researched in literature, the effect of patch size variation of individual neurons of the cou-

pled system has not been thoroughly investigated earlier. Also the effect of sodium and potassium blockers on the synchronization process and metabolic energy consumption has been overlooked.

To explore the effect of patch size and channel blockers, we have considered here a simple coupled neuron system connected via gap junction channels of particular conductance. We calculate the metabolic energy consumed by the ion channels using Hodgkin-Huxley circuit model. The metabolic consumption of energy of action potential has been calculated taking internal channel number fluctuations in account. Channel noise plays very important role in action potential generation. Thus we have incorporated the channel noise in both the neurons. For simplicity we considered both the neurons have same size. In our future work we shall investigate the case of neural synchronization where two neurons are of different size. To be specific in this work we have asked the following questions.

(1) How does the coupled system kinetically and energetically respond to the variable patch size?

(2) To find the effect of sodium blockers, potassium blockers and total blockers on the action potential response and metabolic energy consumption.

(3) What are the qualitative and quantitative differences between these three types of drug blockers?

The layout of the chapter is as follows. In section (7.2) we have discussed the deterministic description of metabolic consumption of a single neuron in presence of external current. Then in section (7.3) we have discussed the kinetic scheme and energetics of the unidirectional coupling. In section (7.4) the channel noise is introduced in the coupled neuron and in various subsections we have studied the effect of patch size on synchronization and average metabolic energy consumption. In section (7.5) we have explored the effect of three types of channel blockers on metabolic energy consumption. Finally the chapter is concluded in section (7.6).

7.2 Single Hodgkin-Huxley Neuron: Deterministic Description

As we have already seen the well known Hodgkin-Huxley equation [12] for the squid giant axon without action potential propagation is given as

$$C_m \frac{d}{dt} V(t) + G_K(t)(V(t) - E_K) + G_{Na}(t)(V(t) - E_{Na}) + G_L(V(t) - E_L) = I_{ext}(t), \quad (7.1)$$

where $V(t)$ is the membrane potential. Parameters are taken from the references by Gerhard Schmid, Igor Goychuk and Peter Hanggi [43–45] and their descriptions are given Table 6.1. Conductance $G_K(t)$ and $G_{Na}(t)$ are given as follows,

$$G_K(t) = g_K^{max} n^4 \quad \text{and} \quad G_{Na}(t) = g_{Na}^{max} m^3 h, \quad (7.2)$$

where n , m and h are the well know gating variables of potassium and sodium channels which describe the mean ratios of the open gates of the working channels. The factor n^4 and $m^3 h$ are the mean portions of the open ion channels within the membrane patch. The dynamics of the opening probabilities for the gates are given by

$$\dot{x} = \alpha_x(V)(1 - x) - \beta_x(V)x, \quad x = n, m, h. \quad (7.3)$$

The expressions of the voltage dependent rates [43–45] are given as follows

$$\begin{aligned} \alpha_m(V) &= (0.1(V + 40))(1 - \exp[-(V + 40)/10])^{-1}, \\ \beta_m(V) &= 4 \exp[-(V + 65)/18], \\ \alpha_h(V) &= 0.07 \exp[-V + 65)/20], \\ \beta_h(V) &= 1 + \exp[-(V - 35)/10]^{-1}, \\ \alpha_n(V) &= (0.01(V + 55))(1 - \exp[-(V + 55)/10])^{-1}, \\ \beta_n(V) &= 0.125 \exp[-(V + 65)/80] \end{aligned}$$

The total electrical energy accumulated in the circuit at a given moment in time is [18]

$$H(t) = \frac{1}{2} C_m V^2 + H_{Na} + H_K + H_L, \quad (7.4)$$

where $\frac{1}{2}C_m V^2$ is the electrical energy accumulated by the capacitor and the last three terms represent the energies in sodium, potassium and leak batteries, respectively. The electrochemical energy accumulated in the batteries are potentially unlimited as the exhaustion of the batteries are not considered here. In the real neuron, the nutrients consumed with food actually prevents the ion pumps from getting exhausted. The rate at which the batteries supply electrical energy to the circuit is equal to the electromotive force of the batteries multiplied by the electrical current through the batteries. The total derivative with respect to time of the above energy is given by [18]

$$\dot{H}(t) = CV\dot{V} + I_{Na}E_{Na} + I_K E_K + I_L E_L, \quad (7.5)$$

where

$$I_{Na} = g_{Na}^{max} m^3 h (V - E_{Na}),$$

$$I_K = g_K^{max} n^4 (V - E_K),$$

and

$$I_L = g_L (V - E_L) \quad (7.6)$$

are the sodium, potassium and leakage currents. Substituting equation (7.1) into (7.5) one can obtain the following relation,

$$\dot{H} = VI_{ext} - I_{Na}(V - E_{Na}) + I_K(V - E_K) + I_L(V - E_L). \quad (7.7)$$

Now substituting equations (7.6) into (7.5) we get

$$\dot{H} = VI_{ext} - g_{Na}^{max} m^3 h (V - E_{Na})^2 - g_K^{max} n^4 (V - E_K)^2 - g_L (V - E_L)^2. \quad (7.8)$$

The above equation is the total derivative of the electrochemical energy in the neuron. The first term in the right-hand summation represents the electrical power supplied to the neuron via the different junctions reaching the neuron such as synapse and the other three terms of the summation represent the total metabolic energy per consumed by all the three types of ion channel per second. The metabolic consumption of the Hodgkin-Huxley neuron is calculated evaluating (7.8) at different values of the external current I_{ext} . For computation we have used second order Runge-Kutta method for solving the differential equations (7.1)-(7.3). The initial voltage at which the steady states $n_\infty, h_\infty, m_\infty$ were calculated is taken as -70 mV. Then the stimulus voltage was provided at -60 mV at two different external current, $I_{ext} = 6.9$ and $10.0 \mu A/cm^2$. Then evaluating equation (7.8)

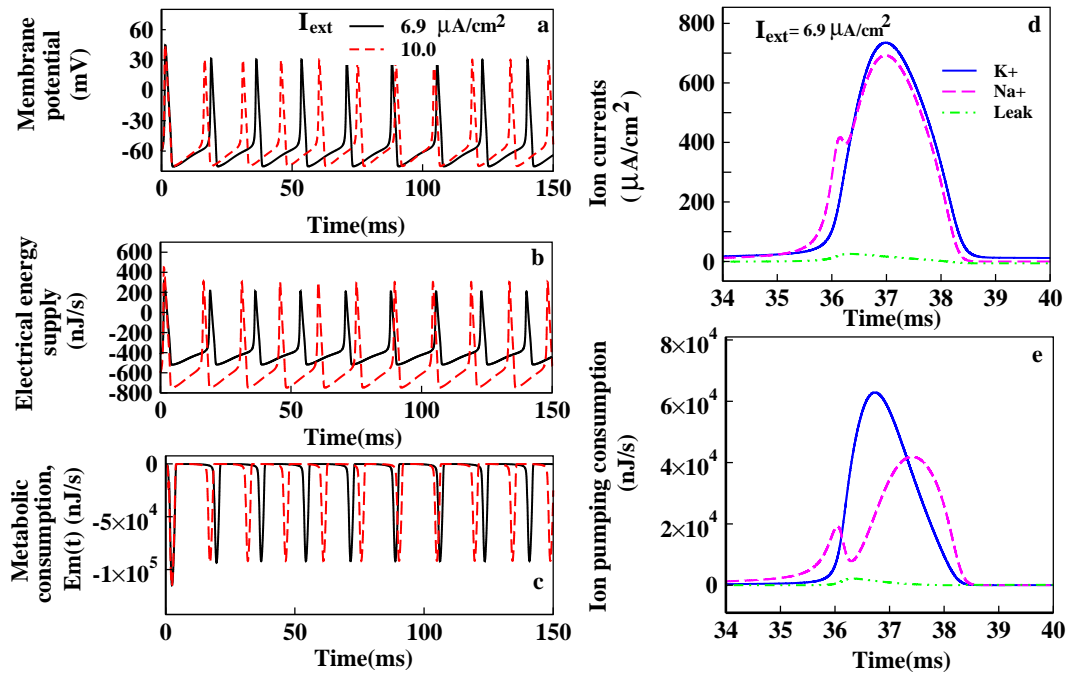


Figure 7.1: Energy Utilization in Hodgkin-Huxley Neuron at $I_{ext} = 6.9$ and $10.0 \mu A/cm^2$. In fig. (a) the action potentials are plotted. In fig. (b) energy supplied/second to the neuron is plotted. In fig. (c) the total metabolic energy consumption rate by all the three ion channels are plotted. (d) Currents of sodium, potassium, and leaks for a single action potential is shown here. Sodium current is negative but to compare with others it is plotted with positive sign. (e) Metabolic energy consumption corresponding to all the ion currents are plotted in positive axis, although all of them are negative.

we have calculated the electrical energy supplied to the neuron and the metabolic energy consumption, $E_m(t)$, for all the three ion channels.

In fig. 7.1(a) we have plotted the action potentials as a function of time(ms) in presence of external current, $I_{ext} = 6.9$ and $10.0 \mu A/cm^2$. With increasing I_{ext} the rate of spiking activity increases. In fig. 7.1(b) the rate, $V I_{ext}$ at which the electrical energy is supplied to the neuron is plotted. In fig. 7.1(c) the total metabolic energy consumption rate of the neuron by its ion channels are represented. It is seen from the peaks of figure 7.1(b) and (c) that the electrochemical energy consumption is much greater than the energy supplied to the neuron. This rate of energy is replenished by the ion pumps and metabolically supplied by hydrolysis of ATP molecules in order to maintain the neuron's activity [18].

In figure 7.1(d) sodium, potassium, and leak currents for a single action potential is shown. The negative sodium current [60] is plotted on positive axis to compare the current. The area of sodium and potassium currents are almost the same which means they neutralize each other to the extent of their mutual overlap and thus the net membrane

current is much smaller. The total number of Na^+ or K^+ ions that permeate the membrane during the action potential is proportional to the area under the curves. In figure 7.1(e) the electrochemical energy consumption associated with each of the ion currents are shown. The energy consumptions are actually negative which are plotted here in positive axis. The total metabolic consumption of the neuron in generating one action potential is directly the sum of these three components.

7.3 Unidirectionally Coupled Two Hodgkin-Huxley Neurons Via Gap Junction: Deterministic Description

So far we have seen the energetic balance in a single neuron. Now we focus on a system where two neurons are coupled to each other. In real system neurons are coupled to each other via electrical synapses or gap junctions and through chemical synapses. We have considered here on the electrical synapse. Electrical synapses owing to have very simple mechanism results in fast or robust signal transmission but can produce only simple behaviors, not all the complex processes where chemical synapses do well [46]. As in gap junction channels there is no need for receptors to recognize chemical messengers, signal transmissions here is more rapid than that in chemical synapses which are generally the most abundant kind of junctions between neurons. Electrical neurotransmission in electrical synapses is less modifiable than chemical neurotransmission as they do not involve neurotransmitters. The response is always the same sign as the source and the relative speed of electrical synapses allow for many neurons to fire synchronously [46–48].

7.3.1 Kinetic scheme of unidirectionally coupled Neurons

To mathematically express the unidirectionally coupled neurons it is considered that both neurons obey two sets of Hodgkin-Huxley equations (7.1) with an addition of a coupling term affecting the postsynaptic neuron only [18]. We have considered that the two neurons are initially in states which are very close to each other. For that reason we have kept the parameters of the master neuron same as described in Table 6.1 and reduced the parameters of the slave neuron by 3%, such as $C_{2m} = 0.97$, $E_{2K} = -74.69$, $E_{2Na} = 48.5$, $E_{2L} = -52.768$, $g_{2L} = 0.291$, $g_{2Na}^{max} = 116.4$, $g_{2K}^{max} = 34.92$. With such parameters both neurons can not share time solutions or they can not be synchronous. The control

action has been implemented in the slave neuron or post synaptic neuron to bring it in synchronization with the master or presynaptic neuron. It is given as the junction current $I_{Junction} = K_{sync}(V_1 - V_2)$, where K_{sync} is the constant conductance of the gap junction or coupling strength in mS/cm^2 . The junction current, $K_{sync}(V_1 - V_2)$ can only flow into the slave neuron through the electrical junction from master neuron making it unidirectional. The difference in electrical potential in the coupled two neuron system is maintained by an amplifier with very large entrance impedance that restricts the energy going back to the first neuron whereas the energy that the second neuron needs at the junction is provided by the amplifier. The slave neuron can not affect the response of the master neuron. We consider that the membrane current of presynaptic neuron, $I_{stimulus}(t)$ is induced by a Gaussian noise, $\xi(t)$ of mean $0.0 \mu A$ and variance $9.0 \mu A$. Thus here $I_{stimulus}(t) = I_{ext} + \xi(t)$ and through out the rest we have taken $I_{ext} = 6.9 \mu A/cm^2$. The postsynaptic neuron is exposed to a total current, I_{noise} induced by a Gaussian noise of mean $0 \mu A$ and variance $1 \mu A$. This noise is attributed to the mean of erratic signals coming to the postsynaptic neuron from all other synapses that we do not specifically consider here. Thus the Hodgkin-Huxley equation for the master and slave neuron stands as,

$$\begin{aligned} C_{1m}\dot{V}_1 &= I_{stimulus}(t) - I_{1Na} - I_{1K} - I_{1L} \\ C_{2m}\dot{V}_2 &= I_{noise}(t) - I_{2Na} - I_{2K} - I_{2L} + I_{Junction}. \end{aligned} \quad (7.9)$$

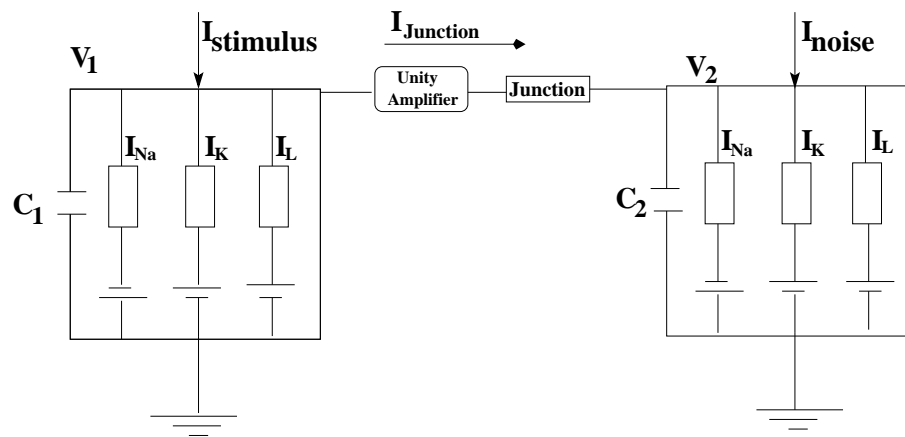


Figure 7.2: Model of Unidirectional coupling of two Hodgkin-Huxley neurons where the master neuron is unaffected by the second or slave neuron by the nature of the amplifier.

7.3.2 Energetic description of the unidirectionally coupled neurons

As the electrical energy of the slave neuron is only affected by the coupling, it is expressed as,

$$H_2(t) = \frac{1}{2}C_{2m}V_2^2 + H_{2Na} + H_{2K} + H_l + H_{Amplifier}. \quad (7.10)$$

The first term in the summation is the accumulated electrical energy in the capacitor and the second, third and the fourth term upon summing up gives the total metabolic consumption of the slave neuron. The last term is the energy available in the gap junction or the amplifier. The total energy derivative in the second neuron is given by

$$\begin{aligned} \dot{H}_2 = & V_2 I_{noise} - g_{2Na}^{max} m_2^3 h_2 (V_2 - E_{2Na})^2 - g_{2K}^{max} n_2^4 (V_2 - E_{2K})^2 - g_{2L} (V_2 - E_{2L})^2 \\ & + K_{sync} V_2 (V_1 - V_2) + K_{sync} V_1 (V_1 - V_2). \end{aligned} \quad (7.11)$$

The last two terms represent energy balance in the junction. Among the last two terms the first one corresponds to the energy consumed at the postsynaptic site of the junction and the second term corresponds to the energy contributed by the amplifier. No energy comes from the master neuron except information [18].

7.4 Effect Of Patch Size In Unidirectionally Coupled Neuron

Until now we have considered only the deterministic description of the neurons. But the Hodgkin Huxley model operates on the average number of open channels disregarding the corresponding number fluctuations or channel noise. These fluctuations are inversely proportional to the number of ion channels. Thus Hodgkin Huxley model is valid only within a large system size. But in actual neuron in a finite patch size there exists a finite number of sodium, potassium and other ion channels. So the role of internal fluctuations can not be neglected a priori. Channel noise alone can give rise to a spiking activity even in the absence of external stimulus [43, 44].

7.4.1 Stochastic generalization of Hodgkin-Huxley model: Langevin description

We use here Fox and Lu's [49, 50] system size expansion method which uses stochastic differential equation or Langevin description to replicates the behavior of the Markov chain model [53, 54] with high accuracy and it is computationally less exhaustive [43–45, 51, 52]. Here the dynamics of the gating variables are considered to be noisy as follows,

$$\dot{x} = \alpha_x(V)(1 - x) - \beta_x(V)x + \eta_x(t), \quad x = n, m, h, \quad (7.12)$$

where the terms with $\eta_x(t)$ are independent Gaussian white noise with zero mean which takes into account of the fluctuations of the number of open gates. The noise strengths depend on the membrane voltage. The noise correlations have the following form for an excitable membrane patch with N_{Na} number of sodium and N_K number of potassium ion channels [49, 50], respectively

$$\langle \eta_x(t)\eta_x(t') \rangle = \frac{2}{N_i} \frac{\alpha_x\beta_x}{\alpha_x + \beta_x} \delta(t - t') \quad i = Na, K, \quad (7.13)$$

where $N_{Na} = \rho_{Na}A$ and $N_K = \rho_KA$ are the numbers of sodium and potassium ion channels in a particular patch size of area A.

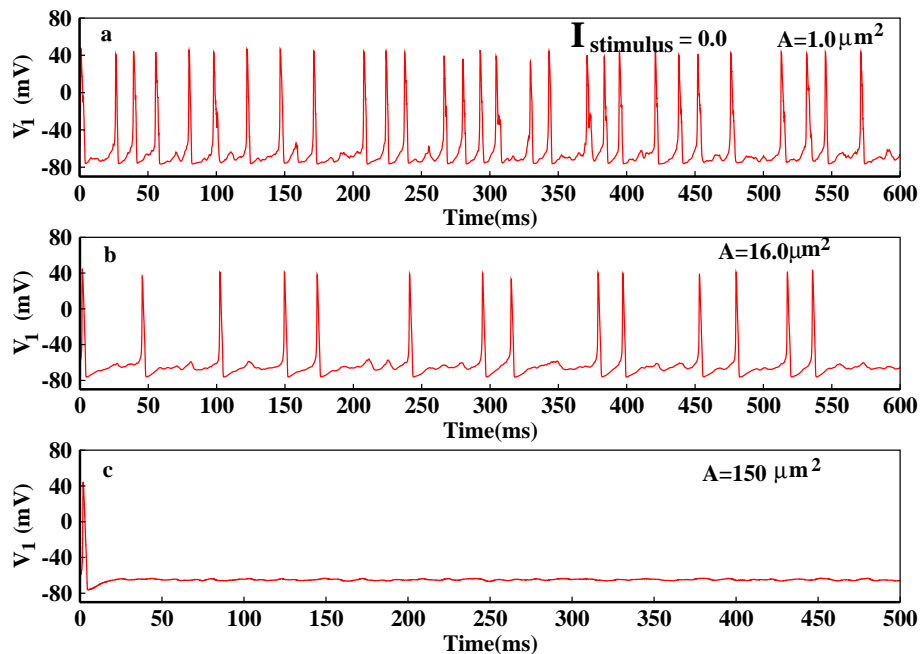


Figure 7.3: Spontaneous generation of action potentials using Langevin description for a single neuron with initial input of $V_1 = -60$ mV and the steady state values of the gating variables, x_∞ are calculated at $V = -70$ mV.

In figure (7.3) we have shown the effect of incorporation of the channel noise into the master neuron only, in absence of any external current, i.e. $I_{stimulus} = 0.0$. Here we show that with decreasing patch size, the spiking activity increases. Thus it is seen that channel fluctuations or channel noise is sufficient to generate spontaneous action potential. With increasing path size system behaves similar to the deterministic dynamics of Hodgkin and Huxley action potential.

Next we have incorporated the channel noise into both the master and slave neurons. For simplicity we consider both of them with equal number of sodium and potassium channels. Here we have used similar set of equations as in equation (7.12) and (7.13) for both the neurons and solved equation (7.9).

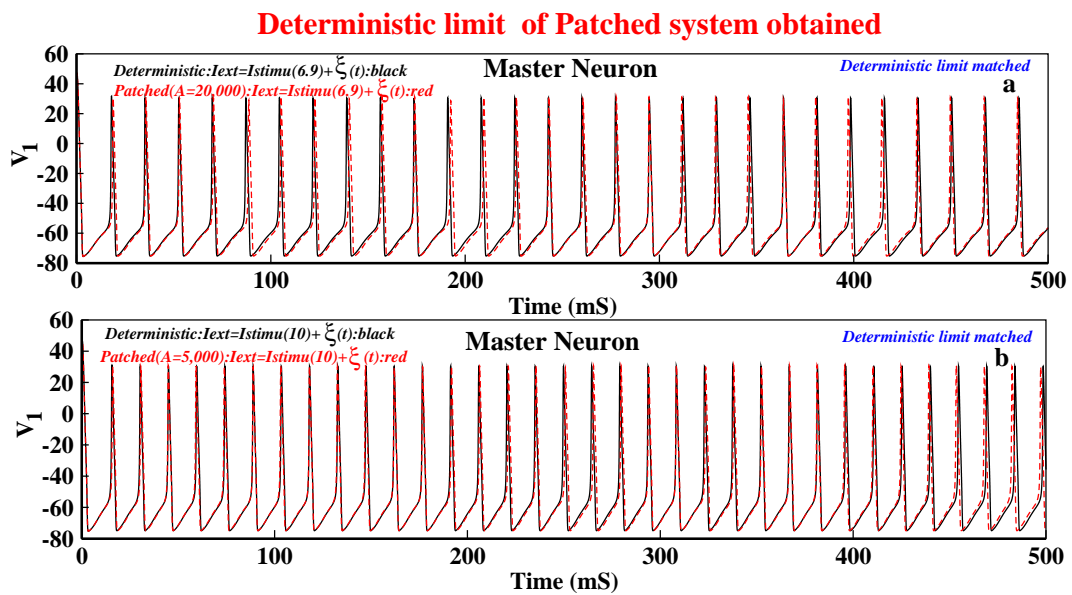


Figure 7.4: Standardization or cross verification of the results at deterministic limit. For $I_{ext} = 6.9 \mu A/cm^2$ and $I_{ext} = 10.0 \mu A/cm^2$ the deterministic limit is achieved at $A=20,000$ and $5,000 \mu m^2$, respectively.

To convince our result to be meaningful one can cross verify the result in the following way. We solved the deterministic Hodgkin -Huxley equation (7.1- 7.3) in presence of noisy external current, $I_{stimulus}(t) = I_{ext} + \xi(t)$, as given earlier in the master neuron with similar set of Gaussian random numbers for both the deterministic and patched programs and varied the patch size from 100 to 20,000 μm^2 . We have found that for an external current of $I_{ext} = 6.9 \mu A/cm^2$ both the deterministic and the patched solutions exactly match each other as seen from figure 7.4(a). It is seen that as we increase the external current the deterministic limit is achieved within a patch size of $A=5,000 \mu m^2$ as seen from figure 7.4(b). Here we have continued our study with $I_{ext} = 6.9 \mu A/cm^2$ taking $A=20,000 \mu m^2$.

7.4.2 Kinetic picture of synchronization

Here we have plotted the action potentials of both master and slave neurons with increasing K_{sync} value. We have shown the synchronization process here in the deterministic limit of $A=20,000$ and $I_{ext} = 6.9 \mu A/cm^2$. From figure 7.5 (a) we can see that the slave neuron is not at all in synchronization with the master neuron for $K_{sync}=0.01$. The master neuron response is same for the K_{sync} values. Thus it is plotted only in the first and last value of the K_{sync} to compare it with slave response. As K_{sync} value increases the slave neuron starts firing initially at a random rate and then gradually the rate becomes equal to the master neuron at $K_{sync}= 0.2$. Although there exists little phase lag between the two neurons at $K_{sync}= 0.2$ which gradually eliminates at higher K_{sync} values.

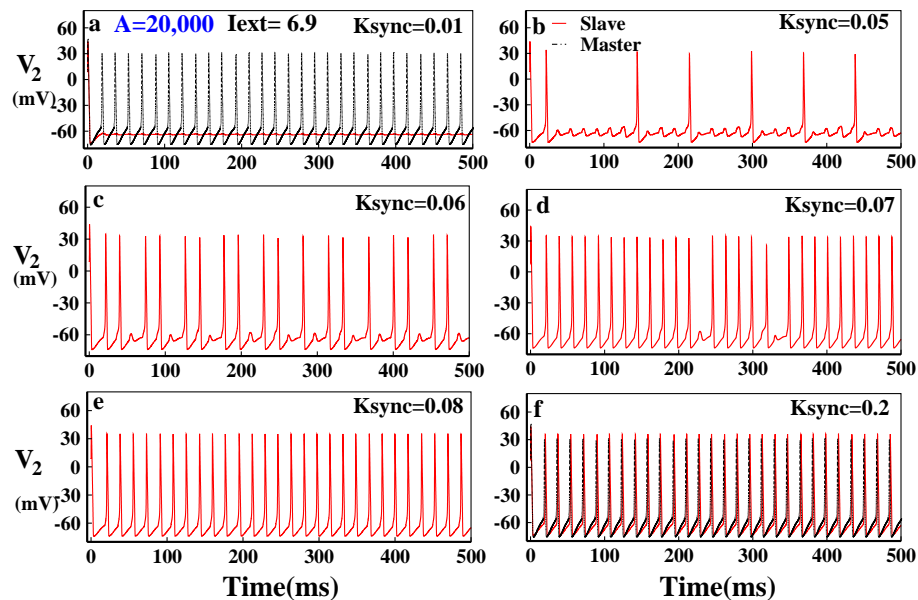


Figure 7.5: Action potential, $V_2(t)$ trains of the slave neuron at different K_{sync} values, for $A=20,000 \mu m^2$, $I_{stimulus}(t) = I_{ext}(= 6.9) + \xi(t)$. In figure (a) and (f) the black dashed curves which correspond to the master neuron is same for all values of K_{sync} . In (f) it is seen that the slave neuron is almost synchronized with the master neuron at $K_{sync} = 0.2$.

7.4.3 Energetics of the unidirectional synchronization

Next we have shown the total metabolic energy consumption, $E_m(t)$, by all the three channels together with time. It is seen from figure 7.6(a) that at very low value of K_{sync} the average metabolic energy consumption of the slave neuron is very less. As soon as K_{sync} increases the spiking activity increases and as a result. Interesting fact here is that for each spike the maximum of the $E_m(t)$ is almost same for almost all the spikes and

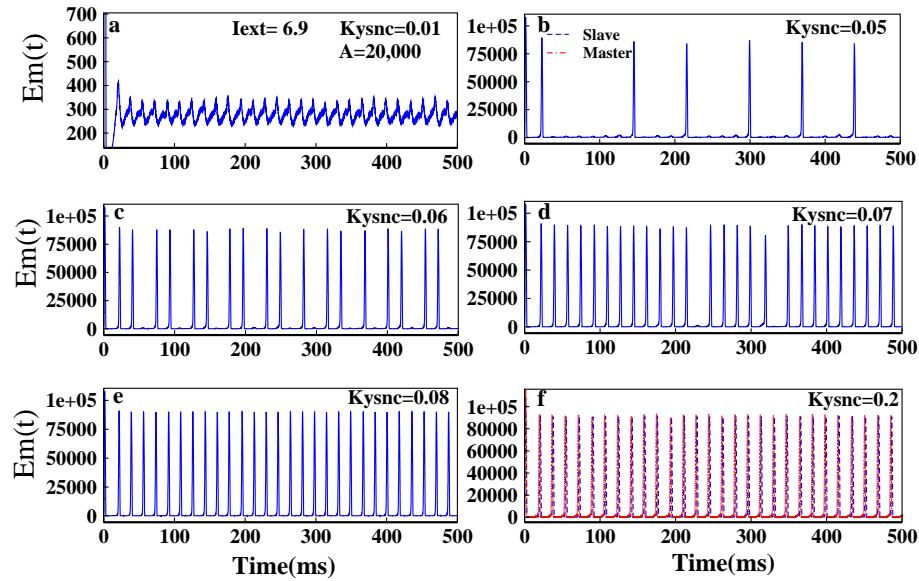


Figure 7.6: Metabolic consumption of energy, $E_m(t)$ of slave neuron at different K_{sync} values, for $A=20,000\mu m^2$, $I_{stimulus}(t) = I_{ext}(= 6.9) + \xi(t)$. In (f) red dashed curve which corresponds to the master neuron is same for all values of K_{sync} . In (f) it is seen that the slave neuron is almost synchronized with the master neuron at $K_{sync}=0.2$.

for all K_{sync} values. At $K_{sync}=0.2$ the $E_m(t)$ for both master and slave neurons becomes almost equal as seen from figure 7.6(f) .

Next we have plotted the average consumption of metabolic energy with increasing K_{sync} value. As the spiking activity is stochastic in nature we take the average over a long period of time. As it is unidirectional coupling the coupling constant has no effect on master neuron. It is seen from figure 7.7 that the average total metabolic energy, $\langle E_m \rangle$, for the master neuron is around 9000 nJ/s. The average metabolic energy for slave neuron from around 350 nJ/s at $K_{sync} = 0 mS/cm^2$ gradually increases and eventually meets master neuron at $K_{sync} = 0.1$.

7.4.4 Effect of patch size variation on metabolic energy consumption

Next we have studied the effect of patch size on the metabolic energy consumption. It is not possible for a neuron to have infinite numbers of ion channels in a finite patch size. As we have also seen that the patch size plays very important role. A low patch size channel noise can alone give rise to spontaneous spiking activities. Thus studying the nature of metabolic energy consumption with variable patch size is very important. In the figure (7.8) we have shown the action potential spikes and the metabolic energy

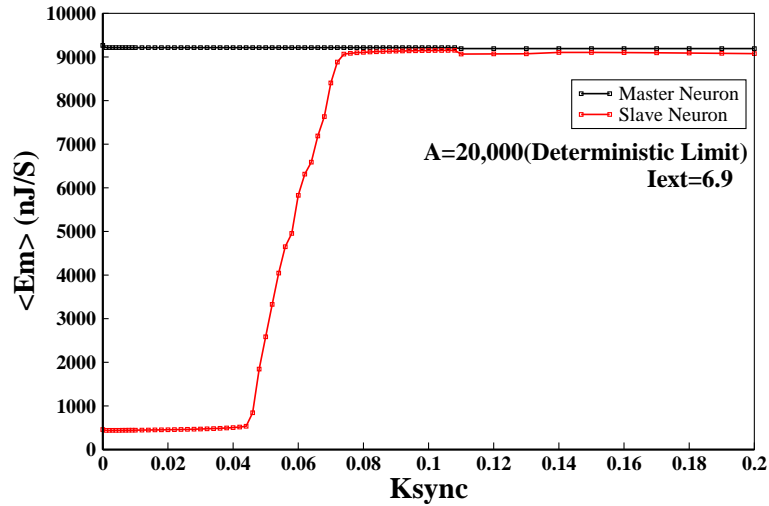


Figure 7.7: The average metabolic energy consumption of the master and slave neuron is plotted here for different K_{sync} values at $A=20,000 \mu m^2$ and $I_{stimulus}(t) = I_{ext}(= 6.9) + \xi(t)$. Each average was taken over very long time trajectories as shown in figure (7.6).

consumption of slave neuron at $K_{sync}=0.2$ in left and right panels, respectively. In this K_{sync} value both the slave and master responds almost equally as seen from figure (7.5). Here we have shown the variation of patch size from $A=100$ to $20,000$. In figure 7.8(a) one can see that with decreasing patch size channel noise plays very important role in action potential generation and consequently the metabolic energy consumption also increases as we decrease the patch size. Thus as we keep on increasing the patch size the spiking activity starts decreasing and suddenly and surprisingly at $A=2000$ the spiking activity totally vanishes and the corresponding metabolic consumption rate also falls down abruptly. This certain phenomenon continues with increasing value of A until $A=6500$ is arrived as seen from figure 7.8(c) and (d). Again after $A=7000$ to $20,000$ the spiking activity becomes almost similar to the deterministic result as seen from figure 7.8(e) and (f).

Thus there exist three different patch size ranges where the neurons behave differently. At very low patch size(e.g. $A= 100-1500$) the system dynamics and energetics are mainly governed by the channel noise or channel number fluctuations. In the mid range (e.g. $A =2000-6500$) the neurons can not even generate action potentials. This patch size range can be called as dead range. Then with increasing patch size($7000-20,000$) the system gradually starts behaving as it behaves in deterministic limit.

Next we have done a detailed analysis of the effect of patch size on average metabolic energy, $\langle Em \rangle$. In figure 7.9(a) we have plotted $\langle Em \rangle$ with different K_{sync} values for different patch sizes. It is seen that with increasing patch size the average metabolic

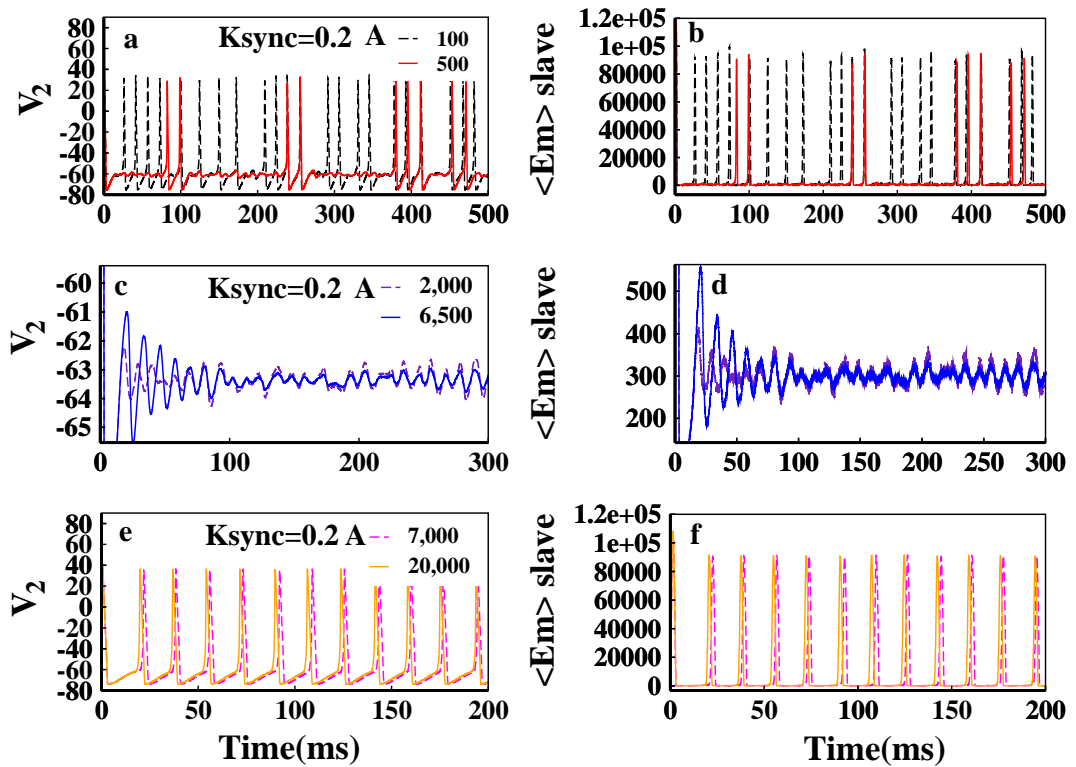


Figure 7.8: Effect of patch size variation on action potentials and metabolic energy consumption is shown in this plot. Only the slave neuron responses have been plotted, as in K_{sync} the master and slave neuron is almost synchronized. In the left column the slave action potentials and in the right corresponding $Em(t)$ s are plotted.

energy consumption for both master and slave neuron decreases. It continues to occur until around $A=1500$. After that for $A=2000$ to 6500 the $\langle Em \rangle$ becomes very low and again after $A=7000$ to $20,000$ $\langle Em \rangle$ almost remains close to the deterministic average. In figure 7.9(b) $\langle Em \rangle$ is plotted with patch size for different K_{sync} values. The dependence on the patch size as depicted earlier is now evident from this picture. There exist three distinct dependency of patch size on average metabolic energy consumption. The very low and very high patch size region shows opposite dependence of patch size and the mid range acts as an dead or inactive zone. For an unidirectionally coupled neuron system this mid range of patch size for both master and slave neurons probably are not a good combination for the generation of action potential unidirectionally.

From figure 7.9(a) it is also seen that with decreasing patch size, the K_{sync} value at which the $\langle Em \rangle$ of master and slave neuron matches, is gradually right shifted. This means the synapse is now finding difficulties in bringing the two neuron in synchronization. Thus with decreasing patch size the synapse needs to work more to synchronize the energies of the two neurons.

Effect of channel noise in average metabolic energy

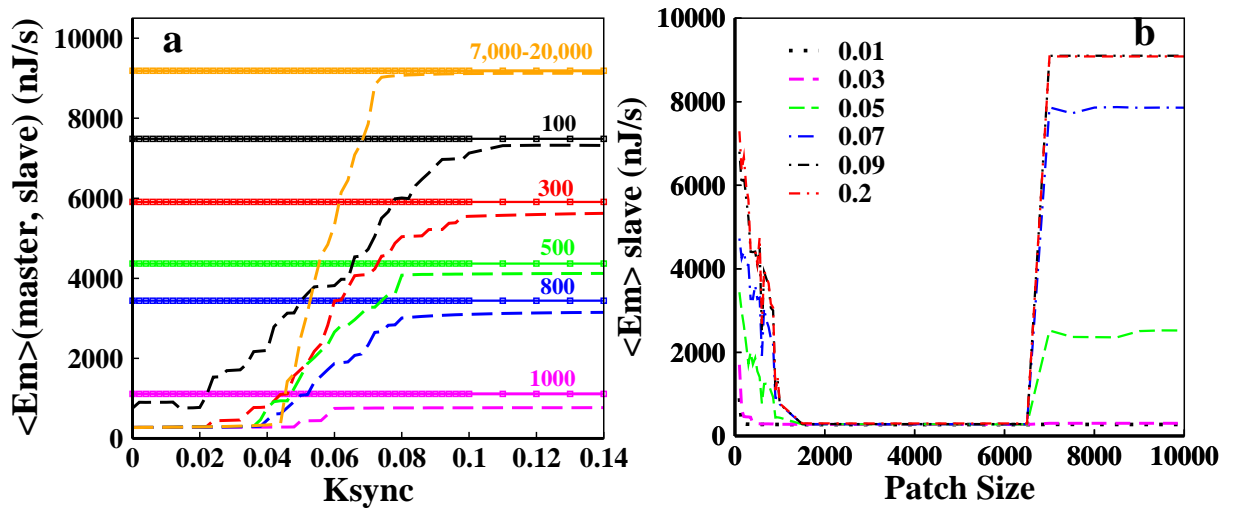


Figure 7.9: In figure (a) the $\langle Em \rangle$ for master and slave neurons are plotted with different K_{sync} values for different patch size. In figure (b) $\langle Em \rangle$ are plotted for different patch size for different K_{sync} values.

7.5 Effect Ion Channel Blocking Drugs

Here we have studied the effect of three different types of drug blockers on the spiking activity and metabolic energy consumption rate. We have taken examples of three types of drug blocking. Among them one is sodium only blockers, e.g. tetrodotoxin (TTX), second one is potassium blockers, e.g. tetraethylammonium (TEA) and the third type is total blockers [55–57]. These drugs selectively blocks either sodium or potassium channels and thus the available number of channels left for ion conduction gets reduced. This why drug binding study here actually falls under the study of patch size effect. Here we have considered that both the master and slave neuron have equal number of ion channels left after the addition of drugs or we can say that both of the neurons are similarly affected by the drugs [58]. For considering the effect of drugs the sodium and potassium conductance modifies as follows [58],

$$G_K(t) = g_K^{max} x_K n^4 \quad \text{and} \quad G_{Na}(t) = g_{Na}^{max} x_{Na} m^3 h, \quad (7.14)$$

where x_K and x_{Na} are the fractions of working ion channels which are not blocked by drugs among the overall number of potassium channels, N_K , or sodium ion channels, N_{Na} , respectively. Thus equations (7.1), (7.12), (7.13) and (7.14) form a stochastic Hodgkin-Huxley model takes drug blocking into account. This set of equations with very high patch sizes, e.g. $A=20,000$ corresponds to the deterministic limit.

7.5.1 Sodium channel blockers

Here we have studied the effect of sodium blockers on action potential and metabolic energy consumption. We have found very drastic effect of sodium blocks here. Here it is shown that even a very minute change in number of available sodium channel the repetitive spiking action totally vanishes surprisingly. We have studied the effect of sodium blockers for $x_{Na} = 0.8, 0.6$, and 0.4 as seen from figure 7.10(a). The master and slave action potentials have been shown here. We can see that at $K_{sync}=0.2$ there is no considerable change in the trends of action potentials for different x_{Na} values but importantly the synchronization between master and slave is obviously destroyed. The corresponding $Em(t)$

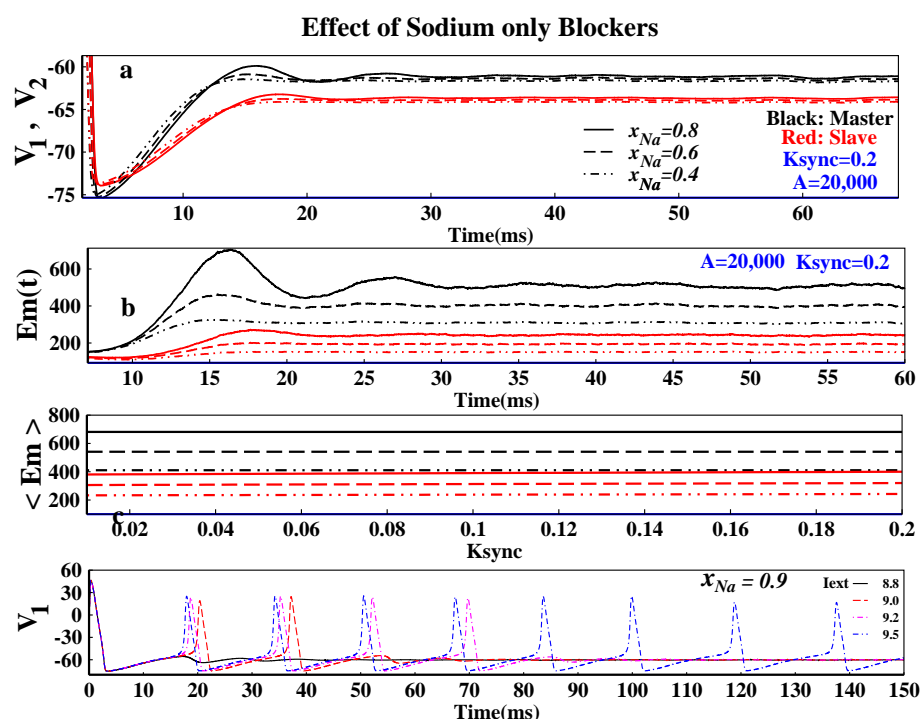


Figure 7.10: Effect of Sodium Blockers on action potential and metabolic energy consumption, deterministic limit. In figure (a) the master and slave neurons for have been plotted for $x_{Na} = 0.8, 0.6$ and 0.4 . In (b) corresponding $Em(t)$ and in figure (c) $\langle Em \rangle$ is plotted for different K_{sync} values. In figure (d) the master neuron's action potentials are shown for $I_{ext} = 8.8, 9.0, 9.2$ and 9.5 for $x_{Na} = 0.9$.

is shown in figure 7.10(b) and the $\langle Em \rangle$ with Ksync has been plotted in figure 7.10(c). From these two figures we can see that the average metabolic consumption rate drastically falls. Thus minute variation in sodium ion channels in a particular external current will cause drastic effect on action potential train. However we have shown that with these fractions of sodium channel the spiking activities can be seen if the I_{ext} is increased gradually as seen from figure 7.10(d). Here the I_{ext} used are 8.8, 9.0, 9.2, 9.5 for $x_{Na} = 0.9$.

Here also we have seen that the master and slave neurons are not synchronized. Also as we decrease the fraction x_{Na} , such as $x_{Na} = 0.8$, higher magnitude of I_{ext} is required to resurrect the spikes again.

7.5.2 Potassium channel blockers

Next we have studied the effect of potassium blockers for $x_K = 0.8, 0.6, 0.4$ and 0.1 . Unlike sodium blockers the potassium blockers have no instant drastic effect on action potential of both master and slave neurons. In figure 7.11 the effect of potassium blockers have been shown for $K_{sync}=0.2$ where both master and slave neurons remain almost synchronized. Thus in figure 7.11 we have shown only the effect on slave neuron.

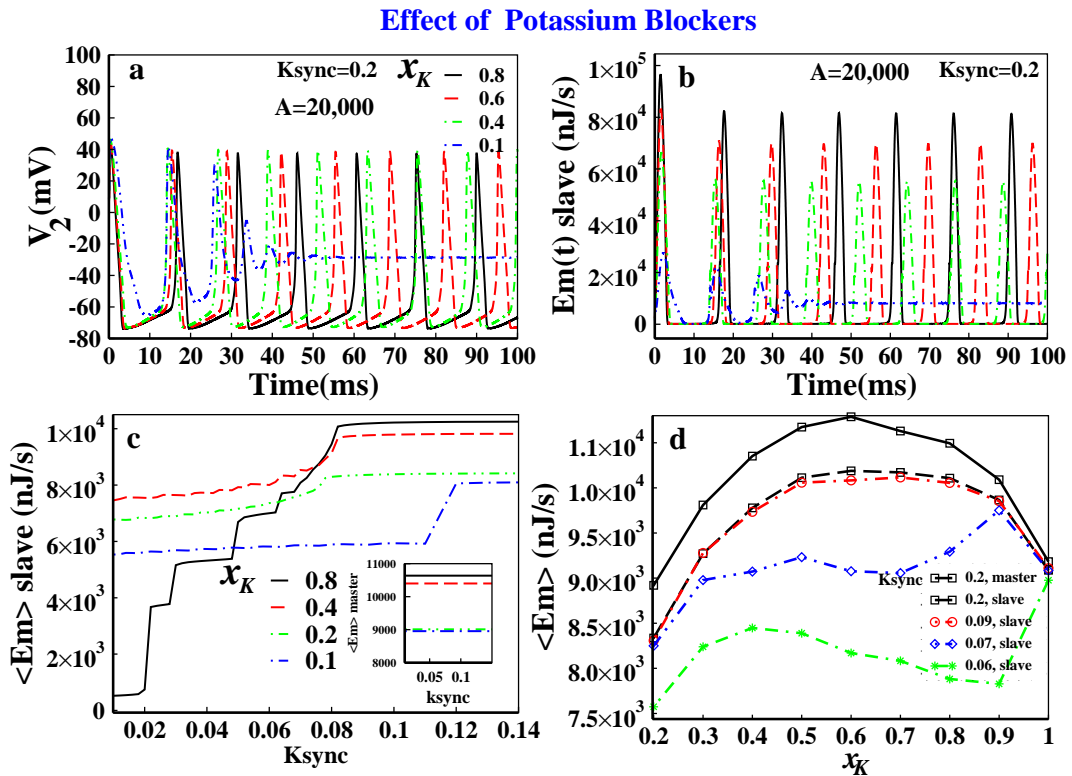


Figure 7.11: Effect of potassium blockers on metabolic energy consumption in the deterministic limit. In figure (a), (b) and (c) the slave neuron action potentials, $Em(t)$ and $\langle Em \rangle$ is plotted for $x_K=0.8, 0.6, 0.4$ and 0.1 , respectively. In figure (d) $\langle Em \rangle$ is plotted with x_K for different K_{sync} values.

From figure 7.11(a) it is seen that initially with decreasing x_K value from $x_K = 1.0$ the spiking activity increases and continues to increase until a certain x_K and then gradually decreases. Here we have shown the picture for first 100 ms only to avoid congestion. A similar trend is observed in the metabolic energy consumption rate as seen from figure

7.11(b). With increasing drug concentration or decreasing available potassium channels the maximum of spikes decreases as seen from figure 7.11(b). In figure 7.11 (c) we find that at $x_K = 0.8$ and 0.4 the $\langle Em \rangle$ at $K_{sync}=0.2$ are almost similar. It is also seen that at very low K_{sync} such as 0.01 or 0.02 etc the $\langle Em \rangle$ of $x_K = 0.4, 0.2$ or 0.1 of the slave neuron starts from relatively much higher magnitude than $x_K = 0.8$ or 1.0 . For better understanding we have plotted the $\langle Em \rangle$ for a particular K_{sync} value for different x_K in figure 7.11(d). Here we can clearly see for $K_{sync}=0.2$, the average metabolic consumption initially increase with decreasing x_K until $x_K = 0.6$ is reached. After that $\langle Em \rangle$ again decreases both for master and slave neurons. This initial increase in spiking activity is attributed to the noise enhanced spiking activity(as reported earlier [58]). Figure 7.11 (d) shows that the noise enhanced spiking activity is also evident in metabolic energy calculations. Now as we decrease the K_{sync} value we see that the noise enhanced phenomena shows different nature in different K_{sync} values.

7.5.3 Total blockers

Here we study the effects of drugs that may block both sodium and potassium channels. For simplicity we keep both $x_{Na} = x_K = x_{Na/K} = 0.8$ and 0.5 in figure 7.12 with $k_{sync}=0.2$. In the left panel the transient action potentials have been shown in presence of no drug and for $x_{Na/K} = 0.8$ and $x_{Na/K} = 0.5$ in figure 7.12 (a), (b), (c) respectively. It is interesting to see that there are not much kinetic differences between the three different concentrations of drug except phase difference and may be slight difference in spiking rate. But for energetic analysis it is seen that all the three types are energetically very distinct process as seen from figure 7.12(d). It is seen that with increase in the drug concentration or decrease in the available number of ion channels available the average metabolic energy consumption decreases. Also one thing can be noticed that with increasing number of channel blockers the value of K_{sync} at which both master and slave neuron's average energy consumption becomes equal, is gradually right shifted. This means synapse also finds it difficult to bring to neurons in synchronization. Synapse needs to work more with increasing number of blocked ion channels.

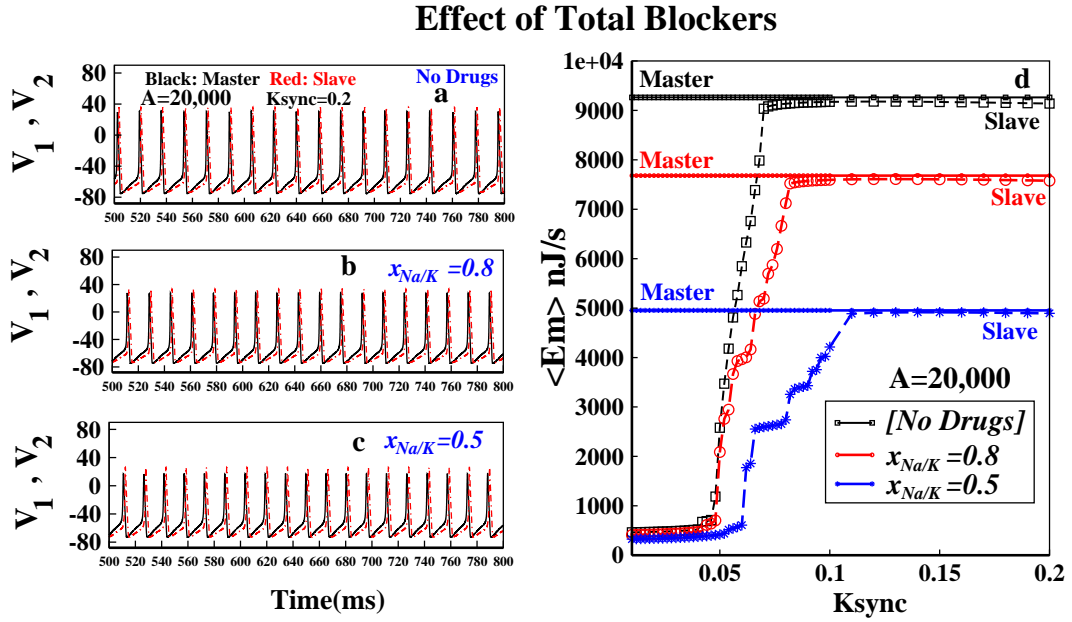


Figure 7.12: Effect of Total blockers on average metabolic energy consumption in the deterministic limit. In the left panel from (a)-(c) the effect of total blockers on action potentials for both the master and slave neurons are plotted but not that much observable effect or difference is seen. On the contrary in figure (d) the blockers have pretty distinguishable effect on energetic.

7.6 Conclusion

In this work we have studied the energetic cost of the signaling activity through generation of spikes for single neuron as well as unidirectionally coupled neurons with an electrical synapse. The basic ingredient of internal noise arising from individual stochastic dynamics of the ion channels are utilized here to characterize spiking for a critical patch size. However, here our main focus was on the effect of the patch size on metabolic energy consumption of the master and slave neurons during the process of synchronization. The detailed results can be summarized as follows.

- (1) To standardise the existing system parameters of squid giant axon we have shown that for a single neuron without the presence of any external current the deterministic limit is reached within very low patch size ($A=150 \mu\text{m}^2$), but for two coupled neurons with an external current (such as $6.9 \mu\text{A}/\text{cm}^2$) a very large number of system size (e.g. $A=20,000$ and $A=5,000$) for a critical value of external current ($I_{ext} = 10.0 \mu\text{A}/\text{cm}^2$) is required to produce deterministic result. With increasing external current the required patch area decreases to reach the deterministic limit.

(2) There exist three different ranges of patch size where the coupled system behaves in a very different manner. At very low patch size range (e.g. $A=100-1500$) the system dynamics and energetics are mainly governed by the channel noise or channel number fluctuations. In the mid range (e.g. $A=2000-6500$) the system fails to respond properly. It can not generate trains of action potentials in this range which adequately can be called as dead range. Then with increasing patch size the system gradually starts behaving as it should follow in deterministic limit.

(3) The range of patch size where channel noise predominates, with increasing patch size metabolic energy consumption decreases as channel noise decreases and with increase in patch size the spontaneous spiking activity decreases. Next in the mid range as there exist no spiking trains, the metabolic consumption of energy falls drastically. Then again in high patch size range with increasing spiking activity both master and slave neuron starts firing pattern close to deterministic limit with increasing metabolic energy consumption.

(4) We have found very interesting effect of sodium, potassium and total blockers on both spiking activity and energetic costs. Both the synchronization process and the spiking activity of action potentials are greatly affected by sodium channel blockers. A minute change in the number of available open sodium channels totally destroys the spiking activity. There is no considerable change in action potential with increasing number of blocked sodium channels as well, but there exists minute changes visible in metabolic consumption. Although with increasing external current spikes resurrects but neurons remain synchronized.

(5) There exists a strikingly different result for potassium channel blockers. Initially with increasing concentration of drug the metabolic energy increases and reaches a maximum for a particular K_{sync} value, spiking activity also increases, which is attributed to the noise enhanced spiking phenomena. Then again with decreasing number of available potassium channel metabolic consumption decreases.

(6) For total blockers with decreasing number of available ion channels the average metabolic energy consumption decreases which can be understandable from the property of internal noise dynamics. Comparing all types of blockers we have found that with increasing number of blocked ion channels the synaptic efficiency plays a vital role to bring synchronization between two neurons. Generally speaking the synapse finds it difficult to bring the neurons in synchronization in presence of drug or in other words the synapse needs to be more conducting with increasing number of blocked ion channels.

Bibliography

- [1] D.D. Clarke, L. Sokoloff, Circulation and energy metabolism of the brain, G.J. Siegel (Ed.), et al., Basic neurochemistry: molecular, cellular and medical aspects, Lippincott-Raven, Philadelphia (1999), pp. 637-669.
- [2] D. Attwell, S.B. Laughlin, An energy budget for signalling in the gray matter of the brain, *J. Cereb. Blood. Flow Metab.* (2001), 21, pp. 1133.
- [3] S.B. Laughlin, Energy as a constraint of the coding and processing of sensory information, *Curr. Opinion Neurobiol.* (2001), 11 , pp. 475.
- [4] P. Siekevitz, Producing neural energy, *Science* (2004), 306, pp. 410.
- [5] B. Sengupta, M. Stemmler, S. B. Laughlin, and J. E. Niven, *PLoS Comput. Biol.* (2010), 6, e1000840.
- [6] Crotty, T. Sangrey, and W. B. Levy, *J. Neurophysiol.* (2006), 96, 1237 .
- [7] H. Alle, A. Roth, and J. R. P. Geiger, *Science* (2009), 325, pp. 1405-1408.
- [8] A. L. Hodgkin, *Phil. Trans. R. Soc. B* (1975), 270, pp.297-300 .
- [9] D. Attwell and C. Iadecola, *Trends Neurosci.* (2002), 25, pp. 621 .
- [10] P. Lennie, *Curr. Biol.* (2003), 13, pp. 493 .
- [11] W. D. Stein, *Int. Rev. Cytol.* (2002), 215, pp. 231.
- [12] AL. Hodgkin Evidence for electrical transmission in nerve Part I. *J Physiol* (1937) 90: 183; AL. Hodgkin Evidence for electrical transmission in nerve Part II. *J. Physiol* (1937) 90: 211; AL. Hodgkin and AF. Huxley, A quantitative description of membrane current and its application to conduction and excitation in nerve, *J. Physiol.* (1952) 117: 500; A. Huxley, From overshoot to voltage clamp, *Trends in Neurosciences* (2002) 25: 553.
- [13] R. H. Adrian, *Proc. R. Soc. B* (1975), 189, pp. 81 .
- [14] A. Destexhe, M. Rudolph, J. Fellous, T. Sejnowski, *Neuroscience* (2001), 107, pp. 13.
- [15] F. Bezanilla, R. E. Taylor, J. M. Fernandez, *J. Gen. Physiol.*(1982), 79, pp. 21 .
- [16] T. D. Sangrey, W. O. Friesen, W. B. Levy, *J. Neurophysiol.*(2004), 91, pp. 2541 .
- [17] FJ. Torrealdea ,A. d'Anjou , M. Grana , C. Sarasola Energy aspects of the synchronization of model neurons. *Phys Rev E.*(2006), 74: 011905.

- [18] A. Moujahid, A. d'Anjou, F. J. Torrealdea, Energy and information in Hodgkin-Huxley neurons, *Physical Review E* (2011), 83, 031912.
- [19] A. Arenas, A. Diaz-Guilera, C.J. Perez-Vicente, Synchronization processes in complex networks, *Physica D* (2006), 224 (1-2) , pp. 27-34.
- [20] K. Czoczynski, P. Perlikowski, A. Stefanski, T. Kapitaniak, Synchronization of self-excited oscillators suspended on elastic structure, *Chaos, Solitons and Fractals* (2007), 32 (3) , pp. 937-943.
- [21] J.Z. Yang, G. Hu, Three types of generalized synchronization, *Phys Lett A* (2007), 361 (4-5), pp. 332-335.
- [22] J.G. Restrepo, E. Ott, B.R. Hunt, Emergence of synchronization in complex networks of interacting dynamical systems, *Physica D* (2006), 224 (1-2), pp. 114-122.
- [23] S.K. Han, W.S. Kim, H. Kook, Synchronization and decoding interspike intervals, *Int J Bifurcat Chaos* (2002), 12 (5), pp. 983-999.
- [24] T. Womelsdorf, P. Fries. The role of neuronal synchronization in selective attention, *Current Opinion in Neurobiology* (2007), 17(2), pp. 154-160.
- [25] D. Chika, R. Borisyuk, Y. Kazanovichb. Selective attention model with spiking elements. *Neural Networks* (2009), 22(7), pp. 890-900.
- [26] A. Senju, MH. Johnson. A typical eye contact in autism: Models mechanisms and development, *Neuroscience and Biobehavioral Reviews* (2009), 33(8), pp. 1204-1214.
- [27] JL. Cantero, M. Atienza, AC Vadell, AS Gonzalez, E. Gil-Neciga. Increased synchronization and decreased neural complexity underlie thalamocortical oscillatory dynamics in mild cognitive impairment. *NeuroImage* (2009), 46(4), pp. 938-948.
- [28] G. Buzsaki, JJ. Chrobak. Temporal structure in spatially organized neuronal ensembles: a role for interneuronal networks. *Current Opinion in Neurobiology* (1995), 5(4), pp. 504-510.
- [29] D. Fricker, R. Miles. Interneurons spike timing and perception, *Neuroscience* (2001), 32(5), pp. 771-774.
- [30] P. Tass, M.G. Rosenblum, J. Weule, J. Kurths, A. Pikovsky, J. Volkmann, A. Schnitzler, H.-J. Freund. Detection of n: m Phase Locking from Noisy Data: Application to Magnetoencephalography[J]. *Physical Review Letters* (1998), 81(15), pp. 3291-3294.
- [31] F. Mormann, T. Kreuz, R.G. Andrzejak, P. David, K. Lehnertz, C.E. Elger. Epileptic seizures are preceded by a decrease in synchronization, *Epilepsy Research* (2003), 53(3), pp. 173-185.
- [32] SJ. Simon, RA. Barker. Understanding the dopaminergic deficits in Parkinsons disease: Insights into disease heterogeneity. *Journal of Clinical Neuroscience* (2009), 16(5), pp 620-625.

- [33] F. Amor, S. Baillet, V. Navarro, CA Jacques. Martinerie Michel Le Van Quyen. Cortical local and long-range synchronization interplay in human absence seizure initiation. *Neuro Image* (2009), 45(3), pp. 950-962.
- [34] A. Ucar, KE. Lonngren, E-W Bai . Synchronization of the coupled FitzHugh-Nagumo systems. *Chaos Solitons and Fractals* (2004). 20(5), pp.1085-90.
- [35] S. Zhou, X. Liao, J. Yu, K-W. Wong . Chaos and its synchronization in two-neuron systems with discrete delays. *Chaos Solitons and Fractals* (2004), 21(1), pp.133-42.
- [36] M. Meister, RO. Wong, DA. Baylor, CJ. Shatz . Synchronous bursts of action potentials in ganglion cells of the developing mammalian retina. *Science* (1991), 252, pp.939-43.
- [37] AK. Kreiter, WJ. Singer. Stimulus-dependent synchronization of neuronal responses in the visual cortex of the awake macaque monkey. *J Neurosci* (1996), 16, pp.2381-96.
- [38] RC. Elson, AI. Selverston, R. Huerta, NF. Rulkov, MI. Rabinovich, HD. Abarbanel . Synchronous behavior of two coupled biological Neurons. *Phys Rev Lett* (1999), 87, pp.5692-5.
- [39] O. Cornejo-Perez, R. Femat, Unidirectional synchronization of Hodgkin-Huxley neurons, *Chaos, Solitons and Fractals* (2005), 25, pp. 43-53.
- [40] HJ. Yu, JH. Peng, Chaotic synchronization and control in nonlinear-coupled Hindmarsh-Rose neural systems, *Chaos, Solitons and Fractals* (2006), 29 (2), pp. 342-348.
- [41] J. Wang, B. Deng, XY. Fei, Chaotic synchronization of two coupled neurons via nonlinear control in external electrical stimulation, *Chaos, Solitons and Fractals* (2006), 27 (5), pp. 1272-1278.
- [42] TB. Kepler , E. Marder , LF. Abbott. The effect of electrical coupling on the frequency of model neuronal oscillators. *Science* (1990),248:83
- [43] G. Schmid, I. Goychuk, P. Hanggi. Channel noise and synchronization in excitable membranes, *Physica A* (2003), 325, pp. 165 -175.
- [44] P. Hanggi, G. Schmid, I. Goychuk. Excitable membranes: Channel Noise, Synchronization, and Stochastic Resonance. *Advances in Solid State Physics* (2002), 42, pp 359-370.
- [45] G. Schmid, I. Goychuk, P. H,anggi. Stochastic resonance as a collective property of ion channel assemblies. *Europhys. Lett.* (2001), 56 (1), pp. 22-28.
- [46] ER. Kandel, JH. Schwartz, TM. Jessell. (2000). *Principles of Neural Science* (4th ed.). New York: McGraw-Hill. ISBN 0-8385-7701-6.
- [47] JR. Gibson , M. Beierlein , BW. Connors . Functional properties of electrical synapses between inhibitory interneurons of neocortical layer 4. *J. Neurophysiol.* (2005), 93, pp. 467-80.

- [48] MV. Bennett , RS. Zukin . Electrical coupling and neuronal synchronization in the Mammalian brain. *Neuron* (2004). 41 (4), pp. 495-511.
- [49] RF. Fox, Stochastic versions of the Hodgkin-Huxley equations. *Biophys. J.* (1997), 72, pp. 2069-2074.
- [50] RF. Fox, Y. Lu, Emergent collective behavior in large numbers of globally coupled independently stochastic ion channels *Phys. Rev. E* 49 (1994), pp.3421.
- [51] JH. Goldwyn, , NS. Imennov, M.Famulare , E. Shea-Brown, Stochastic differential equation models for ion channel noise in hodgkin-huxley neurons. *Physical Review E* 83(4), 041,908 (2011).
- [52] JH. Goldwyn , E. Shea-Brown,,: The what and where of adding channel noise to the hodgkin-huxley equations. *PLoS Comput Biol.* (2011), 7(11), e1002, 247.
- [53] CC. Chow, JA. White. Spontaneous action potentials due to channel fluctuations. *Biophys. J.* (1996), 71, pp.3013-3021.
- [54] E. Skaugen, L. Wall0e, Firing behaviour in a stochastic nerve membrane model based upon the Hodgkin-Huxley equations. *L. Acta Physiol. Scand.* (1979),107, pp. 343-363.
- [55] B. Hille , 1992. Ionic channels of excitable membranes. 2nd edition, Sinauer Associates, Sunderland, Mass.
- [56] K. Pal, G. Gangopadhyay , Probing kinetic drug binding mechanism in voltage-gated sodium ion channel: open state versus inactive state blockers. *Channels* (2015), 9 (5), pp. 307-16.
- [57] K. Pal, G. Gangopadhyay , Dynamical characterization of inactivation path in voltage-gated Na C ion channel by non-equilibrium response spectroscopy, *Channels* (2016), 10 (6), pp.478-497.
- [58] G. Schmid, I. Goychuk, P. Hanggi, Effect of channel block on the spiking activity of excitable membranes in a stochastic Hodgkin-Huxley model, *Phys. Biol.*(2004) , 1, pp.61-66.
- [59] JR. Clay , LJ. DeFelice. Relationship between membrane excitability and single channel open-close kinetics. *Biophys J.* (1983), 42, pp. 151-7.
- [60] K. Pal, G. Gangopadhyay. Nonequilibrium response of a voltage gated sodium ion channel and biophysical characterization of dynamic hysteresis, *Journal of Theoretical Biology* (2017), 415, pp. 113-124.

In every end, there is also a beginning...